UNIVERSITY OF ICELAND

Ph.D. Thesis

in Bioengineering

Decoding the model diatom *Phaeodactylum tricornutum* for developing photosynthetic cell factories

Yixi Su

May 2024

FACULTY OF INDUSTRIAL ENGINEERING, MECHANICAL ENGINEERING AND COMPUTER SCIENCE

Decoding the model diatom *Phaeodactylum tricornutum* for developing photosynthetic cell factories

Yixi Su

Dissertation submitted in partial fulfillment of a
Philosophiae Doctor degree in Bioengineering

Ph.D. Committee
Weiqi Fu
Sigurður Brynjólfsson
Snædís Huld Björnsdóttir
Ólafur Sigmar Andrésson

Opponents
Tryggvi Stefánsson
Maria Barbosa

Faculty of Industrial Engineering, Mechanical Engineering
and Computer Science
School of Engineering and Natural Sciences
University of Iceland
Reykjavik, May 2024

Decoding the model diatom Phaeodactylum tricornutum for developing photosynthetic cell factories
Dissertation submitted in partial fulfillment of a *Ph.D.* degree in Bioengineering

Faculty of Industrial Engineering
School of Engineering and Natural Sciences
University of Iceland
Dunhagi 5
107 Reykjavik
Iceland

Telephone: 525 4000

Bibliographic information:
Yixi Su, 2024, *Decoding the model diatom Phaeodactylum tricornutum for developing photosynthetic cell factories*, Ph.D. thesis, Faculty of Industrial Engineering, University of Iceland.

Author ORCID: https://orcid.org/0000-0001-7223-6010
ISBN 978-9935-9769-5-6

Abstract

Climate change, caused by greenhouse gas (GHG) emissions, has jeopardized sustainability. The urgent demand for carbon neutrality is driving the development of microalgae-based carbon capture technology. There is a desire to utilize untapped carbon sources from industrial flue gas to produce value-added microalgal biomass. However, direct use of flue gas poses challenges to microalgae cultivation such as inhibitory impacts of acidic pH on algal growth. Adaptive laboratory evolution (ALE) was conducted on the model diatom *Phaeodactylum tricornutum* under constant acidic conditions, resulting in adapted strains with improved growth. Meanwhile, stress responses and adaptive mechanisms were investigated through genomics and transcriptomics, reveling important pathways that could confer higher acid resistance on the adapted strains. Several ion/electron carrier genes, which are likely to influence intracellular pH homeostasis, were selected for further reverse genetics studies. Overexpression modifications of the ferredoxin (PtFDX), cation/proton antiporter (PtCPA), and bicarbonate transporter (PtSLC4-2) enabled positive growths of corresponding transgenic strains under acidic stress that completely inhibited the wild-type (WT). These modifications alleviated oxidative stress and partially rescued photosynthetic function in the transgenics. While the PtFDX transgenic exhibited transcriptome profiles similar to the WT, overexpressing the proton and bicarbonate pumps caused elevated expression of various transmembrane transporters, which may be responsible for the acidic tolerant trait. Furthermore, the photosynthetic carbon fixation efficiency is the main obstacle to be addressed for developing photosynthetic cell factories. We first decode the circadian regulation mechanism underlying *P. tricornutum* under conditions without environment cues (i.e., constant light and temperature conditions). These findings pave the way for improving photosynthetic efficiency in microalgae by manipulating the light/dark cycle, shedding light on fundamental features of photobiology, and advancing the understanding of circadian rhythms in photosynthesis regulation.

Útdráttur

Loftlagsbreytingar af völdum gróðurhúsaáhrifa stefna sjálfbærni jarðar í hættu. Mikilvægi þess að draga úr losun kolefnis er drifkrafturinn í þróun á aðferðum við bindingu kolefnis með þörungum. Mikill áhugi er á að binda kolefni í afgasi frá iðnaði og nýta afgasið til framleiðslu á lífefnum. Notkun á afgasi beint til ræktunar er erfitt vegna sýrustigsins sem hindrar þörungavöxt. Þörungurinn Phaeodactylum tricornutum var ræktaður í nokkrar kynslóður á rannsóknarstofu við lágt sýrustig til að fá fram afbrigði með aukinn vaxtarhraða við þær aðstæður. Jafnframt voru áhrif þessa álags á erfðamengi og umritunferli þörungsins rannsökuð til þess að leiða í ljós þá mikilvægu efnaferla sem leiða til aukins þols gegn lágu sýrstigi í nýja afbrigðinu. Nokkur gen sem sem talin eru hafa áhrif á pH jafnvægi voru valin til erfðafræðirannsókna. Yfirtjáning ferrodoxín, rafeindferja og bicarbonatferja (PtFDX, PtCPA og PtSLC4-2) gerði þörunga afbrigðinu kleift að vaxa við skilyrði þar sem óbreytta afbrigðið (WT) óx ekki. Þessar breytingar komu í veg fyrir oxunarálag og vörðu ljóstillífun í genabreytta afbrigðinu. Breyting á PtFDX leiddi af sér svipaða niðurstöðu umritunar og í óbreytta afbrgðinu en yfirtjáning á rafeinda- og bicarbonatferjunum PtCPA og PtSLC4-2 jók tjáningu á ýmsum himnnuferjum sem mögulega veldur auknu þoli gegn súrum aðstæðum. Þar að auki er nýtni ljóstillífunarferilsins ein helsta áskorun við þróun framleiðsluferla hjá þörungum. Við skoðuðum stýringu á dægursveiflu þörungsins án ytri áhrifa frá umhverfi, þ.e. með stöðugt ljós og fast hitastig. Þessar rannsóknar eru skref í átt að auknum afköstum ljóstillífunar í þörungum með því að hafa áhrif á birtu/myrkur tímabil og varpa ljósi á grundvallaratriði ljóslíffræði og stýringu á dægursveiflu ljóstillífunar.

Table of Contents

List of Figures

List of Tables

List of Publications

The thesis is based on the following original papers:

Paper 1 (included in chapter 2): **Yixi Su**, Maonian Xu, Sigurður Brynjólfsson, Weiqi Fu, (2023). Physiological and molecular insights into adaptive evolution of the marine model diatom *Phaeodactylum tricornutum* under low-pH stress, Journal of Cleaner Production 412 (2023) 137297; https://doi.org/10.1016/j.jclepro.2023.137297.

Paper 2 (included in chapter 3): **Yixi Su**, Jiwei Chen, Jingyan Hu, Chen Qian, JiaHao Ma, Sigurður Brynjolfsson, Weiqi Fu. Rational genetic engineering of the model diatom *Phaeodactylum tricornutum* enables its fast growth under inhibitory low-pH stress. Submitted (2023)

Paper 3 (included in chapter 4):: **Yixi Su**, Jingyan Hu, Jiwei Chen, Weizhao Meng, Cheng Qian, Yuexuan Shu, Chao Wang, Xianwei Wang, Kourosh Salehi-Ashtiani, Sigurður Brynjólfsson, Jianping Lin, Yongquan Li, Haisheng Zhang, Lizhong Wang, Weiqi Fu. An intrinsic circadian clock to regulate phytoplankton photosynthesis. Submitted (2023)

In addition, the candidate has contributed to the following published work related to the doctoral project:

Yixi Su, Zhiqian Yi, Snædís Huld Björnsdóttir, Sigurdur Brynjolfsson, and Weiqi Fu, (2018). Adaptive Laboratory Evolution for Enhanced Carotenoid Production in Microalgae, Microbial Carotenoids: Methods and Protocols, Methods in Molecular Biology, vol. 1852; https://doi.org/10.1007/978-1-4939-8742-9_7.

Zhiqian Yi, **Yixi Su**, Maonian Xu, Andreas Bergmann, Saevar Ingthorsson, Ottar Rolfsson, Kourosh Salehi-Ashtiani, Sigurdur Brynjolfsson, Weiqi Fu, (2018) Chemical Mutagenesis and Fluorescence-Based High-Throughput Screening for Enhanced Accumulation of Carotenoids in a Model Marine Diatom *Phaeodactylum tricornutum*. Mar. Drugs 2018, 16, 272; doi:10.3390/md16080272.

Zhiqian Yi, **Yixi Su**, Paulina Cherek, David R. Nelson, Jianping Lin, Ottar Rolfsson, Hua Wu, Kourosh Salehi-Ashtiani, Sigurdur Brynjolfsson, Weiqi Fu, (2019) Combined artificial high-silicate medium and LED illumination promote carotenoid accumulation in the marine diatom Phaeodactylum tricornutum. Microbial Cell Factories 18 (1); 10.1186/s12934-019-1263-1.

Lars Truttmann, **Yixi Su**, Seonki Lee, Michael Burkhardt, Sigurður Brynjólfsson, Tzyy Haur Chong, Bing Wu, (2020). Gravity-driven membrane (GDM) filtration of algae-polluted surface water, Journal of Water Process Engineering 36 (2020) 1012; https://doi.org/10.1016/j.jwpe.2020.101257.

Zhiqian Yi, **Yixi Su**, Sigurdur Brynjolfsson, Kristin Olafsdottir, Weiqi Fu, (2021). Bioactive polysaccharides and their derivatives from microalgae: biosynthesis, applications, and challenges, Studies in Natural Products Chemistry; https://doi.org/10.1016/B978-0-323-91095-8.00007-6.

Weiqi Fu, Yuexuan Shu, Zhiqian Yi, **Yixi Su**, Yiwen Pan, Fan Zhang, Sigurdur Brynjolfsson, (2022). Diatom morphology and adaptation: Current progress and potentials for sustainable development, Sustainable Horizons 2 (2022) 100015; https://doi.org/10.1016/j.horiz.2022.100015.

Abbreviations

ATP	Adenosine Triphosphate
AFDW	Ash-free dry weight
ALE	Adaptive Laboratory Evolution
AD	Anaerobic Digestion
ASP	Aquatic Species Program
BP	Biological Processes
BWA	Burrows-Wheeler Aligner
CBB	Calvin-Benson-Bassham
CCS	Carbon Capture and Storage
CCM	Carbon Concentrating Mechanisms
CO_2	Carbon Dioxide
CC	Cellular Component
CAGR	Compound Annual Growth Rate
CDS	CoDing Sequence
CAT	Chloramphenicol Acetyl Transferase
CRISPR	Cluster of Regularly Interspaced Palindromic Repeats
CCAP	Culture Collection of Algae and Protozoa
CAPS	3-(Cyclohexylamino)-1-PropaneSulfonic acid
CDK	Cyclin-Dependent Kinase
DEA	DiEthanolAmine
DEG	Differentially Expressed Gene
DIC	Dissolved Inorganic Carbon
DPA	DiPhenylAmine
DHA	DocosaHexaenoic Acid
DNA	DeoxyriboNucleic Acid

DW	Dry Weight
ETC	Electron Transport Chain
EPA	EicosaPentaenoic Acid
EGFP	Enhanced Green Fluorescent Protein
FACS	Fluorescence-Activated Cell Sorting
FCM	Flow cytometry
FCP	Fucoxanthin Chlorophyll binding Proteins
FPKM	Fragments Per Kilobase per Million mapped fragments
FBA	Fructose-Bisphosphate Aldolase
GC	Gas Chromatography
GMO	Genetically Modified Organism
GO	Gene Ontology
GHG	GreenHouse Gas
GAPDH	GlycerAldehyde-3-Phosphate DeHydrogenases
HSP	Heat Shock Protein
HGT	Horizontal Gene Transfer
HDR	Homology-Directed Repair
IGCC	Integrated Gasification Combined Cycle
InDel	Insertion-Deletion
KEGG	Kyoto Encyclopedia of Genes and Genomes
LHC	Light harvesting complex protein
mRNA	microRNA
MF	Molecular Function
MEA	MonoEthanolAmine
MES	2-*N*-MorpholinoEthane-Sulfonic acid
NO_x	Nitrogen Oxide

NPQ	Non-Photochemical Quenching
NHEJ	Non-Homologous End Joining
OD	Optical Density
PM	Particular Matter
PMSF	PhenylMethylSulfonyl Fluoride
PS	PhotoSystems
PAR	Photosynthetically Active Radiation
PE	Photosynthetic Efficiency
PBR	PhotoBioReactor
PMA	Plasma Membrane H^+-ATPase
PLA	PolyLactic Acid
PBS	PolyButylene Succinate
PUFA	PolyUnsaturated Fatty Acid
PHA	PolyHydroxyAlkanoates
PK	Pyruvate Kinase
QY	Quantum Yield
RNA	RiboNucleic Acid
RIN	RNA Integrity Number
RuBP	Ribulose BisPhosphate
ROS	Reactive Oxygen Species
RUBISCO	Ribulose-1,5-bisphosphate carboxylase/oxygenase
SNP	Single Nucleotide Polymorphisms
snRNA	small nuclear RNA
snoRNA	small nucleolar RNA
SO_x	Sulfur Oxide
TALEN	Transcription-Activator-Like Effector Nuclease

TF	Transcription Factor
TAG	TriAcylGlyceride
TCA	TriCarboxylic Acid
UV	UltraViolet
UNSDG	United Nations Sustainable Development Goal
vvm	Volume per culture Volume per Minute
WT	Wild Type
ZT	Zeitgeber Time
ZFN	Zinc Finger Nucleases

Acknowledgements

I am grateful to my parents for the infinite support and encouragement, which helped me to get through all the difficult times.

I want thank my supervisors, Prof. Weiqi Fu and Prof. Sigurdur Brynjolfsson, for providing me the opportunity to pursue the research I am truly interest in and for granting me the freedom to develop my ideas. Additionally, I sincerely thank them for years of generous support, patience and inspiring advice.

I would also like to express my gratitude to all staff, coworkers and friends at the University of Iceland, including Zhiqian, Maonian, Guðný, Cyril, Han, Qiong, and others who contributed to my work and made my time working here memorable.

I appreciate for financial supports provided by the Icelandic Research Fund (grant number 207298-052) and the Technology Development Fund (grant number 163922-0613).

1 Introduction

Since the advent of the industrial era, numerous anthropogenic activities such as fossil fuel combustion for power generation, transportation and industries, have accelerated the accumulation of greenhouse gas (GHG) in atmosphere, making it the primary cause of global climate change [1]. China (28%), the USA (15%), the EU (9%) and, India (7%) are the main contributors of the growing GHG emissions that is currently rising by 1.5% per year [2]. Although awareness of the GHG problem has led to the rapid development of alternative energy sources such as wind and solar power, CO_2 emissions are expected to continue increasing in the next 30 years, because economic growths at present is tightly coupled with exploitation of environmental resources and carbon emissions [3, 4]. As a consequence, the global surface temperature is projected to increase by 1.5 ℃ between 2030 and 2052 [2]. Foreseeable consequences of global warming resulting from GHG emission include glacier melting, ocean warming and acidification and sea-level rise, which are globally emerging and correlated with recent increase in weather-related disasters worldwide. These risks threaten livelihoods, ecosystems, biodiversity and coastal environments [5, 6]. Between 2000 and 2019, more than 11,000 extreme weather events occurred globally and caused over 475,000 deaths and an economic loss of around USD 2.56 trillion [7]. To combat the climate crisis, the concept of carbon neutrality, which involves offsetting the generated CO_2 through carbon capture, storage and conversion has been proposed to achieve "zero emission" of GHGs [8]. In 2015, the Paris Agreement adopted by 196 parties, set the goal of achieving net-zero emission in the second half of this century. By 2021, more than 130 countries had proposed emission reduction goals and strategies based on their national conditions [4].

This chapter presents literature reviews on relevant topics. Section 1.1 provides a summary of technological options for carbon capture, highlighting microalgal biotechnology as the most promising solution to address the current problem. Section 1.2 introduces basic knowledge on evolution and biology of microalgae, with a specific focus on the diatom, which is the research subject of this project. Section 1.3 discusses the promising applications of microalgal biotechnology, highlighting the opportunities for a microalgae-based sustainable bioeconomy, as well as challenges that hinder commercialization of microalgae. In Section 1.4, various strain improvement strategies are outlined, presenting available technological choices and reviewing the state-of-the-art in microalgae engineering. This section identifies under-researched areas that have the potential to lead to novel engineering developments. Section 1.5 outlines the research objectives and questions that arise from the motivation to convert waste geogas into value-added microalgal biomass.

1.1 Routes to carbon neutrality

Carbon dioxide (CO_2) accounts for more than 60% of GHG and is the primary driver of climate change [6]. As of 2021, atmospheric CO_2 levels have reached 37 billion tons [9]. Currently, carbon capture strategies can be categorized into pre-combustion, oxy-fuel combustion and post-combustion process. Pre-combustion capture is commonly employed in integrated gasification combined cycle (IGCC) power plants. In this process, the fuels are

initially gasified into syngas, which is a mixture of CO and H_2. CO is then converted into CO_2, and the resulting CO_2 is removed before the combustion of hydrogen. In oxy-fuel combustion capture, pure oxygen instead of air is needed to burn the fuels to reduce N_2. This results in an enriched mixture of CO_2 and H_2O, simplifying the process of CO_2 capture through water condensation. These approaches have the advantage of producing flue gas with higher percent of CO_2, which facilitates easier capture. However, these processes involve additional steps such as gasification and oxygen purification, which increase energy requirement and cost. In contrast, the post-combustion capture process involves separating CO_2 after combustion of fossil fuel, which is suitable for all existing power plants and is therefore the most widely used approach [10].

In order to mitigate carbon footprint, various techniques for carbon capture and storage (CCS) have been proposed. These techniques can be generally classified into physical, chemical, and biological processes [11]. Currently, CO_2 released from fossil fuel combustion is usually captured through absorption using physical solvents like selexol or rectisol, or chemical solvent like diethanolamine (DEA) and monoethanolamine (MEA). However, these methods are capital and energy-intensive during the regeneration process [12]. Alternatively, physical and chemical adsorbents can be used to selectively capture CO_2 via electrostatic and Van der Waals forces (physisorption) or covalent bonding (chemisorption) [10]. Membrane separation, based on the Knudsen diffusion principle and the Fick's molecular diffusion, is also considered a cost-effective separation method [13]. Nevertheless, membrane technique face challenges related to selectivity, permeability for CO_2 and tolerance to harsh operating conditions in flue gas environments [10]. For storage, the separated supercritical CO_2 can be physically injected into deep ocean or subsurface geological sites [3] However, these operations are costly and may pose environmental concerns due to potential long-term CO_2 leakage [12]. Another approach involves the precipitation of CO_2 through mineral carbonation, where CO_2 reacts with metal cations such as Ca^{2+}, Mg^{2+} or Fe^{2+} to form stable carbonate that can be stored. While mineralization processes hold potential for managing significant quantities of CO_2, their development is hindered by technical and economic challenges [14]. Biological CCS technology is based on photosynthesis, where CO_2 is converted into biomass. Strategies for biological carbon capture include forestation, oceanic fertilization, and microorganism-based carbon capture. Forestation and oceanic fertilization aim to promote the growth of terrestrial and oceanic biomass but may carry risks of unpredictable impacts on ecology and biodiversity. Microalgae, on the other hand, have the potential to fix 1.83 kg of CO_2 per 1 kg of biomass, making them a promising carbon sink [15]. Currently, microalgal carbon capture is considered the most promising biological sequestration method [12].

1.2 Microalgae

1.2.1 Evolution and classification

Microalgae are a diverse group of organisms that encompass unicellular photosynthetic organisms, including eukaryotic photosynthetic protists and prokaryotic cyanobacteria [16]. Oxygenic photosynthesis originally occurred in cyanobacteria. Other photosynthetic protists evolved through multiple endosymbiotic events involving a heterotrophic eukaryotic host and a cyanobacterium or a eukaryotic alga. During the establishment of symbiosis, some genes from the engulfed organism were transferred into the host's nucleus, and the

endosymbiont became a plastid organelle [17]. Three phyla, namely Chlorophytes (green algae), Rhodophytes (red algae), and Glaucophytes, emerged independently in the primary endosymbiosis, where a cyanobacterium was engulfed by a heterotrophic eukaryote (Figure 1.1). The resulting primary plastids are surrounded by two membranes. Other eukaryotic lineages acquired photosynthesis through secondary endosymbiosis, where a heterotrophic eukaryote engulfed a green or red alga containing a primary plastid, eventually leading to plastids surrounded by four membranes [18] (Figure 1.1). The phylum Dinofalgellata represents a special case, as it possesses plastids from at least four different sources (Chlorophyta, Cryptophyta, Stramenopiles and Haptophyta) through the uptake of a secondary plastid-containing alga or sequential secondary endosymbiosis [18]. The classification of microalgae is based on various data, including protein, DNA, pigmentation, morphology and basic biology (e.g. reproduction), which reflect their evolutionary relationships [19]. Determiing the phylogeny of microalgae is complex due to the different origins of participants in endosymbiosis. For example, Stramenopiles, Apicomplexa, Chromeridae and Dinophyta, along with Cryptophyta and Haptophyta, belong to the red lineage supergroup, Chromalveolata. However, based on phylogenetic relationships at the host level, they are closer to the green lineage algae, Rhizaria. Stramenopiles, Alveolata (Apicomplexa, Chromeridae and Dinophyta) and Rhizaria are classified in the SAR supergroup [18] (Figure 1.1). In addition to endosymbiosis, the evolution of microalgae is driven by mutation, selection, genetic drift and gene flow as well as horizontal gene transfer (HGT), enabling their versatile adaptability and diverse distribution in various environments [20].

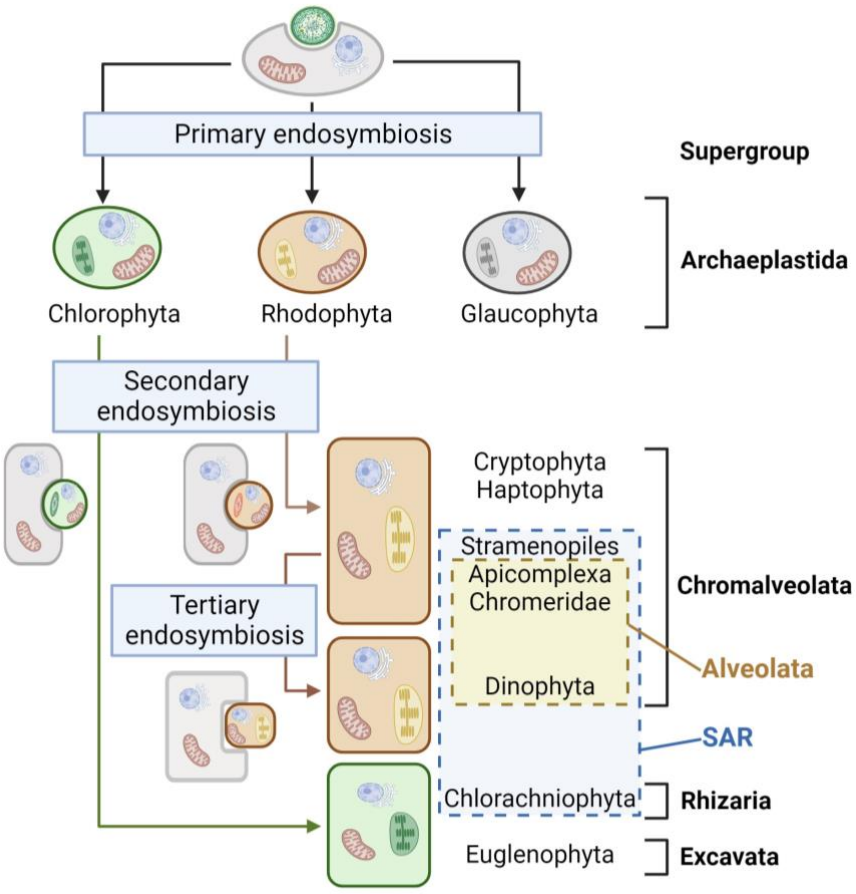

Figure 1.1. *Algae evolution and taxonomic classification.*

1.2.2 Diatoms

Diatoms belong to the red algae lineage, Stramenopiles, and are characterized by their unique silicified cell wall called frustules. The frustules are composed of nanometer-sized particles of SiO_2 arranged in diverse and regular geometric patterns. Traditional classification of diatom is primarily based on the morphological features of the frustule [21]. Diatoms are generally categorized into the centric diatoms, which have circular frustules with radial symmetry, and the pennate diatoms, which have elongated frustules with primarily bilateral symmetry. The pennate diatoms are further divided into the raphid and araphid diatoms depending on the presence and absence of raphe, a longitudinal slit on the frustule. In the late 20th century, a significant classification proposed three classes of diatom: the centric (Coscinodiscophyceae), pennate without raphe (Fragilariophyceae), and pennate with a raphe (Bacillariophyceae) [22]. The frustule, which is the key feature of diatoms, consists of two valves, the epivalve and hypovalve. The epivalve is slightly larger than the hypovalve, and they are connected by silica bands called the girdle or cingulum, forming a petri dish-like structure. The frustule can be observed from two views, the valve view and the girdle view. The valve view displays variations in shape, symmetry as well as topography, ranging from flat to convex. The girdle view is less variable and typically consists of multiple bands that allow the cell to expand in a pervalvar direction [23]. The frustule wall is perforated by pores called areolae, which are occluded on the inner side by a thin porous layer of silica called velum. The arrangement and spacing of areolae form species-specific features known as striae, which are used for identification purposes. Centric diatoms typically have a radiating pore arrangement, while pennate diatoms have elongated and bilaterally symmetric pore patterns [24]. It is important to note that while the artificial classification based on frustule features can aid recognition, it may not necessarily reflect the true evolutionary relationship in a natural classification scheme. In molecular era, comparative analysis of ribosomal RNA (rRNA) sequences has provided insights into the phylogenetic relationships among the diatoms at higher taxonomic levels [21]. Based on these molecular studies, three classes of diatoms have been established accordingly: Clade 1includes Coscinodiscophyceae (radial centric diatoms), Clade 2 includes Mediophyceae (bi-or multipolar centric diatoms and the radial Thalassiosirales) and Clade 3 includes Bacillariophyceae (pennate diatoms) [25]. These molecular classifications help to elucidate the evolutionary relationships among diatoms beyond their morphological characteristics.

Among diatoms, the model species, *P. tricornutum* stands out as a pennate diatom with a unique characteristic known as pleiomorphism [26]. Pleiomorphism refers to the existence of multiple distinct morphotypes within a single species. In the case of *P. tricornutum*, four main morphotypes have been described: fusiform, triradiate, oval, and cruciform [27-29]. The fusiform and triradiate are often found in planktonic environments, while the oval morphotype is predominantly benthic [26]. The fusiform and triradiate morphotypes of *P. tricornutum* possess elongated shapes with additional volume in the form of vacuoles within their arms. These vacuoles increase buoyancy, aiding in planktonic lifestyle of these cells [30]. In contrast, oval morphotype is characterized by silicified frustules, and it is believed that the silica raphe structure of oval cells plays a role in locomotion on solid surface [31]. Oval cell also have the ability to excrete mucilaginous material, which serves to promote cell aggregation, sedimentation and adherence to the culture flask wall [32]. The pleiomorphism observed in *P. tricornutum* highlights the remarkable adaptability and versatility of diatoms in different ecological niches. The ability to exhibit various morphotypes within a single species allows *P. tricornutum* to occupy diverse habitats and effectively respond to environmental conditions.

Although the fusiform cell is typically the most prevalent morphotype in laboratory cultures, different morphotypes of this diatom can interchangeably and commonly coexist within a culture. Current understanding suggests that morphological preference and stability are likely to vary among strains and determined by genotype, while morphotype transformation is likely regulated epigenetically and influenced by external factors [30]. De Martino et al. (2007) conducted a study on ten geographically distinct strains of *P. tricornutum*, where seven cultures were predominantly composed of fusiform cells, while specific strains exhibited a predominance of triradiate or oval morphotypes. The average growth rates of the fusiform accessions (0.97 ± 0.06 d^{-1}) were approximately 1.4 times higher than those of oval (0.71 ± 0.03 d^{-1}) and triradiate (0.73 ± 0.04 d^{-1}) cultures [26]. Suboptimal conditions induce an increase in oval cells while causing the elimination of triradiate cells [26, 28]. The formation of oval cells can be promoted by low temperature [26, 33, 34], hyposalinity [33], solid medium [32, 35] and culture aging [26, 33]. These observations suggest that the oval morphotype represents a stress-resistant form, as supportedly gene expression analysis showing the overexpression of typical stress pathways in cultures predominantly composed of oval cells [33]. Therefore, different morphotype of *P. tricornutum* may be specifically associated with growth under particular conditions, indicating that morphological transformation can serve as an adaptive mechanism in response to environmental changes [30].

1.2.3 Photosynthesis

Photosynthesis generally refers to oxygenic photosynthesis that in cyanobacteria, algae and terrestrial plants produces oxygen and carbohydrates from light, water and carbon dioxide [36]. Photosynthesis, serving as the foundation of all life on Earth, contributes to a global net primary production of 107.3 Pg C $year^{-1}$. Terrestrial and oceanic photosynthesis account for 51.1% and 48.9% of this production, respectively [37]. The basic mechanisms of photosynthesis comprising the light reaction and the dark reaction are described in any comprehensive biochemistry textbook. Briefly, the light-dependent reaction, occurring on the thylakoid membrane, converts the captured light energy into chemical energy through electron transfer in an electron transport chain (ETC). This process leads to the synthesis of ATP and NADPH, providing energy and reducing power for stromal carbon fixation. The dark reaction, known as the Calvin-Benson-Bassham (CBB) cycle or the reductive pentose phosphate cycle is responsible for carbon fixation and conversion of inorganic CO_2 into carbohydrates (Figure 1.2).

The photosynthetic machinery encompasses photosynthetic pigments, photosystems I (PSI) and II (PSII), electron transport systems and CO_2 reduction pathways. Damages to these apparatus can impair the overall photosynthetic capacity [38]. Given the crucial role of photosynthesis in plant growth, the effects of abiotic stresses, particularly temperature, salinity, and drought on crop photosynthesis have been extensively studied and reviewed by Ashraf and Harris [38], Singh and Thakur [39], Sharma, et al. [40] and Muhammad, et al. [41]. Reduction in pigment biosynthesis is frequently observed under stress conditions. This reduction is presumed to be caused by (i) transcriptional down-regulation of genes involved in biosynthesis, (ii) impaired enzymatic activities in biosynthetic pathways and (iii) accelerated pigment breakdown [40]. For instance, temperature stress was reported to reduce expression of enzymes involved in chlorophyll biosynthesis in celery, cucumber and wheat [42, 43]. Pigment degradation in *Arabidopsis* is associated with an ABC1-like kinase gene whose expression is elevated by an oxidative stress, resulting in reduced contents of

chlorophyll and carotenoids [44]. Another susceptible target is the thylakoid membrane, whose stability can be disrupted by ROS mediated oxidative damage induced by high temperature, salt and drought stress, thereby resulting in obstruction of electron transport [41]. In addition to heavy metal and high temperature, excessive light poses a particular risk to PSII, as it can cause damage to the key D1 core proteins, resulting in photoinactivation of PSII [40, 45]. In crops, abiotic stress-induced stomatal closure has a significant impact on the carbon assimilation pathway. Stomatal closure is triggered by abiotic stresses to limit water loss, but it also reduces CO_2 conductance through stomata and mesophyll cells, consequently decreasing the activities of Rubisco and the capacity for ribulose bisphosphate (RuBP) regeneration [38, 39].

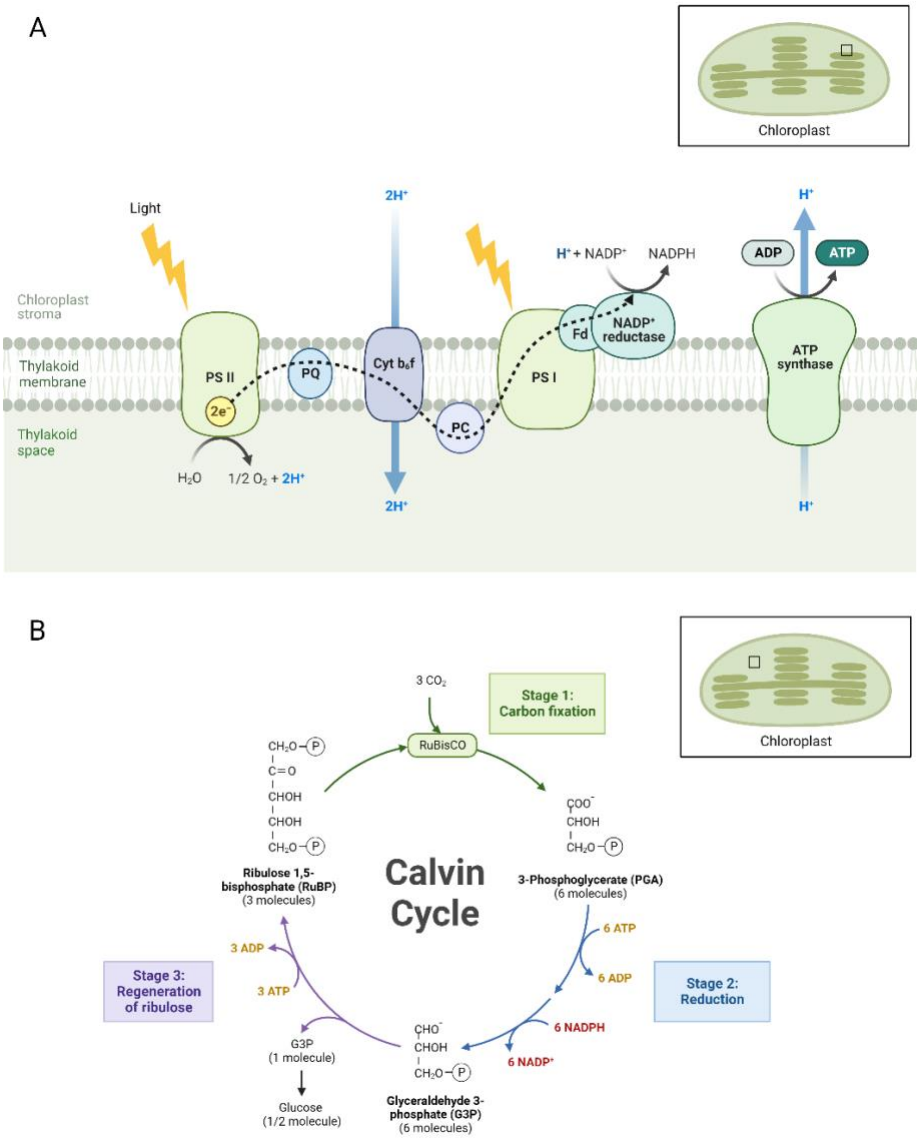

Figure 1.2. Light reaction and dark reaction of photosynthesis

During photosynthesis, only a fraction of solar irradiation within the visible light spectrum (between 400 nm and 700 nm) can be absorbed and utilized for photochemical conversion. This portion, known as photosynthetically active radiation (PAR), accounts for approximately 45% of the solar radiance that reaches the Earth's surface [46]. In theoretical

calculations, the maximum efficiency of converting photon energy into biomass, known as photosynthetic efficiency (PE), is estimated to be approximately 10.7% in photosynthetic organisms. However, this theoretical maximum is unattainable due to various adverse factors in cultivation, as well as the inevitable decrease in actual quantum yield when the photon flux density approaches light saturation [46, 47]. A more realistic PE estimation is 4.5% for C3 plants or microalgae [47]. Microalgae, which benefit from their simple structure are capable of fast growth with more efficient CO2 fixation compared to terrestrial plants [48]. Experimental data on PE derived from microalgae cultivation, whether in open systems or closed photobioreactors (PBRs), can range from 0.31 to 4.2% [49] that are higher than most crops with 0.2 – 1 % PE of solar light [50].

1.2.4 Factors affecting microalgal growths

In algaculture, the optimization of abiotic factors is critical for successful microalgae production. Factors such as irradiance (light intensity), temperature, pH, salinity, carbon dioxide levels, and nutrient availability have significant impacts on microalgal growth, biomass productivity, and the chemical composition of the produced biomass [51]. Microalgal growth depends on maintaining homeostasis by balancing the equilibrium of physiological processes and cellular composition with the organism's environment. Cells react to stress-induced disruptions of homeostasis by changing cellular metabolism to restore equilibrium and, thus, maintain growth [51].

In terms of irradiance impact, microalgal growth is affected by light intensity, quality, and duration. The impact of light intensity on microalgal growth (photosynthesis) can be graphically represented by the photosynthesis-irradiance (P-I) curve, which can be divided into three distinct regions: (i) In the light-limitation region, characterized by low light intensity, the photosynthetic rate and growth of algae are constrained by the rate of photon capture, which is directly proportional to irradiance; (ii) In the light-saturation region, when the light intensity reaches a saturation threshold, photosynthesis becomes irradiance-independent and is limited by the maximum reaction rate of photosynthesis; (iii) In the photoinhibition region, characterized by light intensity exceeding an inhibitory threshold, photosynthesis begins to decline due to irreversible damage to the photosynthetic apparatus [52]. Studies have demonstrated that blue and red light can induce shifts in protein and carbohydrate metabolism [53] . Furthermore, light quality, particularly the blue light has been associated with regulation of photoprotection in diatoms [54]. Moreover, the length of photoperiod, which refers to the light-dark cycle determining the duration of active photosynthesis, significantly impacts biomass productivity [48]. Continuous light is believed to support a prolonged photosynthesis, thereby maximizing productivity. However, biomass accumulation is often not positively correlated with the duration of photoperiod [55, 56].

Temperature and pH affect microalgal growth through influencing both physicochemical carbon dioxide availability and cellular metabolism. Higher temperatures lead to reduced CO_2 solubility [57], while low pH decreases dissolved inorganic carbon (DIC) and shifts the carbonate equilibrium towards higher dissolved free CO_2 [58]. Additionally, temperature and pH affect enzyme activities, thereby influencing the metabolic rates of microalgae. Microalgae typically inhabit a temperature range of 15 to 30 ℃ with optimal temperature between 20 and 25℃. Regarding pH, microalgae generally thrive in the neutral to slightly alkaline range (pH 6 – 8.3) [48]. The availability of nutrients, particularly carbon, nitrogen, and phosphorus sources, is crucial for providing the fundamental substances

required for the construction of the organism [51]. Nutrient deficiency is well-known to shift metabolic pathways from growth to storage of high energy content. Nitrogen and phosphorus limitation has been extensively studied to enhance lipid accumulation. However, this strategy has limited success in increasing the lipid productivity due to low biomass growth [48].

Given the concern over increasing greenhouse gas emissions, extensive research has been conducted to examine the effects of elevated CO_2 and ocean acidification on phytoplankton physiology, with a particular focus on primary productivity. It is evident that strain-specific physiological characteristics, along with interactions between abiotic factors such as CO_2 and light levels, synergistically contribute to growth responses to elevated CO_2 [59]. While some inconsistent results have been observed, likely due to species-specific factors and variations in experimental procedures, previous studies have generally shown that CO_2 enrichment promotes algal growth under limited to moderate light levels [60-63]. However, it can also render cells more susceptible to light stress under oversaturating irradiance [62, 64]. Several studies have provided physiological evidence [64-66] and examined gene expression data [67] to support the effects of rising CO_2 on various aspects, including inorganic carbon acquisition (e.g., carbon concentrating mechanisms [CCMs]), photosynthetic performances (e.g., maximum carbon fixation, photosynthetic efficiency, photorespiration), photoprotection, and mitochondrial respiration (e.g., the citric acid cycle).

1.3 Applications: microalgae-based bioeconomy

Microalgae featured by efficient carbon fixation are very productive biomass and can produce a range of products from low to high value. Microalgae have long been suggested for applications such as biofuels, aquafeed, food, bioactive compounds, and more. However, the high cost of production has remained a significant barrier to their widespread adoption. The growing concern about climate change has sparked enthusiasm for the development of microalgae-based carbon capture technology. Bioremediation, which involves utilizing waste resources like exhaust flue gas and wastewater for cultivating microalgae, has the potential to lower costs and carbon footprints [68]. This section presents the opportunities and challenges associated with microalgae production in a bio-based economy.

1.3.1 Algal bioproducts

Microalgae are rich in primary metabolites, including lipids, carbohydrates, and proteins, which are vital for their survival. They also produce secondary metabolites, such as carotenoids, which serve specific physiological functions [69]. Unlike terrestrial crops that can only be partially utilized, microalgal biomass, in the context of a biorefinery concept, can be almost entirely utilized for the production of diverse bioproducts [70]. Compositions of microalgae can vary depending on the species, leading to specific applications in certain microalgae markets [71]. Table 1.1 provides a summary of common microalgal species that have commercial applications and the corresponding bioproducts.

Table 1.1. Microalgal species and bioproducts with commercial applications.

Microalgal strains	Bioproducts	Applications
Cyanobacteria		
Arthrospira platensis	Biomass, vitamin	Food, nutraceuticals, cosmetics, biofertilizer, animal feed, bioplastics
Red microalgae		
Porphyridium cruentum	Polysaccharides, phycobilins	Food, cosmetics
Green microalgae		
Chlorella sp.	Biomass, lutein	Food, biodiesel, nutraceuticals, biofertilizer, animal feed, bioplastics
Scenedesmus sp.	Biomass, lutein	Biodiesel, nutraceuticals, animal feed, biofertilizer
Dunaliella salina	β-carotene	Aquafeed, pharmaceuticals, nutraceuticals, animal feed, cosmetics
Harmatococcus pluvialis	Astaxanthin	Aquafeed, pharmaceuticals, nutraceuticals, cosmetics
Botryococcus braunii	Lipid	Biodiesel
Haptophytes		
Pavlova salina	PUFA	Aquafeed, nutraceuticals
Isochrysis galbana	PUFA	Aquafeed, nutraceuticals
Stramenopiles		
Phaeodactylum tricornutum	Fucoxanthin, PUFA	Aquafeed, pharmaceuticals, nutraceuticals
Chaetoceros sp.	PUFA	Aquafeed
Thalassiosira pseudonana	PUFA	Aquafeed
Schizochytrium sp.	PUFA	Aquafeed, nutraceuticals, animal feed
Nannochloropsis sp.	PUFA	Aquafeed, nutraceuticals, animal feed, cosmetics
Dinophyta		
Crypthecodinium cohnii	PUFA	Nutraceutical

Currently, microalgae applications are limited to medium- and high-value products due to their high production cost [72]. These applications are primarily found in the food, feed, health-related, and cosmetic sectors [73]. Carotenoids and polyunsaturated fatty acids (PUFA) represent the most valuable and profitable microalgae-derived products. Carotenoids are generally classified into hydrocarbon carotenes, such as β-carotene and their oxygenated derivatives, known as xanthophylls including lutein, astaxanthin and fucoxanthin. Carotenoids, which appear as orange-yellow pigments, absorb light in the blue-green region (400 to 600 nm) and contribute to light harvesting in photosynthesis. Additionally, carotenoids act as strong antioxidants, quenching reactive oxygen species (ROS) and protecting the photosynthetic apparatus from photooxidative damage [74]. In vitro and in vivo studies have recognized the therapeutic applications of carotenoids in anti-cancer, anti-diabetes, and anti-inflammatory treatments [74, 75]. Consequently, carotenoids, priced between 300 and 10,000 USD/kg, are highly valuable ingredients in drugs, nutraceuticals, and functional foods, contributing to a projected global market value of USD 1.85 billion by the end of 2026 [76]. Some microalgal species contain outstandingly high carotenoid contents. For instance, *D. salina* can accumulate up to 14% of its dry weight as β-carotene, while *H. pluvialis* containing can contain 7% of its dry weight as astaxanthin, making them the best natural sources of these carotenoids [71]. Moreover, PUFA/omega-3 fatty acids including eicosapentaenoic acid (EPA) and docosahexaenoic acid (DHA) are essential nutrients for human health. PUFAs play important roles in neurological and cardiac function and are commonly used as nutritional supplements to lower risk of cardiovascular diseases, nervous systems disorders, and aid in development of central nervous system [70, 77]. The sale of EPA and DHA at a price range of 100 to 120 USD/kg [78] contributes a global omega-3 market that is projected to reach USD 15.1 billion by the end of 2032. Currently, omega-3 fatty acids are primarily sourced from fish. However, due to overfishing and the depletion of fisheries, marine microalgae such as *Schizochytrium* sp., *C. cohnii, P. tricornutum, Nannochloropsis* sp. have emerged as alternative sources of PUFAs [79].

Since 1970s, the research on microalgae has been motivated by the pressing need for alternative energy source to substitute fossil fuels. Bioenergy derived from microalgae and genetically modified (GM) microalgae are termed as the third-generation and fourth-generation biofuel, respectively [77]. Microalgal biomass can serve as a feedstock for producing a wide range of bioenergy, including liquid and gaseous fuels [71]. Due to their high lipid content (typically 20 – 50% [77]), microalgae have predominantly attracted attention in research on bioenergy, particularly in the production of biodiesel. Extracted algal lipids can be converted into biodiesel through the process of transesterification, resulting in long-chain alkyl esters. This research area particularly focuses on *Nannochloropsis* sp., *Chaetoceros* sp. and *B. braunii,* which are known for their high lipid yields [71]. In addition, untreated algal biomass or organic residues remaining after oil extraction can be utilized in anaerobic digestion (AD) to produce biomethane (CH_4)/biogas and biohydrogen. The AD is a biochemical conversion process that involves hydrolysis, acidogenesis, acetogenesis, and methanogenesis. It facilitates the decomposition of organic matter derived from microalgae by bacteria and archaea, resulting in the production of biogas, primarily methane (CH_4) [80]. During the acidogenesis step, hydrogen, an intermediate by-product, can be enriched by selectively inhibiting the growth of methanogens responsible for the conversion of H_2 into CH_4 [81]. Alternatively, the carbohydrates present in microalgae can undergo fermentation to yield bioalcohols, including ethanol, butanol, and propanol [77]. For bioethanol production [71], starch-rich species like *Chlorella vulgaris*, *Spirogyra* and *Chlorococcum* are commonly preferred. Moreover, numerous studies have

explored the utilization of microalgal biomass in thermal conversion processes, such as pyrolysis, liquefaction, and gasification, for the production of bio-oil or biogas (syngas) [71, 77, 81]. Nevertheless, the presence of high moisture content hampers the efficiency of thermochemical conversion processes. For instance, gasification can accommodate feedstocks with moisture content as high as 20 – 30%, while pyrolysis requires an acceptable moisture content of approximately 10% [82]. Due to the challenging nature of dewatering algal biomass, microalgae may not be an optimal feedstock for thermochemical conversion. Despite the immense global market potential for bioenergy, projected to reach USD 256.42 billion by 2030 (Table 1.3), none of the current microalgae-based bioenergy forms are financially competitive within today's energy market [83].

The increasing demand for high-quality protein driven by the growing population has placed a significant burden on the production of feed for aquaculture and livestock. As an alternative to conventional crops and fishmeal, the utilization of microalgae as aquatic and animal feed capitalizes on the superior nutrition provided by algal biomass, which is rich in high-quality protein, beneficial pigments, PUFAs, vitamins, and minerals. The incorporation of microalgae in feed provides several benefits to aquaculture and animal farming, including increased weight gain, enhanced immunity and disease resistance, and improved meat quality with higher PUFA content, among others [84]. Moreover, specific microalgae with high carotenoid contents are employed to enhance the coloration of salmon, lobster, and egg yolks, thereby increasing their market value [85]. In aquaculture, the genera *Isochrysis*, *Pavlova*. *Nannochloropsis*, *Arthrospira*, *Chlorella*, *Dunaliella*, *Haematococcus*, and *Schizochytrium* are often employed to breed fish, shellfish as well as larval in hatchery production [86]. Additionally, the use of *A. platensis*, *Chlorella* sp., *Dunaliella* sp., *Nannochloropsis* sp., and *Schizochytrium* sp. as animal feed has been tested in poultry, pigs, cows and sheep [77]. The global animal feed market, currently dominated by traditional feeds, is projected to reach USD 110.29 billion by 2025 [84]. Microalgal biomass can be utilized as whole-cell feed or processed into formulated feed ingredients, such as algal meal, omega-3 and pigment. The higher cost of microalgal alternatives (5 – 15 USD/kg) poses a significant challenge to their viable substitution for traditional feed ingredients, which are commonly priced around 0.5 USD/kg [87]. Therefore, microalgal products, including astaxanthin, fucoxanthin, and DHA powder (priced between 27 and 530 USD/kg), are primarily employed as high-value nutrient additives that are blended into other feed formulations. [85, 87].

Table 1.2. Global markets of emerging microalgae-based bioproducts.

Bioproduct	Feedstocks/ product type	Applications	CAGR	Projected market size (billion USD)
Bioenergy	Agriculture waste, woody biomass, solid waste	Power generation, heat generation, transportation	7.5%	256.42
Biodiesel	Vegetable oil, animal fat	Fuel, power generation	8.1%	79.12
Bioethanol	Starch based, cellulose-based	Transportation, beverages, cosmetics, pharmaceuticals	13.2%	124.5
Bioplastics	Biodegradable, non-biodegradable	Packing, consumer goods, agriculture, textile, building & construction	17.8%	63.55
Biofertilizer	Nitrogen fixing, phosphate solubilizing	Seed treatment, soil treatment	12.3%	6.83
Biostimulants	Humic substances, seaweed extracts, microbial amendments, amino acids	Seed treatment, soil treatment	11.4%	10.25

CAGR: compound annual growth rate. Data source: https://www.precedenceresearch.com/.

Furthermore, microalgae have emerged as promising applications in the production of bioplastics and agriculture-related products such as biofertilizers and biostimulants [73]. Due to the resistance of petroleum-based plastics to degradation by various chemicals and microbes, plastic debris that leaks into the environment can persist and potentially enter the food chain, posing a threat to ecosystems and human health [88]. Bioplastics, as a substitute for conventional plastics, are experiencing rapid market growth, projected to increase from USD 12.42 billion in 2022 to USD 63.55 billion by 2032. Bioplastics encompass bio-based plastics derived from renewable biomass sources or biodegradable materials that can undergo complete degradation [89]. Additionally, certain biodegradable plastics derived from fossil fuels are also classified as bioplastics [90]. While biomass meets sustainability requirements, only degradable polymers can be considered environmentally friendly [91]. The market offers a range of commercially available fossil-based and bio-based polymers for bioplastic manufacturing, with prices ranging from 0.7 to 8 USD/kg [90]. The most commonly used biodegradable bioplastics, produced from bacteria and food crops like

sugarcane, corn, and potatoes, include polylactic acid (PLA), polyhydroxyalkanoates (PHA), polybutylene succinate (PBS), and starch blends [88]. Microalgae, emerging as a feedstock for bioplastics production, offer advantages such as minimal competition with human food consumption and low nutrient requirements for cultivation [88]. The utilization of microalgae as biofertilizers and biostimulants aims to mitigate environmental damage resulting from excessive application of chemical fertilizers, which can lead to imbalanced nitrogen (N), phosphorus (P), and potassium (K) ratios, soil hardening, salinization, and groundwater pollution [92]. Microalgae, when used as biofertilizers, contribute to soil fertility by depositing nutritious biomass that enriches the soil with organic carbon and nutrients. In contrast, biostimulant products exploit bioactive compounds of microalgae such as protein, amino acids, plant hormones and antimicrobial substances to stimulate plant growth. Specifically, microalgal phytohormones such as cytokinins, gibberellins, auxins, salicylic acid, and abscisic acid are key regulators of plant growth and development [93]. *Chlorella* and *Spirulina*, which are rich in polysaccharides, are the most extensively studied species for bioplastic production [91]. Moreover, these microalgae, which provide valuable organic carbon, nitrogen, and phosphorus compounds, are considered promising candidates to offer agricultural benefits [93, 94].

1.3.2 Bioremediation

Nutrients and CO_2 are necessary inputs for algae cultivation and can account for a considerable portion of operation cost. Integration of microalgae production with other industrial facilities such as power plants and wastewater treatment plants, has been suggested as a means to achieve simultaneous bioremediation and generation of marketable biomass. This integrated approach offers dual benefits in terms of environmental and economical advantages [95]. However, these integrated schemes face challenges due to the adverse effects of waste gases or water on the growth of microalgae.

Wastewaters commonly contain eutrophicating organic/inorganic carbon as well as nitrogen and phosphorus components, which can serve as an alternative source of macronutrients to lower the expenses for nutrients in microalgae cultivation [96]. Microalgae-based wastewater treatment provides advantages over conventional methods, including nutrient recovery, production of valuable biomass, low energy consumption, and negative carbon emissions [97, 98]. Microalgae species not only demonstrate high efficiencies in removing inorganic nitrogen and phosphorus, with reported removal rates ranging from 80% to 100% in various studies, but they also have the potential for eliminating specific hazards, such as pesticides and heavy metals, from diverse industrial and agricultural sectors [99]. The primary challenges in microalgae-based wastewater treatment relate to creating favorable conditions (abiotic/biotic) for microalgae growth. This necessitates the selection of appropriate microalgal species and process design that align with the specific characteristics of the wastewater [100]. Wastewaters from different sources such as municipality, industry and agriculture can contain various and complex compositions of pollutants that can pose hazards to microalgae [101]. Furthermore, the dark color of wastewater limits the penetration of light into the medium, hindering efficient photosynthesis. Additionally, the treatment of large volumes of water in wastewater treatment presents economic challenges related to biomass harvesting and dewatering processes [96].

Due to the low atmospheric CO_2 concentration (0.04%), the provision of additional CO_2 is crucial to facilitate the rapid growth of microalgae in large-scale cultures. Therefore, utilizing industrial exhaust gas as a cost-effective substrate becomes imperative to reduce the operational expenses in microalgae production. Depending on fuel types, flue gas from combustion processes could contain complex constituents, including CO_2, NO_x, SO_x, CO, C_xH_x, particular matter (PM), heavy metals, etc.[102]. These compounds could provide carbon, nitrogen, and sulfur for biomass production [103], but their application raises concerns about potential negative impacts on algal growth due to high CO_2 concentrations, the presence of inhibitory compounds, and exposure to sudden high temperatures [104]. Flue gas emitted from fueled boiler typically contains 10-20% CO_2 and small amounts of nitrogen oxides (NO_x) and sulfur oxide (SO_x) [105], which can impair algal growth probably due to the dramatical reduction of pH at presence of acidic gases [106-108]. In this case, selection or development of microalgal strains that tolerate these adverse effects becomes crucial for biomass production with exhaust gas [109]. According to the literature, *Chlorella* sp. and *Scenedesmus* sp. have shown the most robust growth in cultivation using flue gas [104, 110]. In the context of the current project, a positive growth of *P. tricornutum* was reported in semi-continuous cultivation aerated with 15% CO_2 at a pH 6.3 for the initial two cycles [106].

In recent decades, research on the exploitation of flue gases in microalgae production focused on optimizing cultivation conditions [109, 111-114] and isolation/breeding of tolerant algal strains [115-118]. Effective operating strategies such as pH control [119], increasing cell inoculum concentration [109], and adjusting flue gas concentration [111, 120], gas flow rate [121], and supply of nutrients [122] have effectively improved algal growths under the stressful conditions with flue gas inputs. Moreover, microalgal strains that have potentially adapted to acidic conditions can be isolated from water samples collected near power plants. Previous studies often reported the frequent isolation of *Chlorella* strains that exhibit resistance to high concentrations of CO_2 from regions near power plants [115, 118, 123]. Additionally, efforts were also made to mutate and select high-CO_2 tolerant strains of green microalgae, including *Chlorella* sp. [124-126] and *H. pluvialis* [127]. Due to the inevitable drop in pH resulting from the introduction of flue gas, it has been unclear whether the inhibition of microalgae is caused by the toxicity of flue gas components or the induced low pH. A study by Aslam et al. (2017) demonstrated that the negative impact of flue gases on microalgal growth can be mitigated by adjusting the pH to a neutral level. Accordingly, it can be hypothesized that high levels of CO_2 inhibit microalgal growth through the detrimental effects of low pH on photosynthesis.

1.3.3 Challenges

Pioneer research on microalgae started in Germany during World War II to cope with the petroleum shortage. In the post-war period, research focus shifted towards utilizing microalgae as a protein source to meet the needs of a rapidly growing population. Extensive investigation on microalgae for commercial applications gained momentum during the oil crisis in 1970s. In 1987, the United States initiated the "Aquatic Species Program (ASP)" to explore the production of biofuels from microalgae [70, 128]. Despite enduring interest in microalgae-derived biofuels over years, the high production costs associated with microalgae production make it economically unfeasible for marketing low-value products. Firstly, microalgae cultivation necessitates significant capital investments in cultivation systems, such as open ponds or closed photobioreactors (PBRs). Even the relatively less

expensive open raceway ponds entail higher costs compared to investments in conventional arable land. Secondly, harvesting microalgal biomass from diluted suspensions necessitates costly industrial centrifuges, and the subsequent processes of concentration, dewatering, and product extraction are also energy-intensive. Furthermore, microalgae cultivation, similar to terrestrial farming, is susceptible to pest contamination, which can destroy microalgal cultures within days and cannot be entirely prevented, even in closed photobioreactors (PBRs). As a result, microalgal bioproducts are not cost-competitive in the low-value, high-volume markets that are presently dominated by conventional products derived from agriculture and petroleum-based industries [70]. Process optimization with incorporations of wastewater and flue gas treatment and genetic engineering for high productivity are current research focuses to improve economics of microalgae production. However, these approaches face not only the aforementioned technical challenges but also societal challenges. For applications as food and feed, GM microalgae and products derived from waste streams may pose risks to human health, requiring thorough safety assessments and compliance with complex legislation and regulations. [68].

1.4 Strain improvement strategies

Biomass productivity and product yields from microalgae must be enhanced to reduce the costs associated with producing unit products. In the pursuit of strain improvement, three fundamental approaches are employed: random mutagenesis, adaptive laboratory evolution (ALE), and genetic engineering. Random mutagenesis and ALE rely on artificial selection of induced or spontaneous mutations, whereas genetic engineering entails targeted manipulations of known genes, such as overexpression, silencing, and knockout. One advantage of random mutagenesis and ALE is their simplicity, as they necessitate limited knowledge of the biosynthesis pathways for the desired product and involve minimal technical operations. Furthermore, the resulting mutants are exempt from regulations governing genetically modified organisms (GMOs). However, these approaches face uncertainties stemming from the random occurrence of mutations, necessitating arduous screening processes and presenting challenges in establishing genotype-phenotype associations.

1.4.1 Random mutagenesis

Random mutagenesis has been extensively applied to various microalgae, including *Chlorella sp. Nannochloropsis* sp. and *H. pluvialis* for higher lipids or pigments production, demonstrating the effectiveness of this approach for strain improvement (Table 1.4). In this approach, mutations can be created by various methods, therein ultraviolet (UV) irradiation and chemical carcinogens such as EMS, MNNG, and NTG are the most commonly used mutagenesis methods [129], while ion-irradiation [130, 131], atmospheric and room-temperature plasma (ARTP) [132, 133], and insertional cassette (IC) [134] were also reported in a few studies. After mutagenesis, mutants with desired phenotypes need to undergo screening. The screening is the most critical step and a major bottleneck for the mutagenesis approach. Current screening techniques select candidate mutants largely based on cell survival, observable appearance, such as coloration or fluorescence of stainable substances [135].

Traditional mutagenesis-selection procedure is based on plate selection. In brief, survived cells after mutagenesis are spread onto solid medium to isolate genetically homogeneous colonies, which are then picked and amplified in liquid cultures. Then, phenotypes still need to be determined through labor-intensive growth experiments before superior mutants can be selected. The amount of work can be reduced through a primary screening with selective media and microtiter plate to narrow down the scope of mutant candidates. Early studies on breeding carotenoids overproducers were conducted by screening mutants that could resist inhibitors of carotenogenic pathway, such as diphenylamine (DPA), nicotine, norflurazon, glufosinate, and compactin [136-141]. These studies are based the hypothesis that herbicide-resistant mutants possess mutated enzymes with altered quality or quantity which enable synthesis of desired pigments at the presence of inhibitors [142]. With the aid of selective media, fewer survived cells that exhibit obvious colored characteristics could be selected [136]. Recently, the plate technique is still employed to isolate fast growing algal mutants by observing colony size [143-145] or colony color (for chlorophyll-deficient mutants with higher photosynthetic efficiency) [146]. Two recent works selected lipid hyperaccumulators of *Chlorella* sp. based on iodine staining for lower starch content [147, 148].

With application of high-throughput techniques, clones on plates can be picked and inoculated into small volumes of liquid media in a microtiter plate. The small culture in each well of the microplate can be characterized by a microplate reader that measures autofluorescence and/or fluorescent dyes. Microplate assays based on spectrofluorometry offer advantages over flask cultivation due to reduced requirements of laboratory resources, space and time [149]. Alternatively, flow cytometry (FCM) is a more powerful technology that allows high-throughput characterization of individual cells and simultaneous isolation of subpopulation according to features of interest [150]. Like the microplate assays, FCM relies on rapid measurement of fluorescence of cells from pigments or dyes. Autofluorescence (emission wavelength >600 nm), representing the signal of chlorophyll, is usually measured as a proxy of cell growth [151]. A novel application of FCM coupled with staining using fluorescent dyes is known as fluorescence-activated cell sorting (FACS). The use of lipophilic fluorescent dyes, e.g. Nile Red and BODIPY as a detectable proxy of lipid to indicate cells with high lipid contents has provoked a wave of interest on developing lipid hyperaccumulators of microalgae using FACS in the 2010s [152].

Table 1.3. Summary of random mutagenesis applied to strain improvement in microalgae.

Strain	Screening	Selection criteria	Improvement	Ref
Biomass				
Chlorella pyrenoidosa	Plate	Coloration	1.34-fold higher biomass	[146]
Chlorella minutissima	Plate	Size	60% higher biomass, 42% higher lipid content	[143]
Chlorella sp.	Plate	Size, coloration	7.6% higher biomass, increased lipid productivity	[145]
Scenedesmus sp.	Plate	Size	26.3% higher biomass, 37.5% higher lipid content	[144]
Botryococcus braunii	Plate	Size	187.99% higher biomass, 59.95% higher hydrocarbon content	[153]
Lipid				
Chlorella sp. HS2	FACS	BODIPY staining	61.9% increase in lipid content	[154]
Chlorella vulgaris	Plate	Iodine staining	58% increase in lipid, 43% increase in TAGs	[147]
Chlorella vulgaris	Plate	Iodine staining	1.47-fold higher cell concentration, 1.3-fold increase in lipid content	[148]
Chlorella vulgaris	FACS, microplate reader	Nile red staining	12% increase in biomass productivity, 72% increase in fatty acid productivity	[155]
Chlorella sp.	Microplate reader	Nile red staining	2-fold increase in biomass productivity, > 1.2-fold increase in lipid content	[156]
Chlorella vulgaris	Plate	Nile red staining	35% higher biomass, 67% higher lipid content	[157]
Chlorella sp.	Plate	Quizalofop resistance	59% higher lipid content, 53% higher lipid productivity	[158]
Chlorella pyrenoidosa	Plate	Nile red staining	22.07% higher biomass, 16.85% higher lipid productivity	[133]

Strain	Screening	Selection criteria	Improvement	Ref
Chlorella sp. KAS603	FACS	BODIPY staining	1.8 to 2.5-fold increase in TAG accumulation	[159]
Chlorella sorokiniana	Microplate reader	Nile red staining	> 30% increase in lipid content	[160]
Scenedesmus obliquus			33% increase in biomass productivity	
Desmodesmus armatus	FACS, microplate reader	Nile red staining	31% increase in biomass productivity, 30% increase in fatty acid productivity	[155]
Desmodesmus sp.	Microplate reader	Nile red staining	20.67 – 45.50% higher biomass, 8.00 – 10.35% higher lipid content	[161]
Nannochloropsis oceanica	FACS	BODIPY staining	40% increase in neutral lipid content	[134]
Nannochloropsis oceanica	Microplate reader	BODIPY staining	21.44 – 33.54% increase in lipid productivity	[162]
Nannochloropsis salina	FACS, microplate reader	BODIPY staining	76% increase in lipid productivity	[163]
Nannochloropsis sp.	FACS, microplate reader	Nile red staining	1.5 to 2-fold higher total lipid content	[164]
Nannochloropsis oculata	Plate	Cerulenin/erythromycin resistance	29% and 12% increase in EPA content	[165]
Chlamydomonas sp. KOR1	FACS	BODIPY staining	1.5 to 2.1-fold higher lipid content	[130]
Chlamydomonas reinhardtii	Plate, FACS	BODIPY staining	25% increase in lipid productivity	[166]
Parachlorella kessleri	Plate	NA	75% higher biomass productivity, 44% higher lipid productivity	[132]
Euglena gracilis	FACS	BODIPY staining	40% increase in lipid content	[131]

Strain	Screening	Selection criteria	Improvement	Ref
Chlorococcum littorale	FACS	BODIPY staining	1.9-fold higher TAG productivity	[167]
Isochrysis affinis galbana	FACS	Nile red staining	80% increase in lipid productivity	[168]
Tetraselmis suecica	FACS, microplate reader	Nile red staining	114 - 123% increase in neutral lipid content	[169]
Shizochytrium sp	Plate	Iodoacetate acid, malonic acid resistance	34.84% higher lipid content, 38.88% higher DHA content	[170]
Pavlova lutheri	Plate	NA	32.8% higher EPA content, 32.9% higher DHA content	[171]
Phaeodactylum tricornutum	Plate	NA	37 – 44% increase in EPA content	[172]
Pigment				
Chlorella vulgaris	Plate, fluorescence imaging	Fluorescence	3.18-fold increase in violaxanthin production	[173]
Chlorella sorokiniana	Plate	Nicotine, norflurazon resistance	2-fold higher lutein content	[140]
Chlorella regularis S-88	Plate	Coloration	1.5 to 1.8-fold higher carotenoids content	[174]
Haematococcus pluvialis	Plate	DPA resistance	1.7-fold higher astaxanthin content	[136]
Haematococcus pluvialis	Plate	DPA resistance	30% increase in astaxanthin content	[137]
Haematococcus pluvialis	Plate	Glufosinate resistance	23 – 59% increase in astaxanthin content	[141]
Haematococcus pluvialis	Plate	Nicotine, DPA, fluridone, norflurazon resistance	58.3 – 100.1% increase in astaxanthin content	[138]

Strain	Screening	Selection criteria	Improvement	Ref
Haematococcus pluvialis	Plate	Nicotine, DPA, compactin resistance	2.2 to 3.2-fold higher astaxanthin content	[139]
Dunaliella Tertiolecta	Plate	Coloration	10 – 15% higher zeaxanthin content	[175]
Coelastrum sp.	Plate	Glufosinate resistance	2-fold higher total carotenoid and astxanthin accumulation	[176]
Chlorococcum sp.	Plate	Azide resistance	2-fold higher total carotenoid and astxanthin accumulation	[177]
Stress tolerance				
Scenedesmus obliquus	Microplate reader	Low pH	Tolerance to 15% CO_2	[178]
Chlorella pyrenoidosa	Microplate reader	High temperature	Thermotolerance (47 ℃), > 50% increase in lipid content	[179]
Chlorella vulgaris	Microplate reader	Low pH	Tolerance to 15% CO_2	[124]
Chlorella saccharophila	Plate	Low pH	Tolerance to pH 6, > 27% increase in TAG	[180]

Although random mutagenesis remains a popular method for strain improvement due to its simplicity, its effectiveness is constrained by the screening strategy and capacity. Due to the random occurrence of mutations in genomes, unanticipated results can arise, leading to the coexistence of beneficial, neutral, and deleterious mutations in mutants. Since screening is typically based on a single characteristic, mutants selected in this manner are prone to displaying uneven performances [141]. For example, many studies were designed to screen for hyperaccumulators of lipids or pigments. However, these traits were often accompanied by impaired growth due to secondary mutations [141, 162, 163, 177]. Additionally, a diluted aliquot of the mutagenized culture needs to be plated onto solid medium to isolate single colonies. Only a limited number of mutants (up to 96 for microtiter plates) can be further analyzed and selected. Additionally, clones on the plates are typically selected arbitrarily based on visual attributes such as size and color [136, 141, 162, 174], which may not accurately reflect their actual production capabilities. Consequently, the opportunity to obtain mutants with desired traits can be limited. While flow cytometry (FCM) can offer comprehensive analysis of the entire mutagenized population for selection, these costly instruments may not be universally accessible to all researchers. Moreover, since only lipid-targeting dyes are developed for rapid examination of lipid, current application of FACS is largely limited to screening microalgal hyperaccumulators of lipid. With the exception of lipids, there have been few attempts to develop high-throughput methods for selecting strains that overproduce pigments. In a study by Nonomura and Coder (1988), a strain of *D. salina* with doubled β-carotene productivity was isolated by screening autofluorescence greater than 600 nm. Similarly, Mendoza et al. (2008) attempted to select *D. salina* strains that overproduce carotenoids using FACS, relying on an established correlation between carotenoid content and Nile Red fluorescence [181, 182].

1.4.2 Adaptive laboratory evolution

Adaptive laboratory evolution (ALE) is a biotechnological tool used to develop desirable traits of industrial microorganisms, enhancing their robustness against unfavorable conditions such as unusual carbon sources, adverse environments, and chemical inhibitors [183]. In most environments, microbial populations consist of genetic variants that carry spontaneously occurring beneficial, neutral, and deleterious mutations. ALE mimicking natural evolution involves prolonged iterative cultivation under artificially specified pressure. The defined selective pressure drives accumulation of beneficial mutations in the population, preserves mutants with improved fitness in the given environment and thus directs the microbial population to evolve desirable phenotypes over time [184].

Batch cultivation in parallel serial cultures and continuous (chemostat) cultures in bioreactor vessels are the two alternative methods of ALE. In batch cultivation, microorganisms undergo successive propagation in shake flasks, with a portion of culture being periodically transferred to fresh medium at regular intervals. This method offers advantages due to its inexpensive and easy setup, but it has shortcomings such as batch variations in nutrient supply, environmental conditions, population density, and growth rate. In contrast, chemostat cultivation provides tight control over nutrient supply and environmental conditions, thus avoiding fluctuating growth rates and population densities. However, it has a much higher operating cost compared to serial batch cultures [185]. The stress factor that drives evolution is a key element of ALE processes. In practice, the types of stress vary based on the purpose of the experiment or the desired features of the microorganism. Meanwhile, the levels of the designed stress need to be suitable for selection,

that is, they should repress the growth of undesired variants while avoiding the death of the entire population. When the microbial population approaches to adaptation to the designed stress (i.e. mutants with high fitness predominate the population), further improvement in the growth rate can barely be observed. ALE can proceed by modifying or intensifying the stress [186].

In biotechnological applications, ALE can be used to domesticate microorganisms in three main aspects: (i) enhancing tolerance to toxic substances, (ii) improving the utilization of specific substrates, and (iii) optimizing phenotype (Table 1.5) [187]. The ALE approach has long been employed for strain improvement in *Escherichia coli* and *Saccharomyces cerevisiae*, while its application with non-conventional hosts, e.g., microalgae is emerging in the recent decade [188-191]. ALE, by promoting the dominance of advantageous variants over generations, enables the systematic optimization of the fitness landscape without compromising the beneficial traits of microorganisms [192]. Unlike genetic engineering, ALE does not require prior genetic knowledge of the studied organism, providing an advantage over genetic manipulation in microalgae. Additionally, ALE allows for the study of evolutionary processes and identification of beneficial mutations associated with specific selective pressures. In recent years, omics technologies including genomics, transcriptomics and metabolomics, have been increasingly utilized in ALE studies on microalgae to uncover adaptive responses and mutations responsible for tolerance to environmental stresses such as high temperature, salinity and high CO_2 (Table 1.5). For instance, long-term adaptation under the stress of flue gas components, i.e. CO_2, NO_x and SO_x, has highlighted the importance of photosynthesis in maintaining the growth of *Chlorella* sp. [193] and *Nannochloropsis oceanica* [194]. The omics data not only elucidate deeper understanding on the evolutionary mechanisms, but also guide reverse engineering to construct strains carrying only beneficial mutations [192].

Table 1.4. Summary of ALE studies for strain improvement in microalgae.

Organism	Stress	Evolution cycle		Duration	Omics study	Phenotypes of adapted culture	Ref
		Setting	Cycles	(day)			
Phaeodactylum tricornutum	Food waste hydrolysate	8-day	30	240		Higher biomass accumulation, lipid and PUFA content	[194]
Phaeodactylum tricornutum	Light	5-day	11	55		> 2-fold higher biomass productivity and fucoxanthin content	[195]
Nannochloropsis oceanica	High CO_2	8-day	NA	NA	Genomics, transcriptomics	22.7-fold and 3.98-fold higher biomass yield under 6 mL/min and 12 mL/min 15% CO_2	[194]
Nannochloropsis oculata	High temperature	3 to 7-day	24	NA	Metabolomics	1.43-fold higher biomass at 35 ℃	[196]
Chlorella sp. AE10	Simulated flue gas	3-day	46	138	Transcriptomics	Enhanced tolerance to simulated flue gas	[193]
Chlorella sp. AE10	High salinity	3-day	46	138	Transcriptomics	Quadrupled biomass concentration in the ending cycle	[197]
Chlorella sp. L3	Phenol	3-day	31	95	Transcriptomics	> 2-fold biomass concentration under phenol stress	[188]
Chlorella sp.	High CO_2	3-day	31	97		2.94-fold biomass concentration under 30% CO_2	[189]
Chlorella vulgaris	660 nm LED	3-day	38	114		2.5-fold higher biomass concentration	[190]
Schizochytrium sp.	High temperature	1-day	70	NA		60.55% higher growth rate at 34 ℃	[198]

Organism	Stress	Evolution cycle		Duration	Omics study	Phenotypes of adapted culture	Ref
		Setting	Cycles	(day)			
Schizochytrium sp.	High salinity	1-day	NA	150	Transcriptomics	32.7% increase in biomass concentration, 53.31% increase in lipid yield	[199]
Schizochytrium sp.	Agitation (high oxygen)	1-day	40	NA		32.4% increase in biomass concentration	[200]
Chlamydomonas reinhardtii	Cadmium	3-day	140	420	Genomics, Transcriptomics	Enhanced tolerance to 0.5 μM cadmium	[201]
Chlamydomonas reinhardtii	NA	3-day	28	84		1.17 to 1.48-fold increase in biomass concentration	[202]
Nitzschia inconspicua	High temperature	1-day	NA	300		Upper thermal boundary increased by 2 ℃ to 37.5 ℃	[203]
Picochlorum sp.	High temperature	Turbidostat	NA	390	Genomics	Expanded maximal growth temperature of 49 ℃	[204]
Crypthecodinium cohnii	Glucose	NA	260	650	Metabolomics	Enhanced glucose tolerance	[205]
Dunaliella salina	Light	5-day	16	80		1.8-fold higher biomass concentration	[191]
Parachlorella sp.	High salinity	4-day	8	32		Recovered growth under salinity stress	[206]
Synechocystis sp. PCC6803	High salinity	7-day	43	303	Metabolomics, transcriptomics	Higher growth rate and biomass density in media with 3% NaCl	[207]

Organism	Stress	Evolution cycle		Duration	Omics study	Phenotypes of adapted culture	Ref
		Setting	Cycles	(day)			
Synechocystis sp. PCC6803	Cadmium	NA	128	802	Genomics	Enhanced tolerance to 9.0 μM cadmium	[208]
Synechocystis sp. PCC6803	Butanol	NA	94	395	Metabolomics	150% increase in butanol tolerance	[209]
Synechocystis sp. PCC 6803	Toxic amino acids	3 to 4-day	21	75	Genomics, Transcriptomics	Enhanced amino acid tolerance	[210]

1.4.3 Genetic engineering

The development of molecular biology tools for engineering diatoms began approximately three decades ago in 1990s. However, genetical modifications in *P. tricornutum*, a model diatom species had remained largely static until the publication of its full genome sequence [211]. Since then, there has been a growing number of fundamental and applied research on *P. tricornutum*. Here, state of the art available molecular biology tools and recent advances in genetic modifications of *P. tricornutum* are reviewed with particular focus on rational design in the diatom for biotechnological applications.

Molecular tools for engineering *P. tricornutum*

The first attempt to transform *P. tricornutum* was conducted by Apt, et al. [212] who successfully expressed the zeocin resistance gene (S*h ble*) and chloramphenicol resistance gene (*Cat*) under regulation of fucoxanthin binding protein (*Fcp*) promoters. Subsequently, a standard transformation vector (pPhaT1) (Figure 1.3) was designed, containing an expression cassette controlled by the *FcpA* promoter. The pPhaT1 vector and its variants have been the most widely used vectors for genetic modifications in *P. tricornutum*. Other vectors have been customized with different promoters and selective markers for specific applications such as inducible expression (pPhaNR), plastid expression (pPtc) and dual expression (pPhOS2) (Table 1.6).

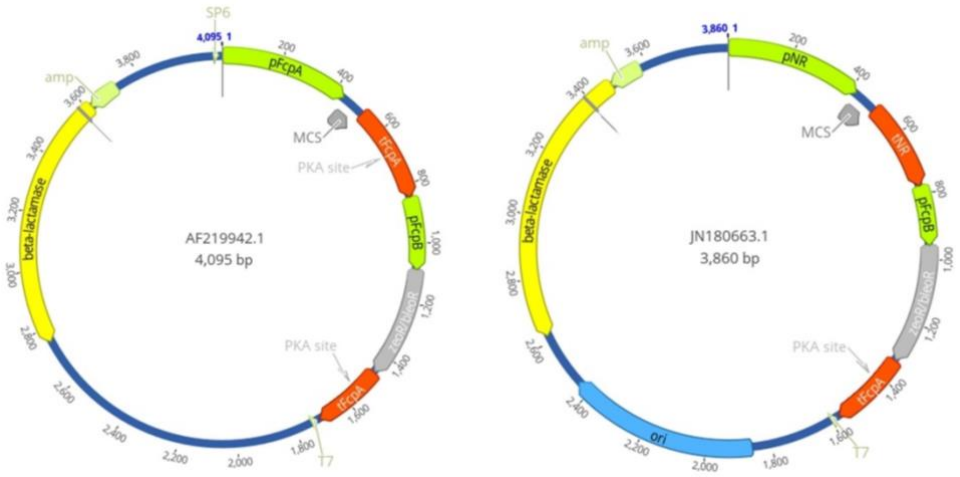

Figure 1.3. *Map of pPhaT1 and pPhaNR vectors designed for gene expression in P. tricornutum.*

Table 1.5. Reported vector designs for genetic engineering P. tricornutum.

Vector	Backbone plasmid	Promoter	Selective marker	Ref
pPhaT1	pSP73	*FcpA*	*Sh ble*	[212]
pPhaNR	NA	*NR*	*Sh ble*	[213]
pHY11/18/21	NA	*FcpC*	*Cat*	[214]
pPtc	pMD19	*rbcL*	*Cat, Myc*	[215]
pPhOS2	pPhaT1 variant	*FcpA*	*Sh ble*	[216]
pPhaT-EF2	pBluescript KS	*EF2*	*Sh ble, Luc*	[217]
pPhaT-BP	pBluescript KS	*FcpB*	*Sh ble, Luc*	[217]

NA, not available.

Promoters containing sequence-motifs that recruit transcription machinery through specific binding are responsible for controlling the rate of transcription. Thus, the choice of promoters is a critical consideration in vector design for genetic engineering. Depending on functional properties (e.g. robustness, response to stimuli), promoters can be generally classified into constitutive promoters that continuously enable gene transcription and inducible promoters that express the gene in response to external stimuli [218]. To date, the *Fcp* class and the nitrate reductase (*NR*) are the most commonly employed for transgene expression. *Fcp* promoters typically drive strong and stable gene expression, and their activity is regulated by light and possibly circadian rhythms as well [219-222]. The *NR* promoter of diatoms, *C. fusiformis*, *T. pseudonana*, and *P. tricornutum* have been characterized responsive to nitrate source, i.e., activated by nitrate and repressed by ammonium [223-225] and it shows stronger expression compared to the *Fcp* promoters [226]. The promoter of the histone H4 gene (*H4*) drives mild and stable expression in various conditions in *P. tricornutum*, rendering it a suitable housekeeping internal reference [221]. Furthermore, the characteristics of additional native or viral promoters are continuously investigated to offer alternative options of promoters for robust and controllable expression (Table 1.7) [227].

Table 1.6. Characterized promoters for transgene expression in P. tricornutum.

Promoter	Source organism	Characteristics	Ref
Fcp	*P. tricornutum* *C. cryptica* *C. fusiformis*	Induced by light, activity depending on circadian rhythms and growth phase	[212]
NR	*P. tricornutum* *C. fusiformis* *T. pseudonana*	Repressed by ammonium, induced by nitrate	[223]
EF2	*P. tricornutum*	Constitutive activity to light variation, stronger than *Fcp* promoters	[141]
H4	*P. tricornutum*	Mild and stable constitutive expression	[221]
RSV-LTR	RSV	Higher average activity than *FcpA* but results significantly varied	[228]
CaMV35s	CaMV		
CIP1	ClorDNAV	Higher average activity than *FcpA* and *NR*, high activity in stationary phase, light-inducible	[229]
PtCA1	*P. tricornutum*	Regulated by CO_2 level, light and circadian rhythm	[230]
PtAP1	*P. tricornutum*	Regulated by phosphorus level, higher expression than *Fcp* and *NR* promoters	[231]
V-ATPase C	*P. tricornutum*	Higher expression than *FcpA*, constitutive expression under light and dark conditions	[232]
HASP1	*P. tricornutum*	Higher expression than *FcpA*, expression during all growth phases, protein secretion	[233]
GS, GapC1	*P. tricornutum*	Higher expression than *FcpA*, expression during all growth phases	[234]

Abbreviation: *Fcp*, fucoxanthin binding protein; *NR*, nitrate reductase; *EF2*, elongation factor 2; *H4*, histone 4; *RSV-LTR*, Rous carcoma virus long terminal repeat; *CA1*, carbonic anhydrase; *AP1*, alkaline phosphatase; *HASP1*, highly

abundant secreted protein; *GS*, glutamine synthetase; *GapC1*, glyceraldehyde-3-phosphate dehydrogenase; ClorDNAV, *Chaetoceros lorenzianus*-infecting DNA virus; CaMV, *Cauliflower mosaic virus*; RSV, *Rous sarcoma virus*.

In pioneer studies on diatom transformation, *P. tricornutum* was found insensitive to commonly used antibiotics. Zeocin is one of the few antibiotics that can inhibit growth of the wild type *P. tricornutum* at low concentration (50 ug/ml) [212, 220]. Thus, the zeocin resistance gene, *Sh ble*, has become the most widely used selectable marker in vector constructs for primary selection. Additionally, alternative selectable markers such as *Nat* (nourseothricin resistance), *Sat* (streptothricin resistance), *NptII* (G418 resistance) can be used for antibiotic selection [235]. Furthermore, reporter genes including luciferase (*Luc*), β-glucuonidase (*uidA*), enhanced green fluorescent protein (*EGFP*), enhanced cyan fluorescent protein (*ECFP*), enhanced yellow fluorescent protein (*EYFP*) and epitope haemagglutinin (*HA*) has been successfully established in *P. tricornutum* [220, 221, 235].

Microprojectile bombardment (biolistics) is used in most genetic engineering studies to introduce foreign DNA into *P. tricornutum* cells. However, this technique has limitations due to laborious sample preparation procedures, costly consumables, and limited transformation efficiency [236]. Generally, transformation efficiency through biolistics techniques varies between 10 and 650 transformants per 10^8 cells [212, 220, 228, 230, 235, 237]. Alternatively, electroporation, which allows for rapid transformation, has been successfully applied to *P. tricornutum*, demonstrating higher efficiency (1000 – 4500 transformants per 10^8 cells) [236, 238]. Due to the costly equipment required for biolistics and electroporation, a cost-effective bacterial-mediated conjugation method has been developed for diatoms [239]. Bacterial conjugation delivers DNA in the form of an artificial chromosome or episome that exist as an additional chromosome in the diatom cell. Therefore, the transgene does not integrate into the genome, which is advantageous for reproducible transgene expression between cell lines. However, this method is limited due to difficulty in cloning large episomal plasmid (> 15 kb) and possible loss of episomal genetic elements [227].

Metabolic engineering in *P. tricornutum*

Over the past two decades, molecular tools for *P. tricornutum* have been well-established, allowing for the rational engineering of cell genotypes to acquire desired traits. Nowadays, reverse genetics can be easily performed for gene function studies and biotechnological applications, aided by genomic information [211]. Genetic modifications are generally achieved by overexpression and/or downregulation of the target genes [240]. Essentially, the overexpression strategy involves driving the expression of the target gene using robust constitutive promoters, bypassing the control of its native promoter. Downregulation is accomplished through RNA interference (RNAi), where designed antisense RNA binds to complementary target mRNA, leading to mRNA degradation and reducing the expression of the targeted gene [241]. Lipids and carotenoids, especially fucoxanthin are the primary desired metabolites in *P. tricornutum*. Since the development of genetic manipulation techniques for this model species diatom, metabolic networks in *P. tricornutum* have been extensively engineered to achieve transgenics that overproduce fucoxanthin as well as lipids including TAG and PUFA (Table 1.8). To date, most metabolic

engineering studies have followed two strategies to achieve high yields of these metabolites. Firstly, carbon fluxes can be directed towards the target products by overexpressing enzymes involved in the biosynthetic pathways. Secondly, the yield or accumulation of the target product can be enhanced by suppressing competing pathways and product catabolism [242].

Diatom lipids consist of storage components, such as triacylglycerols (TAG), and a structural fraction represented by polyunsaturated fatty acids (PUFA). Briefly, fatty acids are synthesized in the plastid through the de novo fatty acid biosynthesis pathway, which begins with the ATP-dependent carboxylation of acetyl-CoA to malonyl-CoA [243]. Fatty acids are synthesized through the sequential condensation of two-carbon building blocks of malonyl-ACP, leading to the elongation of the fatty acid chain and the consumption of NADPH as the reducing power. In the cytosolic phase of the endoplasmic reticulum (ER) membrane, fatty acid molecules are attached to glycerol to form a wide range of glycerolipids [244, 245]. A number of pathways involved in this process have been engineered to increase the carbon flux channeled to lipids (Figure 1.4). In a recent study, a plastidial pyruvate transporter was overexpressed, presumably enhancing influx of pyruvate into plastids and, consequently, the supply of acetyl-CoA for fatty acid synthesis. This led to an increase in lipid content by 11 – 30% in transgenic *P. tricornutum* [246]. Within the mitochondria, the production of acetyl-CoA from pyruvate is catalyzed by the pyruvate dehydrogenase complex (PDC), which can be deactivated through reversible phosphorylation by pyruvate dehydrogenase kinase (PDK). Silencing the PDK to increase the mitochondrial pool of acetyl-CoA resulted in approximately 82% enhanced lipid accumulation [247]. Overexpressing acetyl-CoA carboxylase, which catalyzes the conversion of acetyl-CoA to malonyl-CoA, resulted in a 1.77-fold increase in lipid accumulation [248]. Alternatively, several studies have focused on increasing NADPH levels by overexpressing the malic enzyme (ME) in the tricarboxylic acid (TCA) cycle [249-251] and glucose-6-phosphate dehydrogenase (G6PDH) in the pentose phosphate pathway (PPP) [252, 253]. These strategies have resulted in up to a 2.7-fold increase in lipid content. In a recent study, a modification of a 3-oxoacyl acyl carrier protein reductase (FabG) was carried out to increase fatty acid biosynthesis [87]. Additionally, glycerol synthesis could be significantly enhanced by overexpressing glycerol-3-phosphate dehydrogenase (GPDH) [254]. The TAG biosynthesis pathway comprising sequential steps catalyzed by GPAT, LPAT and DGAT has been extensively studied to enhance TAG accumulation [255-260]. As alternative strategies, lipid content can be enhanced by repressing the degradation pathway of TAG and competing pathways that divert carbon flows from lipid synthesis. For instance, the silencing of UDP-glucose pyrophosphorylase (UGPase) by RNAi resulted in 61.93% decrease in chrysolaminarin content accompanied by a 24.58% increase in lipid content [261]. Similarly, a comparable metabolic shift was observed by repressing the expression of a 1,3-β-glucan synthase gene (*Ptbgs*) [262]. The knockdown of a TAG lipase resulted in a 2-fold relative increase of TAG level in the engineered strain [263]. Additionally, several studied made efforts to modify saturation of fatty acids by overexpressing delta-5 and deta-6 desaturase for PUFA accumulation [216, 264, 265]. In terms of carotenoid biosynthesis, the entire pathway from acetyl-CoA to diadinoxanthin (the precursor of fucoxanthin) have been previously engineered to enhance the fucoxanthin accumulation [229, 266-269] (Figure 1.4). The best result was reported by Manfellotto, et al. [269] who developed triple transformants with overexpressed

violaxanthin de-epoxidase (*Vde*), vde-related (*Vdr*) and zeaxanthin epoxidase 3 (*Zep3*) showing up to 4-fold higher fucoxanthin content.

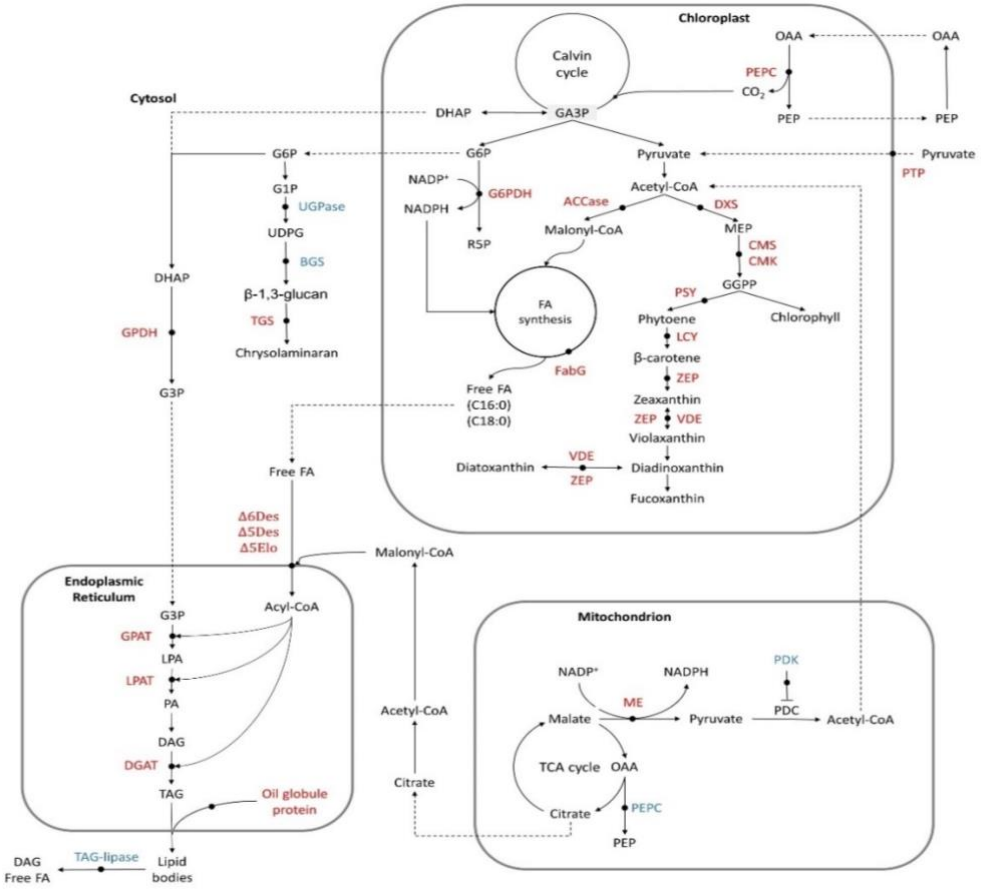

Figure 1.4. *Map of previous metabolic engineering modifications in P. tricornutum. Upregulation and downregulation highlighted in red and blue, respectively. Targets: PEPC, phosphoenolpyruvate carboxykinase; PTP, pyruvate transporter; G6PDH, glucose-6-phosphate dehydrogenase; ACCase, acetyl-coA carboxylase; DXS, 1-deoxy-D-xylulose 5-phosphate synthase pathway; CMS, 2-C-methyl-D-erythritol 4-phosphate cytidylyltransferase; CMK, 4-(cytidine-5-diphospho)-2-C-methyl-D-erythritol kinase; PSY, phytoene synthase; LCY, lycopene cyclase; ZEP, zeaxanthin epoxidase; VDE, violaxanthin deepoxidase; FabG; GPDH, glycerol-3-phosphate dehydrogenase; TGS, 1,6-β-transglycosylase; G3PDH, glycerol-3-phosphate dehydrogenase; UGPase, UDP-glucose pyrophosphorylase; BSG, 1,3-β-glucan synthase; Δ6Des, Δ6-fatty acid desaturase; Δ5Des, Δ5-fatty acid desaturase; Δ5Elo, Delta-5-elongase; GPAT, glycerol-3-phosphate acyltransferase; LPAT, lysophosphatidic acid acyltransferase; DGAT, diacylglycerol acyltransferase; oil globule protein; PDK, pyruvate dehydrogenase kinase; PDC, pyruvate dehydrogenase complex; ME, malic enzyme. Abbreviation: PEP, phosphoenolpyruvate; OAA, oxaloacetate; DHAP, dihydroxyacetone phosphate; GA3P, glyceraldehyde 3-phosphate; G1P, glucose-1-phosphate; G3P, glycerol-3-phosphate; G6P, glucose-6-phosphate; GGPP, geranylgeranyl diphosphate; UDPG, uridine diphosphate glucose; R5P, ribulose-5-phosphate; MEP, 2-C-methyl-D-erytritol 4-phosphate; GGPP, geranylgeranyl diphosphate; FA, fatty acid; LPA, lysophos phatidic acid; PA, phosphatidic acid; DAG, diacylglycerol; TAG, triacylglycerol.*

Table 1.7. Summary of metabolic engineering modifications in P. tricornutum.

Objective	Target protein	Type of modification	Effect of genetic modifications	Ref
Biomass/lipid	Pyruvate transporter (PtPTP)	Overexpression	Enhanced biomass (13.6 – 21.9%), lipid contents (11 – 30%) and growth (3.3 – 8.0%)	[246]
Biomass	Plastocyaninn (Pc)	Heterologous expression	Up to 60% increase in growth under Fe-deficiency	[270]
Biomass	Phosphoenolpyruvate carboxykinase (PtPEPC1)	Overexpression	12% increase in biomass concentration	[271]
Biomass	Enhanced green fluorescent protein (EGFP)	Heterologous expression	50% increase in biomass productivity	[272]
Lipid	Glucose-6-phosphate dehydrogenase (G6PDH)	Overexpression	Higher lipid content and growth	[253]
Lipid	Glucose-6-phosphate dehydrogenase (G6PDH)	Overexpression	2.7-fold increased lipid content	[252]
Lipid	Malic enzyme (ME)	Overexpression	87.02% increase in lipid productivity	[251]
Lipid	Malic enzyme 1 (ME1)	Overexpression	48.42% increase in lipid content	[250]
Lipid	Malic enzyme (ME)	Overexpression	2.5-fold higher in total lipid content	[249]
Lipid	3-Oxoacyl acyl carrier protein reductase (FabG)	Overexpression	1.49-fold higher lipid and 1.31-fold higher fatty acid biosynthesis	[273]
Lipid	Acetyl-CoA carboxylase (PtACC2)	Overexpression	1.77-fold increase in neutral lipid content	[248]
Lipid	Glycerol-3-phosphate acyltransferase 2 (GPAT2)	Overexpression	2.9-fold higher TAG content	[256]

Objective	Target protein	Type of modification	Effect of genetic modifications	Ref
TAG	Glycerol-3-phosphate acyltransferase (GPAT1) Lysophosphatidic acid acyltransferase (LPAT1)	Overexpression	2.3-fold higher TAG content	[255]
Lipid	Diacylglycerol acyltransferase 1 (DGAT1)	Overexpression	2-fold higher TAG and total lipids content	[257]
Lipid	Diacylglycerol acyltransferase 2 (DGAT2B)	Overexpression	Higher lipid yields and DHA content	[258]
Lipid	Diacylglycerol acyltransferase 2 (DGAT2D)	Overexpression	1.6 to 2-fold higher FA and TAG content	[259]
PUFA	Diacylglycerol acyltransferase 2 (DGAT2)	Overexpression	35% increase in neural lipid content	[260]
Lipid	Glycerol-3-phosphate dehydrogenase (GPDH)	Overexpression	6.8-fold higher glycerol content, 60% increase in neutral lipid content	[254]
Lipid	Oil globule protein	Heterologous expression	Slight increase in TAG contents	[274]
TAG	TAG lipase	Silencing	2-fold higher TAG content	[263]
Lipid	Phosphoenolpyruvate carboxykinase (PEPCK)	Silencing	22 – 40% increase in lipid content	[275]
Lipid	UDP-glucose pyrophosphorylase (UGPase)	Silencing	24.58% increase in lipid content	[261]
Lipid	1,3-β-glucan synthase (PtBGS)	Silencing	9 – 39.6% increase in neutral lipid content	[262]
Lipid	Pyruvate dehydrogenase kinase (PtPDK)	Silencing	82% increase in neutral lipid content	[247]

Objective	Target protein	Type of modification	Effect of genetic modifications	Ref
PUFA	Delta-5-desaturase (PtD5b)	Overexpression	58% increase in PUFA content	[264]
DHA	Delta-5-elongase (OtElo5b), Delta-6-desaturase (OtDes6)	Heterologous expression	8-fold higher DHA content	[216]
EPA	Delta-6-desaturase (PtDes6)	Overexpression	16.40 – 18.64% increase in total lipid, 47.66% increase in EPA content	[265]
Chrysolaminaran	1,6-β-transglycosylase (PtTGS1)	Overexpression	>60% increase in chrysolaminarin content	[276]
Fucoxanthin, β-carotene	1-Deoxy-D-xylulose 5-phosphate synthase (TpDXS), lycopene cyclase (TpLCYB)	Overexpression	75% increase in fucoxanthin content, 71% increase in β-carotene content	[267]
Fucoxanthin	1-Deoxy-D-xylulose 5-phosphate synthase (DXS), Phytoene Synthase (PSY)	Overexpression	> 1.8-fold higher fucoxanthin content	[266]
Fucoxanthin	Phytoene Synthase (PSY)	Overexpression	1.45-fold higher fucoxanthin content	[229]
Fucoxanthin	CMS, CMK	Overexpression	1.8-fold higher fucoxanthin content	[268]
Carotenoids	Violaxanthin deepoxidase (VDE), violaxanthin deepoxidase-related protein (VDR), zeaxanthin epoxidase3 (ZEP3)	Overexpression	4-fold higher fucoxanthin content	[269]
Ovothiol	5-Histidylcysteine sulfoxide synthase ovoA (PtOvoA)	Overexpression	2-fold higher ovothiol B content	[277]
Antimicrobial peptides	S-Thanatin, bovin lactoferricin	Heterologous expression	Antimicrobial activity in lysate of transgenic strain	[278]
Therapeutic protein	IgG Hepatitis B antibody	Heterologous expression	IgG accumulate to 8.7% of total soluble protein, 21 mg/g algal dry weight	[279]

Objective	Target protein	Type of modification	Effect of genetic modifications	Ref
Bioplastic	Ketothiolase (PhaA), acetoacetylCoA reductase (PhaB), PHB synthase (PhaC)	Heterologous expression	PHB yield of 2.3% cell dry weight	[280]
Bioplastic	Ketothiolase (PhaA), acetoacetylCoA reductase (PhaB), PHB synthase (PhaC)	Heterologous expression	PHB accumulate up to 10.6% of algal dry weight	[281]
Trophic conversion	Hexose uptake protein (Hup1)	Heterologous expression	Heterotrophic growth, 20% increase in biomass accumulation	[282]
Trophic conversion	Human glucose transporter (GLUT1), Phosphofructokinase (PFK), Glucose-6-phosphate dehydrogenase (G6PD), Phosphogluconolactonase (PGL)	Heterologous expression	4.5-fold higher biomass yield than autotrophy	[283]
Trophic conversion	Glucose transporter (Glut1, Hup1)	Heterologous expression	Heterotrophic growth on exogenous glucose	[284]

1.5 Motivation, research questions and objectives

Geothermal resources, which supply 62% of the energy for electricity generation and direct heat application, play a major role in the Iceland's primary energy supply [285]. Geothermal gases (geogas) containing CO_2, H_2S, H_2, N_2, CH_4 and Ar inevitably contribute to numerous GHG emission. The annual CO_2 emission from the Hellisheiði (operated since 2006) and Nesjavellir (operated since 1990) Power Plants amount to 61,800 tons [286]. By implementing the CarbFix gas injection procedure (scaled up in 2017), it is possible to inject 10,000 tons of CO_2 into the geothermal reservoir, which corresponds to 34% of the annual emissions from the Hellisheiði plant [287]. To achieve carbon neutrality, CO_2 emission need to be further reduced and ideally the untapped carbon source from geogas could be exploited to produce microalgal biomass for higher economic profits. In this context, it is essential to assess and develop microalgae-based carbon capture and storage (CCS) technology for practical implementation. To achieve this, it is necessary to understand how microalgae respond to stress conditions associated with geogas, as this knowledge is crucial for engineering microalgal cell factories.

Table 1.8. Composition of geogas from the Hellisheiði plant.

Sample	**CO_2 %**	**H_2 %**	**O_2 %**	**N_2 %**	**CH_4 %**	**H_2S %**
Gas sample 1	60.8	30.98	0.967	5.53	0.238	2.2
Gas sample 2	61.4	30.55	0.895	5.38	0.236	1.9
Gas sample 3	62.8	29.93	0.864	5.14	0.23	2
Average	61.13	30.77	0.93	5.45	0.24	2.1

Our group focuses on algal biotechnology and aims to produce value-added products from microalgae using local resources in Iceland. **The primary objective of this project was to develop photosynthetic cell factory for diatoms to enable mass production from the geogas resource.** Applying system biology, we attempt to investigate bioengineering strategies to improve growth features of diatom, focusing on stress tolerance and photosynthetic efficiency.

In a preliminary test, the extremely high CO_2 concentration in the geogas (Table 1.8) led to acidic equilibrium pH close to 5.0 in the artificial seawater medium. This condition, as reported in the literature, poses a significant challenge that inhibits cell growth in microalgae cultivation. Experimental evidence has demonstrated the importance of maintaining pH to alleviate the overall negative impact of flue gas on microalgal growth [107, 120], suggesting a principal inhibitory role the low pH in flue gas-induced inhibition. Therefore, we consider it is feasible to overcome the challenge of acidic condition through strain improvement via bioengineering. From the perspective of photosynthetic efficiency, oscillatory photosynthetic performance was observed under continuous light (Appendix A, Figure A1). We hypothesize that photosynthetic efficiency in diatoms may be influenced by an intrinsic circadian clock, which could constrain continuous biomass

production. In pursuit of developing an applicable microalgal platform, this PhD project was designed with scientific and engineering objectives, which are as follows:

Objective 1: to adapt *P. tricornutum* to low-pH stress and decipher underlying adaptive mechanisms (Paper 1)

Objective 2: to develop low-pH resisting diatom strains and study role of key pathways/genes in stress tolerance (Paper 2)

Objective 3: to uncover potential mechanisms that constrain photosynthetic efficiency (Paper 3)

Regarding the objectives above, following questions are asked:

Research Question 1 (RQ1): How does *P. tricornutum* react and adapt to the low-pH stress?

Research Question 2 (RQ2): What pathways/genes contribute to adaptation/tolerance of *P. tricornutum* to acidic conditions?

Research Question 3 (RQ3): Are there intrinsic circadian rhythms in the diatom that affect photosynthesis and cell growth?

2 Physiological and molecular insights into adaptive evolution of the marine model diatom *Phaeodactylum tricornutum* under low-pH stress

Yixi Su, Maonian Xu, Sigurður Brynjólfsson, Weiqi Fu, Physiological and molecular insights into adaptive evolution of the marine model diatom *Phaeodactylum tricornutum* under low-pH stress, Journal of Cleaner Production, Volume 412, 2023, 137297, ISSN 0959-6526, https://doi.org/10.1016/j.jclepro.2023.137297.

Keywords*: Phaeodactylum tricornutum*, adaptive laboratory evolution, low pH tolerance, transcriptomics, whole-genome re-sequencing

2.1 Abstract

The direct use of industrial flue gas in microalgae production is desired for mitigating CO_2 emissions, but the low pH resulting from the inflow of acidic gases (mainly CO_2, NO_x, and SO_x) imposes detrimental effects on microalgal growth and is considered the main technical challenge for simultaneous biomass production and CO_2 sequestration. In this study, we investigated the adaptive responses of the model marine diatom *Phaeodactylum tricornutum* to acidic stress at pH 6.0. Gradual changes in the ratio of morphotypes, chlorophyll content, and photosynthetic efficiency were observed as a result of adaptive laboratory evolution (ALE) under constant acidic stress. The evolved strains showed a significant increase in growth rate in acidic conditions after ALE, and phenotypic characterization demonstrated a stable trait of acid tolerance with an average increase in growth by 110.4%, 46.1%, and 27.5% at pH 5.5, 6.0, and 6.5, respectively compared with the parental wild-type strain. Furthermore, RNA sequencing and whole-genome re-sequencing analyses revealed that core pathways, including photosynthesis, pH regulation/ion transport, and carbohydrate and fatty acid metabolism, were upregulated across all three evolved strains, though they exhibited different evolutionary trajectories. This study demonstrated the feasibility of recovering photosynthetic capability after acidic stress in the marine diatom *P. tricornutum* through ALE and provided molecular data to reveal essential alterations in genetic regulations that could enable cells to tolerate low environmental pH.

Highlights

- Acidic pH significantly impaired the photosynthesis and growth of *P. tricornutum*
- Low-pH tolerance in *P. tricornutum* was improved through the adaptive laboratory evolution process
- Transcriptomics analysis revealed upregulated photosynthesis, pH regulation/ion transport, carbohydrate and fatty acid metabolism in acid-adapted populations
- Whole genome resequencing showed distinct evolutionary trajectories among the evolved strains

2.2 Introduction

The relentless rise in atmospheric CO_2 levels leads to climate change, which has become a severe environmental problem that disrupts sustainability. The coupling of microalgae cultivation with industries emitting greenhouse gasses (GHG) to mitigate global warming and ocean acidification has shown promise for simultaneous biomass production and CO_2 sequestration [288]. Microalgal biomass productivity and product yields are influenced by various factors such as cultivation methods and growth conditions [289]. Biomitigation of CO_2 via microalgal systems is challenging because the direct use of flue gas is likely to impose extreme conditions that few algal species can tolerate [290]. Flue gas from combustion processes can contain complex constituents that provide carbon, nitrogen, and sulfur for biomass production [103], but excessive inputs inhibit microalgal growth [291, 292]. As a direct effect, the dissolution of acidic gases leads to a dramatic decrease in pH in the media. In large-scale cultivation, an inflow of >5% CO_2 resulted in a solution pH of 5.6 – 6.5, and the use of 100% flue gas could greatly reduce the pH of the medium to 2.4 – 4.5 [120, 293, 294]. The decrease in pH of media complicates microalgal growth and cellular composition with species-specific variations [295] and is considered the main inhibitory factor for the direct use of CO_2 in microalgae production [290, 294]. Based on observations on microalgal physiology, high-CO_2 tolerance is often associated with increasing ATP generation by photosynthetic apparatus, upregulation of proton pumping systems, the shutdown of CO_2-concentrating mechanisms, and adjustment of membrane fatty acids composition, which are proposed as key mechanisms to maintain cellular pH homeostasis [296]. However, the pH-responsive effects have not been well characterized in microalgae, although a recent study reported distinct gene expression patterns in the model green alga *C. reinhardtii* in response to high-CO_2 and low-pH conditions [297].

In recent decades, research on the exploitation of flue gases in microalgae production has focused on optimizing cultivation conditions [114, 119, 291] and isolation/breeding of stress-tolerant algal strains [294, 298]. While pH moderation has been applied to improve the tolerance limit of microalgae, other strategies to mitigate the toxicity of flue gas include intermittent flue gas supply, the addition of gas solubility enhancers such as amines, carbonate, and sodium hydroxide, and use of high biomass density [299]. Evidently, the detrimental influence of flue gases on microalgal growth can be alleviated by adjusting the pH to neutral [120], but buffering agents can be uneconomical for microalgae cultivation processes [299]. An inexpensive bicarbonate/phosphate (BP) buffer system was designed to neutralize the pH decrease induced by CO_2 injection, which was capable of maintaining the pH of media in a constant range against 10% (v/v) CO_2 [119]. Nevertheless, the buffer capacity of this system was inadequate to counteract the impacts of high concentration CO_2 and the addition of phosphate buffer could have adverse effects on microalgal growth [119, 293]. Apart from pH moderation, microalgae production in high pH cultures with alkali-tolerant strains was proposed for better solubilization of CO_2 and carbon fixation [300]. Alternatively, acid-tolerant microalgal strains are desired to overcome hazardous acidic conditions induced by industrial flue gas [290].

By mimicking natural evolution, adaptive laboratory evolution (ALE) is effective in screening spontaneously raised genetic diversity under controlled

scenarios, allowing systematic optimization of the fitness landscape of microorganisms [186]. Implementing appropriate stress can direct the evolution of variants of the microbial population that bear desired traits and have a selective advantage to gradually predominate the population over time. The diatom *Phaeodactylum tricornutum* has several advantages over other microalgal species in the context of this study. This marine diatom can be cultivated with seawater on a large scale and possesses enriched value-added compounds such as unsaturated fatty acids and carotenoids. It can be subjected to efficient genetic modifications using molecular biological tools, making it feasible to improve phenotypic traits such as acid tolerance in microalgae. In *P. tricornutum*, ALE has been successfully applied to improve biomass and carotenoid productivity under light stress [195]. Recently, Wang, et al. [301] domesticated a polyunsaturated fatty acid (PUFA)-hyperproducing *P. tricornutum* strain that was adapted to thrive on food waste hydrolysate. Research efforts [302, 303] have been made to develop acid-tolerant cyanobacteria and green microalgae. However, the effect of pH on *P. tricornutum* growth and the adaptative mechanism of the model diatom to acidic conditions during evolution remains largely unknown.

Hence, in this study, we attempted to tackle algal growth inhibition due to low-pH stress [304] by using ALE to improve the fitness of three parallel populations of the model diatom *P. tricornutum*. To further understand acidic tolerance in the diatom, we conducted transcriptome and genome re-sequencing to investigate the critical genes involved in low-pH adaptation. To the best of our knowledge, this is the first study to investigate diatom adaptation under low-pH conditions using transcriptomic and genomic analyses, which provides new insights into the potential of marine diatoms for the bio-sequestration of CO_2 in the flue gas.

2.3 Materials and methods

2.3.1 Microalgal species and culture conditions

Axenic diatom *P. tricornutum* (CCAP 1055/1) culture was purchased from the Culture Collection of Algae and Protozoa (CCAP), Scotland, UK. The inoculum was maintained at room temperature (22 ± 2 ℃) in an f/2 medium [305] under a white LED lamp with a low intensity of 30 μmol photons m^{-2} s^{-1}. All experiments were conducted with axenic monoalgal cultures that were maintained at 22 ± 2 ℃ and illuminated by a red LED panel (with a peak wavelength of 630 nm) from one side at a light intensity of 100 ± 5 μmol photons m^{-2} s^{-1}. Cultures were mixed daily by manual shaking.

Steady pH conditions were maintained using buffers as follows: 40 mM MES (2-*N*-morpholinoethane-sulfonic acid) for pH 5.5–6.5, 40 mM Tris-HCl for pH 7.0–9.0, and 40 mM CAPS [3-(cyclohexylamino)-1-propanesulfonic acid] for pH 10.0–10.5. Media were sterilized by filtration using a 0.22 μm membrane filter (S-PAK, Millipore). The pH of the culture was measured and monitored using a pH meter (Beckman, USA).

2.3.2 Assessment of pH tolerance

To investigate the effects of pH on cell growth, batch culture experiments were conducted in 500 mL flasks with a 200 mL working volume in triplicate. The effect of pH on diatom growth was evaluated under acidic (pH 5.5) and alkaline (pH 10.5) conditions. The control group was grown in a non-buffered f/2 medium at an initial pH of 8.0. The optical density at a wavelength of 750 nm (OD_{750}) and chlorophyll fluorescence were measured daily.

2.3.3 Adaptive laboratory evolution

Based on the assessment of the pH effect, the scenario was designed to use environmental pressure to screen for variants that had better fitness against stress, and these variants were expected to predominate the population and exhibit improved overall growth among the population. Three parallel populations of the parental wild-type *P. tricornutum* were subjected to low-pH stress by semi-continuous cultivation in 5-day cycles in 250 ml flasks with 75 ml working volume. An appropriate aliquot of cells was harvested by centrifugation at 1500 × g for 10 min and resuspended in fresh media, ensuring a fixed initial cell concentration (OD_{750} = 0.100±0.005) for each cycle. The OD, chlorophyll content, photosynthetic efficiency, and morphology were assessed at the end of each cycle. Ten milliliters of the parental culture and the endpoint-evolved cultures were harvested by centrifugation. Cell pellets were washed with 1 mL of sterile milliQ water and stored in 1 mL of sample protector reagent (Takara, Japan) at -20 ℃ for genome re-sequencing.

To assess the pH tolerance of the evolved strains, the parental culture and three endpoint cultures (denoted as ALE1, 2, and 3) were sub-cultured in standard f/2 media (pH 8.0) for two 5-day cycles. They were then transferred into buffered media

with pH values of 5.5, 6.0, and 6.5, respectively. OD_{750} was monitored and 20 mL of the culture was collected for biochemical analyses on the fifth day. This experiment for growth characterization was repeated twice with duplicates for each group and the combined results were reported. Samples for transcriptomic study were made in another growth experiment with triplicated cultures of each strain under pH 6.0 treatment where 20 mL of aliquots were collected on the fifth day by centrifugation (4000 x g, 4 ℃) for 10 min. After washing with 1 mL sterile milliQ water, the samples were stored in 1 mL of sample protector reagent (Takara, Japan) at -20 ℃ for further transcriptomic analysis.

2.3.4 Physiological analyses

Measuring OD_{750}, which was monitored using a DR1900 spectrophotometer (Hach, US), enabled the estimation of the dry weight (DW) of the biomass by using an established relationship between OD_{750} and DW (g L^{-1}) or cell number ($\times 10^4$ mL^{-1}) as follows (Appendix A, Figure A2):

$$\mathrm{DW} = 0.7429 \cdot OD_{750} \ (R^2 = 0.999)$$

For dry weight determination, 10 ml of cell culture was filtered through a pre-combusted (540 ℃) and pre-weighed Whatman GF/C glass microfiber filter. The filtered biomass was rinsed with 10 ml of 0.5 M ammonium bicarbonate and dried at 105 ℃ for 24 hours or to a constant weight, cooled down in a vacuum desiccator, and then weighed [306]. The specific growth rate (μ, d^{-1}) was calculated using the following equation: $\mu = (\mathrm{In}X_t - \mathrm{In}X_0)/(t - t_0)$ where X_t and X_0 are the OD at time t and the beginning of the time interval (t_0), respectively.

During ALE, the chlorophyll content in the samples from each cycle was estimated using a spectrophotometric method based on ethanol extraction [307]. Chlorophyll fluorescence was measured using AquaPen-C AP 110 (Photon Systems Instruments, Czech Republic). The effective quantum yield (Φ_{PSII}) was measured immediately after sample collection. For further analysis, the sample was incubated in the dark for 15 min, and fluorescence was measured according to a built-in program (non-photochemical quenching (NPQ) protocol 3) that generated photosynthetic data, including maximum quantum yield (F_v/F_m), Φ_{PSII}, and NPQ.

For morphological analysis, neutral red staining of the cytoplasm and vacuoles in the plant cells was done to distinguish viable cells from dead cells [308]. Diatom cells were stained by adding 50 µL of 0.33% neutral red solution (Sigma, USA) to 1 mL samples and observed using a light microscope (Leica, Germany) after 30 min of incubation.

The lipid content was measured by the gravimetric method using the chloroform-methanol (1:1, v/v) extraction protocol [309]. Total protein and carbohydrates were quantified following a previously described approach [310]. In brief, protein, and carbohydrate were extracted using 1 ml of extraction buffer (50 mM Tris, pH 7.2; 500 mM NaCl) supplemented with freshly prepared phenylmethylsulfonyl fluoride (PMSF) 1.0 mM and dithiothreitol 2.0 mM. The cells were disrupted through three cycles of sonication (30 s, 10 amplitude), followed by centrifugation at 4000 x g for 10 min. The supernatant cell lysate was collected for

protein and carbohydrate determination through the Bradford assay (Sigma, US) and the cysteine-sulfuric acid assay [311], respectively.

Data were analyzed using IBM SPSS statistics version 26 by Student's t-test or one-way ANOVA, with a significance level of $p<0.05$. Tukey's multiple comparison test was used to examine the differences among low-pH treatments.

2.3.5 Transcriptome sequencing and analyses

RNA-sequencing (RNA-seq) was conducted to investigate the differences in acid-responsive expression between the ALE strains and the wild-type (WT). Total RNA was extracted using the mirVana miRNA ISOlation kit (Ambion, USA) by following the manufacturer's protocol. RNA integrity was evaluated using an Agilent 2100 Bioanalyzer (Agilent Technologies, USA). Samples with an RNA integrity number (RIN) ≥ 7 were subjected to subsequent analysis. Transcriptome sequencing and analysis were conducted by OE Biotech Co. Ltd. (Shanghai, China). Raw data (raw reads) were processed using Trimmomatic [312]. The clean reads were mapped to the reference genome using Hisat2 [313]. Fragments per kilobase of exon per million mapped fragments (FPKM) and read counts of each transcript (protein-coding gene) were calculated using Bowtie2 [314] and eXpress [315]. Differentially expressed genes (DEGs) were identified using the DESeq (2012) R package. P-value < 0.05 and fold change ratios (ALE/WT) ≥ 2 or fold change ratios (ALE/WT) ≤ 0.5 were set as the threshold for significant expression. Gene ontology (GO) and Kyoto Encyclopedia of Genes and Genomes (KEGG) pathway enrichment analyses of DEGs were performed using R based on the hypergeometric distribution.

2.3.6 Whole-genome re-sequencing and analyses

Genomes of the ALE strains and the WT were re-sequenced and analyzed by OE Biotech Co., Ltd. (Shanghai, China). DNA libraries were constructed by fragmenting the genomic DNA into 350–500 bp inserts and sequencing on an Illumina platform (NovaSeq 6000). Raw data were filtered using a preprocessor fastp [316] to remove low-quality reads and then aligned to the reference genome of *P. tricornutum* (release-51, http://protists.ensembl.org/Phaeodactylum_tricornutum/Info/Index) using the Burrows-Wheeler Aligner (BWA) [317]. GATK4 [318] was used to detect single nucleotide polymorphisms (SNPs) and insertion-deletion (InDel) mutations.

2.4 Results and discussion

2.4.1 Assessment of pH tolerance

In this study, we evaluated the effects of pH on the growth of *P. tricornutum* and found that variations in the pH between 6.5 to 9.5 had no significant effect on the maximal specific growth rate (Figure. S2.1). Cultures at pH lower than 6.5 or higher than 9.5 exhibited significantly lower growth rates than the control did (Figure S2.1). The highest biomass productivity of 18.86 $\pm$ 2.28 mg $L^{-1}d^{-1}$ was achieved at pH 9.5, whereas the lowest productivity of 1.32 $\pm$ 0.25 mg $L^{-1}d^{-1}$ was observed at pH 5.5. Under alkaline conditions (pH > 8.5), cell aggregation and attachment to the glass flasks occurred because of bioflocculation induced by high pH in the culture [319]. These findings were in accordance with previous studies [320-322] that *P. tricornutum* is insensitive to pH variations between 7.0 and 9.0, and its growth rates substantially decline when the external pH decreases from 7.0 to 6.0 [320]. Complete inhibition of diatom growth was observed at pH 5.0 in another experiment (Figure S2.2), indicating a low pH limit for the positive growth of *P. tricornutum* (Figure S2.1). Since fresh f/2 medium at low pH 6.0 contained a sufficient amount of carbon source for diatom growth [58], carbon limitation was unlikely to have been the reason for repressed cell growth at the beginning of cultivation with low cell densities.

Moreover, pH may directly affect cell physiology by affecting membrane potential, energy partitioning, and enzyme activity [323]. As illustrated in kinetic data (Figure S2.1), similar Φ_{PSII} curves were observed under conditions of pH 8.0–10.0, whereas a lower pH (pH < 8.0) resulted in a more rapid reduction in Φ_{PSII}. This result indicated that photosynthetic efficiency in *P. tricornutum* was generally unaffected by alkaline pH, whereas lowering the pH had an increasingly negative influence on photosynthesis. Remarkably, photosynthesis was inhibited at pH 5.5 throughout the cultivation period along with a dramatic decrease in the Φ_{PSII} after inoculation. Similar results have been reported for the marine diatom *Chaetoceros muelleri* [324]. Therefore, impaired photosynthesis, which could be a consequence of the induced low pH, could play a significant role in retarding the growth of *P. tricornutum*.

2.4.2 Adaptation to low pH

Based on the results of the experiment to determine the effect of pH on *P. tricornutum*, it was noticed that photosynthesis was not entirely prohibited in *P. tricornutum* at pH 6.0, which was selected as the appropriate stress level for the ALE experiment. Instead of white light (used for inoculum maintenance), red LED (630 nm) was applied in all experiments for more efficient energy conversion [325] and controllable specifications of the light source. Although the use of light with different spectra may induce changes in gene expression and thus metabolism in microalgae, red light evidently can support the fast growth of diatoms comparable to the performance of white light with broad spectrum [326, 327]. Therefore, we consider the red light did not introduce additional stress on cell growths, and evolution was directed under a single selective pressure (i.e. low-pH stress) during the ALE process. ALE under acidic pH stress was conducted for 16 cycles (Figure

1). The average growth rate in each cycle was calculated by measuring the initial and endpoint cell optical density. Compared to growth in non-buffered f/2 media (0.306 d^{-1}), an acidic environment (pH 6.0) caused a 76.7% decline in the average growth of triplicate cultures in the first cycle. The average growth rate of the endpoint strains was 0.176 ± 0.007 d^{-1}, which was 1.4-fold ($p<0.05$) of the growth rate after the initial acid shock (0.125 ± 0.006 d^{-1}) (cycle 1). For each cycle, pH was monitored and measured with a variation of less than 0.03 between the initial and endpoint cultures, demonstrating appropriate pH control with MES buffer (Figure 2.1B). Carbon availability was considered a possible cause for the limited cell density during the ALE process (16 cycles). ALE cycle 16 was followed with three additional cycles in which filtered air was pumped at a rate of 0.3 *vvm* (air volume per culture volume per minute) into ALE cultures to increase CO_2 availability. However, this did not have a positive effect on the growth (Figure S2.3). Therefore, the evolved strains obtained at the end of ALE cycle 16 were used for further phenotypic characterization.

The proportions of the different morphotypes fluctuated throughout the adaptation process (Figure S2.4). Fusiform was the predominant morphotype accounting for $94.9 \pm 1.63\%$ of the population in the seed culture (ALE-cycle 0). Upon treatment with acidic stress, the fusiform ratio in all viable cells gradually decreased to the lowest level ($78.4 \pm 4.5\%$) in the sixth cycle; meanwhile, the oval cells showed an inverse trend by increasing dramatically from $0.3 \pm 0.3\%$ (at ALE cycle 0) to $20.5 \pm 3.7\%$ (at ALE-cycle 6). With the recovery of growth (Figure 2.1B), the population of fusiform and oval morphotypes approached equilibrium, accounting for approximately 90% and 10% of all morphotypes, respectively, towards the end of the experiment. By contrast, the triradiate form decreased from $4.8 \pm 1.4\%$ (at ALE-cycle 0) to $0.4 \pm 0.4\%$ (ALE-cycle 16). Current knowledge suggests that morphological preference and stability are likely strain-specific and determined by genotypes, but morphotype transformation is probably epigenetically controlled and sensitive to external factors [30]. For many *P. tricornutum* strains, fusiform cells predominate under non-stressful or optimal growth conditions. Under suboptimal conditions, more oval cells are induced, whereas triradiate cells are eliminated [328]. The proportion of triradiate cells in the culture increased as pH increased from 7.9 to 9.5 [329]. Thus, we deduced that the formation of the triradiate morphotype of *P. tricornutum* could be induced by a change in pH.

After the shock of acidic stress, the chlorophyll content and quantum yield decreased substantially, and the NPQ levels increased 5-fold in the first two cycles (ALE cycles 1-2) in comparison with cycle 0 (Figure S2.4). The quantum yields quickly recovered to a level equivalent to that of the seed culture at ALE cycle 3, accompanied by a decrease in NPQ levels. Then, maximum and effective (Φ_{PSII}) quantum yields were maintained at relatively lower levels of approximately 0.51 and 0.35 (ALE cycles 6-16), respectively, while the NPQ level fluctuated at approximately 0.15 (Figure S2.4). Decreased chlorophyll synthesis may be a potential defense strategy to survive in detrimental environments by limiting excess electron flow, thus limiting the generation of oxygen radicals and reducing equivalents [310]. This implies a weakened light-harvesting capacity, which could be a reason for the retarded cell growth. Additionally, the Φ_{PSII} of the ALE culture was lower than that of the starting cultures of *P. tricornutum*, which implied that less energy was utilized for carbon fixation. A recent study indicated that excitation

energy transfer around or within chlorophyll molecules could be acidic or alkaline pH-induced to enhance energy quenching or transfer, which may explain the lower efficiency of energy utilization and higher NPQ levels observed in our low-pH-stressed ALE study [330].

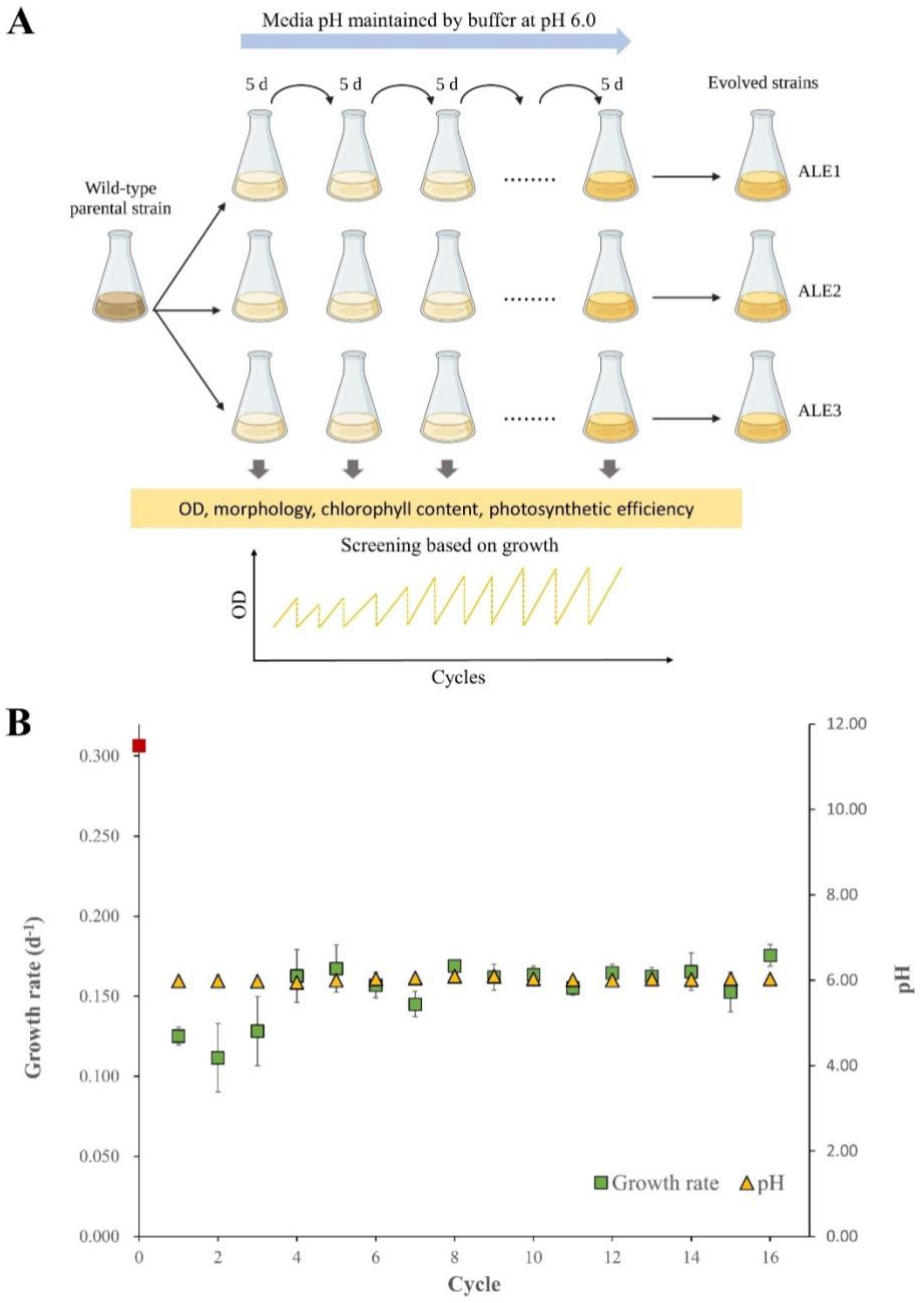

Figure 2.1. *Adaptive laboratory evolution (ALE) process for P. tricornutum at pH 6.0. (A) Conceptual representation of diatom strain improvement through adaptive laboratory evolution (ALE) for acid resistance. (B) Average growth rate under constant acidic stress over the ALE process. Three parallel populations derived from the same parental culture were subjected to constant low pH stress at 6.0 in 5-day cycles. The ALE experiment was conducted for 16 cycles (80 days). Values are shown as mean* $\pm$ ***SD*** *(n = 3). Data for cultures before starting ALE (cycle 1) were illustrated in red as cycle 0.*

Stimulated *P. tricornutum* growth was reported at a low pH value of approximately 6.0 due to high CO_2 supply inflow to successive semi-continuous cultures, but impaired growth was observed after two cycles of semi-continuous cultivation [106, 304]. Elevated CO_2 has been shown to have a stimulatory effect on diatom growth during the light period, which could counteract the inhibitory effect of low-pH stress [331]. Meanwhile, algal cellular respiration was also stimulated by the high CO_2, which caused increased biomass loss during the night period [331]. In this context, reduced chlorophyll synthesis under acidic stress may impair photosynthesis, which break the balance between photosynthesis and respiration. Consequently, high CO_2 inflow could cause unsustainable culviation of diatom in the long run.

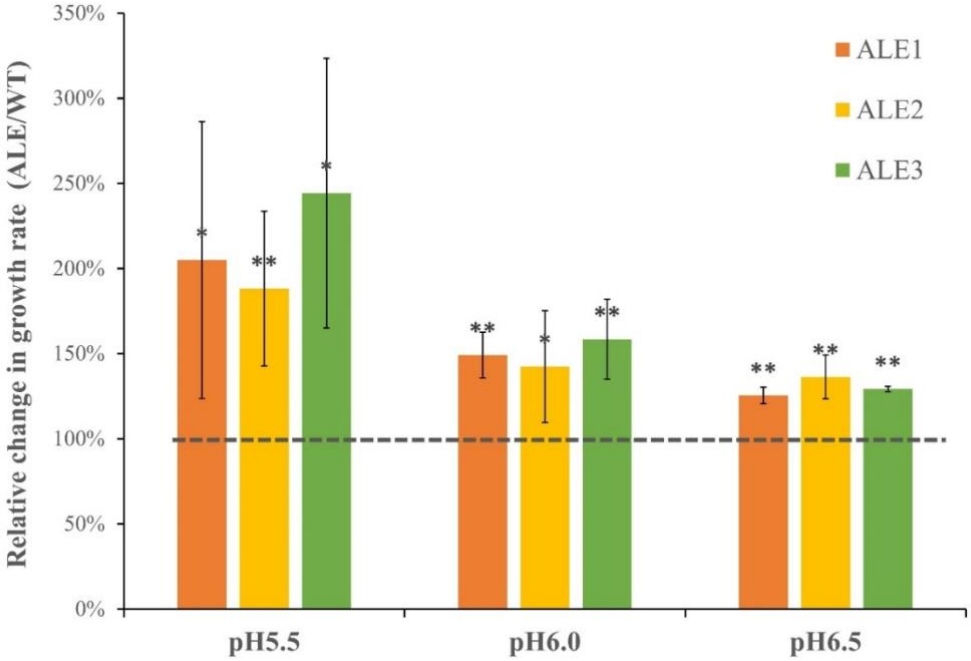

Figure 2.2. *Relative change in growth rate comparing the adaptive laboratory evolution (ALE) and the wild-type (WT) strains under acidic treatments. Results were obtained from two repeated experiments with duplicates (dash line indicates ALE/WT = 1). Values are shown as mean ± SD (n = 4). (* $p < 0.05$, ** $p < 0.01$).*

Microorganisms adapt to new environments or stress conditions through the selection of genetic variability resulting from spontaneous mutations or through physiological adaptation due to phenotypic plasticity [332]. To determine the stability of the new traits of ALE-evolved strains, we cultivated ALE-evolved and WT strains in f/2 media under unstressed conditions to eliminate low-pH-induced physiological responses in ALE strains before low-pH treatments at pH 5.5, 6.0, and 6.5. As demonstrated in Figure 2.2, the ALE strains that had undergone long-term adaptation to pH 6.0 exhibited significant increases in growth rate than the parental strain did in all experimental groups. Average improvements in the growth of ALE strains compared with that of the WT were 110.4%, 46.1%, and 27.5% at pH 5.5, 6.0, and 6.5, respectively. Furthermore, significantly higher contents of protein and carbohydrate were observed in ALE strains, while the difference in lipid content between the WT and ALE strains was insignificant in all low pH treatments (Figure

S2.5). Scholz [333] demonstrated that protein and chlorophyll contents in five marine diatoms decreased as the pH deviated from the optimal pH of 8.0 for all tested taxa. Hence, the relatively higher protein contents may imply alleviated impacts of acidic stress on ALE strains. As for other macromolecules, carbohydrate and lipid content exhibited species-specific responses to pH change in both short- and long-term experiments [333].

2.4.3 Transcriptomic responses to acidic stress

A transcriptomic study was performed to investigate the pH tolerance mechanisms in the acidic adapted strains. Gene expression profiles of the three populations of evolved strains were compared with that in the wild-type strain under the same acidic stress. As summarized in Table S2.1 (see Supplementary Material), the transcriptome dataset with Q30 bases comprising 93.88 – 94.51% of the clean read data and >94% mapping rate was considered qualified for further gene expression analysis. On analyzing the gene expression in the WT, we identified 772, 561, and 1458 DEGs with two-fold changes ($p < 0.05$) in ALE1, ALE2, and ALE3, respectively. The detailed numbers of upregulated and downregulated genes in each strain are summarized in Table 2.1. Since the three populations of *P. tricornutum* underwent long-term ALE process independently, genetic variation and thus different expression patterns could be raised or selected underlying the evolution towards similarly improved stress resistance. The divergence among ALE-evolved strains was reflected by the PCA plot and sample-to-sample distance (Figure S2.6). Compared with that of ALE1 and ALE2, the transcriptome of ALE3, showed an enormous distance to the WT.

Table 2.1. Identified differentially expressed genes (DEGs) in adaptive laboratory evolution (ALE) strains against the gene expression profile in the wild type (WT).

Strain	Total DEGs	Upregulated	Downregulated
ALE1	772	317	455
ALE2	561	319	242
ALE3	1458	539	919

DEGs in different strains were analyzed through GO enrichment analysis and categorized based on biological processes (BP), cellular component (CC), and molecular function (MF). As the resulting transcriptomes from the population samples were associated with the collective low-pH tolerant features of the evolved populations, GO terms with p-value < 0.05 present in at least two ALE strains were selected for further investigation. As a result, upregulated DEGs were assigned to 22 shared GO terms (Figure 2.3A), whereas 9 GO terms were commonly found in ≥2 ALE strains for downregulated DEGs. Our transcriptomic results highlighted the upregulation of genes involved in photosynthesis, pH regulation/ion transport, carbohydrate metabolism, and fatty acid biosynthesis in acid-adapted strains (Figure 2.3A), whereas downregulated DEGs were only enriched in GO terms related to DNA integration/recombination (not shown).

Regarding photosynthesis, extensive upregulation of light-harvesting complexes (LHCs) and electron transport chain (ETC) enzymes, as well as repression of key enzymes in chlorophyll biosynthesis, were commonly observed in the ALE strains (Table 2.2). LHCs play crucial roles in light harvesting and photoprotection of photosystems [334, 335], whereas ETC is essential for converting light energy into ATP. As observed in this study, the gradual decrease in chlorophyll content during the adaptation process was consistent with the transcriptome profiles that indicated a reduced photon capture capacity, and enhanced energy dissipation and conversion in the acid-adapted strains, which suggested a direction of adaptation towards avoiding photodamage.

In eukaryotes, protons regulate cellular metabolism via transmembrane H^+ transport, H^+ buffering, and metabolic H^+ consumption [336]. Experiments have shown that the intracellular pH of diatoms is proportionally influenced by the external pH [337]. In photosynthetic organisms, low pH can cause damage to photosystems and inhibit photosynthesis by inactivating critical enzymes of the Calvin cycle via acidification of the stroma [338]. To resist the adverse effects of external pH on cellular metabolism, pH homeostasis in algal cells is maintained by the active transport of protons and regulation of the CO_2-concentrating mechanism (CCM) [296]. Accordingly, we found that the expression of proton pumping systems comprising multiple paralogues of bicarbonate transporters, carbon/H^+ antiporters, and P-type H^+ ATPases was generally enhanced in all the acid-adapted strains (Table 2.2). A recent study revealed low expression levels of the core H^+ pumping system in high-CO_2 intolerant algal species. Overexpression of plasma membrane H^+-ATPase (PMAs) improved the robustness of *C. reinhardtii* against high CO_2, indicating the importance of proton pumps in microalgae [297]. To counteract the influx of external protons, ALE1 and ALE2 strains behaved similarly to reinforce the expression of proton pumps. In contrast, ALE3 repressed the expression of several proton antiporters (Phatr3_J44149 and Phatr3_J48886) and P-type H^+-ATPases (Phatr3_EG02512, Phatr3_J676, and Phatr3_J47620). The different expression patterns resulting from parallel populations imply that coordination of regulatory pathways may exist in regulating intracellular proton levels in *P. tricornutum*. For instance, increased expression of a P-type ATPase gene, Phatr3_EG01907, was observed in ALE1 and ALE2; instead, a closely homologous protein (Phatr3_EG01908) was significantly upregulated in ALE3.

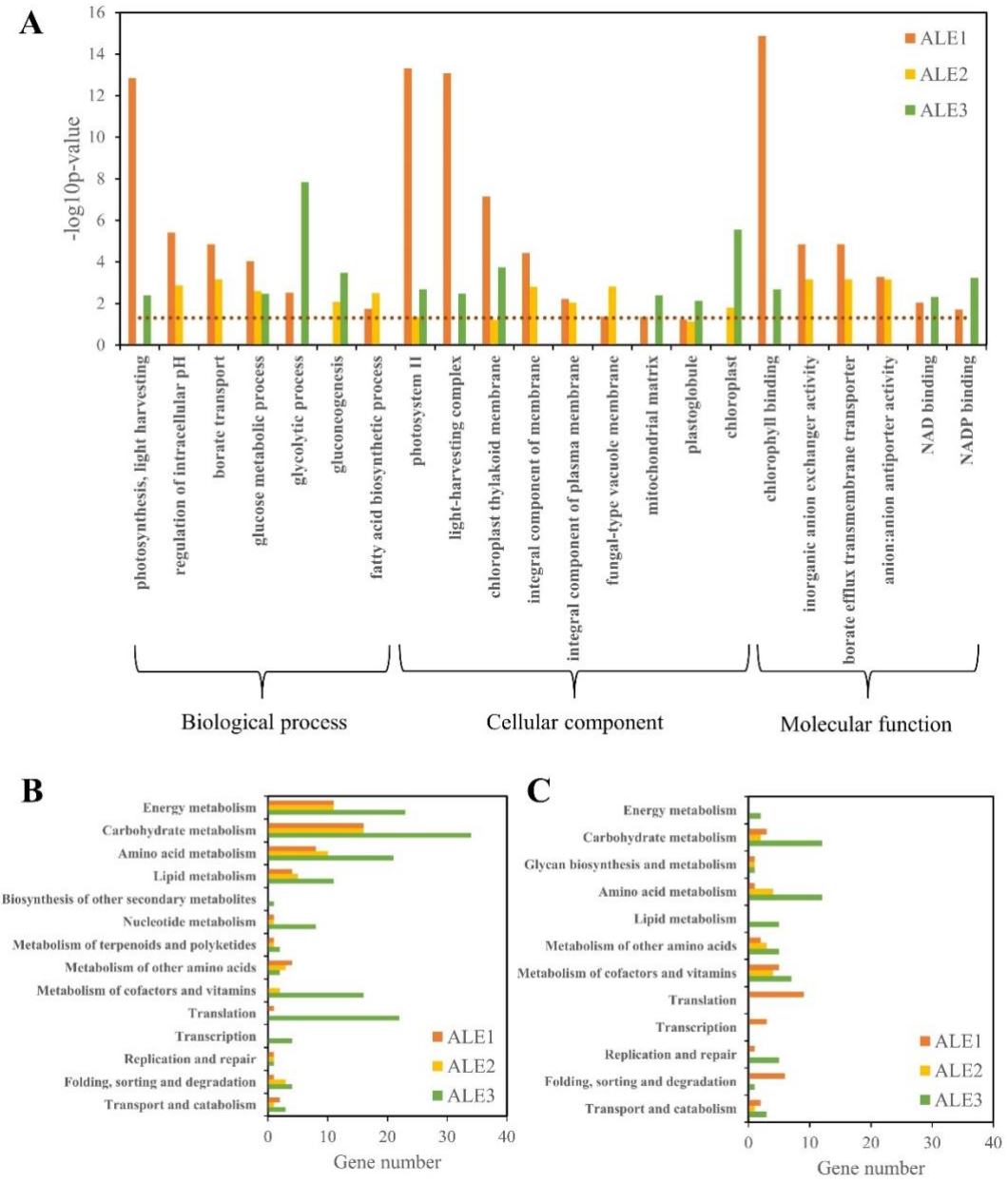

Figure 2.3. *Enrichment analysis on transcriptomes in response to low-pH stress. (A) Gene ontology categories of differentially expressed genes (DEGs) (dash line indicates p-value < 0.05). KEGG pathway classifications of DEGs. (B) Upregulated genes. (C) Downregulated genes.*

The components of the carbon concentration mechanism were further explored, and upregulation of carbonic anhydrase paralogues (Phatr3_J45443, Phatr3_J51305, and Phatr3_J43233) was only observed in ALE1 and ALE2. CCM shutdown was hypothesized to be required for resisting low external pH resulting from high CO_2 levels [296], but our study suggested that the CCM was not necessarily regulated by external pH. Previous studies on microalgal response to rising CO_2 levels [339, 340] have shown that it affects the expression of several carbonic anhydrases but does not influence bicarbonate transporters. These results are partially consistent with those of our low-pH-responsive study, indicating the differential regulation underlying CO_2 and pH-responsive mechanisms.

KEGG classification (Figure 2.3B and C) revealed the enrichment of upregulated DEGs in energy, carbohydrate, amino acid, and lipid metabolism in ALE strains. These were partially supported by physiological data (Figure S2.5) with increased total protein and carbohydrate content in the ALE-evolved strains. As illustrated in Figure 2.4, pathways involving carbon fixation, carbohydrate metabolism, pyruvate metabolism, and fatty acid synthesis in the ALE strains were enhanced compared with those in the WT. Transcriptional regulation in the three ALE strains coincided with these metabolic pathways, although they showed distinct expression levels for many individual genes. Upregulated DEGs were broadly observed in pathways directing carbon fluxes to fatty acids and chrysolaminarin, including multiple paralogous genes encoding glyceraldehyde-3-phosphate dehydrogenases (GAPC), fructose-bisphosphate aldolases (FBA), and pyruvate kinase (PK). Although the transcriptomic data suggested enhanced metabolisms for all macromolecules, i.e. protein, carbohydrate, and lipid, this may not be reflected on the metabolomic level because different pathways could compete for the limited carbon and complicated post-transcriptomic regulation may be involved in the metabolism.

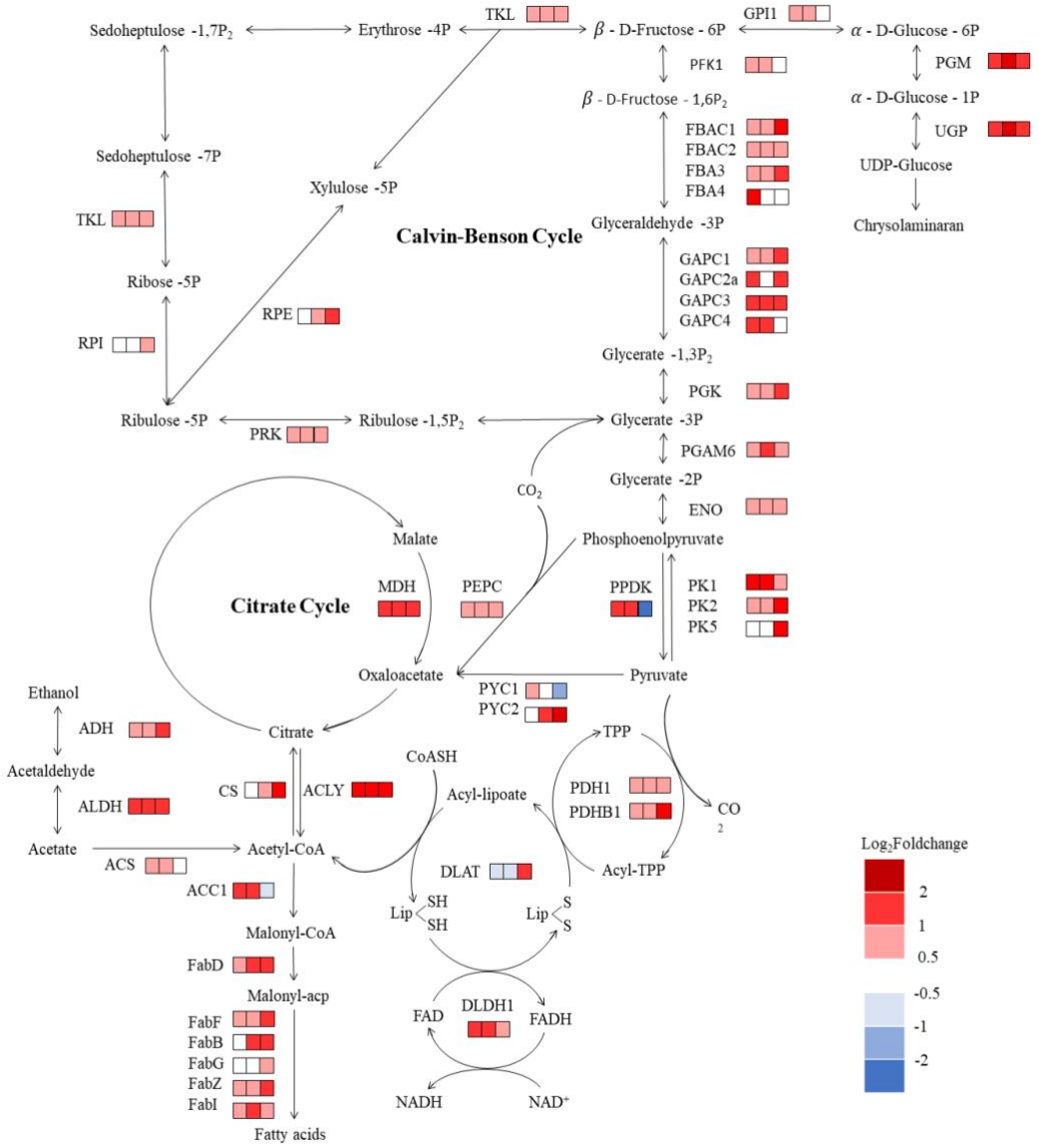

Figure 2.4. *Expression levels of genes involving carbon fluxes in adaptive laboratory evolution (ALE) strains. Colored squares from left to right indicate the regulation of genes in ALE1, ALE2, and ALE3 against gene expression in the wild type (WT) as the control (n = 3). Abbreviation: PGK, phosphoglycerate kinase; GAPC, glyceraldehyde-3-phosphate dehydrogenase; FBA, fructose-bisphosphate aldolase; PFK, pyrophosphate-dependent phosphofructokinase; TKL, transketolase; RPI, ribose-5-phosphate isomerase; RPE, ribulose-phosphate 3-epimerase; PRK, phosphoribulokinase; GPI, glucose-6-phosphate isomerase; PGM, phosphoglucomutase; UGP, UDP-glucose-pyrophosphorylase; PGAM, phosphoglycerate mutase; ENO, enolase; PK, pyruvate kinase; PPDK, pyruvate phosphate dikinase; PEPC, phosphoenolpyruvate carboxylase; MDH, malate dehydrogenase; PYC, pyruvate carboxylase; PDH, pyruvate dehydrogenase; DLAT, dihydrolipoamide acetyltransferase; DLDH, dihydrolipoamide dehydrogenase; ACLY, ATP-citrate synthase; CS, citrate synthase; ADH, alcohol dehydrogenase; ALDH, aldehyde dehydrogenase; ACS, acetyl-coenzyme synthetase; ACC, acetyl-CoA carboxylase.*

Table 2.2. Significantly differentially expressed genes (DEGs) that appeared in multiple acid-adapted strains under low-pH treatment. LogFC represents the average logarithmic fold change against the wild type (WT) ($p < 0.05$, $n = 3$).

Gene ID	Gene Name	Description	LogFC		
			ALE1	ALE2	ALE3
GO:0009765, GO:0015979 photosynthesis, light harvesting					
Phatr3_J48882	LHCF15	fucoxanthin chlorophyll a/c protein	2.19	1.76	1.29
Phatr3_J30643	LHCF6	fucoxanthin chlorophyll a/c protein	1.37	0.92	0.73
Phatr3_J9799	LHCR3	fucoxanthin chlorophyll a/c protein	1.21	0.88	0.74
Phatr3_J29266	LHCF6	fucoxanthin chlorophyll a/c protein	1.41	0.95	0.71
Phatr3_J17531		fucoxanthin chlorophyll a/c protein	1.18	0.89	1.00
Phatr3_J30648	LHCF5	fucoxanthin-chlorophyll a-c binding protein E	1.56	1.03	1.12
Phatr3_J22680	LHCF13	fucoxanthin chlorophyll a/c protein	0.86	0.72	0.90
Phatr3_J24119		fucoxanthin chlorophyll a/c protein	0.84	0.62	0.78
Phatr3_J54027	LHCR12	fucoxanthin chlorophyll a/c protein	1.04	0.68	0.58
Phatr3_J18049	LHCF1	fucoxanthin chlorophyll a/c protein	1.33	0.90	
Phatr3_J30031	LHCF9	fucoxanthin chlorophyll a/c protein	1.04	0.81	
Phatr3_J25172	FCPB	fucoxanthin-chlorophyll a-c binding protein B	1.06	0.62	
Phatr3_J50705	LHCF4	fucoxanthin-chlorophyll a-c binding protein C	0.84	0.47	2.23

Gene ID	Gene Name	Description	LogFC		
			ALE1	ALE2	ALE3
Phatr3_J25168	LHCF4	fucoxanthin-chlorophyll a-c binding protein C	0.60		1.47
Phatr3_J18180	LHCR7	fucoxanthin chlorophyll a/c protein	-0.70	-0.86	
Phatr3_J23717		ferredoxin--NADP reductase	0.61	1.09	1.48
Phatr3_J33543		electron transport chain	0.71	0.96	1.57
Phatr3_EG02261	PEPC1	phosphoenolpyruvate carboxylase	0.89	0.98	
Phatr3_J27976	PEPC2	phosphoenolpyruvate carboxylase	0.77	0.75	
Phatr3_J21988	PPDK	pyruvate, phosphate dikinase	1.48	1.56	-2.52
Phatr3_J10640	HEMF2	chlorophyll biosynthetic process	-2.83	-5.15	-3.34
Phatr3_J43164		chlorophyll biosynthetic process	-1.36	-1.25	-0.97
Phatr3_J34307		chlorophyll biosynthetic process	-0.82		-2.33
GO:0051453, GO:0006885 regulation of pH					
Phatr3_Jdraft1806	SLC4-2	solute carrier (SLC) bicarbonate transporter	4.70	5.19	2.86
Phatr3_EG02360	SLC4-4	solute carrier (SLC) bicarbonate transporter	1.46	1.87	0.88
Phatr3_J45656	SLC4A_1	solute carrier (SLC) bicarbonate transporter	1.01		1.89

Gene ID	Gene Name	Description	LogFC		
			ALE1	ALE2	ALE3
Phatr3_J1534		solute carrier (SLC) bicarbonate transporter		0.60	0.70
Phatr3_EG02538		solute carrier (SLC) bicarbonate transporter	1.00	1.03	
Phatr3_J44149		proton transmembrane transport	0.71	1.47	-2.09
Phatr3_J50516		proton transmembrane transport	1.39	1.44	1.08
Phatr3_J39274		proton transmembrane transport		0.68	1.05
Phatr3_J14403		sodium/hydrogen exchanger	1.17	2.09	
Phatr3_J48886		sodium/hydrogen exchanger	-1.31	-0.79	-1.94
Phatr3_EG01907		P type ATPase	1.51	1.92	
Phatr3_J16222		P type ATPase	1.29	1.12	
Phatr3_EG02512	ATPSE2	P type ATPase	0.76	-1.01	-1.85
Phatr3_J676		P type ATPase	0.61		-1.36
Phatr3_J47620		P type ATPase		-0.64	-2.32

2.4.4 Genome SNP/Indel analysis.

As differential gene expression underlying the physiological changes in the acid-adapted strains was unraveled, we attempted to mine genetic mutations associated with changes in physiology and genetic regulation. Cell samples from three parallel populations of ALE strains and WT were re-sequenced and compared to the reference genome of *P. tricornutum*. Although monoclonal strains were not isolated in the present study, the data derived from population samples that represent all genetic variants are also significant for revealing a wide pool of mutations that can potentially be responsible for the collective traits of populations [341]. Using the WT as a baseline, 1101, 984, and 1123 SNPs and 157, 173, and 196 indel mutations were identified in ALE1, ALE2, and ALE3 strains, respectively. Most SNPs were present in the coding sequence (CDS) (43.8 $\pm$ 2.5%), upstream (39.9 $\pm$ 0.7%), and

intergenic (12.4 ± 1.4%) regions of genes, while indels mainly occurred in the upstream (70.8 ± 1.8%) and CDS (17.0 ± 3.0%) region (Figure S2.7). Since the results were not obtained from monoclonal samples, all the ALE-unique mutations were identified as heterozygotes, indicating heterogeneity of the ALE populations. As illustrated in Figure S2.7, mutations were widespread in all chromosomes of the genome in ALE strains, while the three independently evolved populations showed evolutionary divergence at many sites as well.

SNP/indel mutations were identified in 390, 350, and 393 genes in ALE1, ALE2, and ALE3, respectively, with 137 genes in common (Figure 2.5A). These results suggested distinct genetic paths for the three ALE-evolved populations under identical stress conditions. GO enrichment analysis revealed that most mutated genes were commonly related to DNA integration, DNA metabolic processes, and sequence-specific DNA binding in all ALE strains (Figure 2.5B). Since microorganisms tend to increase the mutation rate for genetic diversity to survive environmental stress [342], the genotypes for stress-induced mutagenesis were found to be extensively changed under selective pressure. On exploring annotations, 23 mutant genes across all three evolved strains were found to function in transcription regulation (5 genes), metabolic processes (8 genes), and membrane component or transmembrane transportation (10 genes), which may be responsible for altered metabolism and enhanced low-pH resistance in the ALE strains. In particular, five heat shock transcription factors (Phatr3_J44684, Phatr3_J45391, Phatr3_J40994, Phatr3_J49594, and Phatr3_J36499) were identified as containing SNP or Indel mutations in the gene upstream or CDS region.

While mutations in the CDS region of genes can influence the functions of the encoded proteins, mutations in the upstream sequence and the 5'UTR region may affect the expression of the corresponding genes. Further analysis combined with genome and RNA-seq data revealed 65, 26, and 68 mutated genes in ALE1, ALE2, and ALE3, respectively, exhibiting differential expression levels. Specifically, most downregulated mutant genes in ALE strains were related to mobile genetic elements, such as retrotransposon, nucleocapsid, and transposable-element-derived proteins (PGBDs), that could facilitate genome remodeling. These mutations may be responsible for the inactive DNA recombination detected using transcriptomics, suggesting an adaptation in ALE strains after long-term ALE. However, none of the mutated genes with upstream intergenic mutations were associated with DEGs related to acid-tolerant physiological changes.

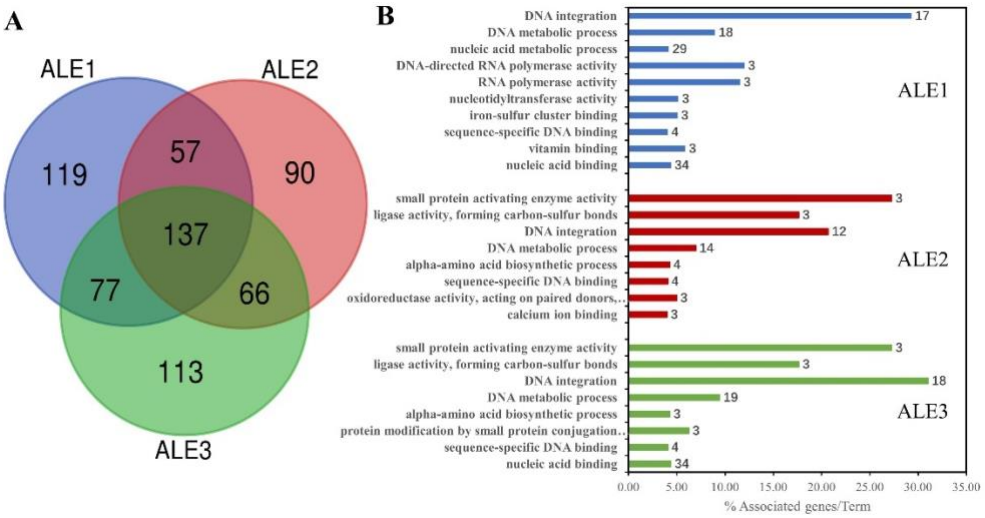

Figure 2.5. *Independent evolution of the three adaptive laboratory evolution (ALE) populations. (A) Venn diagram indicating the comparison of mutant genes among ALE strains. (B) Enrichment analysis on mutant genes present in different strains. Columns represent percentages of associated genes (x-axis) for each term, and labels present the number of genes grouped based on gene ontology (GO) terms.*

2.4.5 Implications, limitations, and recommendations

The present study based on transcriptomics and genomics contributes to understanding adaptive mechanisms in a model diatom under long-term acidic stress, and also to identifying and determining crucial genes responsible for acidic stress resistance, which is important for developing feasible diatom strains for efficient biofixation of flue gas CO_2. Specifically, there are three implications as follows. (1) Due to the crucial role of diatoms as primary producers, understanding their long-term response to changing environments such as ocean acidification is meaningful for assessing the impacts of human activities on ecosystems. (2) These findings could provide valuable information for further reverse genetic study on functions of particular genes in acidic stress responses. (3) Transcriptomics-guided design may efficiently facilitate the engineering of microalgae for biotechnological applications, which could pave the way for the direct utilization of high-CO_2 flue gas by diatoms to achieve carbon neutrality. These dual values on technological development and science are significant for achieving United Nations Sustainable Development Goals (UNSDGs) concerning food and energy security (SDGs 2 and 7) as well as climate action and ocean ecosystem (SDGs 13 and 14).

As a primary goal of this study, the ALE process was designed to achieve evolved diatom strains with improved acidic tolerance and high biomass production. Indeed, the adapted strains exhibited significantly improved growth in a normally prohibiting condition, which demonstrated enhanced low-pH tolerance of *P. tricornutum* after long-term adaptation. However, the recovery of growth after ALE is still limited under the low-pH stress conditions compared to the growth rate under standard conditions at pH 8, which implied the limitation of stress-driven adaptation. Further, the identified DEGs that were potentially associated with the stress-tolerant phenotype in the evolved strains should be investigated through reverse genetics and

synthetic biology approaches may be used to engineer and achieve desired diatom strains with acidic stress tolerance more efficiently.

Compared to green microalgae such as *Chlorella*, *Desmodesmus*, and *Scenedesmus* sp. that were often found tolerant to industrial flue gas [294, 298], *P. tricornutum* as a representative of marine diatoms seems fundamentally intolerant to acidic conditions due to its genomic background that has been evolved to adapt to its natural oceanic habitats [299]. Therefore, future work is also recommended to research comparative genomics of low-pH tolerant and intolerant microalgal species for a better understanding of gene regulation networks during evolution under specific environments.

2.5 Conclusion

In this study, we conducted evolutionary engineering for acidic resistance in the model marine diatom *P. tricornutum* and thoroughly examined the physiology and molecular features of the evolved strains. Based on the novel phenotypic traits of three parallel ALE strains, our transcriptomic results highlighted a generic evolutionary path for upregulating photosynthesis, ion transport, and carbohydrate and fatty acid metabolism in the acid-adapted strains.

2.6 Supplementary materials

Table S2.1. Summary of transcriptome data set for different strains under acidic stress.

Sample	Clean Bases	Q30	GC content	Total mapped reads
WTa	5.83G	94.46%	51.96%	39800009 (95.75%)
WTb	6.05G	94.58%	51.89%	41245257 (95.76%)
WTc	5.92G	94.50%	51.77%	40469885 (95.52%)
ALE1a	6.50G	94.42%	52.05%	44042455 (94.74%)
ALE1b	5.78G	94.61%	52.16%	39291679 (95.24%)
ALE1c	6.87G	93.69%	51.83%	46109069 (94.53%)
ALE2a	6.95G	94.00%	51.87%	46871115 (95.46%)
ALE2b	6.54G	93.86%	51.89%	44204393 (95.56%)
ALE2c	6.69G	93.83%	51.92%	45308436 (95.60%)
ALE3a	6.68G	93.96%	51.94%	45343670 (95.83%)
ALE3b	6.84G	93.84%	51.88%	46718320 (95.67%)
ALE3c	6.50G	93.84%	51.85%	44339693 (95.78%)

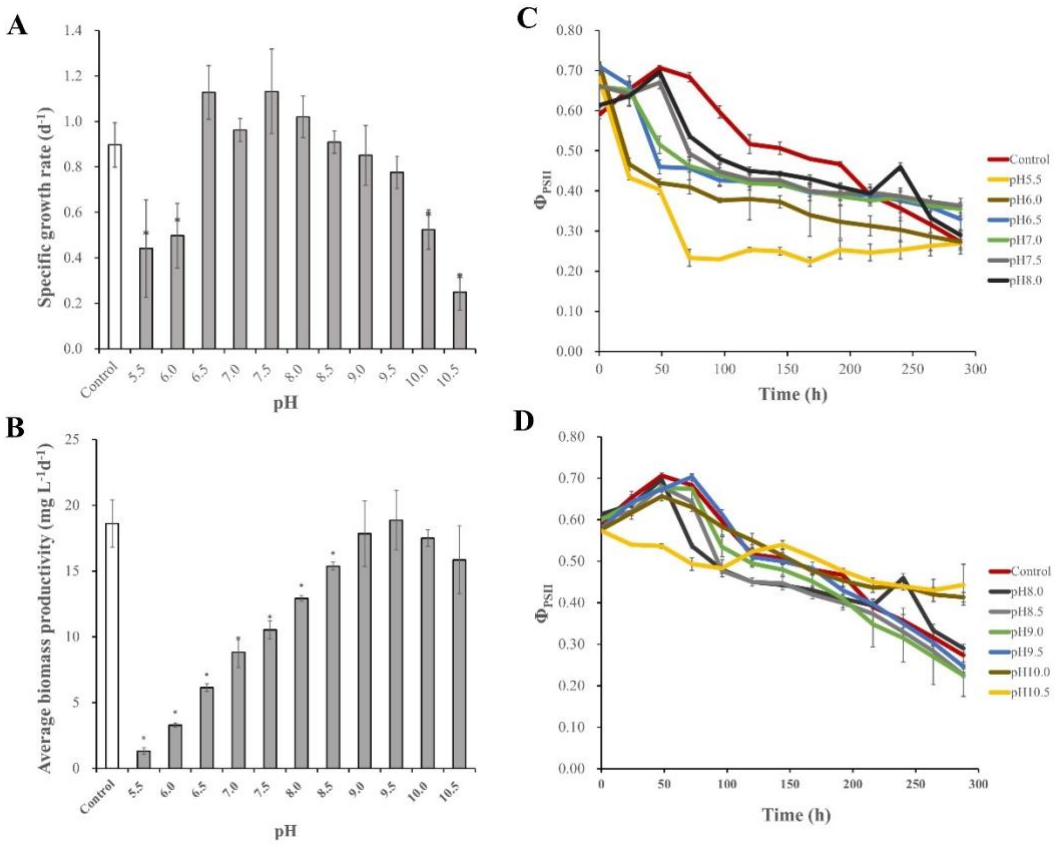

Figure S2.1. *Effects of pH on growth and photosynthesis in P. tricornutum. (A) Maximal specific growth rate. (B) Average biomass productivity. (C) Effective quantum yield (pH 5.5 – 8.0). (D) Effective quantum yield (pH 8.0 – 10.5). In experimental groups, the pH settings were controlled using buffers. The control group was cultured in a non-buffered regular f/2 medium. Values are shown as mean* $\pm$ ***SD*** *(n = 3). The label (*) indicates a significant difference ($p<0.05$) between the experimental group and the control group.*

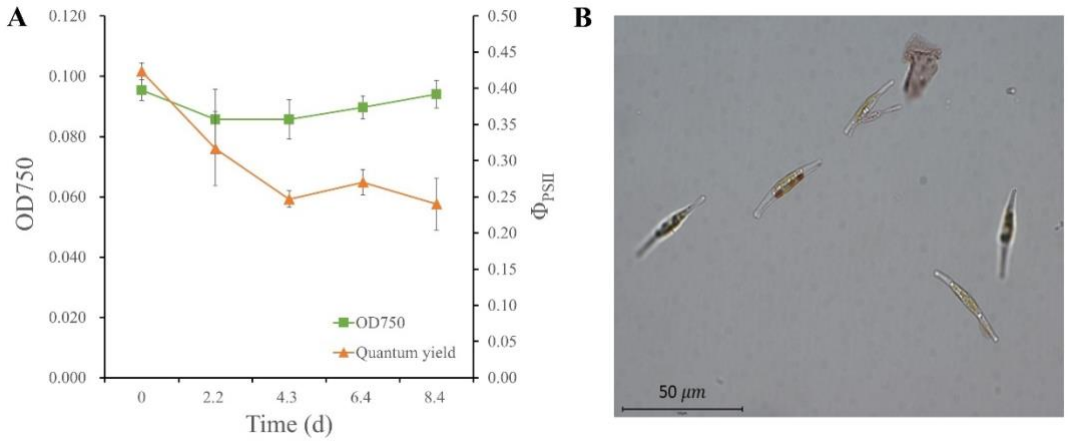

Figure S2.2. *Growth and cell viability at pH 5.0. (A) growth performance parameters, optical density at 750 nm (OD_{750}), and quantum yield in a time course over 8-day cultivation. (B) representative image of cell status under pH 5.0 condition (400 x magnification, live cell stained by 0.3% neutral red). Values are shown as mean* $\pm$ ***SD*** *(n = 3).*

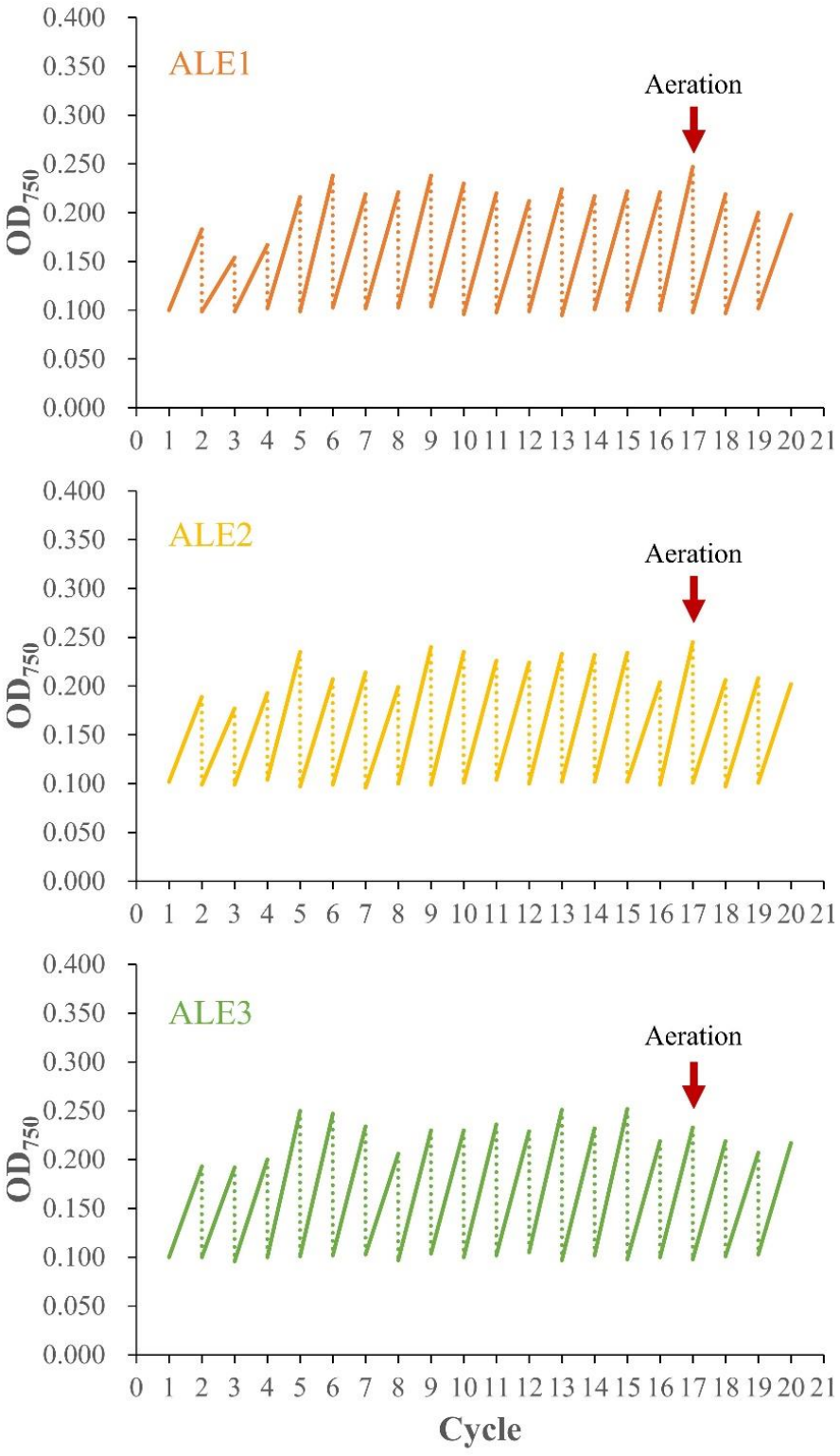

Figure S2.3. *Changes of cell optical density during the adaptive laboratory evolution process. Sixteen 5-day cycles were conducted for three parallel P. tricornutum populations (ALE1, ALE2, and AL3) derived from the same parental culture (with a volume of 75 ml for each flask culture). While initial cell density was adjusted to* OD_{750} *= 0.100±0.005,* OD_{750} *was measured at the end of each cycle. Aeration at a rate of 0.3 vvm was applied after the 16th cycle.*

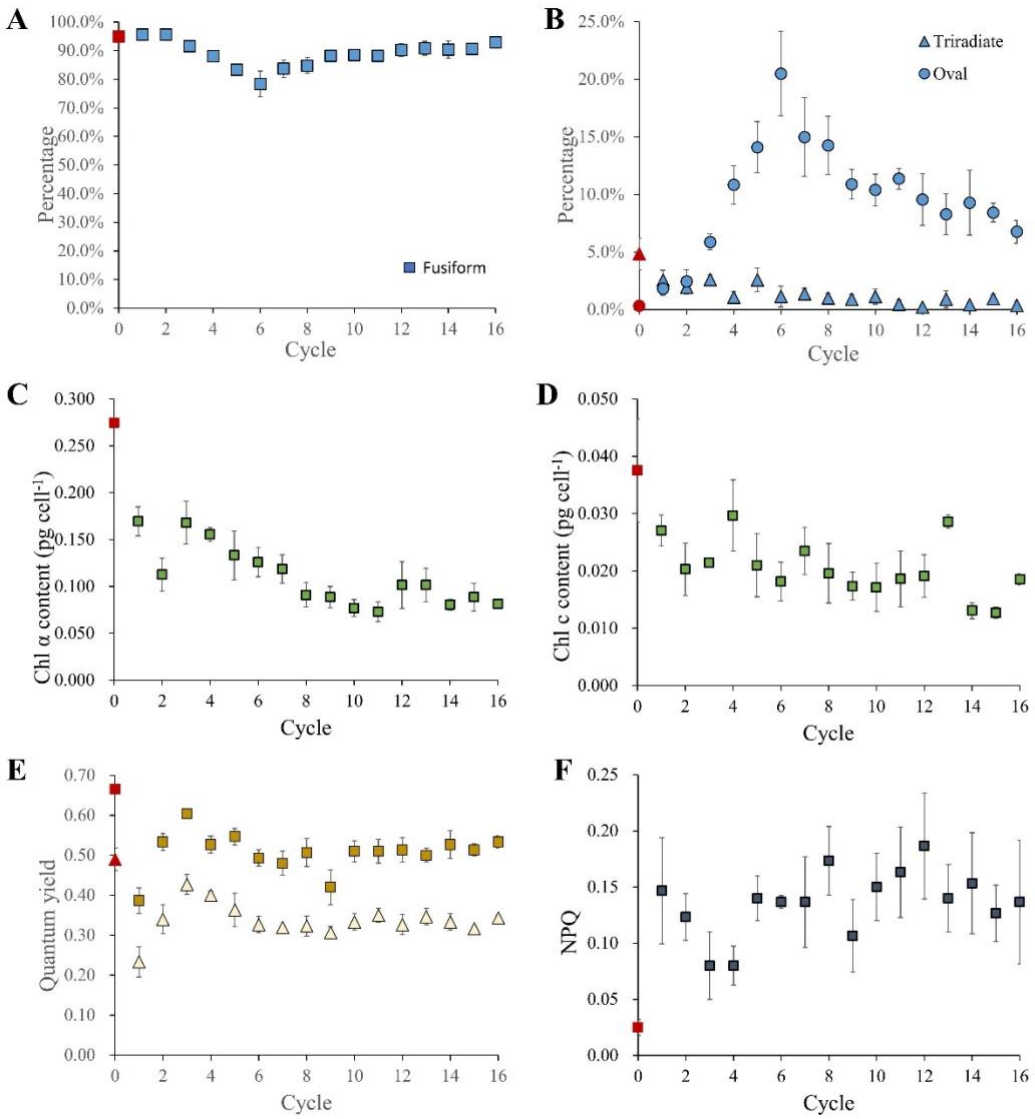

Figure S2.4. *Physiological data during adaptive laboratory evolution (ALE). (A) relative percentage of fusiform morphotype. (B) relative percentage of triradiate & oval morphotype. (C) chlorophyll a content. (D) chlorophyll c content. (E) quantum yields. (F) non-photochemical quenching (NPQ). Chlorophylls were measured by spectrophotometry assay and estimated using a picogram per cell. In C, maximum and effective quantum yields are denoted as square and triangle, respectively. Values are shown as mean* $\pm$ ***SD*** *(n = 3). Data for cultures before starting ALE (cycle 1) were illustrated in red as cycle 0.*

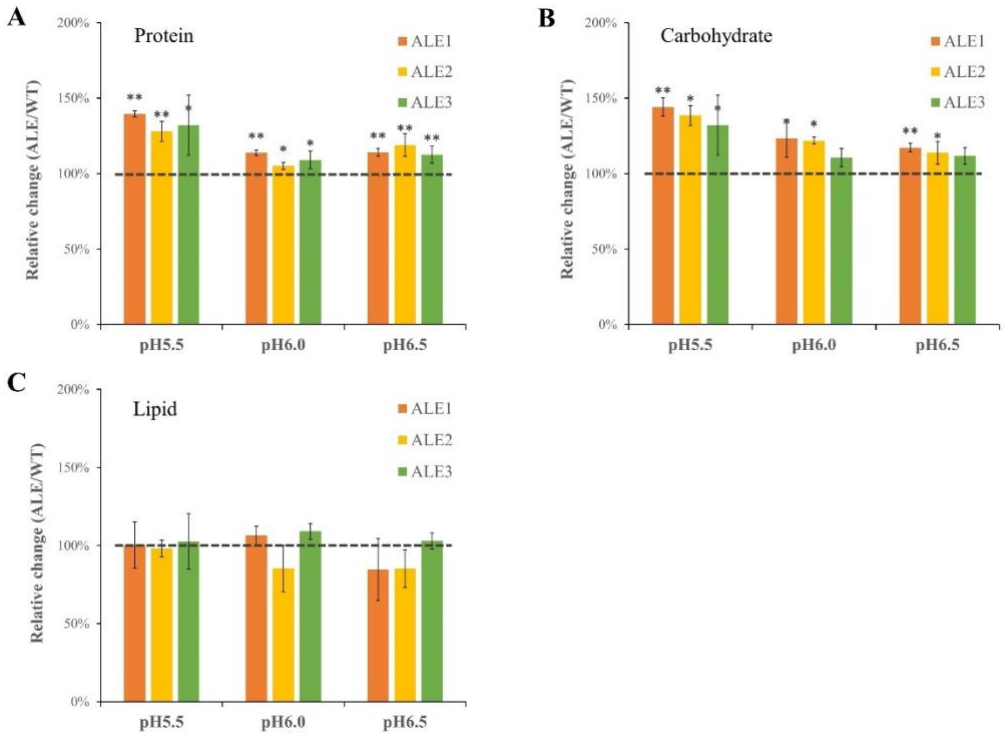

Figure S2.5. *Relative changes in macromolecule contents comparing the adaptive laboratory evolution (ALE) and the wild-type (WT) strains under acidic treatments. (A) protein. (B) carbohydrate. (C) lipid. Results were obtained from two repeated experiments with duplicates (dash line indicates ALE/WT = 1). Values are shown as mean ± SD (n = 4). (* $p < 0.05$, ** $p < 0.01$).*

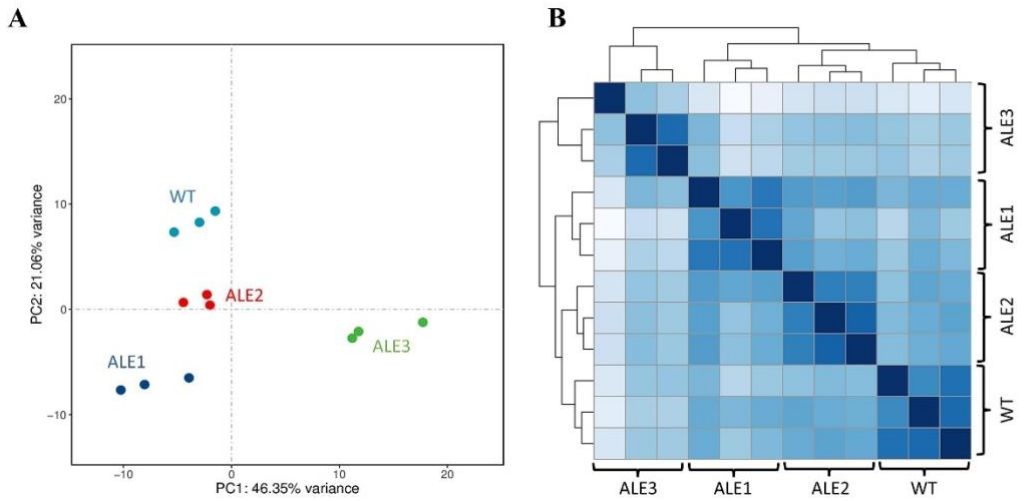

Figure S2.6. *Principal component analysis (PCA) and heat map of correlation analysis. (A) PCA results. (B) Heat map of correlation analysis.*

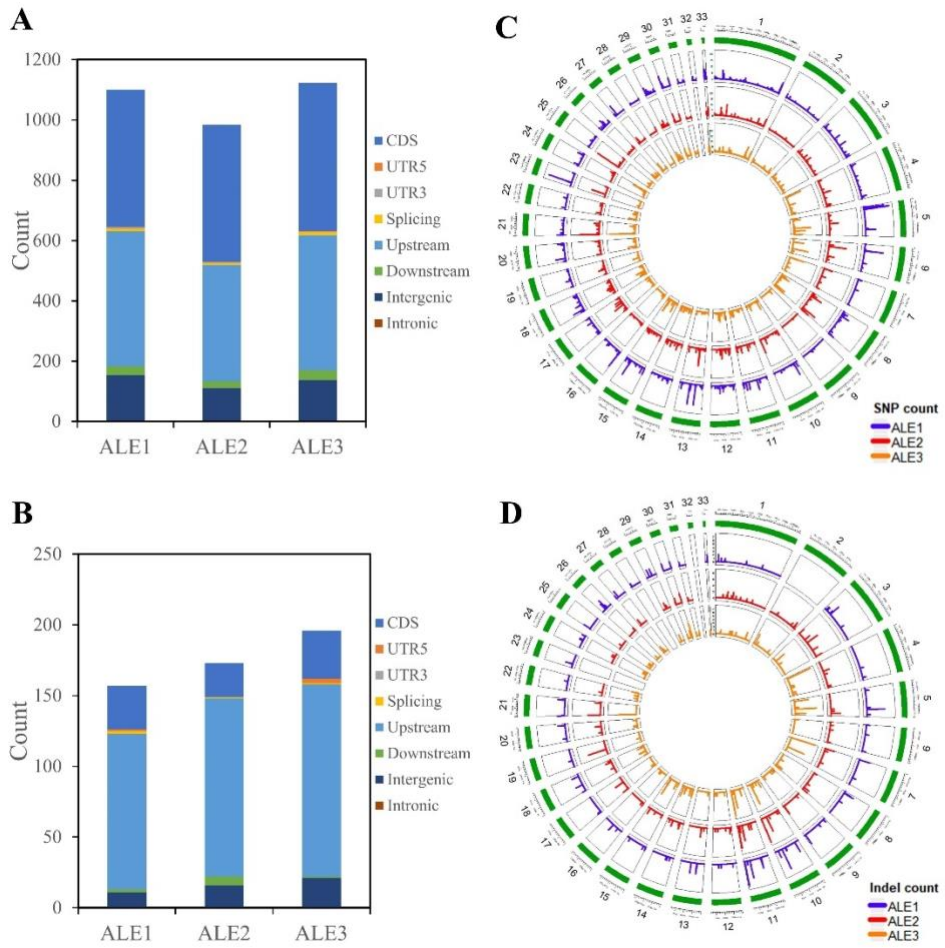

Figure S2.7. *Whole-genome re-sequencing analysis of adaptive laboratory evolution (ALE) strains. Distribution of mutations in different genic regions. (A) SNPs. (B) Indels. The density of mutations across chromosomes of P. tricornutum. (C) SNPs. (D) Indels. CDS, coding sequence; UTR, untranslated region.*

3 Manipulation of ion/electron carrier genes in the model diatom *Phaeodactylum tricornutum* enables its fast growth under acidic stress

Yixi Su[1,2], Jiwei Chen[1], Jingyan Hu[1], Chen Qian[1], JiaHao Ma[1], Sigurður Brynjolfsson[2], Weiqi Fu[1, 2*]

[1] Ocean College, Zhejiang University, Zhoushan, 316021, Zhejiang, China

[2] Center for Systems Biology and Faculty of Industrial Engineering, School of Engineering and Natural Sciences, University of Iceland, Reykjavík 101, Iceland

(*Corresponding Author)

Keywords: CO_2 mitigation, pH stress, diatoms, algal biotechnology, genetic engineering

3.1 Abstract

The growing concerns about climate change due to CO_2 emission have urged the demand for developing microalgal biotechnology to convert CO_2 into value-added products. The major obstacle to exploiting industrial flue gas in microalgae cultivation is the adverse acidic environment, i.e., low pH that suppresses algal growth. We previously identified three outstandingly upregulated genes of potential ion/electron carrier in the low-pH adapted model diatom *Phaeodactylum tricornutum*, namely ferredoxin (PtFDX), cation/proton antiporter (PtCPA), and HCO_3^- transporter (PtSCL4-2). In this study, we individually manipulate these genes in *P. tricornutum* by constructing overexpression strains to investigate their roles in acidic stress (pH 5.0) resistance. The genetic modifications enabled positive growths of transgenic strains under acidic stress that completely inhibited the growth of the wild-type strain. Further physiological study indicated improved photosynthetic function and reduced oxidative stress in the transgenic strains. While PtFDX could alleviate intracellular oxidative stress by facilitating the distribution of electron flow, overexpressing PtCPA and PtSCL4-2 led to broadly elevated expression of various transmembrane transporters that could aid in resisting excessive external protons, thereby preventing the generation of excessive reactive oxygen species (ROS) to suppress cell growth. The present work demonstrated the critical role of ion/electron carrier genes in diatom resistance to acidic stress, deepening the understanding of phytoplankton adaptation to ocean acidification. The developed engineering strategy confers diatom carbon fixation capability under low-pH stress, which could facilitate the initiatives for biological carbon capture and utilization of industrial flue gas CO_2.

3.2 Introduction

The Intergovernmental Panel on Climate Change (IPCC, the United Nations body for assessing the science related to climate change) has found that carbon dioxide (CO_2) missions due to the consumption of fossil fuels play a dominantly important role in causing global warming [3]. In this context, algal biotechnology driven by the need to reduce CO_2 footprint can benefit various sectors such as environment management and the production of renewable fuel, food, and chemicals for a sustainable bioeconomy [343]. To maximize economic profit while mitigating CO_2 emission, incorporating microalgae production into greenhouse gas (GHG) emitting industries is desired to create value-added products from untapped carbon in industrial flue gas. However, challenges caused by flue gas such as inhibitory acidic pH on algal growth must be tackled prior to microalgae-based manufacturing [299]. Apart from various efforts on process optimization for alleviating stresses in cultivation [291, 344], strain improvement strategies including random mutagenesis [126], adaptive laboratory evolution (ALE) [190, 191] and genetic engineering [297] have been employed to enhance microalgae productivity under unfavorable environments. For instance, chemical mutagenesis followed by stress exposure was applied to generate *Chlorella* mutants with improved thermotolerance [345] and alkali tolerance [346]. Through ALE, high-CO_2 tolerant *Chlorella* sp. [290], thermotolerant *Picochlorum* sp. [204], and low-pH tolerant *Phaeodactylum tricornutum* [347] were obtained showing increased growths in stressful conditions. Moreover, *Chlamydomonas reinhardtii* was genetically modified to overexpress a heterologous pyrroline-5-carboxylate synthetase to increase the intracellular proline level for better tolerance against toxic heavy metals [348]. The introduction of green alga plastocyanin that provided redox alternative couples was reported to improve the growth of *P. tricornutum* in iron deficient conditions [270]. A recent study [273] modified fatty acid compositions in *P. tricornutum* by overexpressing a 3-oxoacyl acyl carrier protein reductase, which led to enhanced thermotolerance in the transgenic strains.

P. tricornutum is a model species of marine diatoms featured by efficient photosynthetic conversion of inorganic CO_2 into biomass and high yields of lipids, carotenoids, and protein, which make it a promising cellular factory [349]. In addition to the published genomic sequence [211], molecular techniques for transformation, as well as gene overexpression, silencing, and knockout, have been well-established for *P. tricornutum*, which facilitates rational engineering design for desired traits and reverse genetic study on gene functions [350]. In the past decades, metabolic networks of *P. tricornutum* have been extensively studied for optimizing carbon fluxes to increase accumulation of particular metabolites, especially lipids and carotenoids [251, 262, 267], while a few efforts aimed at increasing biomass production by manipulating the C4 pathway and pyruvate transportation [246, 271]. One recent study reported the enhancement of the pH tolerance of *C. reinhardtii* by overexpressing an H^+-ATPase pump [297]. However, research on genetic manipulation to improve microalgal growth under environmental stress has been obscure.

To investigate the acidic stress that is likely to be encountered in industrial production with flue gas as well as ocean acidification, we previously applied ALE to domesticate low-pH tolerant strains of *P. tricornutum* and studied their adaptive

responses to acidic stimulus in long-term semi-continuous cultivation [347]. Common differentially expressed genes (DEGs) were identified in three parallelly evolved cultures, which suggested the importance of photosynthetic electron transport chain, proton transporters, and bicarbonate transporters in acidic tolerance[347]. More specifically, substantial upregulation of three genes with gene identifiers (IDs) of Phatr3_J33543, Phatr3_J50516, and Phatr3_Jdraft1806 was identified in all low-pH-adapted cultures. Based on conserved polypeptide domains, Phartr3_J33543 and Phatr3_J50516 are predicted proteins that presumably perform electron transfer activity and solute: proton antiporter activity, respectively. Phatr3_Jdraft1806 was previously identified as a solute carrier 4 (SLC4) gene responsible for HCO_3^- transport[351].

The ion/electron carrier genes and their products are likely to impact cellular proton homeostasis, making potential contributions to pH adaptation in diatoms. In photosynthesis, harvested light energy is converted into chemical energy via electron transport chains (ETC). Ferredoxins (FDXs) containing an [2Fe-2S] active center are the soluble electron transport proteins that mediate linear electron transfer (LET) and cyclic electron transfer (CET), which generate proton gradients across the thylakoid membrane to drive adenosine triphosphate (ATP) synthesis[352]. Additionally, FDXs can transfer the excessive electrons from photosynthesis to other metabolic processes such as carbon and nitrogen assimilation, thereby facilitating microalgal growth. Overexpressing FDXs was demonstrated to decrease cellular reactive oxygen species (ROS) levels and enhance stress tolerance in green microalgae[353, 354]. Moreover, the product of Phatr3_J50516 containing a cation/proton antiporter (CPA) domain is expected to directly control pH homeostasis and concentrations of cation ions such as K^+, Na^+, and Ca^{2+}, which could indirectly participate regulation of photosynthesis, protein metabolism and stress responses[355]. For instance, the thylakoid membrane-localized K^+ exchange antiporter 3 (KEA3) in Arabidopsis is responsible for proton translocation between lumen and stroma to reduce non-photochemical quenching (NPQ) and thus allows high photosynthetic efficiency[356]. Finally, SLC4 involving a CO_2-concentrating mechanism (CCM) is important for diatoms to adapt to low-carbon availability environments. Not only does HCO_3^- uptake help regulation of pH homeostasis by providing buffering capacity against acidified conditions but also enhances carbon concentrating in a low-pH environment where total dissolved inorganic carbon (DIC) is reduced [58]. Although PtSLC4-2 and its paralogs (PtSLC4-1 and PtSLC4-4) have been well characterized for their localization and catalytic properties[351, 357], it remains unclear how these bicarbonate transporters affect low-pH tolerance in microalgae.

Here we investigated the potential roles of three ion/electron carrier genes (Phatr3_J33543, Phatr3_J50516, and Phatr3_Jdraft1806) in the model diatom *P. tricornutum* involved in low-pH adaptation through the construction of transgenic strains and their physiological and transcriptomic profile shift. Furthermore, this is the first attempt to rationally engineer diatoms to enable cell growth and carbon fixation under inhibitory acidic stress, which could provide critical insights into gene regulations involved in microalgal response to acidic stress as well as ocean acidification.

3.3 Methods

3.3.1 Strain and culture conditions

Axenic culture of marine diatom *Phaeodactylum tricornutum* (CCAP 1055/1) was purchased from the Culture Collection of Algae and Protozoa (CCAP), Scotland, UK. The inoculum was grown in enriched artificial seawater (EASW) [358] at 22 ± 1 °C under continuous illumination of red/blue (50:50) LED with a light intensity of 40 μmol m^{-2} s^{-1}. The EASW medium was supplemented with 40 mM Tris-HCl to maintain the pH of the media at 8.0. For low-pH treatments, 40 mM MES (2-N-morpholinoethane-sulfonic acid) buffer was applied to control the acidic pH range. Additionally, the medium was supplemented with ampicillin (100 μg mL^{-1}), kanamycin (100 μg mL^{-1}), and streptomycin (100 μg mL^{-1}) and sterilized by filtration using a 0.22 μm membrane filter (S-PAK, Millipore, US) to avoid bacterial contamination.

3.3.2 Expression vector construction, electroporation, and transformant screening

Target genes, Phatr3_J33543 (FDX), Phatr3_J50516 (CPA), and Phatr3_Jdraft1806 (PtSLC4-2) are 780 bp, 2588 bp, and 1913 bp of nucleotides in length, respectively. Their coding sequences (CDS) and amino acid sequences were retrieved from the European Molecular Biology Laboratory (EMBL) database. Homologous proteins were searched against the NCBI server (http://www.ncbi.nlm.nih.gov/) and filtered for > 40% identity. Phylogenetic trees were constructed based on corresponding amino acid sequences using MEGA11 by the Maximum Likelihood algorithm. The conserved domains of each protein were identified using the NCBI CD-search tool.

The transgenic proteins (minus the stop codon) were fused to an enhanced green fluorescence protein (EGFP) at its N-terminus through a 5 × glycine linker (Figure 3.1A). The recombinant gene constructs were codon-optimized and artificially synthesized (Sangon Biotech Co. Ltd., China) and cloned into the multiple cloning sites of pPhaNR plasmid (NCBI accession: JN180663.1) under the control of the nitrate reductase promoter. After linearization by digestion at the NdeI restriction site, the overexpression vectors were introduced into diatom cells through electroporation according to a published protocol[238]. Following transformation, cells were spread onto EASW solid plates (1% w/v, agar) containing 100 μg mL^{-1} Zeocin (Invitrogen, US). In approximately three to four weeks visible colonies on the selective plates were transferred into liquid media containing Zeocin (100 μg mL^{-1}) and subcultured twice in microplates. Nitrate in the ESAW medium was enriched (4.4 mM) to ensure constitutively active expression of the transgenes. Successful transformants were initially screened by detecting EGFP signals against the wild-type (WT) strain using a microplate reader (BioTek, US), which was confirmed by observing green fluorescence under a microscope. Three transformants with strong fluorescent signals (one for each transgene), denoted as HI3310, HI5021, and HI1831 for Phatr3_J33543, Phatr3_J50516 and Phatr3_Jdraft1806, respectively were selected for the following phenotype characterization.

3.3.3 Molecular characterization of the selected transformants

The presence of the target genes in the transformants was validated by genomic PCR amplifying the non-native recombinant fragments of the transgenic constructs (Figure 3.1A). Genomic DNA of transgenic strains was extracted using an HP Plant DNA Kit (Omega, USA) and subsequently used as the templates in genomic PCR using the primer pairs listed in Table S3.1. Green fluorescence was detected by a microplate reader (BioTek, US) and fluorescent microscope at the excitation wavelength (λ_{ex}) of 488 nm and emission wavelength (λ_{em}) of 525 nm.

3.3.4 Growth and photosynthesis performances

Growths of the transformants (HI3310, HI5021, and HI1831) were characterized in comparison with the WT strain by batch cultivation in flasks (250 mL) with 100 mL working volume. Three biological replicates were conducted for all growth experiments. Optimal growths of different strains were determined in the regular ESAW medium (pH 8.0), followed by low-pH treatment. For the transfer, cells in the exponential growth phase were pelleted by centrifugation at 1500 × g for 10 min (15 ℃) and washed once using acidic media (at pH 5.5 and pH 5.0, respectively). Then, cells were centrifuged again and resuspended into the corresponding buffered fresh ESAW media. The initial optical density (OD_{750}) of each group was adjusted to 0.050 ± 0.005.

Cell growth was monitored by measuring OD_{750} using a spectrophotometer (DR3900, Hach, US). The specific growth rate (μ, d^{-1}) was calculated using the following equation:

$$\mu = (\mathrm{In}X_t - \mathrm{In}X_0)/(t - t_0)$$

where X_t and X_0 are the OD at time t and the beginning of the time interval (t_0), respectively. Biomass dry weight (DW) was estimated based on an established correlation (Appendix A, Figure A2) between OD_{750} and DW (mg mL^{-1}) as follows:

$$\mathrm{DW} = 0.4877 \times \mathrm{OD}_{750}\ (R^2 = 0.999)$$

For chlorophyll fluorescence determination, a 3 mL culture was incubated in the dark for 15 min. Photosynthetic parameters including maximum quantum yield (F_v/F_m), effective quantum yield (Φ_{PSII}), and NPQ were measured with an AquaPen-C AP110 fluorometer (Photon Systems Instruments, Czech Republic) using the built-in program (non-photochemical quenching (NPQ) protocol 3).

3.3.5 Stress assessment

Intracellular ROS level was determined using the 2', 7'-dichlorofluorescen diacetate (DCFH-DA) fluorescent probe. For each assay, an aliquot of 2μL DHCF-DA was added to a 200 μL cell sample (final concentration: 10 μM) and incubated at 37℃ for 20 min in dark. Fluorescence at λ_{ex} = 488 nm and λ_{em} = 525 nm was measured with a microplate reader (BioTek, US). The results were presented as the ratio of

fluorescence intensity at 525 nm normalized to cell density (OD_{750}) compared to the WT in control.

3.3.6 RNA extraction and library construction

Total RNA was extracted using the TRIzol reagent (Invitrogen, CA, USA) according to the manufacturer's protocol. RNA purity and quantification were evaluated using the NanoDrop 2000 spectrophotometer (Thermo Scientific, USA). RNA integrity was assessed using the Agilent 2100 Bioanalyzer (Agilent Technologies, Santa Clara, CA, USA). Then the libraries were prepared using VAHTS Universal V6 RNA-seq Library Prep Kit according to the manufacturer's instructions.

3.3.7 RNA sequencing and transcriptomic analysis

The transcriptome sequencing was conducted by OE Biotech Co., Ltd. (Shanghai, China) based on the Illumina Novaseq 6000 platform, generating 150 bp paired-end reads. After trimming by fastp [316], the resulted clean reads data with > 90% Q30 were mapped to the reference genome using Hisat2 [313]. Following reads assembly by StringTie2 [359], gene structure extension and novel transcripts identification were performed by comparing the reference genome and the known annotated genes using Cuffcompare software. Fragments per kilobase of exon per million mapped fragments (FPKM) and read counts of each transcript (protein-coding gene) were calculated using HTSeq-count [360].

By comparing transcriptomes from low-pH treatment/control for each strain and transgenic strains/WT at 0 h and 24 h timepoints, differentially expressed genes (DEGs) were identified using the DESeq (2012) R package. The thresholds with adjusted p-value < 0.05 and $|Log_2FoldChange| \geq 1$ were set for determining significant expression. Based on the hypergeometric distribution, Gene ontology (GO) enrichment analysis of DEGs was performed to reveal the significant enriched term (Padj < 0.05) using the g:Profiler web server[361].

3.3.8 Statistical analysis

All the growth, biochemical and molecular data of transgenic strains were compared to those of the WT. Statistical analyses were performed using a two-tailed Student's t-test on Microsoft Excel. All data were obtained from three independent biological replicates and reported as means ± standard deviation (n = 3).

3.4 Results

3.4.1 Construction of transgenic *P. tricornutum*

Based on our previous study, the expression of three genes (Phatr3_J33543, Phatr3_J50516, and Phatr3_Jdraft1806) was outstandingly enhanced (1.6 to 36.5-fold compared to corresponding genes in the WT) in all the evolved strains that had been acclimated in acidic conditions. The Phatr3_J33543 protein contains an FDX and a PDZ domain. Phylogenetic analysis indicated that the FDX is widely conserved in diatoms and cyanobacteria, but the PDZ domain is only present in diatoms (Figure S3.1). Furthermore, the proteins encoded by Phatr3_J50516 and Phatr3_Jdraft1806 contain conserved domains across diatom species (Figure S3.1).

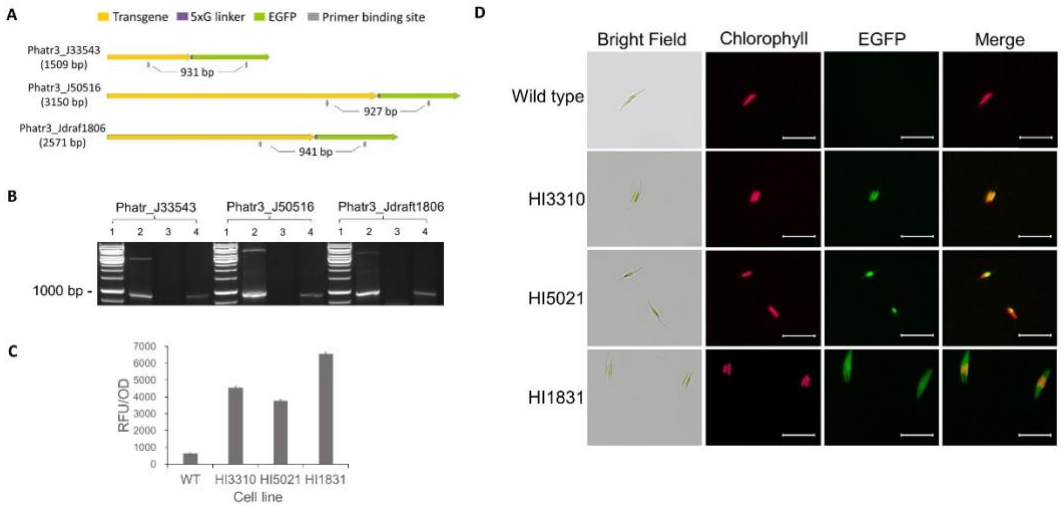

Figure 3.1. *Construction of transgenic P. tricornutum overexpressing recombinant genes. (A) Recombinant gene constructs. (B) PCR analysis of the recombinant gene using genomic DNA as a template. For each transgene::EGFP fusion, lane 1, ladder; lane 2, plasmid (positive control); lane 3, WT; lane 4, transgenic strain. (C) Detection of green fluorescence intensity (excitation wavelength of 488 nm and emission wavelength of 525 nm). RFU, relative fluorescence unit. (D) Fluorescence microscopic image (scale bar indicates 20 μm).*

The present study attempted to overexpress these genes in *P. tricornutum* to investigate their roles in low-pH tolerance. The coding sequence of each gene was tagged with an EGFP gene (Figure 3.1A). Multiple transgenic lines were obtained for each construct and further selection was based on green fluorescence intensity against the WT. Three lines (clone#10 for Phatr3_J33543, clone#21 for Phatr3_J50516, clone#31 for Phatr3_Jdraft1806) exhibiting the strongest EGFP signal, denoted as HI3310, HI5021, and HI1831, respectively were selected for further characterization.

The presence of recombinant genes in transgenics was determined by genomic PCR amplifying a fragment spanning the transgene::EGFP fusion (Figure 1B). Successful expression of recombinant proteins in the transgenic strains was confirmed by detecting their green fluorescence signals which were 5 to10-fold of that in the WT (Figure 3.1C). By visualizing EGFP using a fluorescent microscope (Figure 3.1D), the recombinant proteins were observed in different organelles of the cell. Specifically, the PtFDX encoded by Phatr3_J33543 was expressed in the entire

chloroplast, while the proton transporter encoded by Phatr3_J50516 was only present in a small compartment inside the chloroplast. For PtSLC4-2 encoded by Phatr3_Jdraft1806, EGFP spread in the cytosol but was intensified at the plasma membrane as previously reported[351].

3.4.2 Growth rate and photosynthetic efficiency at inhibitory pH

The selected HI3310, HI5021, and HI1831 transformants were subjected to growth experiments at pH 8.0 (control), pH 5.5, and pH 5.0. All experiments resulted in the maximal specific rates at 24 h (Figure 3.2). At a favorable pH for diatom growth (pH 8.0), the growth rates of all tested strains were comparable, though HI1831 exhibited a slightly higher maximal growth rate than the WT ($p < 0.05$) (Figure 3.2). The promotive effect of overexpressing PtSLC4-2 on DIC uptake and photosynthesis[351] could explain the phenomenon of a slight increase in the growth of HI1831. At pH 5.5, *P. tricornutum* was still capable of growing with a 6–20% reduction in growth rates on the first day. Significant differences between transgenic strains and the WT were observed at pH 5.0 with a clear inhibition on the growth of WT. By contrast to the dying WT, all three transformants showed positive growths at 24 h, though the low-pH stress caused 73.8%, 39.9%, and 49.6% reduction in maximal growth rate in HI3310, HI5021, and HI1831, respectively (Figure 3.2). While HI3310 declined after 24 h, cell densities of HI5021 and HI1831 were maintained without significant changes in the following four days (Figure S3.2).

At pH 8.0, photosynthetic parameters in the WT and transformants showed similar trends (Figure 3.3). The maximal quantum yield (Fv/Fm) remained at a high level (> 0.6) throughout the cultivation, which suggests a non-stressed environment. While Φ_{PSII} peaked at 24 h and declined afterward, the non-photochemical quenching (NPQ) parameter increased gradually from 48 h until the end of the experiment. These results suggest that photosynthetic efficiency decreased with the growth of cell density, probably due to the shading effect where the proportion of harvested energy used for biomass growth declined with the increasing energy dissipation as heat and fluorescence. Upon transfer into the pH 5.0 media, Fv/Fm in all three transgenic strains dramatically dropped in 24 h, as a sign of inhibition on photosynthesis due to the serious acidic stress. Nevertheless, the Fv/Fm values in transformants were significantly higher than those in the WT ($p < 0.05$), suggesting a relatively reduced stress in reflection of survival of transgenic strains under low-pH conditions. In similar trends, Φ_{PSII} decreased to extremely low levels correlating to ceased growths in all cultures. Interestingly, the NPQ in WT was maintained at a relatively low level throughout the cultivation, but this parameter in transgenic strains substantially increased after 24 h and then decreased to a comparative level as the WT.

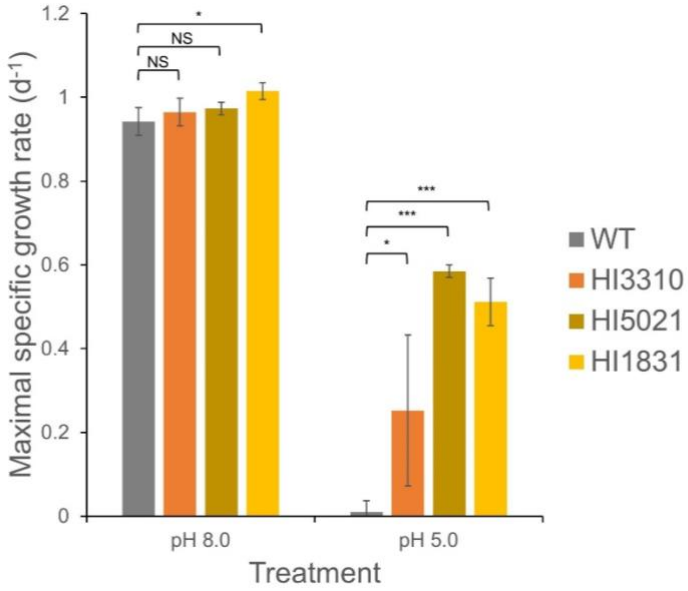

Figure 3.2. *Growth characterization of different strains under low-pH treatments. Different strains were cultivated at pH 8.0 in identical conditions (40 µmol m^{-2} s^{-1} red/blue LED, 22 ± 1 ℃) for 5 days and then transferred into acidic EASW media (pH 5.0) for the low-pH treatments. HI3310, HI5021 and HI1831 are genetically modified strains with overexpressed ferredoxin (Phatr3_J33543), cation/proton antiporter (Phatr3_J50516), and bicarbonate transporter (Phatr3_Jdraft1806). The error bar shows the standard deviation (n=3). (NS, p > 0.05; *p<0.05; **p<0.01; ***p<0.001)*

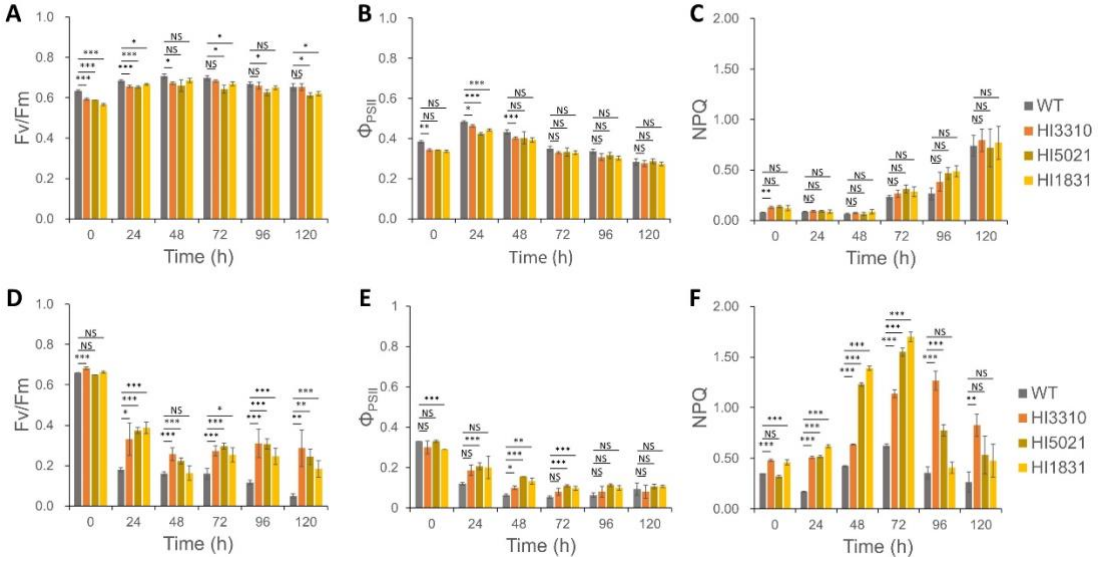

Figure 3.3. *Effects of low-pH treatment on photosynthetic performance in different strains. Different strains were cultivated at pH 8.0 in identical conditions (40 µmol m^{-2} s^{-1} red/blue LED, 22 ± 1 ℃) for 5 days and then transferred into acidic EASW media (pH 5.0). HI3310, HI5021, and HI1831 are genetically modified strains with overexpressed ferredoxin (Phatr3_J33543), cation/proton antiporter (Phatr3_J50516), and bicarbonate transporter (Phatr3_Jdraft1806). (A – C) Photosynthetic parameters at pH 8.0 (A) Fv/Fm, (B) Φ_{PSII}, and (C) NPQ. (D – F) Photosynthetic parameters at pH 5.0 (A) Fv/Fm, (B) Φ_{PSII}, and (C) NPQ. (Fv/Fm, maximal quantum yield of photosystem II. Φ_{PSII}, effective quantum yield for photochemistry. NPQ, non-photochemical quenching. The error bar shows the standard deviation (n=3). NS, p > 0.05; *p<0.05; **p<0.01; ***p<0.001)*

3.4.3 Oxidative stress under low-pH treatment

Intracellular reactive oxygen species (ROS) levels were monitored to assess the effects of medium pH on cell physiological status. In pH 8.0 media, the intracellular ROS levels in all three transgenic strains were increased after inoculation and gradually decreased as acclimation. Upon acidic treatment, intracellular ROS in the WT was significantly higher than that in the transformants. While WT cells underwent continuously increasing intracellular ROS, the ROS levels in transformants were maintained relatively low (Figure 3.4A). These results indicate that transgenic strains were less stressed compared to the WT when growing at pH 5.0. Furthermore, superoxide dismutase (SOD) activities in HI5021 and HI1831 were relatively stable over cultivation. The antioxidant defense in WT and HI33543 showed an increasing tendency (Figure 3.4B), which is correlated with the relatively high ROS levels in these strains.

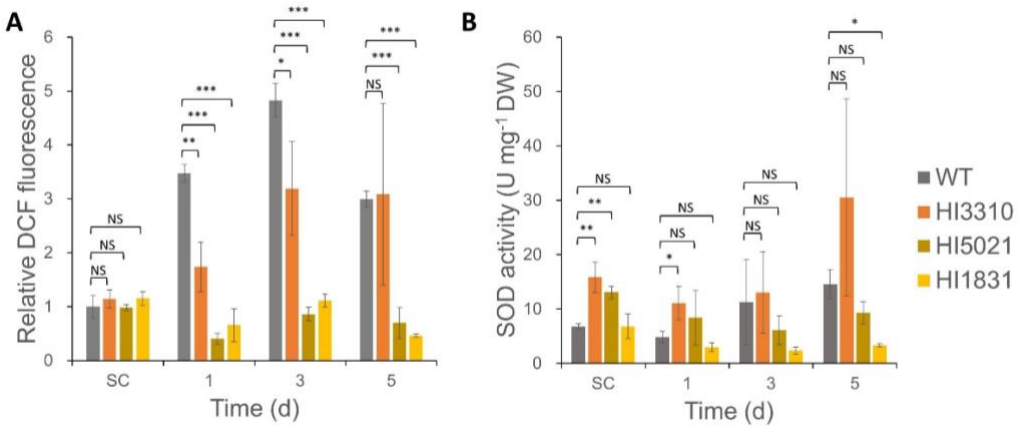

Figure 3.4. *Intracellular oxidative stress and antioxidant capacity assessment. Seed cultures (SC) of different strains were grown at pH 8.0 in identical conditions (40 µmol m^{-2} s^{-1} red/blue LED, 22 ± 1 ℃) for 5 days and then transferred into acidic EASW media (pH 5.0). The data of SC were measured before the low-pH treatment. Oxidative stress and SOD activity during the low-pH treatment were monitored on days 1, 3, and 5. HI3310, HI5021, and HI1831 are genetically modified strains with overexpressed ferredoxin (Phatr3_J33543), cation/proton antiporter (Phatr3_J50516), and bicarbonate transporter (Phatr3_Jdraft1806). (A) Relative reactive oxygen species (ROS) level detected by DCFH-DA fluorescent probe. All DCF intensity data was normalized to corresponding cell density (OD) and compared to the WT in SC. (B) Intracellular superoxide dismutase (SOD) activity.SC stands for seed culture. (DCFH-DA, 2', 7'-dichlorofluorescen diacetate. DCF, 2'-7'dichlorofluorescein. The error bar shows the standard deviation (n=3). NS, p > 0.05; *p<0.05; **p<0.01; ***p<0.001)*

3.4.4 Effect of low-pH stress on gene expression

A transcriptomic study was conducted to investigate molecular responses to acidic pH in diatoms and the underlying mechanisms that could contribute to improved low-pH tolerance. For all three transgenic strains, samples were collected at the start point (T0) from the inoculum culture (pH 8.0) and at 24 h (T1) after the low-pH treatment (pH 5.0). The principal component analysis (PCA) showed distinct clusters between samples at T0 and T1, but different strains under the same pH conditions were less distinguishable (Figure 3.5A).

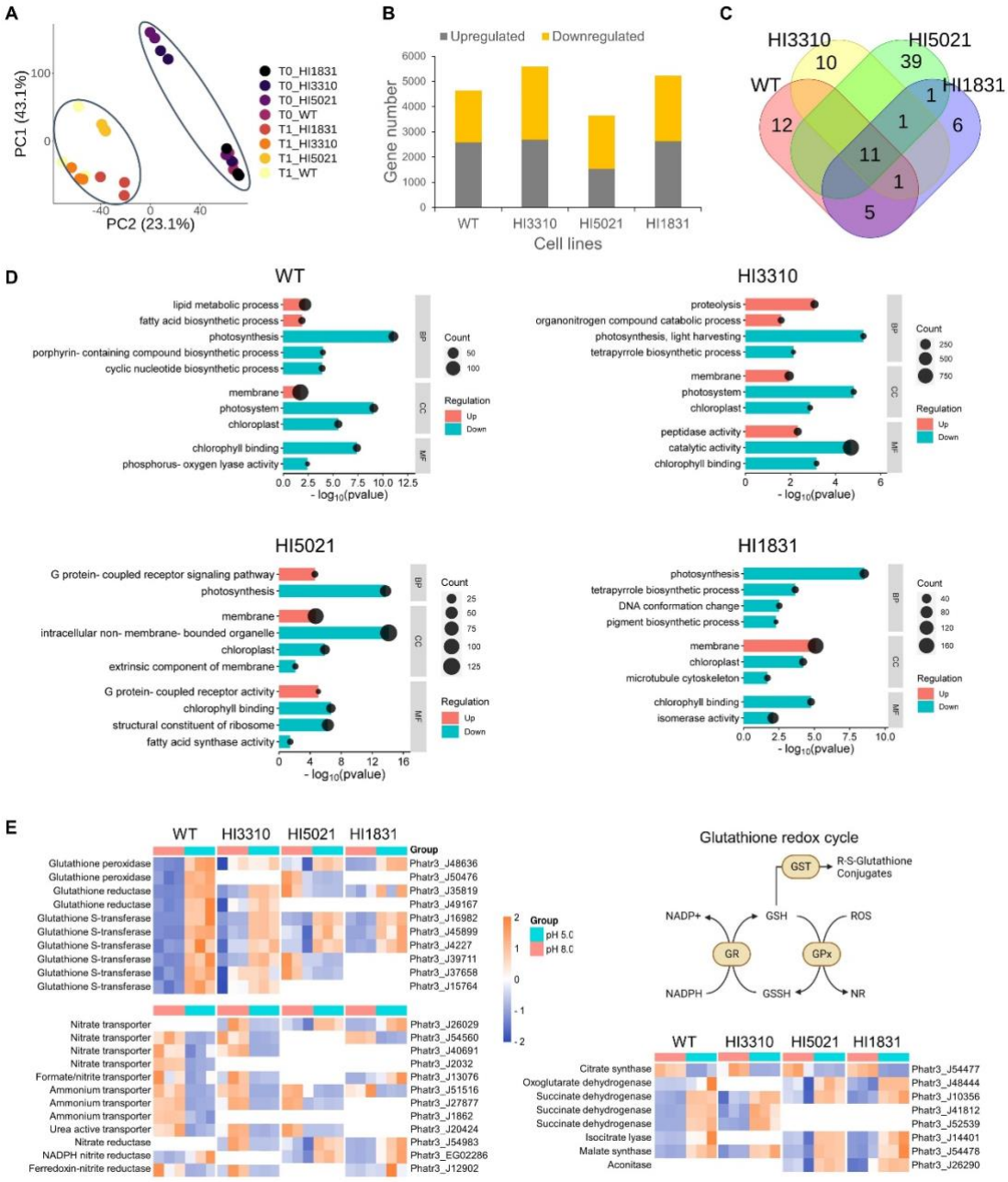

Figure 3.5. *Effect of low-pH stress on gene expression in WT and transgenic strains. (A) Principal component analysis (PCA). T0 stands for timepoint 0 (the control at pH 8.0) and T1 stands for timepoint 1 (at 24 h) of low-pH treatment. (B) The number of differentially expressed genes (DEG). (C) Venn plot of the number of enriched GO terms among different strains. (D) Highlighted driver GO terms (at least one function being presented from every connected component) under low-pH stress. (E) Expression patterns of genes involving glutathione metabolic process and nitrogen assimilation. (GPx, glutathione peroxidase; GR, glutathione reductase; GST, glutathione S-transferase; GSH, glutathione; GSSH, glutathione disulfide)*

As for the transcriptomic responses to low pH (T1/T0), 4641, 5589, 3638, and 5221 differentially expressed genes (DEGs) were identified in WT, HI3310, HI5021, and HI1831, respectively (Figure 3.5B). Upregulated and downregulated DEGs were separately subjected to the Gene Ontology (GO) enrichment analysis that resulted in 34, 26, 52, and 25 significantly enriched GO terms ($P_{adj} < 0.05$) for WT, HI3310,

HI5021, and HI1831, respectively. Based on a greedy search strategy, driver terms were generated presenting at least one function from each connected component[361] (Figure 3.5D). Apparently, the WT and transgenic strains with different genetic bases differed in their gene expression responses to acidic. Nevertheless, 11 enriched GO terms that mostly related to photosynthesis (GO:0015979) were shared in all the strains in a downregulation pattern, including chlorophyll-binding proteins (GO:0016168, GO:0009765, GO:0019684) and chlorophyll biosynthetic processes (GO:0033014, GO:0006778) (Figure 3.5C). Further investigation on the underrepresented terms revealed commonly upregulated functions relating to protein transport/repair/degradation/translation (GO:0009987, GO:0046907, GO:0043043, GO:0006412) and regulation of gene expression (GO:0010467).

Considering potential mechanisms involving acidic responses including oxidative stress, proton pumping, and energy supply, we explored annotated genes encoding peroxidases, ATP binding cassette (ABC) transporters, P-type ATPases, and tricarboxylic acid cycle (TCA) enzymes. It was found that the glutathione redox cycle including glutathione peroxidase (GPx), glutathione reductase (GR), and glutathione S-transferase was provoked by the acidic stress in WT and HI3310 (Figure 3.5E). Nevertheless, the glutathione metabolism in HI5021 and HI1831 showed different expression patterns with many genes remaining unchanged or downregulated (Figure 3.5E). In all three transgenic strains, expression of a catalase-peroxidase (Phatr3_J18572) and an L-ascorbate peroxidase (APX) (Phatr3_J54731) was substantially increased by 2.5 to 61.8-fold and 2.9 to4.4-fold, respectively, but APX genes were found generally downregulated. P-type adenosine triphosphatase (P-ATPases) and ABC transporters are the two principal active transporters in organisms. For these genes, the ratios of identified upregulated/downregulated genes were 3/9, 5/6, 6/0, and 9/4 in WT, HI3310, HI5021, and HI1831, respectively, which implies stimulated active transportation in HI5021 and HI1831. Notably, considerable upregulation (2.1 to11.2-fold) of an ABC transporter (Phatr3_J14778) and a P-type ATPase (Phatr3_EG02611) was observed in all three transgenic strains. As expected, genes involving the TCA cycle were generally upregulated in all three transgenic strains, including 2-oxoglutarate dehydrogenase, succinate dehydrogenase, isocitrate lyase, malate synthase, and aconitase. However, the expression of a citrate synthase gene (Phatr3_J54477) was markedly decreased (Figure 3.5E). Due to the great demand for protein turnover, nitrogen assimilation mechanisms were explored, which revealed wide downregulation of nitrate, ammonium, and urea transporters in the WT and HI3310. By contrast, many of these genes remained unchanged or upregulated in HI5021 and HI1831 (Figure 3.5E).

3.4.5 Transcriptomic profiles of transgenic strains

To uncover the molecular basis associated with phenotypical changes in the genetically modified strains, further analysis was conducted to study the relative expression between transgenics and WT at the same time points. At T0, transgenic strains had little difference from the WT (Table S3.2), except for HI5021, which exhibited 1620 DEGs (Figure S3.3). Consequently, enrichment analyses based on DEGs revealed limited differential functions under non-stressed conditions. In HI3310, a group was enriched with five sulfur compound binding proteins (GO:1901681), where two homologous genes (Phatr3_J16343, Phatr3_EG01877) of

iron storage ferritins[362] were upregulated, which could be responsible for increasing production of [2Fe-2S]-containing FDXs. Additionally, these results suggested that overexpression of the solute: proton antiporter (Phatr_J50516) led to changes in protein metabolism with increased nitrogen assimilation (KEGG:00910) and hydrolysis of an amine group (GO:0016810), but functions related to protein translation/biosynthesis (GO:0006520) were downregulated. By contrast, a few GO terms were found enriched in HI1831 under the acidic stress condition, which did not reveal the obvious impacts of overexpressing SCL4-2 (Phatr3_Jdraft1806) on cellular metabolism in this condition.

Against the WT, HI5021, and HI1831 in response to acidic stress differentially expressed 4111 and 2468 genes, respectively, whereas HI3310 possessing 1638 DEGs was less differentiated from the WT. According to GO enrichment results, HI3310 in the low-pH treatment only functioned differently in limited biological processes, including DNA integration (GO:0015074) and amino acid metabolic process (GO:0006520). Although many GO terms were only enriched in either HI5021 or HI1831, gene expression patterns in these functions were found alike in both strains, which reflects similar growth performances under acidic stress. Relative changes in HI5021 and HI1831 are illustrated in Figure 3.6C. As a response to low-pH stress, transcription of many heat shock transcription factors was increased in HI5021 and HI1831. Importantly, many transmembrane transporters (GO:0055085) showed enhanced expression, which did not occur in HI3310. For instance, solute carrier family 4 bicarbonate transporters, ABC transporters, potassium channel, P-type ATPase, nitrogen transporters, and ammonium transporters were likely to contribute to low-pH tolerance. Also, HI5021 and HI1831 shared multiple upregulated genes in nitrogen metabolism (KEGG:00910), propanoate metabolism (KEGG:00640), and pentose-phosphate shunt (GO:0006098). Furthermore, many genes functioning in chlorophyll-binding (GO:0016168), tetrapyrrole biosynthetic process (GO:0033014), and small molecule biosynthetic process (GO:0044283) were downregulated in comparison with the WT. Also, lower expression was observed in multiple genes delivering fatty acid synthase activity (GO:0004312) and peroxidative activity (GO:0004601).

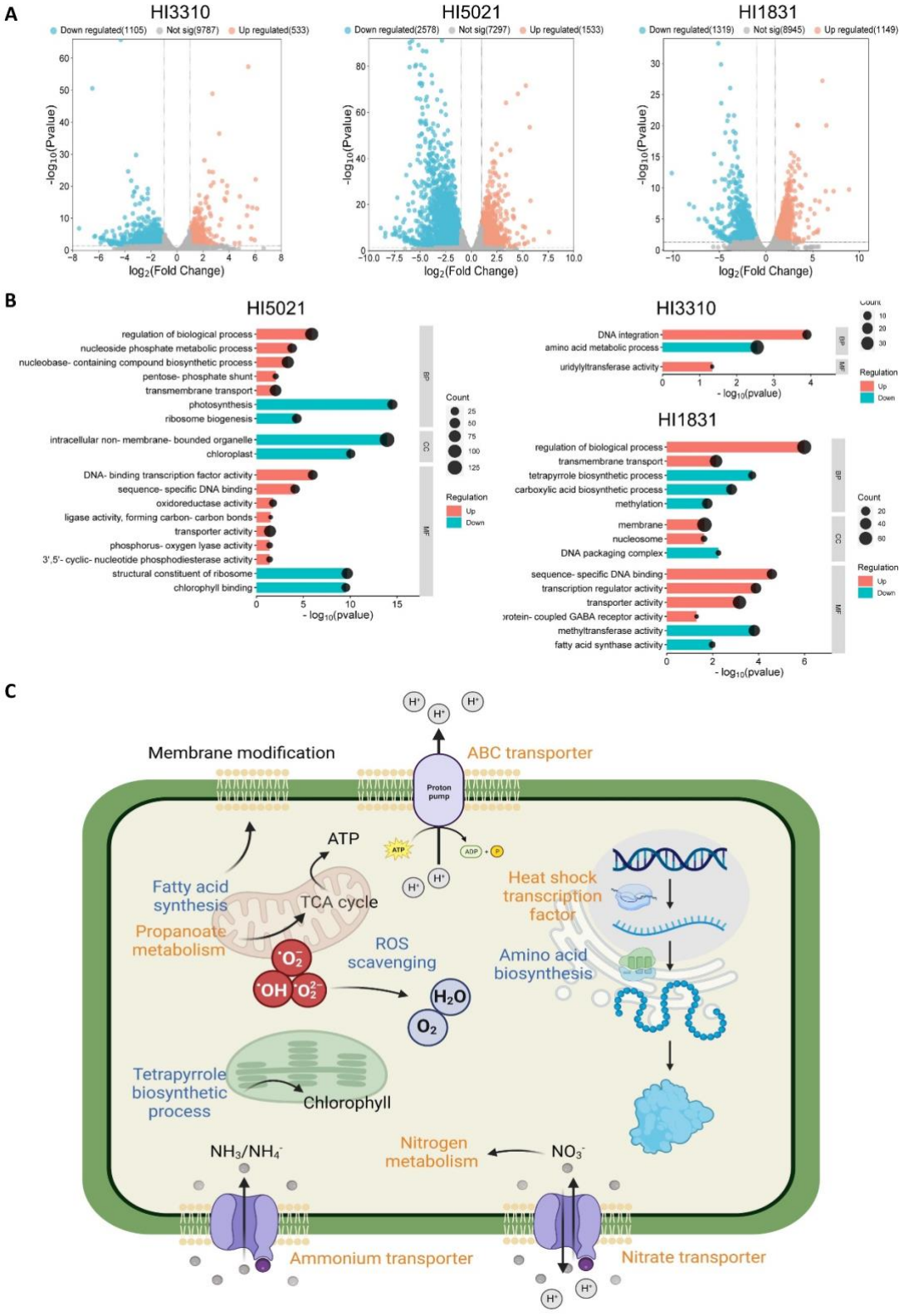

Figure 3.6. *Relative gene expression comparing transgenic strains with the WT. (A) Volcano plots presenting differentially expressed genes (DEGs) in transgenic strains at pH 5.0. (B) Highlighted driver GO terms in transgenic strains. (C) Schematic illustration of differentially expressed pathways in transgenic strains. (Orange color indicates upregulation, blue color indicates downregulation)*

3.5 Discussion

In this study, we attempt to improve acidic tolerance in diatoms. The model marine diatom *P. tricornutum* was engineered to overexpress PtFDX (Phatr3_J33543), PtCPA (Phatr3_J50516), and PtSLC4-2 (Phatr3_Jdraft1806). Our results indicate that these genetic modifications effectively enable *P. tricornutum* to survive under severe low-pH stress, which could be supported from the perspectives of photosynthetic function and oxidative stress responses. Although photosynthetic efficiency was still compromised by the acidic treatment, the inhibitory effect of low-pH was somewhat alleviated in transgenic strains, resulting in significantly higher photosynthetic quantum yields (Figure 3.3). According to the photochemistry model, maximal quantum yield (Fv/Fm) evaluates the potential efficiency of utilizing absorbed light for driving electron transfer from the reaction center chlorophyll to the primary quinone acceptor of photosystem II (Q_A). Stressful conditions lead to an increase in energy dissipation as heat, i.e., NPQ rather than photochemistry, thereby decreasing the maximal fluorescence potential (Fm). Hence, Fv/Fm in general should be reversely related to NPQ [363]. However, our results for transgenic strains showed higher values in both Fv/Fm and NPQ, but NPQ in the WT was unexpectedly kept low. These results indicate that the transgenic strains not only conducted relatively more efficient energy utilization for photochemistry but also dissipated more energy as heat. A possible explanation is that energy capture in the WT might have been impaired at the beginning of low-pH treatment, resulting in a shortage of energy to support downstream photochemistry and heat dissipation.

Moreover, elevated generation of ROS serving as a signaling mechanism is a typical physiological response to environmental stresses, but high levels of ROS could be lethal to cells by damaging macromolecules such as lipids, proteins and DNA [364]. In this study, the growth performances of different strains were clearly correlated with their intracellular ROS levels. While the wild-type *P. tricornutum* suffering from oxidative stress was severely inhibited at pH 5.0, the transgenic strains with significantly lower ROS levels showed positive growth. When ROS levels in both HI5021 and HI1831 were maintained low through the cultivation, oxidative stress in HI3310 increased over time, which could be the reason for declining cell density after 24 h (Figure S3.2). SOD activities in WT and HI3310 showing an increasing trend could be triggered by the increase in ROS levels. Furthermore, significantly lowered ROS levels in both HI3310 and HI5021 may be due to the higher initial antioxidant capacity provided by antioxidants such as SOD in the seed culture. Even though the SOD activity was low, HI1831 managed to maintain a low ROS level. These results suggest that enhanced expression of PtFDX may mitigate ROS by stimulating antioxidant-mediated detoxification, which however had limited resistance against the acidic stress for a prolonged period. In the other two transgenic strains with overexpressed proton and bicarbonate transporters (PtCPA and PtSLC4-2, respectively), different solutions other than antioxidants may be involved in alleviating oxidative stress or preventing the generation of ROS.

Although genetic modifications presented in this study demonstrated effective functions in acidic tolerance, positive growths of transgenic strains ceased after 24 h. To address this issue, gene expression at pH 5.0 was further examined by qPCR

and western blot. Since the recombinant genes were redesigned through codon optimization, their transcripts could be distinguished from the corresponding native genes. The native genes in different strains showed differential expression in response to low pH (Table 3.1). Both qPCR and transcriptomic data confirmed successful transcription of these transgenes at high levels (Figure S3.4). Due to the pH-dependent property of EGFP[365], we could not ensure the expression of the recombinant proteins by detecting EGFP signals in acidic cultures. Anti-EGFP antibody was used in western blot to detect the presence of recombinant proteins in transgenic strains. While the WT (control) was absence of targeted protein signals, recombinant proteins were detectable by the anti-GFP antibody in all transgenic strains cultured in optimal conditions (pH 8.0) and such proteins were still present after incubation at pH 5.0 for 24 h (Figure S3.4), which confirmed translation of the target proteins in corresponding transgenic strains. As stress tolerance could be a systematic response that requires the integration of multiple pathways, the impact of genetic modifications on a single gene might be limited. Interestingly, protein lengths of PtCPA and PtSLC4-2 were predicted to be 115 kD (kilodalton) and 95 kD, respectively, but they were not present at the expected sizes and exhibited multiple bands with different sizes, which suggests the occurrence of mRNA alternative splicing during their expression [366].

Table 3.1. Differential expression (log_2FoldChange) of native genes of Phatr3_J33543 (PtFDX), Phatr3_J50516 (PtCPA), and Phatr3_Jdraft1806 (SLC4-2) in response to low-pH treatment in different strains ($P_{adj} < 0.05$).

Transgene	**WT**	**HI3310**	**HI5021**	**HI1831**
Phatr_J33543	1.92	2.37	0.41*	2.23
Phatr_J50516	-1.11	-0.39*	0.00*	0.49*
Phatr_Jdraft1806	-0.25*	0.38*	-3.49	-2.75

(* represents non-significant changes, $P_{adj} > 0.05$)

To resist the low-pH stress, transcriptomic responses revealed common reactions in all three transgenic strains including enhanced heat shock responses, proteasomal protein catabolism, chaperone-mediated protein folding/ repair, TCA cycle, fatty acid biosynthesis, and defensive mechanisms such as glutathione metabolism. As environmental pH proportionally impacts the intracellular pH of diatom [337], the drop of pH leading to the misfolding of proteins certainly triggered the refolding and turnover of denatured protein to maintain proper cellular functions. Also, enzymes involved in the TCA cycle were generally upregulated, which suggests an increased demand for energy (Figure 3.5E). An acetyl-CoA carboxylase (Phatr3_J55209) that catalyzes the first committed step of fatty acid synthesis was found upregulated in all three transgenic strains, showing a carbon flux channeled to lipid production. ROS-mediated lipid accumulation as a stress response for energy storage, membrane reconfiguration, and ROS scavenging has been widely reported in oleaginous microorganisms [367]. The upregulation of multiple fatty acid desaturases (Phatr3_J46383, Phatr3_J54219, Phatr3_J9316, Phatr3_J25769, Phatr3_J41570) suggests an increased formation of unsaturated fatty acids that may act as antioxidants to balance the ROS level[367]. Additionally, peroxidase-

mediated defenses, especially the glutathione metabolic process were generally provoked in all three transgenic strains to resolve the stress-induced ROS. Transcript abundance of a catalase-peroxidase (Phatr3_J18572) was elevated by 61.8-fold in the WT, which highlighted the importance of this antioxidant to resist H^+ toxicity. This enzyme was also upregulated in all three transgenic strains in response to low-pH but with much lower fold changes i.e., 15.9 folds in HI3310, 2.5 folds in HI5021, and 10.9 folds in HI1831. In addition to the different expression patterns of glutathione redoxes, these results suggest fewer demands of peroxidase activities in the genetically modified strains, which is consistent with the results of intracellular ROS assay. Another common reaction to low-pH was the downregulation of genes related to light harvesting e.g., chlorophyll-binding proteins, and pigment biosynthesis e.g., chlorophyll and carotenoid. This was also observed in our previous ALE experiments[347] as a potential defense strategy to limit ROS generation from excessive electron flow [310].

Further comparison of transcriptome profiles between transgenic strains and the WT found relatively closer expression patterns between the WT and HI3310, while gene expression in HI5021 and HI1831 largely deviated from the WT (Figure 3.6A). These results imply that HI5021 and HI1831 share molecular features that could confer superior low-pH tolerance on them compared to WT and HI3310. Examination of DEGs among different strains revealed higher expression of various transmembrane transporters in HI5021 and HI1831. Therein, ABC transporters and P-type ATPases were likely to participate in proton efflux and translocation. Additionally, elevated ammonium transporters and bicarbonate transporters (paralogs of PtSLC4-2) may aid pH control by absorbing alkaline compounds such as NH_3/NH_4^- and HCO_3^- [368]. Increased expression of multiple nitrate transporters as well as nitrate and nitrite reductases were thought to be required for assimilating nitrogen to support protein synthesis. However, amino acid metabolism and translation machinery were found slightly downregulated in HI5021 and HI1831 (Figure 3.6). Therefore, nitrate/nitrite transporters and reductases may also be demanded for translocating protons. In addition to the nitrate reduction activity, the membrane-bound nitrate reductase plays a role in translocating cytoplasmic protons into periplasm [369]. Furthermore, nitrate uptake via nitrate transporter was shown to alleviate H^+ toxicity to plants by increasing pH in the root's rhyizosphere [370], which may also be applied to diatoms. The differential expression analysis among strains also revealed extensive lower expression of peroxidase systems in HI5021 and HI1831, including catalase (CAT), ascorbate peroxidase (AXP), glutathione peroxidase (GPX) and superoxide dismutase (SOD), which confirmed the fact that ROS scavenging was not urgently demanded in HI5021 and HI1831 (Figure 3.6C). Based on these results, we may propose that ROS generation was avoided in HI5031 and HI1831 by vast upregulation of transporters that could alleviate the impact of protons. The overexpression of Phatr_J33543 caused limited changes in gene expression in response to the environmental change, which is expected for a single modification on a non-regulatory gene. However, the overexpression of a proton pump (Phatr_J50516) and a bicarbonate pump (Phatr_Jdraft1806) led to broader changes in the gene expression patterns associated with many mechanisms and pathways (Table S3.3). These results imply that the direct effects of overexpressing Phatr_J50516 and Phatr_Jdraft1806 may cause fundamental changes, for example, cellular homeostasis that could mediate signaling for global regulation.

3.6 Conclusion

The present study demonstrated the critical roles of ion/electron carrier genes (i.e., Phatr3_J33543, Phatr3_J50516, and Phatr3_Jdraft1806) in the model marine diatom *P. tricornutum* to achieve low-pH resistance. These genetic modifications enabled the growth of *P. tricornutum* under an inhibitory low-pH stress. Physiological and molecular data suggested that these genes functioned differently in stress tolerance by either alleviating oxidative stress or preventing ROS generation. This study demonstrated the first attempt to engineer diatoms to resist inhibitory acidic conditions based on an ALE integrated with a whole-genome transcriptomics approach. We expect the presented rational engineering strategy to facilitate the development of robust transgenic microalgae for turning waste flue gas into valuable algal products, thereby contributing to achieving carbon neutrality for combating climate change.

3.7 Supplementary materials

Table S3.1. Primer designs for genomic PCR.

Primer	Sequence	Amplicon size (bp)
HI33F1	GATCATCAATTCCCCCGAAACC	931
HI33R1	GTGGCGAATCTTGAAGTTGACC	
HI50F1	GGAACACAAGAAGCAACAGTCG	927
HI50R1	ACGTTGTGGGAGTTGTAGTTGTA	
HI18F1	GATTTTCCCTCTTGGCTCTCGA	941
HI18R1	GTTGTATTCGAGCTTGTGACCG	

Table S3.2. Differentially expressed genes (DEGs) in transgenic strains in comparison with WT.

Timepoint	T0		T1	
Strains	Upregulation	Downregulation	Upregulation	Downregulation
HI3310	376	294	533	1105
HI5021	881	739	1533	2578
HI1831	289	124	1149	1319

(T0, starting point with seed culture at pH 8.0; T1, 24 h after low-pH treatment)

Table S3.3. Differential expression of transmembrane transporters in transgenic strains in comparison with WT.

Gene ID	Description	Log_2(Fold Change)		
		HI3310	HI5021	HI1831
Phatr3_EG02538	Solute carrier family 4		2.20	2.93
Phatr3_EG02360	Solute carrier family 4	1.50	1.18	2.42
Phatr3_Jdraft52	Solute carrier family 4			1.62
Phatr3_J83	ABC transporter		2.04	
Phatr3_J21664	ABC transporter		1.74	
Phatr3_J44756	ABC transporter		1.36	1.25
Phatr3_J45195	ABC transporter		1.36	
Phatr3_J31433	ABC transporter	1.05	1.10	1.83
Phatr3_EG01286	ABC transporter		1.08	1.45
Phatr3_J14778	ABC transporter		1.35	2.05
Phatr3_J11674	ABC transporter		1.79	1.19
Phatr3_J43299	ABC transporter		1.58	1.80
Phatr3_J52343	ABC transporter	-1.54	1.16	
Phatr3_J18197	ABC transporter		1.14	
Phatr3_J25218	ABC transporter			1.64
Phatr3_J10151	ABC transporter			1.15
Phatr3_J21548	ABC transporter			1.10
Phatr3_EG01954	ABC transporter			1.05
Phatr3_EG02475	Potassium channel		1.31	
Phatr3_J43530	Potassium channel		1.27	
Phatr3_EG02234	Potassium channel		1.02	
Phatr3_J44535	Potassium voltage-gated channel		1.44	

Gene ID	Description	Log_2(Fold Change)		
		HI3310	HI5021	HI1831
Phatr3_J50123	Potassium voltage-gated channel		1.12	1.05
Phatr3_J46424	Potassium voltage-gated channel		1.58	
Phatr3_EG01907	P-type Na+/K+ transporter		-1.33	1.39
Phatr3_EG01908	P-type Na+/K+ transporter			1.36
Phatr3_EG02611	P type ATPase		2.04	
Phatr3_J52468	P type ATPase		2.02	2.00
Phatr3_J52368	P type ATPase			1.53
Phatr3_EG02512	P-type ATPase	2.30		2.40
Phatr3_J52468	P-type ATPase		2.02	2.00
Phatr3_J16222	P-type ATPase		1.42	1.21
Phatr3_J24978	H^+-transporting ATPase		1.50	
Phatr3_J51058	H^+-transporting ATPase		1.22	
Phatr3_J27923	H^+-transporting ATPase		1.10	
Phatr3_J17928	H^+-transporting ATPase		1.08	1.15
Phatr3_J43023	H^+-transporting ATPase			1.12
Phatr3_J29711	H^+-transporting ATPase			1.03
Phatr3_J28794	H^+-transporting ATPase			1.02
Phatr3_J25840	H^+-translocating transhydrogenase		1.34	1.18
Phatr3_J46424	Hydrogen voltage-gated channel 1		1.58	
Phatr3_J11843	Cation/H^+ exchanger		1.16	1.11
Phatr3_J50516	Cation/H^+ exchanger			1.94
Phatr3_J43052	Cation/H^+ exchanger			1.65

Gene ID	Description	Log_2(Fold Change)		
		HI3310	HI5021	HI1831
Phatr3_Jdraft1692	Aquaporin		1.41	
Phatr3_J20755	Aquaporin		1.34	
Phatr3_J26029	Nitrate transporter		5.78	7.25
Phatr3_J54560	Nitrate transporter		3.04	2.49
Phatr3_J40691	Nitrate transporter		1.45	
Phatr3_J2032	Nitrate transporter		1.02	1.68
Phatr3_J26029	Nitrate transporter		5.78	7.25
Phatr3_J13076	Formate/nitrite transporter		2.93	5.20
Phatr3_J51516	Ammonium transporter	-1.26	2.92	2.06
Phatr3_J27877	Ammonium transporter		2.69	3.43
Phatr3_Jdraft972	Ammonium transporter		1.51	1.76
Phatr3_J1862	Ammonium transporter			1.63
Phatr3_J51516	Ammonium transporter	-1.26	2.92	2.06
Phatr3_J20424	Urea active transporter		1.97	2.82
Phatr3_J54983	Nitrate reductase		5.31	6.41
Phatr3_EG02286	NADPH nitrite reductase		4.54	5.76
Phatr3_J12902	Ferredoxin-nitrite reductase	1.23	2.86	4.74

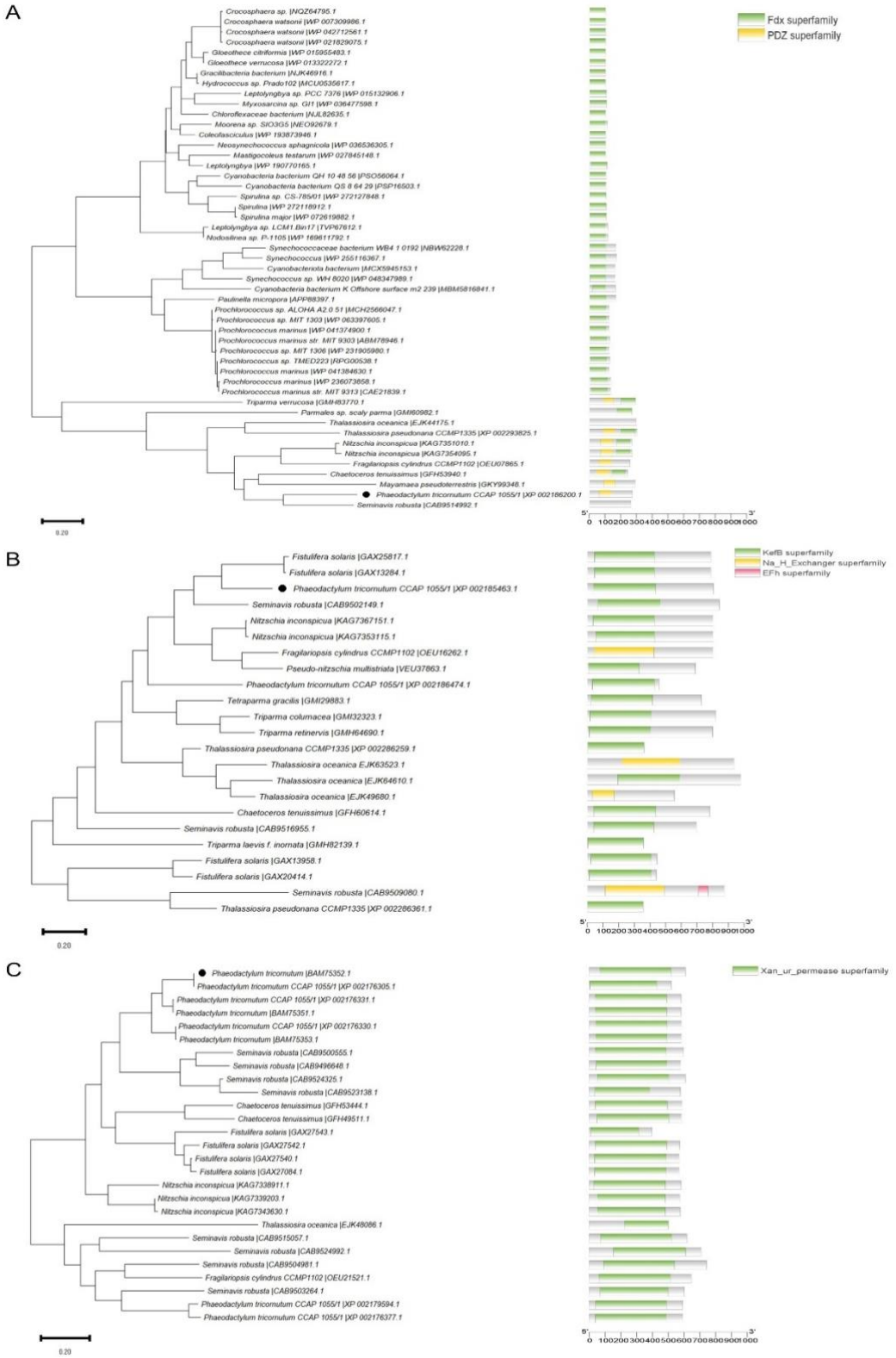

Figure S3.1. *Phylogenetic relationships of the target proteins in various species. Homologous proteins were searched against the NCBI database and filtered for > 40% identity. Phylogenetic trees were constructed using MAGA11 by the Maximum Likelihood algorithm. (A) Phylogenetic tree of ferredoxin (FDX). (B) Phylogenetic tree of cation/proton antiporter (CPA). (C) Phylogenetic tree of $HCO3^-$ transporter (PtSCL4-2).*

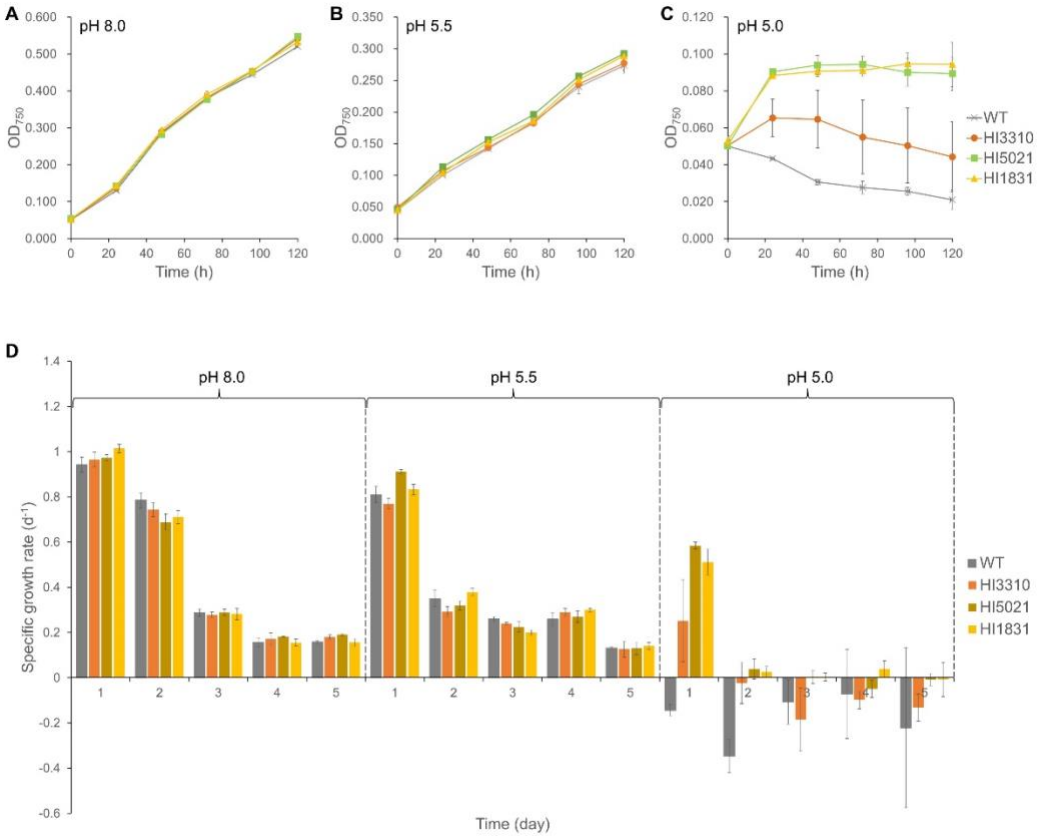

Figure S3.2. *Growth performance of different strains at different pH. (A) Growth curves at pH 8.0. (B) Growth curves at pH 5.5. (C) Growth curves at pH 5.0. (D) Daily specific growth rates of different strains at pH 8.0, pH 5.5, and pH 5.0 over 5-day cultivation. Different strains were cultivated at pH 8.0, pH 5.5 and pH 5.0 in identical conditions (40 µmol* m^{-2} s^{-1} *red/blue LED, 22 ± 1 ℃). HI3310, HI5021 and HI1831 are genetically modified strains with overexpressed ferredoxin (Phatr3_J33543), cation/proton antiporter (Phatr3_J50516), and bicarbonate transporter (Phatr3_Jdraft1806), respectively.*

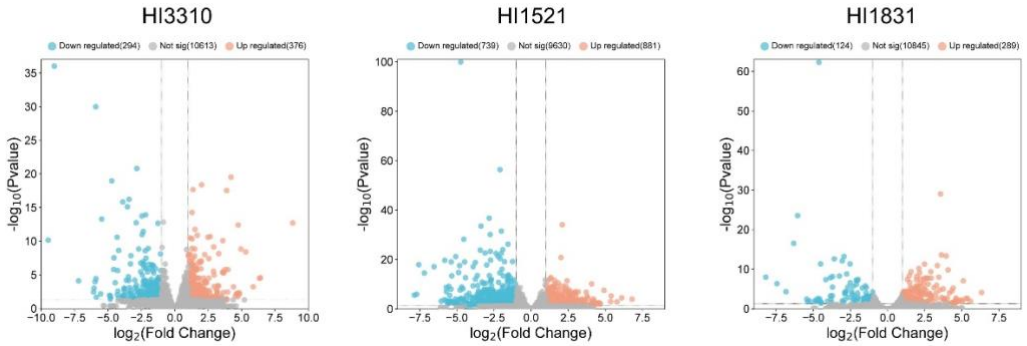

Figure S3.3. *Volcano plots presenting differentially expressed genes (DEGs) in transgenic strains compared to the WT in unstressed condition (pH 8.0).*

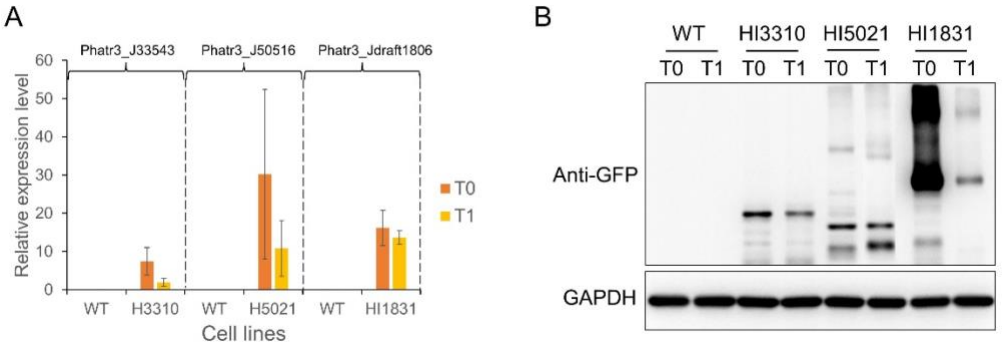

Figure S3.4. *Validation of expression of recombinant proteins in low-pH treatment (pH 5.0). (A) Relative expression of transgenes determined by qPCR at T0 and T1. Histone 4 (H4) gene was used as the internal reference. (B) Western blot detection with anti-GFP antibody using GAPDH as the internal control. The low-pH treatment was conducted by transferring different cell lines from pH 8.0 to pH 5.0 media. Cultures were maintained in identical conditions (40 µmol m^{-2} s^{-1} red/blue LED, 22 ± 1 ℃). HI3310, HI5021, and HI1831 are genetically modified strains with overexpressed ferredoxin (Phatr3_J33543), cation/proton antiporter (Phatr3_J50516), and bicarbonate transporter (Phatr3_Jdraft1806). T0 and T1 stand for starting point (without low-pH treatment) and 24 hours after the low-pH treatment, respectively.*

4 An intrinsic circadian clock to regulate phytoplankton photosynthesis

Yixi Su[1,2], Jingyan Hu[1], Jiwei Chen[1], Weizhao Meng[1], Cheng Qian[1], Yuexuan Shu[1], Chao Wang[1], Xianwei Wang[3], Kourosh Salehi-Ashtiani[4], Sigurður Brynjólfsson[2], Jianping Lin[5], Yongquan Li[6], Haisheng Zhang[1,7], Lizhong Wang[1,8], Weiqi Fu[1,2,9,*]

[1]Ocean College, Zhejiang University, Zhoushan, 316021, Zhejiang, China;

[2]Center for Systems Biology and Faculty of Industrial Engineering, School of Engineering and Natural Sciences, University of Iceland, Reykjavík 101, Iceland;

[3]School of Oceanography, Shanghai Jiao Tong University, Shanghai 200030, China;

[4]Laboratory of Algal, Systems, and Synthetic Biology, Division of Science and Math & Center for Genomics and Systems Biology, New York University Abu Dhabi, P.O. Box 129188, Abu Dhabi, UAE.

[5]Key Laboratory of Biomass Chemical Engineering of Ministry of Education, College of Chemical and Biological Engineering, Zhejiang University, Hangzhou, 310058, Zhejiang, China;

[6]Institute of Pharmaceutical Biotechnology & Research Center for Clinical Pharmacy, The First Affiliated Hospital, School of Medicine, Zhejiang University, Hangzhou, 310058, Zhejiang, China;

[7]Key Laboratory of Offshore Geotechnics and Material of Zhejiang Province, College of Civil Engineering and Architecture, Zhejiang University, Hangzhou, 310058, Zhejiang, China;

[8]Ocean Academy, Zhejiang University, Zhoushan, 316021, Zhejiang, China;

[9]Donghai Laboratory, Zhoushan, 316021, Zhejiang, China;

*Corresponding author: Weiqi Fu

Email: weiqifu@zju.edu.cn or weiqi@hi.is

Keywords: Photosynthesis; circadian clocks; phytoplankton; intrinsic circadian rhythm; *Phaeodactylum tricornutum*

4.1 Abstract

Circadian clocks exist in all types of organisms and coordinate key biological processes, e.g. photosynthesis in phytoplankton (microalgae) and land plants. We asked whether a circadian rhythm sustains in phytoplankton when living under continuous illumination without environmental cues. Here, for the first time, we report a persistent circadian rhythm in the model marine diatom *Phaeodactylum tricornutum* living under constant illumination and temperature without environmental cues. We show that the majority of the rhythmic genes identified under diel light conditions lose their oscillatory expression in the absence of external entrainers and the genes with persistent circadian clocks are predominantly involved in transcriptional regulation and cell division. We find constant illumination leads to an increased average expression of transcription factors and cell division genes, while the Calvin-Benson cycle and the pigment biosynthesis are kept at low expression levels, which causes lowered photosynthetic efficiency. We also show that the downregulation of pigment biosynthesis is targeted by ten microRNAs that are potentially functional in transcriptional regulation. By manipulation of the dark rest period, we confirm a fine-tuned light/dark cycle could dramatically improve photosynthetic efficiency in microalgae. Our results unveil a novel persistent circadian rhythm on photosynthetic regulation in marine phytoplankton and provide critical insights into the interaction between environmental signals and inheritable internal circadian clocks in diatoms.

4.2 Introduction

Our planet Earth is home to billions of different species of organisms. Biological rhythm (clock) has been found ubiquitously developed in almost all living organisms for adaption to a fluctuating environment during evolution[371, 372]. Different rhythmic behaviors of life can be shaped by daily and seasonal changes in the environment due to the Earth's rotation and revolution, among which circadian clocks following an approximately 24-hour cycle in synchronization with solar time have been widely observed with profound biochemical and molecular effects on organisms [373, 374]. However, these biological clocks could be reset by environmental cues, for example, "jet lag" occurs immediately after traveling across the time zone and can be dismissed by adaptation to local time zones shortly.

Unlike human beings, most photosynthetic organisms, such as land plants and phytoplankton operate photosynthesis under daily light/dark cycles with a circadian network of photic and temperature cues[375-377]. Particularly, phytoplankton (microalgae) which constitutes more than half of global primary production via photosynthesis is vital to a sustainable ecosystem and economy for human beings[373, 378-380]. Recently, most major countries/economies have agreed to achieve carbon neutrality by the middle of this century, which is one of humanity's most urgent missions. Among various solutions to address such a grand challenge, nature-based carbon bio-fixation and industrial carbon capture by microalgae have attracted much attention. For example, it was reported that a 10% increase in photosynthetic efficiency in nature could fix an additional 40 billion tons of carbon dioxide (CO_2) annually by plants, roughly equivalent to the amount of CO_2 emissions from fossil fuels and industry in 2021[381, 382]. Therefore, understanding the circadian rhythms of photosynthetic organisms, such as phytoplankton, is critical for optimizing their growth and photosynthetic efficiency, and thus for developing sustainable carbon capture and sequestration technology.

For microalgal production, continuous illumination offering a prolonged period of production is certainly desired for maximizing productivity. However, biomass accumulation is often disproportionate to the duration of the photoperiod [55, 56], which implies an impaired photosynthetic efficiency due to the removal of external entrainer[383, 384]. In nature, the peak primary production in the Arctic Ocean [385] or the Southern Ocean was usually observed at a period away from the summer solstice that has the most daylight (e.g. polar day with continuous daylight of whole 24 hours), although the primary production of the Southern Ocean is difficult to predict directly[386]. Evidently, the primary production peaks in January, which is equal to July in the Northern Hemisphere for the Weddell Sea sector[387]. Oscillatory growths, physiological states, and cellular compositions of microalgae were previously demonstrated under constant culturing conditions[388, 389], which suggests the involvement of an internal circadian clock (Figure 4.1A). Therefore, intrinsic rhythms controlling cellular activities may be responsible for the lower overall biomass yield on light energy (photosynthetic efficiency) under continuous irradiance. In the last decades, changes in diel transcriptome have been studied in several different microalgae under light/dark cycle conditions[375, 389-393]. In addition, a few studies looked into gene changes immediately after the transition from the light/dark cycle condition to a constant light condition using microarray or qPCR analysis[394-396]. However, little has been done to investigate transcriptomic

rhythms in phytoplankton living in habitats with polar-day alike illumination or after adaptation to constant light and temperature conditions and it remains largely unknown whether there is a robust circadian rhythm viable and inheritable in phytoplankton under continuous light conditions. Diatoms are a major group of microalgae that dominate in the modern ocean [227]. Smart regulation and manipulation of controllable photosynthetic processes appear promising in nature as well as in the design of photosynthetic cell factories for sustainable development. In this study, we attempt to answer the key question of robustness for phytoplankton circadian rhythms and decipher the molecular basis of the circadian regulation of photosynthesis in diatoms.

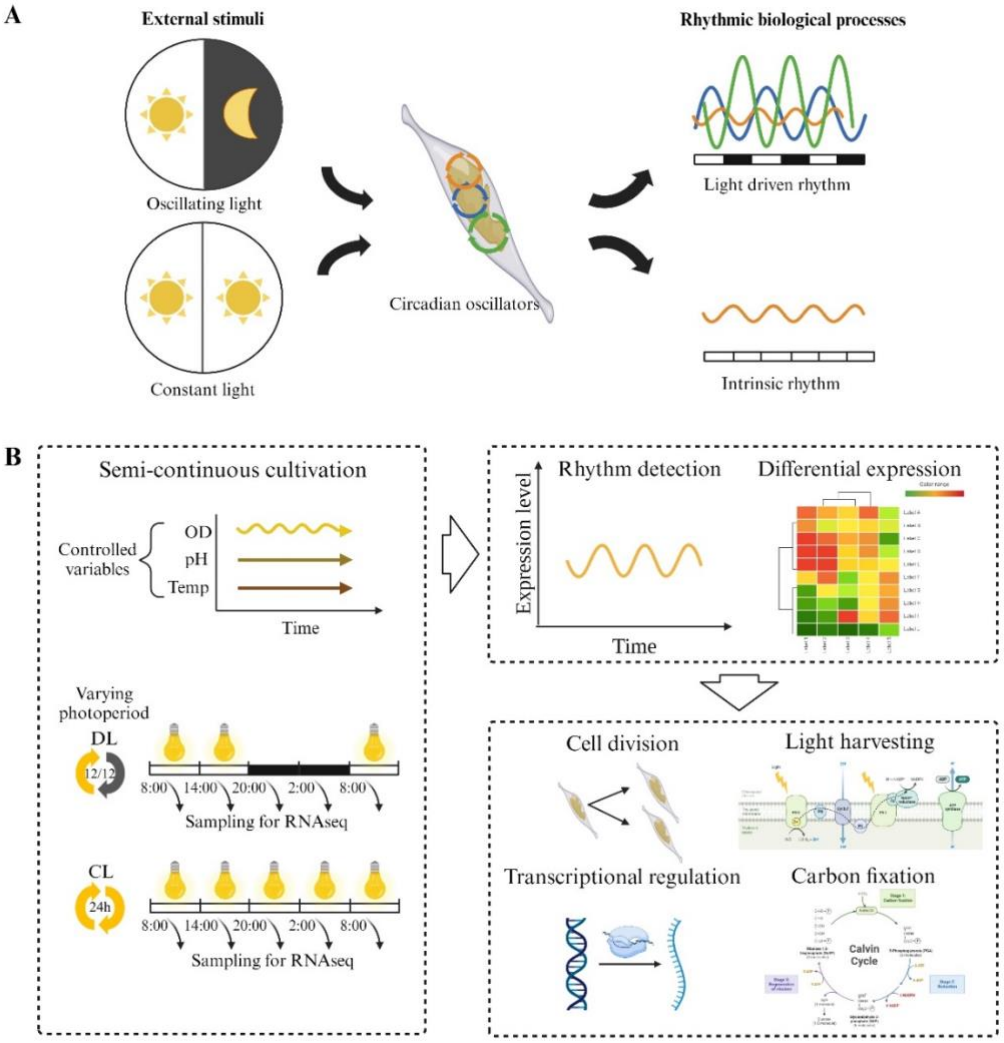

Figure 4.1. *Schematic representation of the circadian system and experimental design. (A) Light-driven rhythm and intrinsic rhythm. (B) Experimental design and procedures. Semi-continuous cultivations were conducted under controlled conditions with fixed temperature, light intensity, and pH. Cell density, OD_{750}=0.22±0.02, and culture volumes =200±40 ml were maintained by adding and removing media every six hours. CL: continuous light; DL: 12h/12h light/dark cycle.*

4.3 Materials and Methods

4.3.1 Strain and culture condition.

Axenic culture of *Phaeodactylum tricornutum* CCAP 1055/1 was purchased from the Culture Collection of Algae & Protozoa (CCAP), Scotland, UK, and had been incubated under continuous illumination (white fluorescent lamp) for two years. The diatoms were grown in filter-sterilized ESAW (Enriched Seawater, Artificial Water) [358] media containing 100 μg mL^{-1} ampicillin, kanamycin, and streptomycin. The culture pH was maintained at 8.10±0.10 by supplying 40 mM Tris-HCl buffer in the media. Illumination using combined red (630±20 nm) and blue (450±20 nm) LED panels (50:50) was set at a light intensity of 40±2.0 μmol $m^{-2}s^{-1}$ and the temperature was maintained at 20±2 ℃.

4.3.2 Semi-continuous cultivation

Before the experiment, two groups of inoculums were acclimated to continuous light (CL) and a diel cycle of 12h light:12h darkness (DL) photoperiod (lights on at 7:00 am; lights off at 7:00 pm) through subcultures for two weeks. Subsequently, the experiment was initiated by batch cultivation with triplicated cultures in 500 mL flasks (200 mL working volume). Aliquots of 3 mL were sampled from each replicate every 3 h to monitor the optical density at 750 nm (OD_{750}) using a DR3900 spectrophotometer (Hach, US) (*SI Appendix,* Dataset S1). To assess photosynthetic efficiency, the sample was incubated in the dark for 15 min, and chlorophyll fluorescence was measured (*SI Appendix,* Dataset S1) using an AquaPen-C (Photon Systems Instruments, Czech Republic) according to a built-in program with (non-photochemical quenching, NPQ) protocol 3 that generated maximum quantum yield (F_v/F_m) and effective quantum yield (Φ_{PSII}). As OD_{750} reached 0.25, cultures were diluted with fresh media, and a certain volume of the culture was removed in a 6-h interval to maintain the optical density (OD_{750}) at 0.225±0.025 and culture volume at 200±40 mL. When stable growths were achieved for both groups, sampling started 1 h after the light was turned on in the morning. In a 6-h interval, 40 mL of culture was collected from each replicate at zeitgeber time, ZT1, ZT7, ZT13, ZT19, and ZT25, which covered a 25-h period. Samples were centrifuged at 4000 x g for 10 min at 4 ℃. Cell pellets were washed once using sterile Milli-Q water and stored in 1 mL of sample protector reagent (Takara, Japan) at -20 ℃ for RNA sequencing.

4.3.3 Calculation of growth rate and productivity

Ash-free dry weight (AFDW) of *P. tricornutum* was measured according to Zhu and Lee (1997). The relationship between AFDW and OD_{750} was established as following, AFDW (mg L^{-1}) = 415.1OD_{750} (R^2 = 0.9915). The specific growth rate (μ, d^{-1}) was calculated using the following equation: $\mu = (\mathrm{In}X_t - \mathrm{In}X_0)/(t - t_0)$ where X_t and X_0 are the OD at time t and the beginning of the time interval (t_0), respectively (*SI Appendix*, Dataset S1). As AFDW was estimated based on OD data, the average biomass productivity (P_b, mg $L^{-1}d^{-1}$) in a period (t) was calculated as accumulated biomass divided by time, $P_b = \Delta AFDW/t$.

4.3.4 Pigment content assay

During semi-continuous cultivation, aliquots of 2 mL were collected in 3 h intervals. The cell pellet was produced by centrifugation at 4000 x g for 10 min at 4 ℃. Pigments were extracted by adding 1 mL 100% ethanol to the cell pellet, followed by sonication for 2 min. Cell debris was pelleted by centrifugation at 12000 x g for 10 min (4 ℃) and the supernatant was transferred to a cuvette for spectrophotometric assay at 630 nm, 664nm, and 470 nm using a DR3900 spectrophotometer (Hach, US). Concentrations of pigments including chlorophyll a, chlorophyll c_1+c_2, and total carotenoids were estimated using equations[307, 397] and then normalized based on the cell concentration of each sample measured using a hematocytometer to obtain the value of pigment contents per cell.

4.3.5 RNA extraction and sequencing

Transcriptome sequencing and analysis were conducted by OE Biotech Co. Ltd. (Shanghai, China). Total RNA was extracted using the mirVana miRNA Isolation Kit (Ambion) following the manufacturer's protocol. RNA integrity was evaluated using the Agilent 2100 Bioanalyzer (Agilent Technologies, Santa Clara, CA, USA) and RT-qPCR. The samples with RNA Integrity Number (RIN) ≥ 7 were subjected to the subsequent analysis. According to the manufacturer's instructions, an amount of 1 ug RNA per sample was used for library construction using TruSeq Stranded Total RNA with Ribo-Zero Gold. Then the constructed libraries were sequenced on the Illumina sequencing platform (HiSeq x-10) and 150 paired-end reads were generated.

4.3.6 Bioinformatic analyses

Raw reads were filtered using Trimmomatic [312] to remove adapter sequences, poly-N containing, and low-quality reads. As a result, RNA sequencing generated 67.8 – 99.9 million reads with an average Q30 base > 94.1% (*SI Appendix*, Dataset S2). The clean reads were mapped to the reference genome using Hisat2 [313] and assembled using StringTie [359]. While more than 98% of total reads were mapped to the genome for all samples, uniquely mapping rates on average were 65.6% and 66.3% for the DL and CL groups, respectively (*SI Appendix*, Dataset S2). The htseq-count[360] was used to count the read abundance of each transcript (protein-coding gene), which was normalized into fragments per kilobase of exon per million mapped fragments (FPKM) using cufflinks[398].

For small RNA, the raw sequence data were processed by removing adaptor sequences, low-quality reads, and reads shorter than 15nt and longer than 41nt to generate the data of clean reads. The clean reads were mapped to the genome of *P. tricornutum* using bowtie (a software package for sequence alignment)[399] (*SI Appendix*, Dataset S3). Non-coding RNAs, including rRNAs, tRNAs, small nuclear RNAs (snRNAs), and small nucleolar RNAs (snoRNAs) were identified using the BLAST[400] search against Rfam v.10.1 (http://www.sanger.ac.uk/software/Rfam)[401] and GenBank databases (http://www.ncbi.nlm.nih.gov/genbank/) using an e-value of 0.01 as cutoff (*SI Appendix*, Dataset S3). Degraded fragments of mRNAs were identified by aligning reads to exons and introns of annotated mRNAs in the genome of *P. tricornutum*.

Additionally, repeat sequences were identified by comparing the clean reads to the Repbase (https://www.girinst.org/repbase/). These fractions of RNAs were removed from the clean reads. Then, the bowtie was used to identify microRNAs (miRNAs) by comparing the clean reads with known plant miRNA sequences deposited in the miRBase v.22 database (http://www.mirbase.org/)[402] and PmiREN (Plant miRNA Encyclopedia, https://www.pmiren.com/) with one mismatch permitted. While between 423 and 1013 miRNAs were identified in CL samples, the number of identified miRNAs in DL samples varied from 580 to 2251 (*SI Appendix,* Dataset S3). The remaining unannotated small RNAs were analyzed using mirdeep2 [403] to predict novel miRNAs. Based on the hairpin structure of a pre-miRNA and the miRBase database, the corresponding miRNA star sequence was also identified. In total, 38 novel miRNAs within 27 novel miRNA families were revealed across all samples (*SI Appendix,* Dataset S3). The expression levels of miRNAs were normalized by transcript per million (TPM).

Rhythmic genes were detected using the JTK_cycle algorithm (MetaCycle R package) based on time course data of triplicated values of expression level (*SI Appendix,* Dataset S4). To assess overall expression in CL and DL groups, read counts (*SI Appendix,* Dataset S4) derived from five points throughout 24 h were subjected to differential gene screening using the DESeq2 R package [404]. The target period was set to be 24 h and an adjusted p-value < 0.05 was used to define significant rhythmic transcripts. The detected cycling genes with maximum FPKM > 1, fold change between maximum and minimum FPKM values > 1.3, and amplitude > 1 were further screened to omit lowly expressed and weak oscillating genes (*SI Appendix,* Dataset S5). With adjusted p-value < 0.05, fold change ratios (CL/DL) ≥ 2 or fold change ratios (CL/DL) ≤ 0.5 were set as the thresholds for significantly differential expression (*SI Appendix,* Dataset S6).

The differentially expressed mRNA and miRNA were analyzed using miRanda [405] with default parameters to predict the potential targeting relationship between mRNA and miRNA. Likely target sites were screened using the parameters as follows: match score $S \geq 90$ and target duplex free energy $\Delta G \leq -20$ kcal mol^{-1} [406]. Gene Ontology (GO) enrichment analysis was performed to assess significant annotations within different clusters of rhythmic genes as well as differentially expressed genes between different light regimes. Annotations of protein-coding genes in *P. tricornutum* were obtained by mapping transcripts to the Swiss-Prot database. The significance of GO term enrichment was examined by a hypergeometric test with a p-value < 0.05.

Concerning cell growth, further research was carried out for specific biological processes of interest, including transcriptional regulation, cell division, photosynthesis, and carbon fixation. Genes for specific functions were listed in *SI Appendix,* Dataset S7. In silico examination indicated that the numbers of putative transcriptional factors with bHLH, Myb, bZIP, and HSF domain in *P. tricornutum* were 9, 39, 23, and 78, respectively. For cell division, we explored 28 cyclins and 17 cyclin-dependent kinases (CDKs) present in *P. tricornutum*. Moreover, genes involved in DNA replication were explored including genes encoding 10 DNA polymerases, 7 DNA mismatch repair proteins, and 10 MCM proteins that serve as DNA replication licensing factors for ensuring the completion of genomic DNA replication[407]. Regarding mitosis, 8 SMC-encoding genes that function in mitotic

anaphase for chromosome condensation were detected in our transcriptome data. Also, we investigated the expression of 13 KIF and 3 kinetochore proteins for chromosome segregation [408]. In addition to 11 genes encoding APC subunits, we investigated other 20 various genes[408] that are presumably involved in cell cycle control. In addition, genes involved in photosynthesis and carbon fixation processes were retrieved from the genome-wide metabolic model of *P. tricornutum* [340]. The gene lists for these processes were completed by searching on KEGG and PLAZA databases.

4.3.7 Statistical analysis

Statistical significance was assessed using a two-tailed Student's t-test on Microsoft Excel. All data include more than three independent biological replicates and reported as means ± standard deviation.

4.4 Results and Discussion

4.4.1 Physiological status of *P. tricornutum* throughout semi-continuous cultivations

To reveal external stimuli-independent rhythms in the model diatom *P. tricornutum*, a comparison in this study was set between parallel cultivations under continuous light (CL) and light/dark cycle (DL) conditions (Figure 4.1). Before experiments, the inoculum culture had been incubated under CL for more than six months with regular subculture to eliminate the occurrence of light-responsive rhythms that may be inherited from a day/night cycle (Figure 4.1). Semi-continuous cultivations were operated with constant light intensity, temperature, pH as well as well-controlled cell density and nutritional levels, to exclude external stimuli other than photoperiod. In agreement with previous studies[409, 410], biomass productivity in cultures with double photoperiod did not reach twice that of the productivity under the light/dark regime (Table S4.1), which suggested a lower biomass yield on the light under the CL condition. Diel oscillations in growth rate and quantum yields (Figure S4.1) were observed under the DL condition as previously reported [375, 389, 410]. However, under continuous light, the fluctuation in growth rate over semi-continuous cultivation did not show obvious regular rhythms, while a slight periodicity can be seen in the effective quantum yields (Figure S4.2). In *P. tricornutum*, circadian rhythms in growth rate, cell size, and pigment contents remained for a short period after switching from the DL cycle to the CL condition [396]. Additionally, oscillatory chlorophyll fluorescence was observed in *P. tricornutum* under constant light over four days following entrainment to the DL cycle [394]. Nevertheless, oscillations in the physiological parameters were dampened as cultures were incubated under constant light for a longer period, which was attributed to the desynchronization of the cell division cycle[409]. It is believed that cell activities in the culture become randomized under continuous light, as the daily resetting of the diel rhythm is abolished[389, 396, 409].

4.4.2 The periodic gene expression under constant and diel illumination

Time series data of the transcriptome covering 24 h were obtained from parallel groups of triplicate cultures under the DL and CL conditions. Due to the low sampling frequency that caused difficulty in discerning fine-scale phase differences, we did not aim at investigating phase shifts under constant light, and the target period was confined to 24 h to identify genes with likely cyclic expression patterns. The resulting rhythmic genes were automatically classified into eight phases in 3 h intervals based on the peaking time of transcript abundance.

In total, 10741 and 10849 transcripts with an average of fragments per kilo base exon per million mapped reads (FPKM) > 1 were identified in the CL and DL groups, respectively. As a result of rhythmicity analysis, 7344 and 1378 rhythmic genes were detected in the DL and CL groups, respectively, showing significant cyclic expression ($P_{adj} < 0.05$). These genes were further screened to omit those with low Max/Min fold change (maximum FPKM/minimum FPKM < 1.3) and amplitude (amp < 1). As a result, the number of rhythmic genes that could potentially lead to significant oscillatory outputs was 6978 in the DL group, which accounted for 64.3% of the transcribed protein-coding genes of *P. tricornutum* under the DL condition. This was comparable to the results of previous transcriptomic studies on *P. tricornutum* that identified 5803 [392] and 4567 [375] rhythmic genes. Moreover, 1028 CL-rhythmic genes remained after the screening, accounting for 9.6% of the total transcripts detected under the CL regime. The ratio of amplitude/maximum FPKM was calculated for each cyclic gene to assess the relative change of oscillation. Most DL-derived rhythmic genes (81.0%) showed relative amplitudes in a range of 10~40% (Figure S4.3). By contrast, the amplitude of 72.1% CL-rhythmic genes was distributed in a narrow range between 10 and 20% of the maximum expression level, which indicates a relatively stable expression of the genes under the CL condition. These results demonstrated that the diel expression of cyclic genes largely relied on external light stimulus. Under constant conditions, most of the rhythmicity on the transcriptomic level was abolished, reflecting the arrhythmic physiological parameters. A small proportion of genes persisted circadian rhythms that were independent of environmental cues. To our best knowledge, the present study provides the first data on the free-running circadian transcriptome under constant conditions in diatoms.

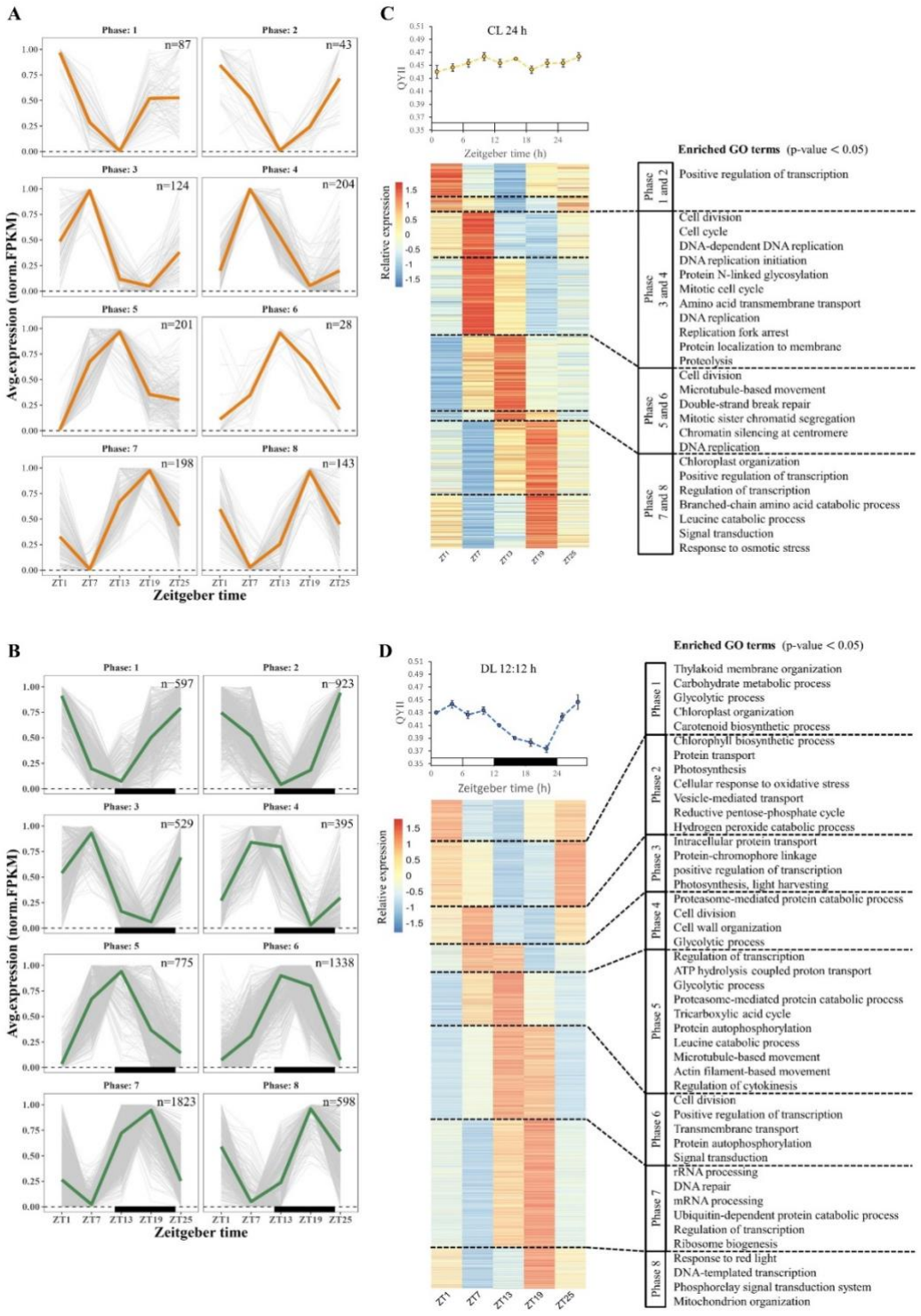

Figure 4.2. *Clustering of rhythmic genes under light/dark cycle and continuous light conditions. (A) and (B) Trendline of 24 h periodic change in transcript expression of rhythmic genes. Fragments per kilobase of exon per million mapped fragments (FPKM) values were normalized between 0 and 1; the thick green and orange lines represent an averaged expression of each cluster in the 12h/12h light/dark (DL) cycle and continuous light (CL) groups, respectively; "n" represents the number of genes in each cluster. Black squares indicate dark periods. (C) and (D) Heatmap of gene clusters associated with physiological data in photosynthetic efficiency (effective quantum yield, Φ_{PSII}) and enriched gene ontology (GO) terms.*

Through the rhythmicity analysis, the identified rhythmic genes were clustered into eight phases according to their expression patterns (Figure 4.2A and B). The distribution of the expression phase in the DL group exhibited a bimodal pattern with relatively more genes peaking in the morning (phase 2) and midnight (phases 6 and 7) (Figure S4.3). Similar findings were also reported in other species, such as *Nannochloroplsis oceanica*[389], *Seminavis robusta* [390], *C. reinhardtii*, *Porphyridium purpureum*, and *Synechocystis* sp. PCC6803[391]. By contrast, expression peaks of rhythmic genes in the CL group were more evenly distributed in different phases (Figure S4.3), which was likely due to the lack of external stimulus that entrained and constrained gene expression into coherent patterns. Furthermore, 717 genes were identified to exhibit periodic expression in both the CL and DL groups (Figure 4.3A). The same set of genes showed significantly higher and broader values of relative amplitude under the DL cycle (Figure 4.3B). This indicated a weaker oscillatory property of the common rhythmic genes under constant conditions, which could be attributed to desynchronization resulted from loss of entrainment. Nevertheless, the Sankey diagram associating common genes in the two groups showed dispersed links of different phases between the free-running and entrained conditions (Figure 4.3C). Notably, major parts of some CL-cyclic gene clusters (phases 5 – 7) showed corresponding relationships with adjacent 4 – 7 phases in the DL group. This result suggests the existence of synchronized populations in triplicate cultures that enabled the detection of persistent circadian rhythmic genes.

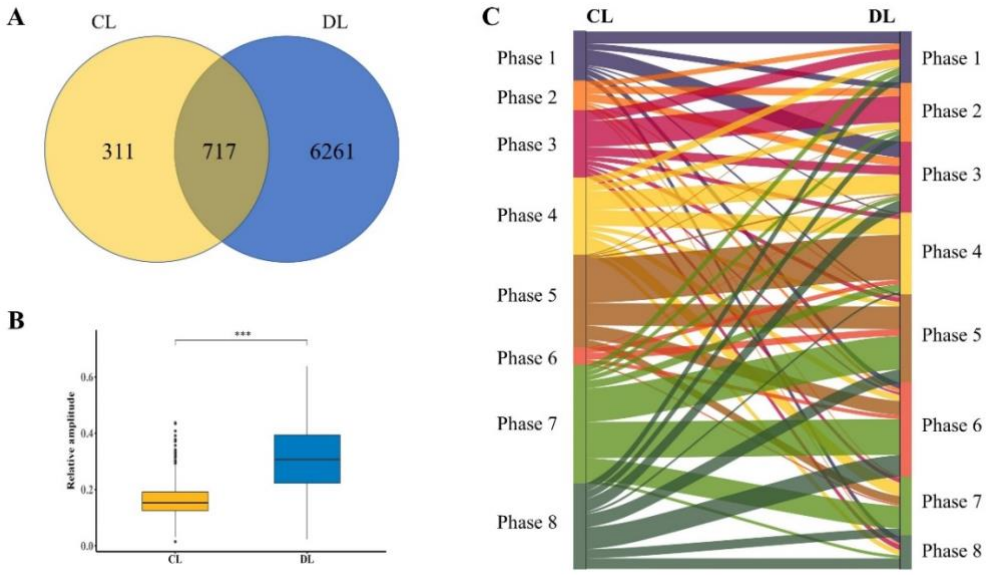

Figure 4.3. *Summary of rhythmic genes detected under light/dark cycle and continuous light conditions. (A) Venn diagram to compare the number of rhythmic genes in the 12h/12h light/dark cycle (DL) group with the continuous light (CL) group. (B) Statistics of relative amplitude (amplitude/maximum FPKM) among common rhythmic genes in DL and CL groups. (C) The association of common rhythmic genes in different expression phases between DL and CL groups. (***, p-value < 0.001).*

4.4.3 Rhythmic patterns associated with specific biological processes

Enrichment analysis of Gene Ontology (GO) annotation was performed to characterize the main functional activities within each phase group. Rhythmic genes in both CL and DL groups were clustered based on gene expression patterns, which can be functionally specialized according to the enriched GO terms shown (Figure 4.2).

For the DL regime, our data are generally consistent with the previous global transcriptomes [375, 392] in *P. tricornutum* concerning the rhythmic order of active biological processes. For instance, a predominant up-regulation of photosynthesis, the Calvin-Benson cycle, carbohydrate metabolism during the day, and an elevated expression of glycolysis and tricarboxylic acid (TCA) cycle in the dark period [375, 392] were also observed in the present study. Activation of processes participating in cell division started from phase 4 to phase 6. Consistently, active cell division at the light-to-dark transition has been widely reported in diatoms and green microalgae[375, 390, 393]. While the proteosome-mediated protein degradation became active several hours before the dark period, terms such as rRNA processing and ribosome biogenesis predominated in the phase several hours before light onset. This suggests that protein degradation and synthesis were separately activated during the day and night, respectively, which have been previously reported in other microalgal species[389, 411].

The relatively small size of each cluster in the CL group necessitated the combination of genes from phases with similar trend lines (Figure 4.2) for the enrichment analysis. Notably, most enriched functions found among CL-rhythmic genes were involved in cell division, including a variety of GO terms relevant to chromatin organization, DNA replication, and mitosis. The associated expression clusters spanning phases 3 to 6 (ZT7 – ZT13) included more than half of the total identified rhythmic genes in the CL group. Specifically, phase 3/4 possessing more genes encoding G2 mitotic-specific cyclins, mini-chromosome maintenance complex-binding proteins (MCM) as well as DNA polymerases and DNA mismatch repair proteins was presumably related to the interphase (G1-S-G2) that is characterized by DNA synthesis and replication. The subsequent phase 5/6 featured a peaking expression of multiple genes encoding structural maintenance of chromosomes (SMC) proteins, cohesion complex subunits, and microtubule components such as kinesin-like protein (KIF), and kinetochores, all of which play a role in the mitotic process [408]. These results demonstrated an intrinsic regulation of cell division genes, which was largely independent of external stimuli.

4.4.4 Rhythms in global regulation and cell growth

Then, we investigated the participation of the identified rhythmic genes in transcriptional regulation and cell growth-related processes, including cell division, photosynthesis, and carbon fixation (Figure 4.4). All annotated genes with functions of interest were searched on the PLAZA database and listed in *SI Appendix*, Dataset S7.

In this analysis, we found that more than 80% of the examined transcription factors (TFs) exhibited rhythmicity in either condition. Nevertheless, different TF families showed distinct characteristics. Relatively large proportions of bHLH-TFs (33.3%) and Myb-TFs (37.2%) had rhythmic features under constant conditions. By contrast, fewer HSF-TFs (16.7%) and bZIP-TFs (4.3%) exhibited self-sustained rhythms. The circadian expression properties of bHLH- and Myb-family TFs have been widely recognized in plants, insects, and mammals[412-415]. Concerning cell division, DNA replication, cyclin, and mitosis represented the groups containing the highest proportions of genes with self-sustained rhythms. By contrast, CDK and APC subunits, including 35.3% and 45.5% of arrhythmic genes, respectively, implied relatively constitutive expression of signal transduction and proteolytic components. These findings agree with the cell cycle mechanism controlled by the cyclin-CDK association. In the cell cycle, levels of CDKs are generally kept constant, while their active functions are regulated by the presence of their cyclin partners. Fluctuating abundance of various cyclins is regulated by their synthesis and proteolysis that has been recognized as an intrinsic oscillator controlling the cell cycle progression [416]. Furthermore, we explored rhythmic genes in photosynthetic processes including the electron transfer chain (ETC), chlorophyll and carotenoid biosynthesis, and carbon fixation processes, including the carbon concentrating mechanism (CCM) and the Calvin-Benson-Bassham (CBB) cycle. These biological processes included very high percentages of rhythmic genes among all genes involved, but the majority of rhythmic genes appeared only with DL diel rhythm. These results indicated that the cyclic expression of light harvesting and carbon conversion processes heavily depended on light stimuli.

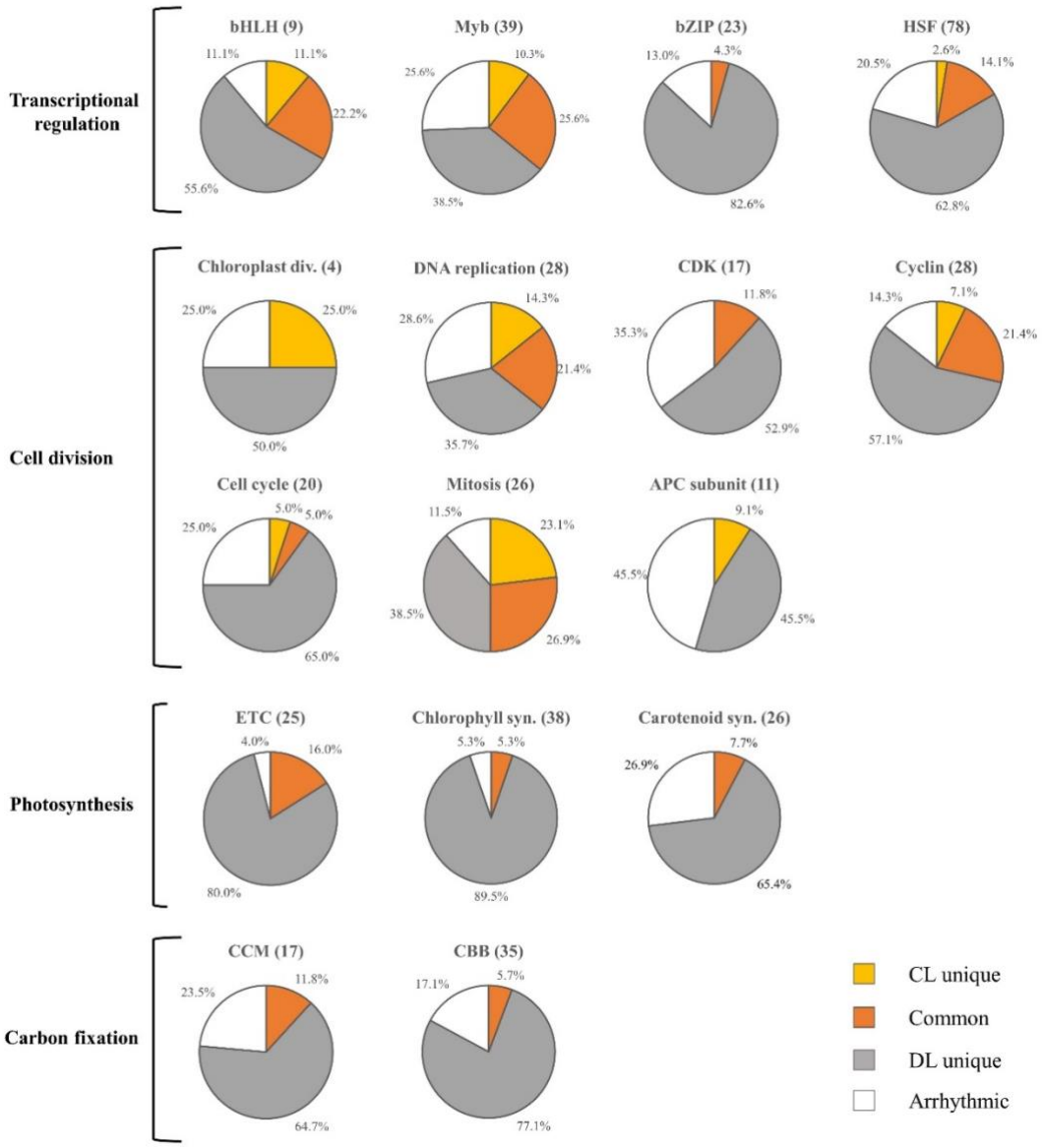

Figure 4.4. *Proportions of self-sustained rhythmic genes in selected biological processes. For a specific function or pathway, all annotated genes present in P. tricornutum were searched on PLAZA. The pie charts indicate the proportions of CL- or DL-derived rhythmic genes within each selected functional group. Abbreviation: bHLH, basic-helix-loop-helix; Myb, myeloblastosis; bZIP, basic region leucine zipper; HSF, heat shock factor; Chloroplast div., chloroplast division; Chlorophyll syn., chlorophyll synthesis; Carotenoid syn., carotenoid synthesis; CCM, carbon concentrating mechanism; CBB, Calvin-Benson-Bassham cycle; CDK, cyclin-dependent kinase; APC, anaphase-promoting complex; ETC, electron transport chain.*

A previous study on *C. reinhardtii* identified 269 circadian rhythmic genes with diverse functions in photosynthesis, respiration, cellular structure, and various metabolic pathways[395]. This may explain the strong circadian rhythms in the physiology of green microalgae[388]. In diatoms, the circadian rhythms were not obvious on the phenotypic level due to the arrhythmic expression of metabolic genes[409]. Our molecular data revealed a persistent oscillator of the cell division

cycle that might be one reason for the controlled pace of cell growth under continuous light. A theory states that cell growth and cell division are coordinately regulated to maintain a cell size homeostasis [417]. Excepting environmental factors that determine the growth of cells, cell cycle is more likely to be regulated by a cell-sensing rather than a timing mechanism [417]. The "sizer" model has been proposed for various cells from bacteria to animal cells [418-420], though research on size-sensing in microalgae has not been seen. Furthermore, a homologous gene family containing ten Myb-genes, including Myb3R1 (Phatr3_J15016) and Myb3R2 (Phatr3_J6839) that based on orthologous annotations suggest a possible connection to the regulation of cell proliferation. In Arabidopsis thaliana, the Myb3R TFs were shown to act as transcriptional repressors to regulate G2/M-specific genes and thus played a role in establishing a post-mitotic quiescent state[421]. The intrinsic expression rhythms of these TF genes may be responsible for the circadian rhythms exhibited by various cell division genes.

4.4.5 Effect of continuous light on gene expression

In this study, it is worth noting that the loss of the entrainment led to arrhythmic expression and substantially reduced oscillations in gene expression. Therefore, the different light regimes may affect cell growth by influencing the overall gene expression levels. To address this hypothesis, differential expression analysis was conducted to compare overall gene expression levels in the two experimental groups across all sampling times. Using the DL group as the control, 507 up-regulated DEGs and 935 down-regulated DEGs ($P_{adj} < 0.05$) were identified in the CL group. As shown in the GO enrichment results (Figure 4.5A and B), top up-regulated biological process GO terms were related to cell division. The kinesin complex, microtubule, and nuclear chromosome kinetochore, which form mitotic machinery components such as the spindle appeared in the top confident cellular component GO terms. For down-regulated DEGs, we found several biological processes that were likely to influence cell growth, including chlorophyll biosynthetic process, ribosome biogenesis, reductive pentose-phosphate cycle (i.e., CBB cycle), photosynthesis, nitrate assimilation, and carotenoid biosynthetic process.

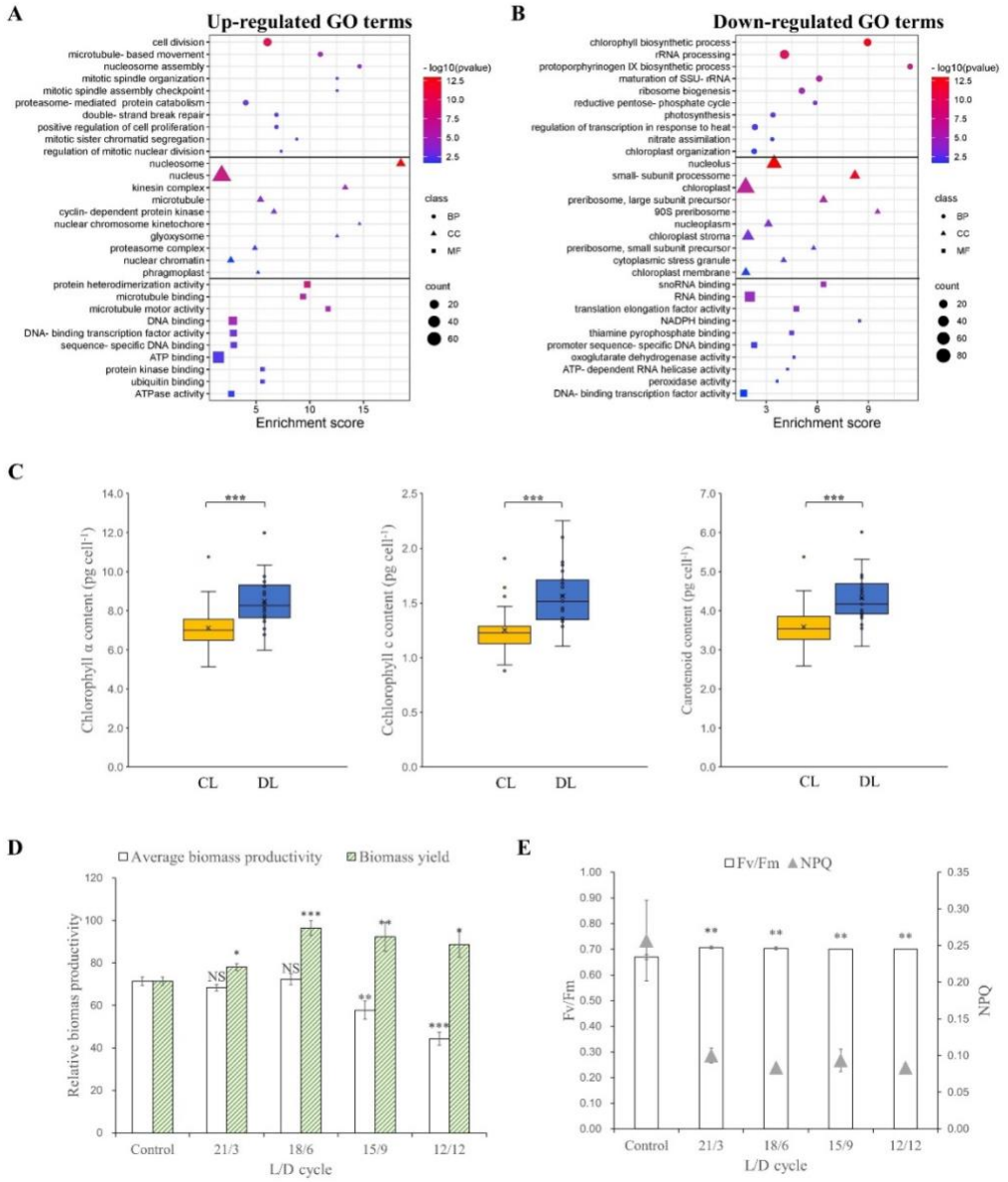

Figure 4.5. *Differential gene expression and contents of pigments in the CL group compared with the DL group. (A) Enrichment of GO terms based on up-regulated DEGs. (B) Enrichment of gene ontology (GO) terms based on down-regulated DEGs. An overall differential gene expression profile between the DL and CL groups was assessed based on data from five time points over a 24 h time course (n = 15). Top enriched GO terms in each category (BP: biological process; CC: cellular component; MF: molecular function) are presented. (C) Comparison of estimated pigment contents between cultures under CL and DL conditions. Samples were collected in 3 h intervals over 24 h time course (n = 27). (D) Effect of light/dark cycles on biomass productivity. (E) Effect of light/dark cycles on photosynthetic efficiency. (NS, no significance; *, p-value < 0.05; **, p-value < 0.01; ***, p-value < 0.001).*

More specifically, three bHLH-TFs, eight Myb-TFs, five bZIP-TFs, and five HSP-TFs were significantly up-regulated in CL compared to DL (Figure S4.4), whereas remarkably more stress-induced HSP-TFs (16 genes) were down-regulated. This result implies a higher intracellular stress under the DL condition, which may be caused by oscillatory changing environments. While up-regulated genes were

extensively found in all functional groups involved in cell division (Figure S4.5), pathways of chlorophyll and carotenoid biosynthesis contained only down-regulated DEGs. Specifically, 17 out of 38 chlorophyll biosynthetic genes were down-regulated under the CL condition, which can be mapped to the entire pathway of synthesizing chlorophyll *a* from L-glutamate (Figure S4.6). Additionally, five genes encoding the pathway of synthesizing lycopene, the precursor of carotene from geranyl-geranyl-PP were significantly down-regulated (Figure S4.7). These results were further proved by pigment determination that demonstrated significantly higher contents of chlorophylls and total carotenoids per cell under the DL condition in comparison with the CL condition (Figure 4.5C). Although most genes in the ETC and CCM pathways did not show significant changes in expression, the expression of eight genes within the CBB cycle was significantly down-regulated (Figure S4.8), which suggests a reduction in carbon fixation. The constantly low expression of essential pathways in pigments biosynthesis and carbon dioxide assimilation provided another likely explanation for the reduced photosynthetic efficiency in diatoms under the continuous light condition. These results suggest that distortions of the regular diel rhythms could impact diatom growth by impairing the overall gene expression in photosynthesis. To further demonstrate the importance of the dark period in maintaining photosynthetic efficiency, an experiment was conducted to examine cell growths under different light/dark cycles. By reducing the photoperiod, biomass accumulation in 15 h and 12 h illumination was only decreased to 81 ± 6% and 62 ± 4% of that generated by 24 h photoperiod (control), whereas the average biomass productivities resulted from 21/3 h and 18/6 h light/dark cycles were statistically indifferent from the control. When only light periods were accounted for in the calculation, all experimental groups with 3 – 12 h dark periods showed 10 – 35% higher ($p < 0.05$) biomass yield on light compared to the control (Figure 4.5). Additionally, significantly lower maximal quantum yield (F_v/F_m) and higher non-photochemical quenching (NPQ) were observed in the control, which suggests that inclusion of a dark period could effectively improve photosynthetic efficiency in diatoms.

4.4.6 Differential expression and targeting analysis of microRNA (miRNA)

Small RNAs were analyzed to recover possible miRNA-mediated regulation of gene expression. Rhythmic analysis indicated significant cyclic expression patterns for eight miRNAs in the CL group and eighty miRNAs in the DL group. However, due to large variations among biological replicates, the patterns of rhythmic expression of these miRNAs were not as clear as the genes (mRNAs). This was probably due to the vulnerabilities of miRNA to degradation during the sample processing. Through differential expression analysis on a 24 h course expression of miRNA transcripts in different conditions, 82 DEGs of miRNA were identified, including 18 up-regulated miRNAs and 64 down-regulated miRNAs in the CL group, in comparison with the DL group. Target prediction suggested 751 and 1281 possible mRNA targets of the up-regulated and down-regulated miRNAs, respectively (Table S4.2). While miRNAs could match and thus regulate many mRNAs, some mRNAs were targets of multiple miRNAs. Further research was focused on 424 genes (Figure 4.4) that, as mentioned above, are associated with global transcriptional regulation and cell growth. Regarding miRNA-mediated gene silencing through mRNA cleavage [422], the expression levels of mRNAs in theory should be

inversely related to the expression levels of miRNAs. Nevertheless, the target identification analysis revealed potential matches of miRNAs with both up-regulated and down-regulated mRNAs (Table S4.2). We only explored the coupling of miRNAs and mRNAs with reverse expression levels, whereas the other possible targets that might be regulated in translation or involved in more complicated regulatory networks with other small RNAs were not investigated here due to a lack of data for analysis. For the coding RNAs of interest, the expression of 47 up-regulated mRNAs and 40 down-regulated mRNAs could be influenced by the differentially expressed miRNAs determined in the present study (Table S4.2). For instance, our results revealed ten up-regulated miRNAs under continuous light, which could repress the expression of 11 enzyme-coding genes in the chlorophyll biosynthesis pathway (Figure 4.6).

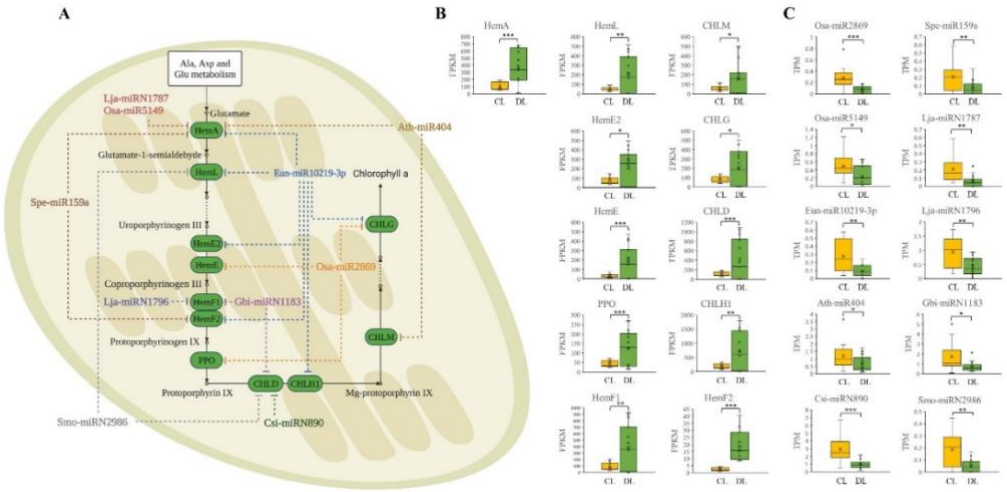

Figure 4.6. *Potential mRNA targets of differentially expressed microRNAs (miRNA) under continuous light conditions. Differential expression analysis using all data across five sampling times covering 24 h was performed to compare gene expression levels between the CL and DL groups. Differentially expressed genes (DEGs) with significant differences (P_{adj} < 0.05) and large fold changes (|log2foldchange| > 1) were screened. (A) Pathways in chlorophyll biosynthesis that were possibly targeted by differentially expressed miRNA within 24 h period. (B) DEG expression levels of coding RNAs targeted by miRNAs. (C) DEG expression levels of miRNAs. CL and DL are presented in yellow and green, respectively. (*, p-value < 0.05; **, p-value < 0.01; ***, p-value < 0.001).*

4.5 Supplementary materials

Table S4.1. Growth performance of P. tricornutum under continuous and light/dark cycle conditions (n = 3).

Group	Semi-continuous cultivation period		24-h sampling period	
	μ (d^{-1})	**P_b (mg $L^{-1}d^{-1}$)**	**μ (d^{-1})**	**P_b (mg $L^{-1}d^{-1}$)**
DL	0.51 ± 0.02	49.82 ± 0.77	0.46 ± 0.02	46.44 ± 1.62
CL	0.90 ± 0.19	79.08 ± 3.03	0.93 ± 0.18	81.43 ± 3.44

CL, continuous light condition; DL, light/dark cycle condition; μ, growth rate; P_b, biomass productivity.

Table S4.2. Potential mRNA targets of differentially expressed miRNAs under continuous and light/dark cycle conditions.

Differentially expressed miRNAs	**Total number of miRNA**	**Total number of target mRNA**	**Target mRNAs of interest**	
			Up-regulated	**Down-regulated**
Up-regulated miRNA	18	751	33	40
Down-regulated miRNA	64	1281	47	63

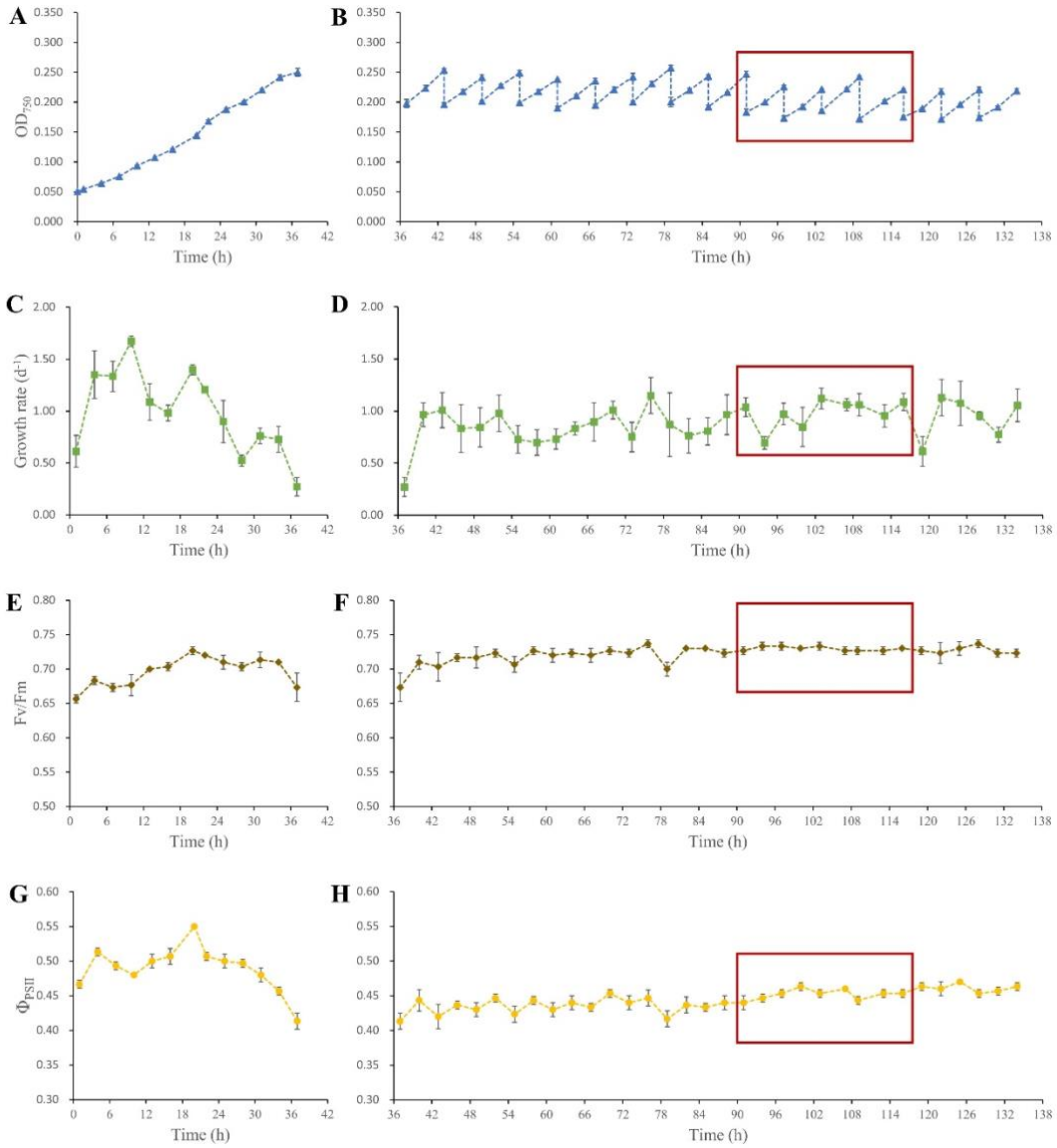

Figure S4.1. Growth performance of P. tricornutum under the continuous light condition. (A) and (B) Cell density (OD750). (C) and (D) Growth rate. (E) and (F) Maximum quantum yield (F_v/F_m). (G) and (H) Effective quantum yield (Φ_{PSII}). Samples were measured every three hours with triplicated cultures. Panels (B), (D), (F), and (H) represent the data during semi-continuous cultivation. The red rectangles indicate the sampling time for molecular analysis.

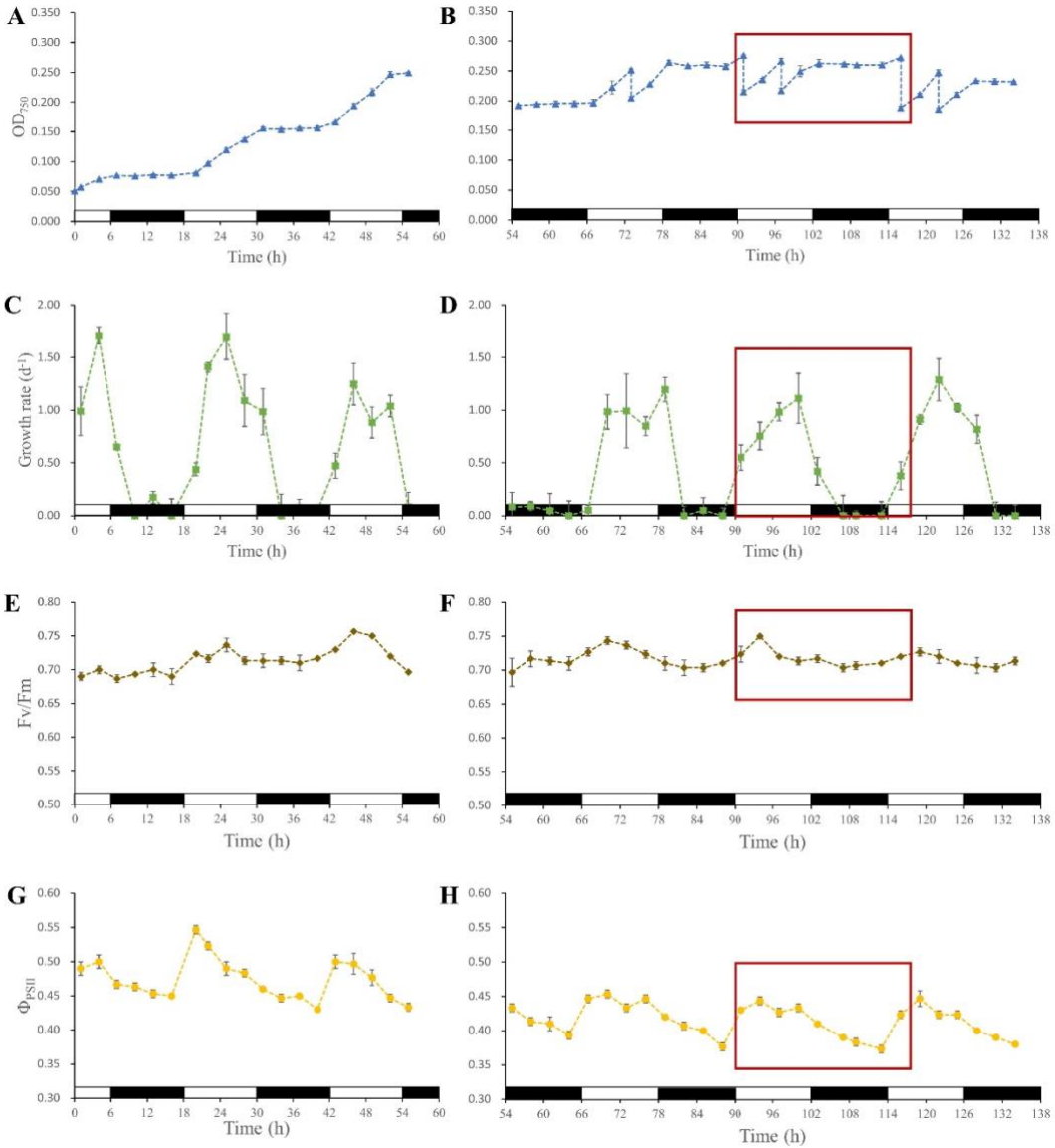

Figure S4.2. Growth performance of P. tricornutum under the light/dark cycle condition. (A) and (B) Cell density (OD750). (C) and (D) Growth rate. (E) and (F) Maximum quantum yield (F_v/F_m). (G) and (H) Effective quantum yield (Φ_{PSII}). Samples were measured every three hours with triplicated cultures. Panels (B), (D), (F), and (H) represent the data during semi-continuous cultivation. Black blocks indicate dark periods. The red rectangles indicate the sampling time for molecular analysis.

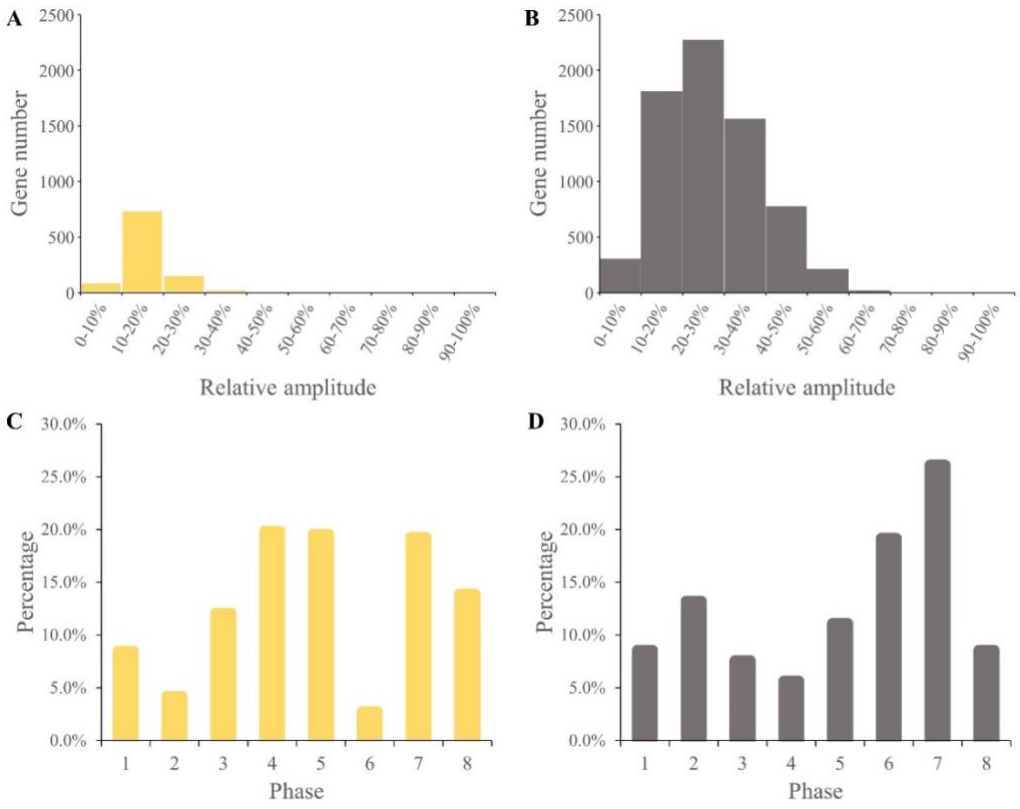

Figure S4.3. Distributions of rhythmic genes in CL and DL groups. (A) and (B) Distribution of amplitudes relative to maximal expression (FPKM) of identified rhythmic genes in the CL (yellow) and DL (grey) groups. (C) and (D) Distribution of identified rhythmic genes in the CL (yellow) and DL (grey) groups in different clusters.

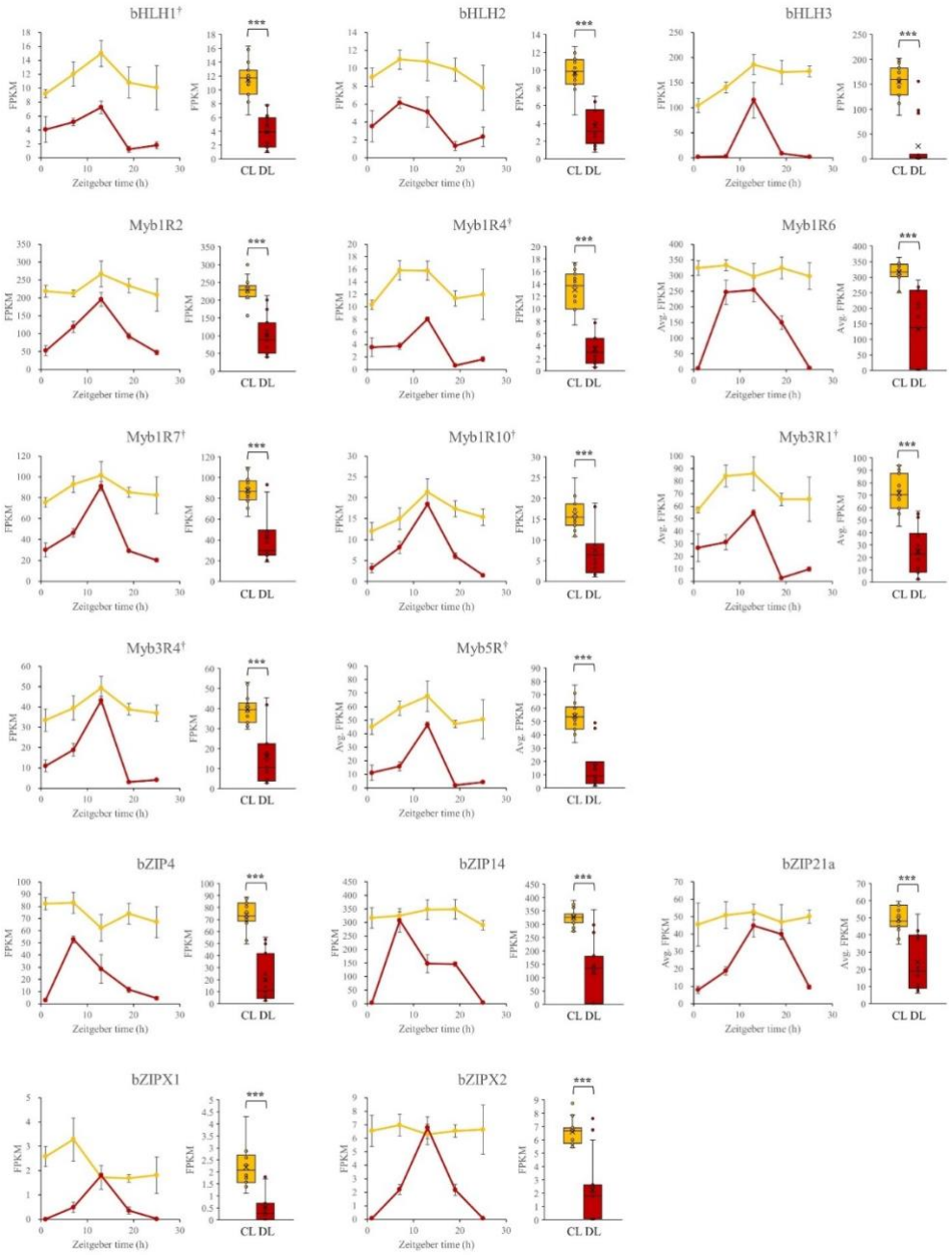

Figure S4.4. Differentially expressed genes (DEGs) of transcription factors comparing expression levels under the continuous light (CL) and light/dark cycle (DL) conditions. Differential expression analysis using all data across five sampling times covering 24 h was performed to compare gene expression levels between the CL and DL groups. DEGs with significant differences (P_{adj} < 0.05) and large fold changes (|log2foldchange| > 1) were screened. Expression data of each identified DEG include a trendline of average FPKM over the sampling period (24 h) and distribution statistics on the data across all time points; CL and DL are presented in yellow and red, respectively. (, p-value < 0.05; **, p-value < 0.01; ***, p-value < 0.001. The label † indicates genes with significant rhythmicity under the continuous light condition).*

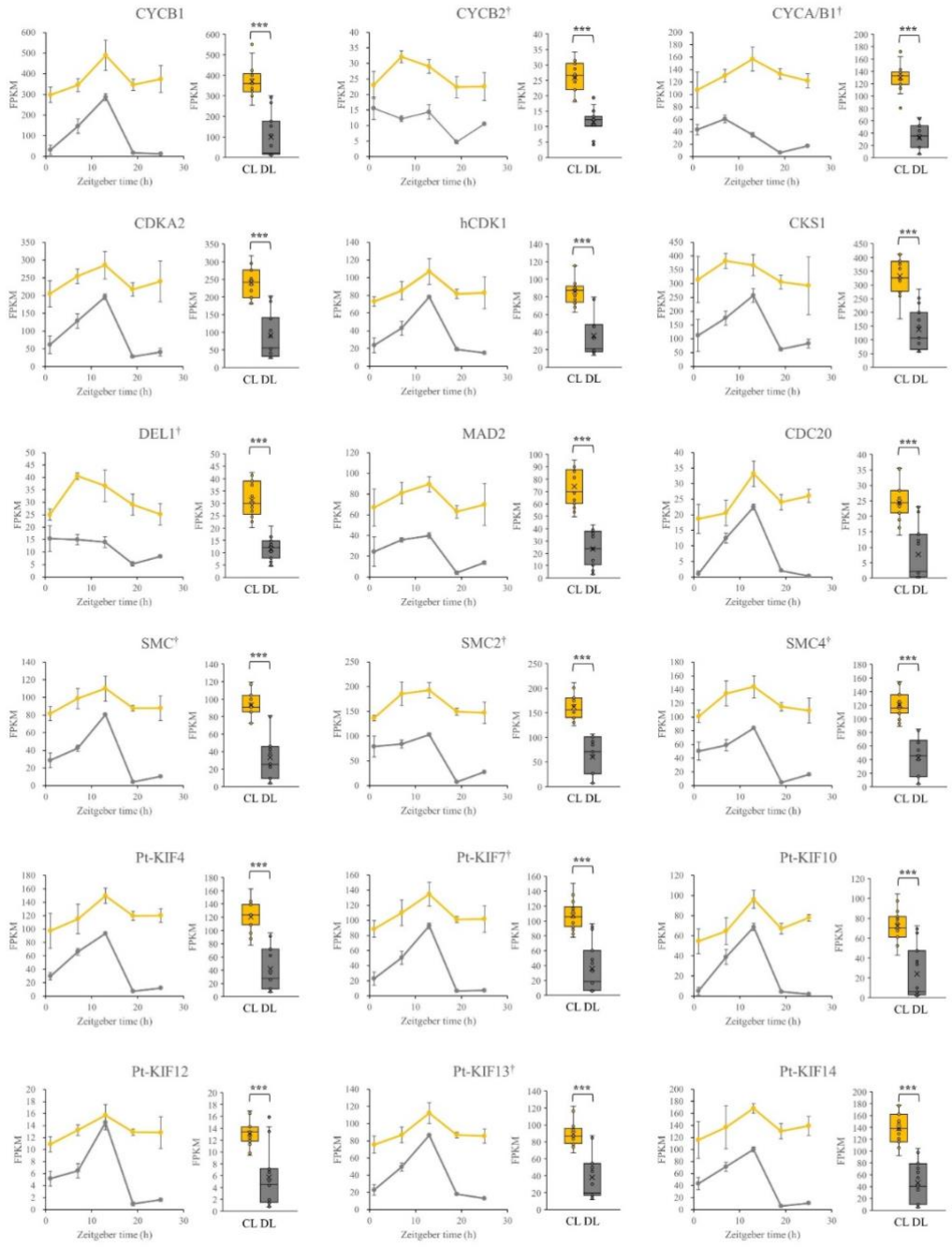

Figure S4.5. Differentially expressed genes (DEGs) involved in cell division comparing expression levels under the continuous light (CL) and light/dark cycle (DL) conditions. Differential expression analysis using all data across five sampling times covering 24 h was performed to compare gene expression levels between the CL and DL groups. DEGs with significant differences (P_{adj} < 0.05) and large fold changes (|log2foldchange| > 1) were screened. Expression data of each identified DEG include a trendline of average FPKM over the sampling period (24 h) and distribution statistics on the data across all time points; CL and DL are presented in yellow and grey, respectively. (, p-value < 0.05; **, p-value < 0.01; ***, p-value < 0.001. The label † indicates genes with significant rhythmicity under the continuous light condition).*

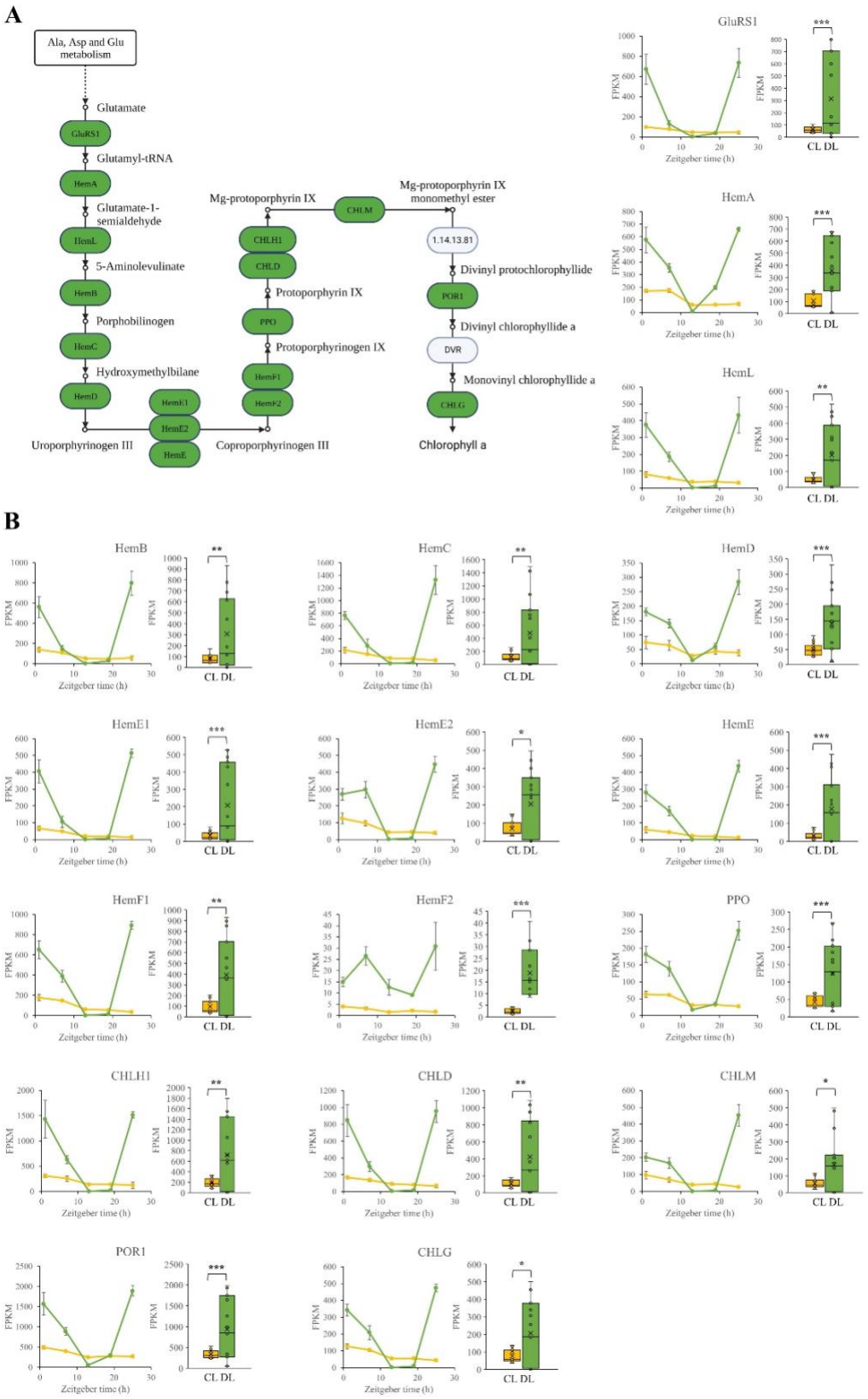

Figure S4.6. Differentially expressed genes (DEGs) in chlorophyll biosynthesis comparing expression levels under the continuous light (CL) and light/dark cycle (DL) conditions. Differential expression analysis using all data across five sampling times covering 24 h was performed to compare gene expression levels between the CL and DL groups. DEGs with significant differences (P_{adj} < 0.05) and large fold changes (|log2foldchange| > 1) were

screened. (A) Mapping of DEGs (CL/DL) in the metabolic pathways of chlorophyll biosynthesis, DEGs are highlighted in green color. (B) Expression data of each identified DEG, including a trendline of average FPKM over the sampling period (24 h) and distribution statistics on the data across all time points; CL and DL are presented in yellow and green, respectively. (, p-value < 0.05; **, p-value < 0.01; ***, p-value < 0.001).*

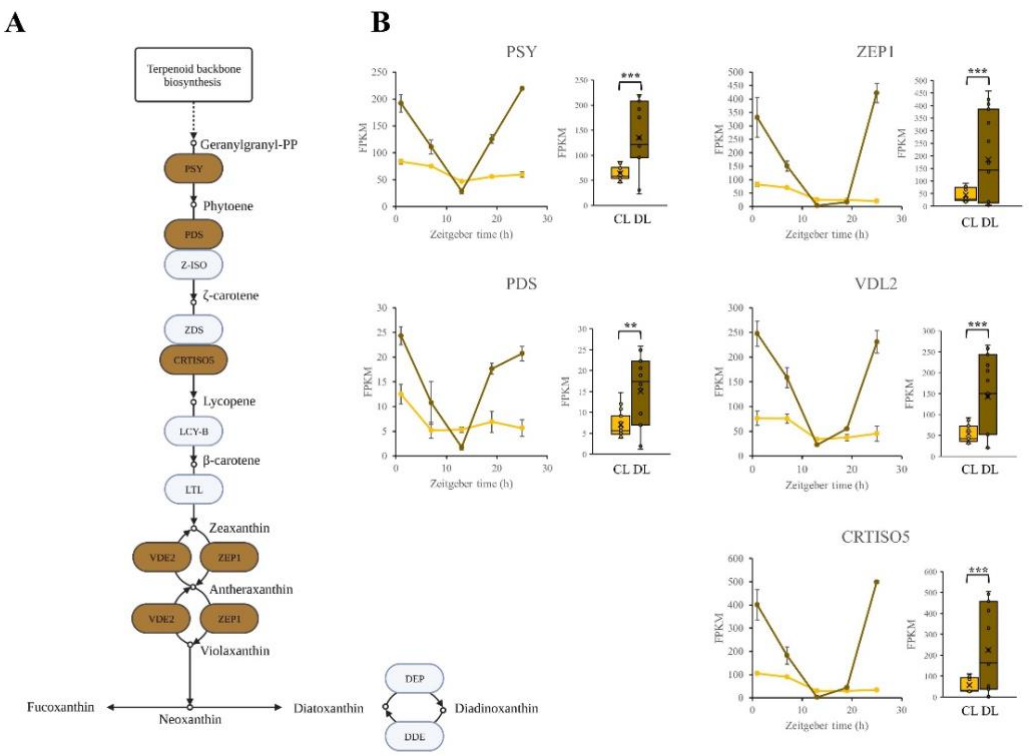

Figure S4.7. Differentially expressed genes (DEGs) in carotenoid biosynthesis comparing expression levels under the continuous light (CL) and light/dark cycle (DL) conditions. Differential expression analysis using all data across five sampling times covering 24 h was performed to compare gene expression levels between the CL and DL groups. DEGs with significant differences (P_{adj} < 0.05) and large fold changes (|log2foldchange| > 1) were screened. (A) Mapping of DEGs (CL/DL) in the metabolic pathways of the carotenoid biosynthesis, DEGs are highlighted in brown color. (B) Expression data of each identified DEG, including a trendline of average FPKM over the sampling period (24 h) and distribution statistics on the data across all time points; CL and DL are presented in yellow and brown, respectively. (, p-value < 0.05; **, p-value < 0.01; ***, p-value < 0.001).*

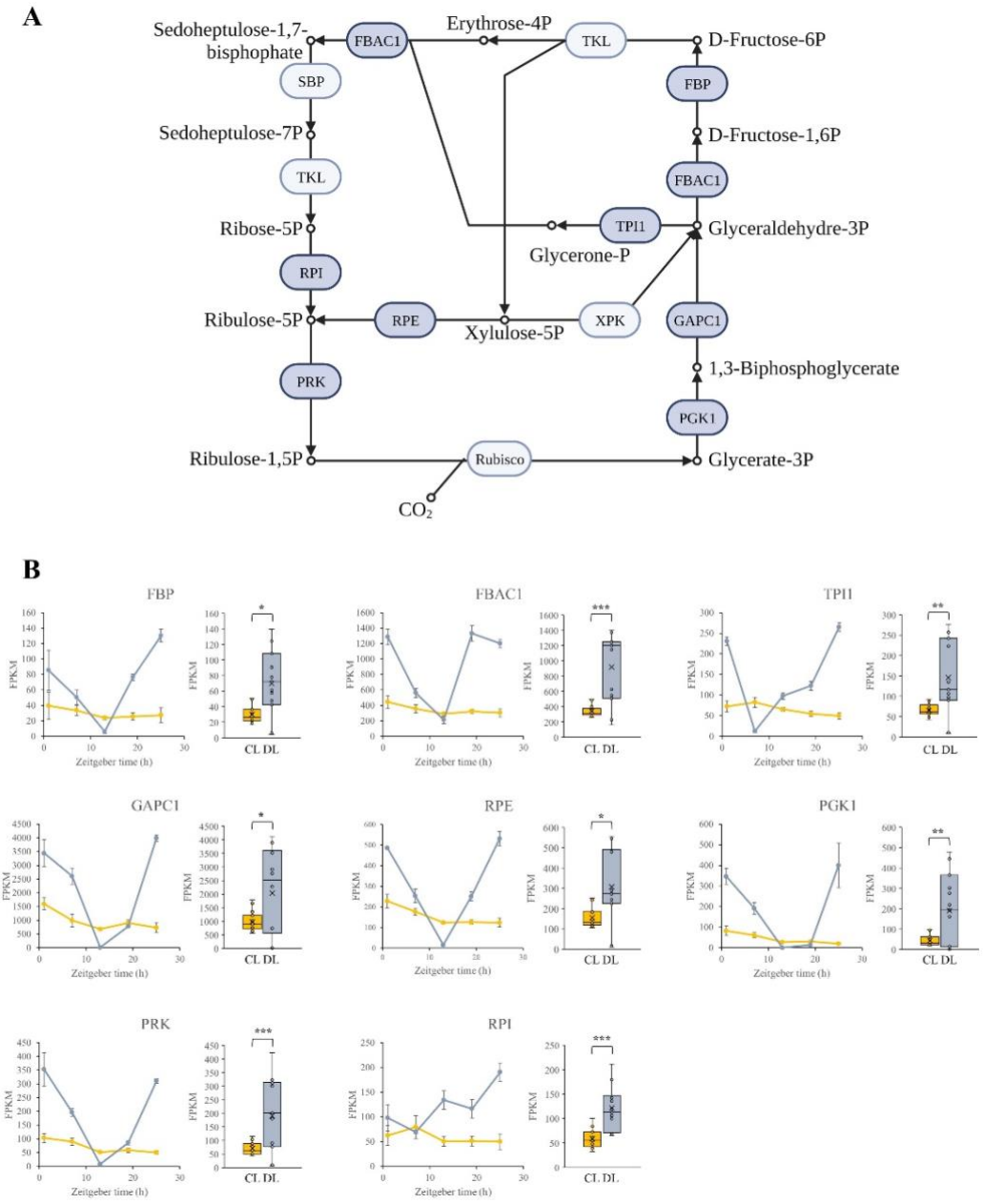

Figure S4.8. Differentially expressed genes (DEGs) in the Calvin-Benson-Bassham (CBB) cycle comparing expression levels under the continuous light (CL) and light/dark cycle (DL) conditions. Differential expression analysis using all data across five sampling times covering 24 h was performed to compare gene expression levels between the CL and DL groups. DEGs with significant differences (P_{adj} < 0.05) and large fold changes (|log2foldchange| > 1) were screened. (A) Mapping of DEGs (CL/DL) in the metabolic pathways of the CBB cycle, DEGs are highlighted in blue color. (B) Expression data of each identified DEG, including a trendline of average FPKM over the sampling period (24 h) and distribution statistics on the data across all time points; CL and DL are presented in yellow and blue, respectively. (, p-value < 0.05; **, p-value < 0.01; ***, p-value < 0.001).*

5 Discussion and conclusions

The model diatom, *P. tricornutum* is of commercial interest due to its high content of fucoxanthin and PUFA. However, *P. tricornutum* exhibits sensitivity to acidic conditions [304, 423], which presents a challenge for its cultivation using industrial flue gas. For strain improvement, this project explored bioengineering approaches, including ALE and genetic modification to enhance the stress resistance of *P. tricornutum* against inhibitory low-pH. ALE led to partial recovery of growth in three parallel cultures. Phenotypic characterization confirmed a 27.5% to 110% increase in growth of the adapted strains under acidic conditions (pH 5.5 to 6.5). Additionally, using the insights gained from gene expression analysis in the ALE strains, transgenic strains of *P. tricornutum* were developed to overexpress specific candidate genes, including Phatr3_J33543 (ferredoxin), Phatr3_J50516 (cation/proton transporter), and Phatr3_Jdraft1806 (bicarbonate transporter). Despite a significant reduction in growth rates, all transgenic strains were able to survive at pH 5.0, which was lethal to the WT. Overall, the objectives 1 and 2 were achieved from an engineering perspective.

To address RQ1, an initial single-factorial experiment was conducted to assess impacts of a wide pH range on the photosynthesis and growth of *P. tricornutum*, revealing progressively more severe negative impacts as the pH decreased to pH 5.0. While the pH 5.5 allowed little cell growth, *P. tricornutum* was completely inhibited by pH 5.0, which defined the low threshold for viable cell growth. Throughout ALE, we noted a higher proportion of oval cells in the initial several subcultures, which may be a result of the selection of stress-resistant cell form [424] under selective pressure. Furthermore, the oval cells may undergo active transformation from other morphotypes as an adaptive mechanism to ensure cell survival in the face of adverse environmental changes [33]. Another adaptive response observed during acclimation was the gradual reduction in chlorophyll levels. Stress-induced degradation of chlorophyll and suppression of chlorophyll biosynthesis are frequently observed in higher plants [42-44], which is proposed as a defense strategy to survive in harsh environments by curtailing excessive energy capture that leads to the generation of harmful oxygen radicals [310]. The suppression of chlorophyll biosynthesis was also evident in the culture subjected to continuous illumination, which could induce stress in *P. tricornutum* as well (Paper 3).

In response to RQ2, the transcriptomic study of the ALE strains revealed upregulated genes associated with photosynthesis, intracellular pH regulation, and carbon fluxes, such as glycolysis/gluconeogenesis and fatty acid biosynthesis. These findings provide an explanation for the enhanced growth, photosynthesis, acidic tolerance, and changes in macromolecular compound composition. Among them, ion/electron carrier genes that potentially impact cellular proton homeostasis were chosen for subsequent reverse genetics investigations. As the genomic and transcriptomic analyses indicated distinct evolutionary paths for the three parallel cultures during adaptation, shared differentially expressed genes (DEGs) among multiple strains are likely to play a crucial role in acidic tolerance. The

overexpression of Phatr3_J33543, Phatr3_J50516, and Phatr3_Jdraft1806 resulted in a significant reduction in cellular oxidative stress and improved photosynthesis. Molecular analyses of the Phatr3_J33543 transgenic strain showed minimal alterations in the transcriptomic response to low-pH stress. In contrast, the overexpression of Phatr3_J50516 (PtCPA) and Phatr3_Jdraft1806 (PtSLC4-2), which encode proton and bicarbonate pumps, respectively, resulted in more extensive differential expression in the corresponding transgenic strains. Specifically, the upregulated expression of diverse transmembrane transporters can facilitate intracellular pH regulation, consequently mitigating the production of reactive oxygen species (ROS).

With respect to the influence of circadian rhythms on photosynthetic efficiency (RQ3), the transcriptomic data demonstrated self-sustained oscillations in the expression of transcription factor genes and cell division genes, while the transcription of genes associated with photosynthesis and carbon fixation relied heavily on light stimuli. Continuous photosynthesis exerted effects on the overall expression levels of multiple pathways. Notably, the absence of the light/dark cycle resulted in consistently low expression levels of pigment biosynthesis and carbon fixation pathways during continuous illumination, potentially contributing to hindered growth and reduced photosynthetic efficiency. The three articles presented in this thesis collectively contribute to developing photosynthetic cell factory of diatoms. While the first two articles focus on maintaining photosynthesis under stressed conditions, the third article investigates circadian rhythms relevant to cell growth. Although it deviates in its focus, the third article sheds lights on potential intrinsic factors that affect photosynthesis and biomass production, which also complements the findings of the first two articles. By examining oscillatory expression of transcriptomes under constant illumination, it provides a broader perspective on strain improvement for biomass production and offers valuable insights into circadian rhythms in diatoms.

5.1 Validation of results

The project encountered certain technical challenges that have the potential to impact the validity of the results. These challenges and their implications are discussed in this section. To overcome these limitations, the implementation of more advanced technologies is necessary.

In many studies investigating the effects of pH, CO_2 streams are introduced into microalgae cultures for pH regulation [304, 423]. However, this method fails to differentiate the impacts of pH and CO_2. Hence, buffers such as MES and Tris-HCl were employed in this project to control the pH without introducing additional variables. While the buffers effectively maintained pH stability in all experiments, the medium pH could still influence carbon availability [58], potentially restricting cell growth. In the absence of CO_2 supply, carbon availability primarily depended on the equilibrium of CO_2 dissolution between the air and the medium.

Approximately 80 clones were obtained from the ALE strains by plating diluted cultures on solid media (refer to Appendix A, Figure A3). Unfortunately, due to limited experimental capacity and the absence of high-throughput screening

technology to assess their growth, the sequencing analyses were not conducted using genetically homogeneous clone samples. Instead, bulk cultures of ALE strains, which could consist of multiple dominant populations, were employed to generate the omics data. Although these results provide valuable insights into the set of genes associated with stress tolerance that contribute to the overall growth improvement of the culture, they may be less reliable for establishing a genotype-to-phenotype relationship. Nevertheless, they offer valuable information regarding the mutations and transcriptomes resulting from the ALE process.

Growth improvements in *P. tricornutum* through either ALE or rational genetic engineering approaches were found to be limited for engineering purposes. In the ALE method, the diatom exhibited very slow growth under the selective pressure of pH 6.0, which could result in insufficient reproduction for generating mutations. Another potential contributing factor could be the relatively short duration of the ALE process, although the growth rates remained stable in several cycles before concluding the experiment. To expand the subjects of mutation in the ALE screening, a combination with induced mutagenesis could be considered as an option. However, a more significant factor is the fundamental intolerance of *P. tricornutum* to acidic conditions, which can be attributed to its inherent characteristics determined by the genomic background. Therefore, we cannot expect that modifications of individual genes alone can rescue and restore the growth of *P. tricornutum* under severe stress.

5.2 Dissertation contribution

This dissertation focuses on the topic of pH stress and its implications for engineering stress-resistant microalgae for biotechnological applications. Additionally, it contributes to scientific advancements in cell biology and our understanding of adaptive mechanisms in marine diatoms in the context of ocean acidification. Although growth improvements through ALE and genetic engineering are still distant from achieving feasible diatom production from geogas, this study presents a significant breakthrough in enabling diatom growth under lethal stress conditions. Moreover, this dissertation showcases the utility of ALE and omics studies in guiding genetic engineering, thus offering a rational engineering strategy supported by molecular evidence. Furthermore, the transcriptomic data provide valuable insights into the global transcriptional regulation in diatoms under the impacts of low-pH stress (Papaer 1) and continuous light (Paper 3). The reverse genetics study conducted in Paper 2, focusing on Phatr3_J33543, Phatr3_J50516, and Phatr3_Jdraft1806, contributes to the characterization of functions of previously uncharacterized ion/electron carrier genes in low-pH tolerance.

5.3 Future research recommendation

5.3.1 Novel screening methods

One challenge encountered in this project was evaluating the growth performances of the isolated clones from ALE cultures. Current screening methods based on herbicide resistance, colony appearance (e.g., size and color), or fluorescence,

primarily focus on observable or detectable metabolites (Table 1.3). However, there are limited approaches available for screening based on rapid growth. ALE is a screening process that selectively promotes the dominance of mutated variants with a competitive advantage in the population. Nevertheless, it is still necessary to isolate and characterize genetically homogeneous strains to identify the best-performing mutants. The microplate assay offers a high-throughput growth screening method that significant accordance with the conventional flask-based growth experiment [425]. However, in practical applications, microtiter cultures have limitations in controlling cultivation parameters such as illumination, mixing, and gas transfer. Insufficient mixing, for example, can result in cell aggregation and attachment to the surface of microplate wells, making it challenging to simulate large-scale liquid suspension cultures. An innovative approach recently demonstrated the use of a droplet microfluidics-based system for high-throughput examination of cell division in single cells encapsulated within droplets of culture media [426]. Since cellular senescence is associated with oxidative stress [423], the level of reactive oxygen species (ROS) can be probed using a fluorescent dye, such as DCFH-DA, to indicate stress-resistant mutants with low cellular ROS levels.

5.3.2 Advanced engineering tools

The conventional method of genetic modification in diatoms has demonstrated its effectiveness in numerous metabolic engineering endeavors. However, the random insertion of the targeted gene into the host genome presents certain challenges. Firstly, the transgene can be influenced by a positional effect at the insertion site. Secondly, the insertion itself may induce mutations in native genes, potentially affecting the fitness of the transgenic cells [226]. The uncertainties arising from copy number variations and random gene insertion result in phenotypic variations. To address this issue, current advancements in bioengineering for diatoms are focused on site-specific genetic modification using genome editing techniques. Evidently, three bi-allelic PtAUREO1a knockout strains showed highly comparable physiological properties in terms of pigment composition and non-photochemical quenching [427]. Concerning need for experiment reproducibility, genome editing represents a more promising approach for future research in this field.

5.3.3 Photosynthetic engineering strategies

In the past decade, the main focus of metabolic engineering in microalgae has been on modifying carbon flow into biosynthetic pathways such as TAG, PUFAs, and fucoxanthin to increase their cellular contents. However, this strategy, which diverts carbon flux away from essential metabolism, can be detrimental to the engineered cells. Numerous studies have reported impaired growth as a result of directing carbon towards lipid production [254, 259, 428]. Consequently, the overall productivity of the desired products may be limited due to the reduced growth rate. In such cases, a more practical strategy could be photosynthetic engineering, aiming to improve light-biomass conversion efficiency and overall biomass productivity by targeting the capture and conversion of light and CO_2 (Figure 5.1) [429]. While these strategies are commonly proposed for crop engineering, some have been implemented in microalgae. For example, the truncated light-harvesting antennae (TLA) strategy has been successfully applied to *C. reinhardtii* to prevent photoinhibition, resulting in significant growth improvement [430-432]. In terms of

carbon concentration mechanisms (CCM), cyanobacteria have been engineered to secrete carbonic anhydrase (CA) into the medium, facilitating the hydration of dissolved CO_2 into HCO_3^- for faster inorganic carbon acquisition. This modification led to a 50% - 60% increase in CO_2 fixation rate and a 1.3-fold increase in biomass productivity [433]. In *P. tricornutum*, the C4 pathway was engineered to enhance biomass production by overexpressing phosphoenolpyruvate carboxylase (PEPCase), resulting in a 12% increase in biomass production while maintaining unchanged lipid contents [434]. However, it seems that photosynthetic engineering has received comparatively less attention in the context of improving microalgal biomass productivity.

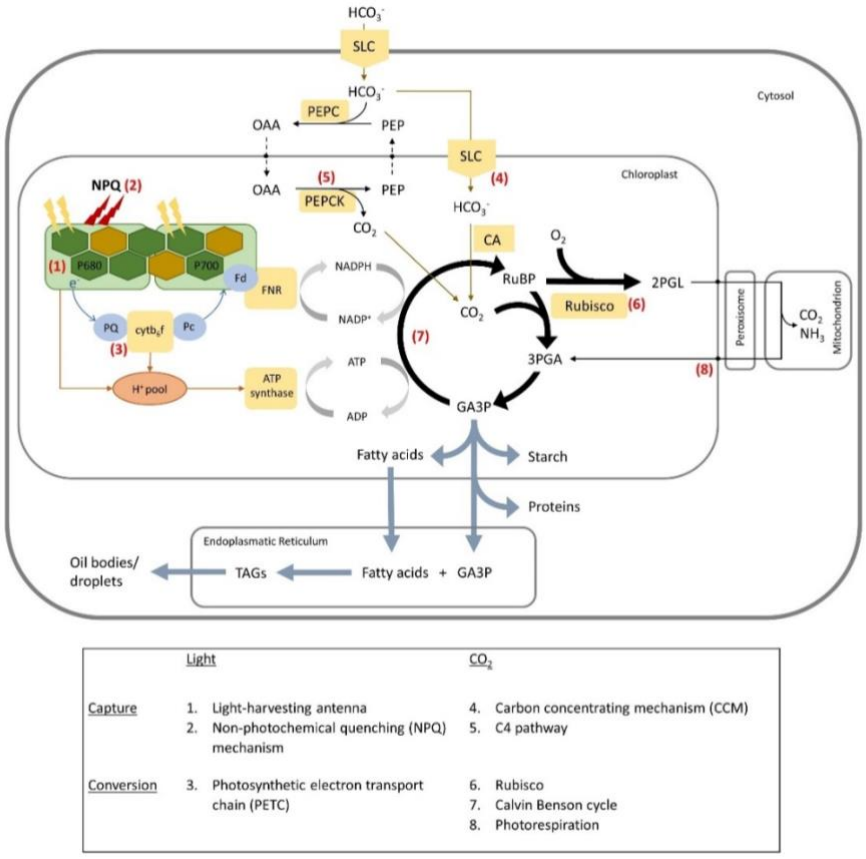

Figure 5.1. *Targets for photosynthetic engineering. Abbreviation: NPQ, non-photochemical quenching; PQ, plastoquinone; cytb6f, cytochrome b6/f; Pc, plastocyanin; Fd, ferredoxin; FNR, ferredoxin NADP oxidoreductase; PEP, phosphoenolpyruvate; OAA, oxaloacetate; PEPC, phosphoenolpyruvate carboxylase; PEPCK, phosphoenolpyruvate carboxykinase; SLC, solute carrier; CA, carbonic anhydrase; RuBP, ribulose-1,5-bisphosphate; 3PGA, 3-phosphoglycerare; GA3P, glyceraldehyde 3-phosphate; Rubisco, ribulose-1,5-bisphosphate carboxylase/oxygenase; 2PGL, 2-phosphoglycolate.*

5.4 Conclusions

Based on findings of this dissertation, the main conclusions can be drawn as follows:

- Significant improvements in low-pH tolerance have been achieved in the marine diatom, *P. tricornutum* through ALE and omics-guided genetic engineering.
- Stress-adapted strains in acidic environments exhibit upregulated photosynthesis, intracellular pH regulation, carbon metabolism, and repressed chlorophyll biosynthetic pathways as adaptive mechanisms.
- Several ion/electron carrier genes have been identified to play a critical role in low-pH resistance in diatoms, enabling the growth of *P. tricornutum* at lethal pH conditions. These genes have varying impacts on stress tolerance, with likely association between acidic resistance and a broad elevated expression of various transmembrane transporters.
- While most genes lose their diel rhythm under continuous illumination, certain transcription factor genes and cell division genes maintain rhythmic expression. The absence of a light/dark cycle leads to an overall downregulation of pigment biosynthesis and carbon fixation, which may explain the impaired photosynthetic efficiency under continuous light.

In addition to deepening our understanding of adaptive mechanisms and stress responses to acidified conditions, this project sheds light on the functions of several genes in acidic tolerance as well as rhythmic transcriptomes under continuous light. Furthermore, the dissertation contributes to the field of bioengineering by demonstrating an ALE-omics-guided rational engineering strategy, which has been successfully applied to develop stress-resistant diatom strains for practical applications.

References

[1] A. K. Sadvakasova *et al.*, "Microalgae as a key tool in achieving carbon neutrality for bioproduct production," *J Algal Research*, p. 103096, 2023.

[2] L. Liu *et al.*, "Household CO_2 emissions: Current status and future perspectives," *J International Journal of Environmental Research*, vol. 17, no. 19, p. 7077, 2020.

[3] A. Tarafdar *et al.*, "Environmental pollution mitigation through utilization of carbon dioxide by microalgae," *J Environmental Pollution*, p. 121623, 2023.

[4] Y. Zhao *et al.*, "Have those countries declaring "zero carbon" or "carbon neutral" climate goals achieved carbon emissions-economic growth decoupling?," *J Journal of Cleaner Production*, vol. 363, p. 132450, 2022.

[5] A. Srivastava, R. Maity, and V. R. Desai, "Assessing global-scale synergy between adaptation, mitigation, and sustainable development for projected climate change," in *Ecological Footprints of Climate Change: Adaptive Approaches and Sustainability*: Springer, 2023, pp. 31-61.

[6] G. Halkos and A. Zisiadou, "The Effects of Climate Change to Weather-Related Environmental Hazards: Interlinkages of Economic Factors and Climate Risk," *J Journal of Risk*, vol. 16, no. 5, p. 264, 2023.

[7] D. Eckstein, V. Künzel, and L. Schäfer, *The global climate risk index 2021*. Bonn: Germanwatch, 2021.

[8] X. Wu, Z. Tian, and J. Guo, "A review of the theoretical research and practical progress of carbon neutrality," *J Sustainable Operations and Computers*, vol. 3, pp. 54-66, 2022.

[9] J. G. Comley, J. A. Scott, and C. A. Laamanen, "Utilizing CO_2 in industrial off-gas for microalgae cultivation: considerations and solutions," *J Critical Reviews in Biotechnology*, pp. 1-14, 2023.

[10] R. Ahmed, G. Liu, B. Yousaf, Q. Abbas, H. Ullah, and M. U. Ali, "Recent advances in carbon-based renewable adsorbent for selective carbon dioxide capture and separation-A review," *J Journal of Cleaner Production*, vol. 242, p. 118409, 2020.

[11] R. Nandhini, B. Sivaprakash, N. Rajamohan, and D.-V. N. Vo, "Carbon-free hydrogen and bioenergy production through integrated carbon capture and storage technology for achieving sustainable and circular economy–A review," *J Fuel*, p. 126984, 2022.

[12] H. Onyeaka, T. Miri, K. Obileke, A. Hart, C. Anumudu, and Z. T. Al-Sharify, "Minimizing carbon footprint via microalgae as a biological capture," *J Carbon Capture Science Technology*, vol. 1, p. 100007, 2021.

[13] T. Wilberforce, A. Olabi, E. T. Sayed, K. Elsaid, and M. A. Abdelkareem, "Progress in carbon capture technologies," *J Science of The Total Environment*, vol. 761, p. 143203, 2021.

[14] C. D. Hills, N. Tripathi, and P. J. Carey, "Mineralization technology for carbon capture, utilization, and storage," *J Frontiers in Energy Research*, vol. 8, p. 142, 2020.

[15] Y. Chisti, "Biodiesel from microalgae," *J Biotechnology Advances*, vol. 25, no. 3, pp. 294-306, 2007.

[16] J. Singh and R. C. Saxena, "An introduction to microalgae: diversity and significance," in *Handbook of Marine Microalgae*: Elsevier, 2015, pp. 11-24.

[17] M. A. Borowitzka, "Biology of microalgae," in *Microalgae in Health and Disease Prevention*: Elsevier, 2018, pp. 23-72.
[18] K. Heimann and R. Huerlimann, "Microalgal classification: major classes and genera of commercial microalgal species," in *Handbook of Marine Microalgae*: Elsevier, 2015, pp. 25-41.
[19] J. P. Sexton and M. W. Lomas, "Microalgal systematics," in *Microalgae in Health and Disease Prevention*: Elsevier, 2018, pp. 73-107.
[20] A. Hopes and T. Mock, "Evolution of microalgae and their adaptations in different marine ecosystems," *J eLS*, pp. 1-9, 2015.
[21] L. Medlin, W. Kooistra, R. Gersonde, and U. Wellbrock, "Evolution of the diatoms (Bacillariophyta). II. Nuclear-encoded small-subunit rRNA sequence comparisons confirm a paraphyletic origin for the centric diatoms," *J Molecular Biology Evolution,* vol. 13, no. 1, pp. 67-75, 1996.
[22] E. J. Cox and D. M. Williams, "Systematics of naviculoid diatoms (Bacillariophyta): a preliminary analysis of protoplast and frustule characters for family and order level classification," *J Systematics and Biodiversity,* vol. 4, no. 4, pp. 385-399, 2006.
[23] E. J. Cox, "Morphology, cell wall, cytology, ultrastructure and morphogenetic studies: overview and specific observations," *J The Diatom World*, pp. 21-45, 2011.
[24] Z. V. Finkel and B. Kotrc, "Silica use through time: macroevolutionary change in the morphology of the diatom fustule," *J Geomicrobiology Journal,* vol. 27, no. 6-7, pp. 596-608, 2010.
[25] L. K. Medlin and I. Kaczmarska, "Evolution of the diatoms: V. Morphological and cytological support for the major clades and a taxonomic revision," *J Phycologia,* vol. 43, no. 3, pp. 245-270, 2004.
[26] A. D. De Martino, A. Meichenin, J. Shi, K. Pan, and C. Bowler, "Genetic and phenotypic characterization of *Phaeodactylum tricornutum* (Bacillariophyceae) accessions 1," *J Journal of Phycology*, vol. 43, no. 5, pp. 992-1009, 2007.
[27] M. A. Borowitzka and B. E. Volcani, "The polymorphic diatom *Phaeodactylum tricornutum*: ultrastructure of ITS morphotypes 1, 2," *J Journal of Phycology*, vol. 14, no. 1, pp. 10-21, 1978.
[28] D. P. Wilson, "The triradiate and other forms of *Nitzschia closterium* (Ehrenberg) Wm. Smith, forma minutissima of Allen and Nelson," *J Journal of the Marine Biological Association of the United Kingdom,* vol. 26, no. 3, pp. 235-270, 1946.
[29] L. He, X. Han, and Z. Yu, "A rare *Phaeodactylum tricornutum* cruciform morphotype: culture conditions, transformation and unique fatty acid characteristics," *J PloS One,* vol. 9, no. 4, p. e93922, 2014.
[30] B. Tesson, C. Gaillard, and V. Martin-Jezequel, "Insights into the polymorphism of the diatom *Phaeodactylum tricornutum* Bohlin," *J Botanica Marina,* 2009.
[31] K. Iwasa and A. Shimizu, "Motility of the diatom, *Phaeodactylum tricornutum*," *J Experimental Cell Research,* vol. 74, no. 2, pp. 552-558, 1972.
[32] J. C. Lewin, R. Lewin, and D. Philpott, "Observations on *Phaeodactylum tricornutum*," *J Microbiology*, vol. 18, no. 2, pp. 418-426, 1958.
[33] A. De Martino *et al.*, "Physiological and molecular evidence that environmental changes elicit morphological interconversion in the model

diatom *Phaeodactylum tricornutum*," *J Protist,* vol. 162, no. 3, pp. 462-481, 2011.
[34] K. Lu, X. Lin, and Y. Qian, "Studies on the morphotype and morphological variation of *Phaeodactylum tricornutum*," *J Journal of Ocean University of Qingdao,* vol. 31, no. 1, pp. 61-68, 2001.
[35] S. A. Gutenbrunner, J. Thalhamer, and A. M. M. Schmid, "Proteinaceous and immunochemical distinctions between the oval and fusiform morphotypes of *Phaeodactylum tricornutum* (Bacillariophyceae) " *J Journal of Phycology,* vol. 30, no. 1, pp. 129-136, 1994.
[36] L. O. Björn, D. Shevela, and G. Govindjee, "What Is Photosynthesis?—A Broader and Inclusive View," *Nova Science Publishers, Inc.,* 2023.
[37] A. D. Friend, R. J. Geider, M. J. Behrenfeld, and C. J. Still, "Photosynthesis in global-scale models," *Springer Nature,* pp. 465-497, 2009.
[38] M. Ashraf and P. J. Harris, "Photosynthesis under stressful environments: An overview," *J Photosynthetica,* vol. 51, pp. 163-190, 2013.
[39] J. Singh and J. K. Thakur, "Photosynthesis and abiotic stress in plants," *J Biotic Abiotic Stress Tolerance in Plants,* pp. 27-46, 2018.
[40] A. Sharma *et al.*, "Photosynthetic response of plants under different abiotic stresses: a review," *J Journal of Plant Growth Regulation,* vol. 39, pp. 509-531, 2020.
[41] I. Muhammad, A. Shalmani, M. Ali, Q.-H. Yang, H. Ahmad, and F. B. Li, "Mechanisms regulating the dynamics of photosynthesis under abiotic stresses," *J Frontiers in Plant Science,* vol. 11, p. 615942, 2021.
[42] W. Huang *et al.*, "Comparative proteomic analysis provides novel insights into chlorophyll biosynthesis in celery under temperature stress," *J Physiologia Plantarum,* vol. 161, no. 4, pp. 468-485, 2017.
[43] S. Mohanty, B. Grimm, and B. C. Tripathy, "Light and dark modulation of chlorophyll biosynthetic genes in response to temperature," *J Planta,* vol. 224, pp. 692-699, 2006.
[44] S. Yang *et al.*, "AtACDO1, an ABC1-like kinase gene, is involved in chlorophyll degradation and the response to photooxidative stress in Arabidopsis," *J Journal of Experimental Botany,* vol. 63, no. 10, pp. 3959-3973, 2012.
[45] S. Mathur, D. Agrawal, and A. Jajoo, "Photosynthesis: response to high temperature stress," *J Journal of Photochemistry and Photobiology B: Biology,* vol. 137, pp. 116-126, 2014.
[46] J. Masojídek, G. Torzillo, and M. Koblížek, "Photosynthesis in microalgae," *J Handbook of Microalgal Culture: Applied Phycology Biotechnology,* pp. 21-36, 2013.
[47] D. A. Walker, "Biofuels, facts, fantasy, and feasibility," *J Journal of Applied Phycology,* vol. 21, no. 5, pp. 509-517, 2009.
[48] M. Morales, L. Sánchez, and S. Revah, "The impact of environmental factors on carbon dioxide fixation by microalgae," *J FEMS Microbiology Letters,* vol. 365, no. 3, p. fnx262, 2018.
[49] J. H. De Vree, R. Bosma, M. Janssen, M. J. Barbosa, and R. H. Wijffels, "Comparison of four outdoor pilot-scale photobioreactors," *J Biotechnology for Biofuels and Bioproducts,* vol. 8, pp. 1-12, 2015.
[50] A. Melis, "Solar energy conversion efficiencies in photosynthesis: minimizing the chlorophyll antennae to maximize efficiency," *J Plant Science,* vol. 177, no. 4, pp. 272-280, 2009.

[51] B. L. Gatamaneni, V. Orsat, and M. Lefsrud, "Factors affecting growth of various microalgal species," *J Environmental Engineering Science,* vol. 35, no. 10, pp. 1037-1048, 2018.
[52] Q. Béchet, A. Shilton, and B. Guieysse, "Modeling the effects of light and temperature on algae growth: state of the art and critical assessment for productivity prediction during outdoor cultivation," *J Biotechnology Advances,* vol. 31, no. 8, pp. 1648-1663, 2013.
[53] A. Jungandreas, B. Schellenberger Costa, T. Jakob, M. Von Bergen, S. Baumann, and C. Wilhelm, "The acclimation of *Phaeodactylum tricornutum* to blue and red light does not influence the photosynthetic light reaction but strongly disturbs the carbon allocation pattern," *J PloS One,* vol. 9, no. 8, p. e99727, 2014.
[54] B. Schellenberger Costa, A. Jungandreas, T. Jakob, W. Weisheit, M. Mittag, and C. Wilhelm, "Blue light is essential for high light acclimation and photoprotection in the diatom *Phaeodactylum tricornutum*," *J Journal of Experimental Botany,* vol. 64, no. 2, pp. 483-493, 2013.
[55] P. Sirisuk, C.-H. Ra, G.-T. Jeong, and S.-K. Kim, "Effects of wavelength mixing ratio and photoperiod on microalgal biomass and lipid production in a two-phase culture system using LED illumination," *J Bioresource Technology,* vol. 253, pp. 175-181, 2018.
[56] S. Wahidin, A. Idris, and S. R. M. Shaleh, "The influence of light intensity and photoperiod on the growth and lipid content of microalgae *Nannochloropsis* sp," *J Bioresource Technology,* vol. 129, pp. 7-11, 2013.
[57] A. Kumar *et al.,* "Enhanced CO_2 fixation and biofuel production via microalgae: recent developments and future directions," *J Trends in Biotechnology,* vol. 28, no. 7, pp. 371-380, 2010.
[58] T. Berge, N. Daugbjerg, B. B. Andersen, and P. J. Hansen, "Effect of lowered pH on marine phytoplankton growth rates," *Marine Ecology Progress Series,* vol. 416, pp. 79–91, 2010, doi: 10.3354/meps08780.
[59] K. Gao and D. A. Campbell, "Photophysiological responses of marine diatoms to elevated CO2 and decreased pH: a review," *Functional Plant Biology,* vol. 41, no. 5, pp. 449-459, 2014.
[60] S. Burkhardt, I. Zondervan, and U. Riebesell, "Effect of CO2 concentration on C: N: P ratio in marine phytoplankton: a species comparison," *Limnology and Oceanography,* vol. 44, no. 3, pp. 683-690, 1999.
[61] Y. Li, J. Xu, and K. Gao, "Light-modulated responses of growth and photosynthetic performance to ocean acidification in the model diatom Phaeodactylum tricornutum," *PloS one,* vol. 9, no. 5, p. e96173, 2014.
[62] A. McCarthy, S. P. Rogers, S. J. Duffy, and D. A. Campbell, "Elevated carbon dioxide differentially alters the photophysiology of Thalassiosira pseudonana (Bacillariophyceae) and Emiliania huxleyi (Haptophyta)," *Journal of Phycology,* vol. 48, no. 3, pp. 635-646, 2012.
[63] Y. Yang and K. Gao, "Effects of CO2 concentrations on the freshwater microalgae, Chlamydomonas reinhardtii, Chlorella pyrenoidosa and Scenedesmus obliquus (Chlorophyta)," *Journal of Applied Phycology,* vol. 15, no. 5, pp. 379-389, 2003.
[64] K. Gao *et al.,* "Rising CO 2 and increased light exposure synergistically reduce marine primary productivity," *Nature climate change,* vol. 2, no. 7, p. 519, 2012.

[65] H. Hu and K. Gao, "Impacts of CO 2 enrichment on growth and photosynthesis in freshwater and marine diatoms," *Chinese Journal of Oceanology and Limnology*, vol. 26, no. 4, pp. 407-414, 2008.
[66] Y. Wu, K. Gao, and U. Riebesell, "CO2-induced seawater acidification affects physiological performance of the marine diatom Phaeodactylum tricornutum," *Biogeosciences (BG)*, vol. 7, no. 9, pp. 2915-2923, 2010.
[67] G. M. Hennon *et al.*, "Diatom acclimation to elevated CO 2 via cAMP signalling and coordinated gene expression," *Nature Climate Change*, vol. 5, no. 8, p. 761, 2015.
[68] P. Xu *et al.*, "Recent advances in CO_2 fixation by microalgae and its potential contribution to carbon neutrality," *J Chemosphere*, p. 137987, 2023.
[69] M. L. Calijuri *et al.*, "Bioproducts from microalgae biomass: Technology, sustainability, challenges and opportunities," *J Chemosphere*, vol. 305, p. 135508, 2022.
[70] E. S. Thoré, K. Muylaert, M. G. Bertram, and T. Brodin, "Microalgae," *J Current Biology*, vol. 33, no. 3, pp. R91-R95, 2023.
[71] C. Y. B. Oliveira *et al.*, "An overview on microalgae as renewable resources for meeting sustainable development goals," *J Journal of Environmental Management*, vol. 320, p. 115897, 2022.
[72] B. Llamas, M. C. Suárez-Rodríguez, C. V. González-López, P. Mora, and F. G. Acién, "Techno-economic analysis of microalgae related processes for CO_2 bio-fixation," *J Algal Research*, vol. 57, p. 102339, 2021.
[73] F. G. A. Fernández, A. Reis, R. H. Wijffels, M. Barbosa, V. Verdelho, and B. Llamas, "The role of microalgae in the bioeconomy," *J New Biotechnology*, vol. 61, pp. 99-107, 2021.
[74] P. Sirohi *et al.*, "Microalgal carotenoids: therapeutic application and latest approaches to enhance the production," *J Current Issues in Molecular Biology*, vol. 44, no. 12, pp. 6257-6279, 2022.
[75] J. Ávila-Román, S. García-Gil, A. Rodríguez-Luna, V. Motilva, and E. Talero, "Anti-inflammatory and anticancer effects of microalgal carotenoids," *J Marine Drugs*, vol. 19, no. 10, p. 531, 2021.
[76] S. Yaqoob, M. Riaz, A. Shabbir, M. Zia-Ul-Haq, S. S. Alwakeel, and M. Bin-Jumah, "Commercialization and marketing potential of carotenoids," *J Carotenoids: Structure Function in the Human Body*, pp. 799-826, 2021.
[77] S. Y. A. Siddiki *et al.*, "Microalgae biomass as a sustainable source for biofuel, biochemical and biobased value-added products: An integrated biorefinery concept," *J Fuel*, vol. 307, p. 121782, 2022.
[78] E. Jacob-Lopes, M. M. Maroneze, M. C. Deprá, R. B. Sartori, R. R. Dias, and L. Q. Zepka, "Bioactive food compounds from microalgae: An innovative framework on industrial biorefineries," *J Current Opinion in Food Science*, vol. 25, pp. 1-7, 2019.
[79] G. K. S. H. Nishshanka, R. A. D. P. Anthonio, P. H. V. Nimarshana, T. U. Ariyadasa, and J.-S. Chang, "Marine microalgae as sustainable feedstock for multi-product biorefineries," *J Biochemical Engineering Journal*, vol. 187, p. 108593, 2022.
[80] C. Gonzalez-Fernandez, B. Sialve, and B. Molinuevo-Salces, "Anaerobic digestion of microalgal biomass: challenges, opportunities and research needs," *J Bioresource Technology*, vol. 198, pp. 896-906, 2015.

[81] M. Moon *et al.*, "Utilization of whole microalgal biomass for advanced biofuel and biorefinery applications," *J Renewable Sustainable Energy Reviews*, vol. 160, p. 112269, 2022.
[82] P. Tanger, J. Field, C. Jahn, M. DeFoort, and J. Leach, "Biomass for thermochemical conversion: targets and challenges," (in English), Review vol. 4, 2013-July-01 2013, doi: 10.3389/fpls.2013.00218.
[83] I. Chanana, P. Kaur, L. Kumar, P. Kumar, and S. Kulshreshtha, "Advancements in microalgal biorefinery technologies and their economic analysis and positioning in energy resource market," *J Fermentation*, vol. 9, no. 3, p. 202, 2023.
[84] D. Nagarajan, S. Varjani, D.-J. Lee, and J.-S. Chang, "Sustainable aquaculture and animal feed from microalgae–nutritive value and techno-functional components," *J Renewable Sustainable Energy Reviews*, vol. 150, p. 111549, 2021.
[85] M. A. Siddik, M. Sørensen, S. M. Islam, N. Saha, M. A. Rahman, and D. S. Francis, "Expanded utilisation of microalgae in global aquafeeds," *J Reviews in Aquaculture*, 2023.
[86] G. Dineshbabu, G. Goswami, R. Kumar, A. Sinha, and D. Das, "Microalgae–nutritious, sustainable aqua-and animal feed source," *J Journal of Functional Foods*, vol. 62, p. 103545, 2019.
[87] J. Yarnold, H. Karan, M. Oey, and B. Hankamer, "Microalgal aquafeeds as part of a circular bioeconomy," *J Trends in plant science*, vol. 24, no. 10, pp. 959-970, 2019.
[88] Y. Arora, S. Sharma, and V. Sharma, "Microalgae in Bioplastic Production: A Comprehensive Review," *J Arabian Journal for Science Engineering*, pp. 1-17, 2023.
[89] N. Nanda and N. Bharadvaja, "Algal bioplastics: current market trends and technical aspects," *J Clean Technologies Environmental Policy*, vol. 24, no. 9, pp. 2659-2679, 2022.
[90] J.-G. Rosenboom, R. Langer, and G. Traverso, "Bioplastics for a circular economy," *J Nature Reviews Materials*, vol. 7, no. 2, pp. 117-137, 2022.
[91] M. Nandal, P. Khyalia, A. Ghalawat, H. Jugiani, M. Kaur, and J. S. Laura, "Review on the use of Microalgae Biomass for Bioplastics Synthesis: A Sustainable and Green approach to control Plastic Pollution," *J Pollution*, vol. 8, no. 3, pp. 844-859, 2022.
[92] S. Guo, P. Wang, X. Wang, M. Zou, C. Liu, and J. Hao, "Microalgae as biofertilizer in modern agriculture," *J Microalgae Biotechnology for Food, Health High Value Products*, pp. 397-411, 2020.
[93] J. C. Braun and L. M. Colla, "Use of Microalgae for the Development of Biofertilizers and Biostimulants," *J BioEnergy Research*, vol. 16, no. 1, pp. 289-310, 2023.
[94] T. N.-D. Cao *et al.*, "Roles of microalgae-based biofertilizer in sustainability of green agriculture and food-water-energy security nexus," *J Science of The Total Environment*, vol. 870, p. 161927, 2023.
[95] J. P. Maity, J. Bundschuh, C.-Y. Chen, and P. Bhattacharya, "Microalgae for third generation biofuel production, mitigation of greenhouse gas emissions and wastewater treatment: Present and future perspectives–A mini review," *J Energy*, vol. 78, pp. 104-113, 2014.

[96] A. Abdelfattah *et al.*, "Microalgae-based wastewater treatment: Mechanisms, challenges, recent advances, and future prospects," *J Environmental Science Ecotechnology,* vol. 13, p. 100205, 2023.
[97] X. You, L. Yang, X. Zhou, and Y. Zhang, "Sustainability and carbon neutrality trends for microalgae-based wastewater treatment: A review," *J Environmental Research,* vol. 209, p. 112860, 2022.
[98] S. D. Priyadharshini, P. S. Babu, S. Manikandan, R. Subbaiya, M. Govarthanan, and N. Karmegam, "Phycoremediation of wastewater for pollutant removal: A green approach to environmental protection and long-term remediation," *J Environmental Pollution,* vol. 290, p. 117989, 2021.
[99] S. Mustafa, H. N. Bhatti, M. Maqbool, and M. Iqbal, "Microalgae biosorption, bioaccumulation and biodegradation efficiency for the remediation of wastewater and carbon dioxide mitigation: Prospects, challenges and opportunities," *J Journal of Water Process Engineering,* vol. 41, p. 102009, 2021.
[100] S. Rani, N. Gunjyal, C. Ojha, and R. P. Singh, "Review of challenges for algae-based wastewater treatment: strain selection, wastewater characteristics, abiotic, and biotic factors," *J Journal of Hazardous, Toxic, Radioactive Waste,* vol. 25, no. 2, p. 03120004, 2021.
[101] F. Wollmann *et al.*, "Microalgae wastewater treatment: Biological and technological approaches," *J Engineering in Life Sciences,* vol. 19, no. 12, pp. 860-871, 2019.
[102] S. Van Den Hende, H. Vervaeren, and N. Boon, "Flue gas compounds and microalgae:(Bio-) chemical interactions leading to biotechnological opportunities," *J Biotechnology Advances,* vol. 30, no. 6, pp. 1405-1424, 2012.
[103] A. K. Vuppaladadiyam *et al.*, "Impact of flue gas compounds on microalgae and mechanisms for carbon assimilation and utilization," *J ChemSusChem,* vol. 11, no. 2, pp. 334-355, 2018.
[104] H. W. Yen, S. H. Ho, C. Y. Chen, and J. S. Chang, "CO2, NOx and SOx removal from flue gas via microalgae cultivation: A critical review," *Biotechnology journal,* vol. 10, no. 6, pp. 829-839, 2015.
[105] S. P. Cuellar-Bermudez, J. S. Garcia-Perez, B. E. Rittmann, and R. Parra-Saldivar, "Photosynthetic bioenergy utilizing CO2: an approach on flue gases utilization for third generation biofuels," *Journal of Cleaner Production,* vol. 98, pp. 53-65, 2015.
[106] M. Negoro, N. Shioji, K. Miyamoto, and Y. Miura, "Growth of microalgae in high CO_2 gas and effects of SOx and NOx," *J Applied Biochemistry Biotechnology,* vol. 28/29, 1991.
[107] J. N. Lee, J. S. Lee, C. S. Shin, S. C. Park, and S. W. Kim, "Methods to enhance tolerances of Chlorella KR-1 to toxic compounds in flue gas," *J Applied Biochemistry Biotechnology,* vol. 84-86, pp. 329-42, Spring 2000, doi: 10.1385/abab:84-86:1-9:329.
[108] J.-S. Lee *et al.*, "Effects of SO_2 and NO on growth of *Chlorella* sp. KR-1," *J Bioresource Technology,* vol. 82, pp. 1-4, 2002.
[109] S. Y. Chiu, C. Y. Kao, C. H. Chen, T. C. Kuan, S. C. Ong, and C. S. Lin, "Reduction of CO_2 by a high-density culture of *Chlorella* sp. in a semicontinuous photobioreactor," *J Bioresource Technology,* vol. 99, no. 9, pp. 3389-96, Jun 2008, doi: 10.1016/j.biortech.2007.08.013.

[110] W. Y. Cheah, P. L. Show, J.-S. Chang, T. C. Ling, and J. C. Juan, "Biosequestration of atmospheric CO2 and flue gas-containing CO2 by microalgae," *Bioresource technology,* vol. 184, pp. 190-201, 2015.
[111] Y. Jiang, W. Zhang, J. Wang, Y. Chen, S. Shen, and T. Liu, "Utilization of simulated flue gas for cultivation of *Scenedesmus dimorphus*," *J Bioresource Technology,* vol. 128, pp. 359-64, Jan 2013, doi: 10.1016/j.biortech.2012.10.119.
[112] M. Anjos, B. D. Fernandes, A. A. Vicente, J. A. Teixeira, and G. Dragone, "Optimization of CO_2 bio-mitigation by *Chlorella vulgaris*," *J Bioresource Technology,* vol. 139, pp. 149–154, 2013, doi: 10.1016/j.biortech.2013.04.032.
[113] N. R. Moheimani, "*Tetraselmis suecica* culture for CO_2 bioremediation of untreated flue gas from a coal-fired power station," *J Journal of Applied Phycology,* vol. 28, no. 4, pp. 2139-2146, 2015, doi: 10.1007/s10811-015-0782-3.
[114] B. Zhao, Y. Su, Y. Zhang, and G. Cui, "Carbon dioxide fixation and biomass production from combustion flue gas using energy microalgae," *J Energy,* vol. 89, pp. 347-357, 2015, doi: 10.1016/j.energy.2015.05.123.
[115] M. G. de Morais and J. A. V. Costa, "Isolation and selection of microalgae from coal fired thermoelectric power plant for biofixation of carbon dioxide," *Energy Conversion and Management,* vol. 48, no. 7, pp. 2169-2173, 2007, doi: 10.1016/j.enconman.2006.12.011.
[116] M. Olaizola, "Microalgal removal of CO_2 from flue gases: changes in medium pH and flue gas composition do not appear to affect photochemical yield of microalgal cultures," *J Biotechnology and Bioprocess Engineering,* vol. 8, pp. 360-367, 2003.
[117] C. Yoo, S. Y. Jun, J. Y. Lee, C. Y. Ahn, and H. M. Oh, "Selection of microalgae for lipid production under high levels carbon dioxide," *J Bioresource Technology,* vol. 101 Suppl 1, pp. S71-4, Jan 2010, doi: 10.1016/j.biortech.2009.03.030.
[118] L. Yue and W. Chen, "Isolation and determination of cultural characteristics of a new highly CO_2 tolerant fresh water microalgae," *J Energy Conversion and Management,* vol. 46, no. 11-12, pp. 1868-1876, 2005, doi: 10.1016/j.enconman.2004.10.010.
[119] Y. Y. Choi *et al.,* "Development of large-scale and economic pH control system for outdoor cultivation of microalgae *Haematococcus pluvialis* using industrial flue gas," *J Bioresource Technology,* vol. 244, pp. 1235-1244, 2017.
[120] A. Aslam, S. R. Thomas-Hall, T. A. Mughal, and P. M. Schenk, "Selection and adaptation of microalgae to growth in 100% unfiltered coal-fired flue gas," *Bioresour Technol,* vol. 233, pp. 271-283, Jun 2017, doi: 10.1016/j.biortech.2017.02.111.
[121] C. M. Kuo *et al.,* "Simultaneous microalgal biomass production and CO_2 fixation by cultivating *Chlorella* sp. GD with aquaculture wastewater and boiler flue gas," *J Bioresource Technology,* vol. 221, pp. 241-250, Dec 2016, doi: 10.1016/j.biortech.2016.09.014.
[122] R. Praveenkumar *et al.,* "Improved biomass and lipid production in a mixotrophic culture of *Chlorella* sp. KR-1 with addition of coal-fired flue-gas," *J Bioresource Technology,* vol. 171, pp. 500-5, Nov 2014, doi: 10.1016/j.biortech.2014.08.112.

[123] K. D. Sung, J. S. Lee, C. S. Shin, and S. C. Park, "Isolation of a new highly CO_2 tolerant fresh water microalga *Chlorella* SP.KR-1," *J Renewable Energy* vol. 16, pp. 1019-1022, 1999.
[124] F. Qi, H. Pei, W. Hu, R. Mu, and S. Zhang, "Characterization of a microalgal mutant for CO_2 biofixation and biofuel production," *J Energy Conversion and Management,* vol. 122, pp. 344-349, 2016.
[125] J. Cheng, Y. Huang, J. Feng, J. Sun, J. Zhou, and K. Cen, "Mutate *Chlorella* sp. by nuclear irradiation to fix high concentrations of CO_2," *J Bioresource Technology,* vol. 136, pp. 496-501, May 2013, doi: 10.1016/j.biortech.2013.03.072.
[126] C.-Y. Kao *et al.*, "A mutant strain of microalga *Chlorella* sp. for the carbon dioxide capture from biogas," *J Biomass Bioenergy,* vol. 36, pp. 132-140, 2012.
[127] J. Cheng, K. Li, Z. Yang, H. Lu, J. Zhou, and K. Cen, "Gradient domestication of *Haematococcus pluvialis* mutant with 15% CO_2 to promote biomass growth and astaxanthin yield," *Bioresour Technol,* vol. 216, pp. 340-4, Sep 2016, doi: 10.1016/j.biortech.2016.05.095.
[128] M. A. Borowitzka, "Energy from microalgae: a short history," in *Algae for Biofuels and Energy*: Springer, 2012, pp. 1-15.
[129] W. A. Fathy *et al.*, "Insights into random mutagenesis techniques to enhance biomolecule production in microalgae: Implications for economically viable bioprocesses," *J International Aquatic Research,* vol. 15, no. 2, pp. 85-102, 2023.
[130] T. Oyama *et al.*, "Development of mutant microalgae that accumulate lipids under nitrate-replete conditions," *J Algal Research,* vol. 60, p. 102544, 2021.
[131] K. Yamada *et al.*, "Production of a thermal stress resistant mutant *Euglena gracilis* strain using Fe-ion beam irradiation," *J Bioscience, Biotechnology, Biochemistry,* vol. 80, no. 8, pp. 1650-1656, 2016.
[132] M. E. Elshobary, H. M. Zabed, X. Qi, and R. A. El-Shenody, "Enhancing biomass and lipid productivity of a green microalga *Parachlorella kessleri* for biodiesel production using rapid mutation of atmospheric and room temperature plasma," *J Biotechnology for Biofuels Bioproducts,* vol. 15, no. 1, pp. 1-17, 2022.
[133] S. Cao *et al.*, "Improving of lipid productivity of the oleaginous microalgae *Chlorella pyrenoidosa* via atmospheric and room temperature plasma (ARTP)," *J Bioresource Technology,* vol. 244, pp. 1400-1406, 2017.
[134] C. Südfeld *et al.*, "High-throughput insertional mutagenesis reveals novel targets for enhancing lipid accumulation in *Nannochloropsis oceanica*," *J Metabolic Engineering,* vol. 66, pp. 239-258, 2021.
[135] M. Hlavova, Z. Turoczy, and K. Bisova, "Improving microalgae for biotechnology—From genetics to synthetic biology," *J Biotechnology Advances,* vol. 33, no. 6, pp. 1194-1203, 2015.
[136] N. Wang, B. Guan, Q. Kong, H. Sun, Z. Geng, and L. Duan, "Enhancement of astaxanthin production from *Haematococcus pluvialis* mutants by three-stage mutagenesis breeding," *J Journal of Biotechnology,* vol. 236, pp. 71-77, 2016.
[137] P. I. Gómez, I. Inostroza, M. Pizarro, and J. Pérez, "From genetic improvement to commercial-scale mass culture of a Chilean strain of the green microalga *Haematococcus pluvialis* with enhanced productivity of the red ketocarotenoid astaxanthin," *J AoB Plants,* vol. 5, p. plt026, 2013.

[138] Y. Chen, D. Li, W. Lu, J. Xing, B. Hui, and Y. Han, "Screening and characterization of astaxanthin-hyperproducing mutants of *Haematococcus pluvialis*," *J Biotechnology Letters,* vol. 25, pp. 527-529, 2003.
[139] U. Tripathi, G. Venkateshwaran, R. Sarada, and G. Ravishankar, "Studies on *Haematococcus pluvialis* for improved production of astaxanthin by mutagenesis," *J World Journal of Microbiology Biotechnology,* vol. 17, pp. 143-148, 2001.
[140] B. F. Cordero, I. Obraztsova, I. Couso, R. Leon, M. A. Vargas, and H. Rodriguez, "Enhancement of lutein production in *Chlorella sorokiniana* (Chorophyta) by improvement of culture conditions and random mutagenesis," *J Marine Drugs,* vol. 9, no. 9, pp. 1607-1624, 2011.
[141] B. S. Kamath, R. Vidhyavathi, R. Sarada, and G. Ravishankar, "Enhancement of carotenoids by mutation and stress induced carotenogenic genes in *Haematococcus pluvialis* mutants," *J Bioresource Technology,* vol. 99, no. 18, pp. 8667-8673, 2008.
[142] A. E. Tjahjono, T. Kakizono, Y. Hayama, N. Nishio, and S. Nagai, "Isolation of resistant mutants against carotenoid biosynthesis inhibitors for a green alga *Haematococcus pluvialis*, and their hybrid formation by protoplast fusion for breeding of higher astaxanthin producers," *J Journal of Fermentation Bioengineering,* vol. 77, no. 4, pp. 352-357, 1994.
[143] J. Mehtani *et al.*, "Augmented lipid accumulation in ethyl methyl sulphonate mutants of oleaginous microalga for biodiesel production," *J Bioresource Technology,* vol. 242, pp. 121-127, 2017.
[144] R. Sivaramakrishnan and A. Incharoensakdi, "Enhancement of lipid production in *Scenedesmus* sp. by UV mutagenesis and hydrogen peroxide treatment," *J Bioresource Technology,* vol. 235, pp. 366-370, 2017.
[145] S. Liu *et al.*, "Improving cell growth and lipid accumulation in green microalgae *Chlorella* sp. via UV irradiation," *J Applied Biochemistry Biotechnology,* vol. 175, pp. 3507-3518, 2015.
[146] M. V. Vani, P. O. Basha, N. Rajesh, and K. Riazunnisa, "Development of *Chlorella pyrenoidosa* EMS mutants with enhanced biomass and lipid content for biofuel production," *J Systems Microbiology Biomanufacturing,* pp. 1-9, 2022.
[147] P. P. M. Bruno, W. L. Rivera, and P. G. Vital, "UV-irradiation mutagenesis of *Chlorella vulgaris* Beijerinck SP17 to enhance lipid production for potential biodiesel application," *Philippine Science Letters* 2021.
[148] J. D. Carino and P. G. Vital, "Characterization of isolated UV-C-irradiated mutants of microalga *Chlorella vulgaris* for future biofuel application," *J Environment, Development Sustainability,* pp. 1-18, 2022.
[149] S. W. Geis, K. L. Fleming, E. T. Korthals, G. Searle, L. Reynolds, and D. A. Karner, "Modifications to the algal growth inhibition test for use as a regulatory assay," *J Environmental Toxicology Chemistry: An International Journal,* vol. 19, no. 1, pp. 36-41, 2000.
[150] P. Hyka, S. Lickova, P. Přibyl, K. Melzoch, and K. Kovar, "Flow cytometry for the development of biotechnological processes with microalgae," *J Biotechnology Advances,* vol. 31, no. 1, pp. 2-16, 2013.
[151] J. Van Wagenen, S. L. Holdt, D. De Francisci, B. Valverde-Pérez, B. G. Plósz, and I. Angelidaki, "Microplate-based method for high-throughput screening of microalgae growth potential," *J Bioresource Technology,* vol. 169, pp. 566-572, 2014.

[152] J. Rumin *et al.*, "The use of fluorescent Nile red and BODIPY for lipid measurement in microalgae," *J Biotechnology for Biofuels and Bioproducts,* vol. 8, no. 1, pp. 1-16, 2015.
[153] T. Thurakit, W. Pathom-Aree, C. Pumas, T. W. Brocklehurst, J. Pekkoh, and S. Srinuanpan, "High-efficiency production of biomass and biofuel under two-stage cultivation of a stable microalga *Botryococcus braunii* mutant generated by ethyl methanesulfonate-induced mutation," *J Renewable Energy,* vol. 198, pp. 176-188, 2022.
[154] M. Nayak *et al.*, "Directed evolution of *Chlorella* sp. HS_2 towards enhanced lipid accumulation by ethyl methanesulfonate mutagenesis in conjunction with fluorescence-activated cell sorting based screening," *J Fuel,* vol. 316, p. 123410, 2022.
[155] T. Smalley, F. J. Fields, A. J. Berndt, J. T. Ostrand, V. Heredia, and S. P. Mayfield, "Improving biomass and lipid yields of *Desmodesmus armatus* and *Chlorella vulgaris* through mutagenesis and high-throughput screening," *J Biomass Bioenergy,* vol. 142, p. 105755, 2020.
[156] R. Rachmayati, E. Agustriana, and D. Y. Rahman, "UV mutagenesis as a strategy to enhance growth and lipid productivity of *Chlorella* sp. 042," *J J. Trop. Biodivers. Biotechnol,* vol. 5, no. 3, p. 218, 2020.
[157] E. Sarayloo, S. Simsek, Y. S. Unlu, G. Cevahir, C. Erkey, and I. H. Kavakli, "Enhancement of the lipid productivity and fatty acid methyl ester profile of *Chlorella vulgaris* by two rounds of mutagenesis," *J Bioresource Technology,* vol. 250, pp. 764-769, 2018.
[158] O.-u.-M. Tanadul, W. Noochanong, P. Jirakranwong, and S. Chanprame, "EMS-induced mutation followed by quizalofop-screening increased lipid productivity in *Chlorella* sp," *J Bioprocess Biosystems Engineering,* vol. 41, pp. 613-619, 2018.
[159] K. Manandhar-Shrestha and M. Hildebrand, "Development of flow cytometric procedures for the efficient isolation of improved lipid accumulation mutants in a *Chlorella* sp. microalga," *J Journal of Applied Phycology,* vol. 25, pp. 1643-1651, 2013.
[160] H. Vigeolas *et al.*, "Isolation and partial characterization of mutants with elevated lipid content in *Chlorella sorokiniana* and *Scenedesmus obliquus*," *J Journal of Biotechnology,* vol. 162, no. 1, pp. 3-12, 2012.
[161] Y. Zhang *et al.*, "Breeding of high biomass and lipid producing *Desmodesmus* sp. by Ethylmethane sulfonate-induced mutation," *J Bioresource Technology,* vol. 207, pp. 268-275, 2016.
[162] S. Wang, L. Zhang, G. Yang, J. Han, L. Thomsen, and K. Pan, "Breeding 3 elite strains of *Nannochloropsis oceanica* by nitrosoguanidine mutagenesis and robust screening," *J Algal Research,* vol. 19, pp. 104-108, 2016.
[163] T. Beacham, V. M. Macia, P. Rooks, D. White, and S. Ali, "Altered lipid accumulation in *Nannochloropsis salina* CCAP849/3 following EMS and UV induced mutagenesis," *J Biotechnology Reports,* vol. 7, pp. 87-94, 2015.
[164] T. T. Y. Doan and J. P. Obbard, "Enhanced intracellular lipid in *Nannochloropsis* sp. via random mutagenesis and flow cytometric cell sorting," *J Algal Research,* vol. 1, no. 1, pp. 17-21, 2012.
[165] R. Chaturvedi and Y. Fujita, "Isolation of enhanced eicosapentaenoic acid producing mutants of *Nannochloropsis oculata* ST-6 using ethyl methane sulfonate induced mutagenesis techniques and their characterization at

mRNA transcript level," *J Phycological Research,* vol. 54, no. 3, pp. 208-219, 2006.
[166] B. Lee, G.-G. Choi, Y.-E. Choi, M. Sung, M. S. Park, and J.-W. Yang, "Enhancement of lipid productivity by ethyl methane sulfonate-mediated random mutagenesis and proteomic analysis in *Chlamydomonas reinhardtii*," *J Korean Journal of Chemical Engineering,* vol. 31, pp. 1036-1042, 2014.
[167] I. T. D. Cabanelas, M. Van Der Zwart, D. M. Kleinegris, R. H. Wijffels, and M. J. Barbosa, "Sorting cells of the microalga *Chlorococcum littorale* with increased triacylglycerol productivity," *J Biotechnology for Biofuels and Bioproducts,* vol. 9, no. 1, pp. 1-12, 2016.
[168] G. Bougaran *et al.*, "Enhancement of neutral lipid productivity in the microalga *Isochrysis affinis Galbana* (T - Iso) by a mutation - selection procedure," *J Biotechnology Bioengineering,* vol. 109, no. 11, pp. 2737-2745, 2012.
[169] D. K. Lim, H. Schuhmann, K. Sharma, and P. M. Schenk, "Isolation of high-lipid *Tetraselmis suecica* strains following repeated UV-C mutagenesis, facs, and high-throughput growth selection," *J BioEnergy Research,* vol. 8, pp. 750-759, 2015.
[170] M. Lian, H. Huang, L. Ren, X. Ji, J. Zhu, and L. Jin, "Increase of docosahexaenoic acid production by *Schizochytrium* sp. through mutagenesis and enzyme assay," *J Applied Biochemistry Biotechnology,* vol. 162, pp. 935-941, 2010.
[171] L. A. Meireles, A. C. Guedes, and F. X. Malcata, "Increase of the yields of eicosapentaenoic and docosahexaenoic acids by the microalga *Pavlova lutheri* following random mutagenesis," *J Biotechnology Bioengineering,* vol. 81, no. 1, pp. 50-55, 2003.
[172] D. L. Alonso, C. I. Segura del Castillo, E. M. Grima, and Z. Cohen, "First insights into improvement of eicosapentaenoic acid content in *Phaeodactylum tricornutum* (bacillariophyceae) by induced mutagenesis 1," *J Journal of Phycology,* vol. 32, no. 2, pp. 339-345, 1996.
[173] J. Kim, M. Kim, S. Lee, and E. Jin, "Development of a *Chlorella vulgaris* mutant by chemical mutagenesis as a producer for natural violaxanthin," *J Algal Research,* vol. 46, p. 101790, 2020.
[174] E. Ishikawa, H. Sansawa, and H. Abe, "Isolation and characterization of a *Chlorella* mutant producing high amounts of chlorophyll and carotenoids," *J Journal of Applied Phycology,* vol. 16, pp. 385-393, 2004.
[175] M. Kim, J. Ahn, H. Jeon, and E. Jin, "Development of a *Dunaliella tertiolecta* strain with increased zeaxanthin content using random mutagenesis," *J Marine Drugs,* vol. 15, no. 6, p. 189, 2017.
[176] A. Tharek *et al.*, "Improvement and screening of astaxanthin producing mutants of newly isolated *Coelastrum* sp. using ethyl methane sulfonate induced mutagenesis technique," *J Biotechnology Reports,* vol. 32, p. e00673, 2021.
[177] D. Zhang and Y. Lee, "Enhanced accumulation of secondary carotenoids in a mutant of the green alga, *Chlorococcum* sp," *J Journal of Applied Phycology,* vol. 9, pp. 459-463, 1997.
[178] F. Qi, D. Wu, R. Mu, S. Zhang, and X. Xu, "Characterization of a microalgal UV mutant for CO_2 biofixation and biomass production," *J Biomed Research International,* vol. 2018, 2018.

[179] N. Sachdeva, R. P. Gupta, A. S. Mathur, and D. K. Tuli, "Enhanced lipid production in thermo-tolerant mutants of *Chlorella pyrenoidosa* NCIM 2738," *J Bioresource Technology,* vol. 221, pp. 576-587, 2016.
[180] J. I. Teco-Bravo, L. F. Barahona-Pérez, C. F. Reyes-Sosa, Á. F. Ku-González, V. A. Herrera-Valencia, and S. Peraza-Echeverria, "Enhanced production of triacylglycerols and polyunsaturated fatty acids in novel acid-tolerant mutants of the green microalga *Chlorella saccharophila*," *J Bioprocess Biosystems Engineering,* vol. 42, pp. 1561-1571, 2019.
[181] H. Mendoza *et al.*, "Characterization of *Dunaliella salina* strains by flow cytometry: a new approach to select carotenoid hyperproducing strains," *J Electronic Journal of Biotechnology,* vol. 11, no. 4, pp. 5-6, 2008.
[182] A. M. Nonomura and D. M. Coder, "Improved phycocatalysis of carotene production by flow cytometry and cell sorting," *J Biocatalysis,* vol. 1, no. 4, pp. 333-338, 1988.
[183] J. D. Winkler and K. C. Kao, "Recent advances in the evolutionary engineering of industrial biocatalysts," *Genomics,* vol. 104, no. 6, pp. 406-411, 2014.
[184] K.-K. Hong, *Advancing Metabolic Engineering through Combination of Systems Biology and Adaptive Evolution*. Chalmers University of Technology, 2012.
[185] M. Dragosits and D. Mattanovich, "Adaptive laboratory evolution–principles and applications for biotechnology," *Microbial cell factories,* vol. 12, no. 1, p. 1, 2013.
[186] B. Zhang, J. Wu, and F. Meng, "Adaptive laboratory evolution of microalgae: A review of the regulation of growth, stress resistance, metabolic processes, and biodegradation of pollutants," *J Frontiers in Microbiology,* vol. 12, p. 737248, 2021.
[187] M. Mavrommati, A. Daskalaki, S. Papanikolaou, and G. Aggelis, "Adaptive laboratory evolution principles and applications in industrial biotechnology," *J Biotechnology Advances,* vol. 54, p. 107795, 2022.
[188] L. Wang, C. Xue, L. Wang, Q. Zhao, W. Wei, and Y. Sun, "Strain improvement of *Chlorella* sp. for phenol biodegradation by adaptive laboratory evolution," *J Bioresource Technology,* vol. 205, pp. 264-268, 2016.
[189] D. Li, L. Wang, Q. Zhao, W. Wei, and Y. Sun, "Improving high carbon dioxide tolerance and carbon dioxide fixation capability of *Chlorella* sp. by adaptive laboratory evolution," *J Bioresource Technology,* vol. 185, pp. 269-75, Jun 2015, doi: 10.1016/j.biortech.2015.03.011.
[190] W. Fu, O. Gudmundsson, A. M. Feist, G. Herjolfsson, S. Brynjolfsson, and B. Palsson, "Maximizing biomass productivity and cell density of *Chlorella vulgaris* by using light-emitting diode-based photobioreactor," *J Journal of Biotechnology,* vol. 161, no. 3, pp. 242-249, 2012.
[191] W. Fu *et al.*, "Enhancement of carotenoid biosynthesis in the green microalga *Dunaliella salina* with light-emitting diodes and adaptive laboratory evolution," *J Applied Microbiology Biotechnology,* vol. 97, pp. 2395-2403, 2013.
[192] G. Wang, Q. Li, Z. Zhang, X. Yin, B. Wang, and X. Yang, "Recent progress in adaptive laboratory evolution of industrial microorganisms," *J Journal of Industrial Microbiology Biotechnology,* vol. 50, no. 1, p. kuac023, 2023.

[193] D. Cheng *et al.*, "Adaptive evolution and carbon dioxide fixation of *Chlorella* sp. in simulated flue gas," *J Science of The Total Environment,* vol. 650, no. Pt 2, pp. 2931-2938, Feb 10 2019, doi: 10.1016/j.scitotenv.2018.10.070.
[194] Z. Wang, J. Cheng, W. Song, X. Du, and W. Yang, "CO2 gradient domestication produces gene mutation centered on cellular light response for efficient growth of microalgae in 15% CO2 from flue gas," *J Chemical Engineering Journal,* vol. 429, p. 131968, 2022.
[195] Z. Yi, M. Xu, M. Magnusdottir, Y. Zhang, S. Brynjolfsson, and W. Fu, "Photo-oxidative stress-driven mutagenesis and adaptive evolution on the marine diatom *Phaeodactylum tricornutum* for enhanced carotenoid accumulation," *J Marine Drugs,* vol. 13, no. 10, pp. 6138-6151, 2015.
[196] N. Arora, E. Lo, and G. P. Philippidis, "A two-prong mutagenesis and adaptive evolution strategy to enhance the temperature tolerance and productivity of *Nannochloropsis oculata*," *J Bioresource Technology,* vol. 364, p. 128101, 2022.
[197] X. Li *et al.*, "Exploring stress tolerance mechanism of evolved freshwater strain *Chlorella* sp. S30 under 30g/L salt," *J Bioresource Technology,* vol. 250, pp. 495-504, Feb 2018, doi: 10.1016/j.biortech.2017.11.072.
[198] X. Hu, X. Tang, Z. Bi, Q. Zhao, and L. Ren, "Adaptive evolution of microalgae *Schizochytrium* sp. under high temperature for efficient production of docosahexaeonic acid," *J Algal Research,* vol. 54, p. 102212, 2021.
[199] X.-M. Sun, L.-J. Ren, Z.-Q. Bi, X.-J. Ji, Q.-Y. Zhao, and H. Huang, "Adaptive evolution of microalgae *Schizochytrium* sp. under high salinity stress to alleviate oxidative damage and improve lipid biosynthesis," *J Bioresource Technology,* vol. 267, pp. 438-444, 2018.
[200] X.-M. Sun, L.-J. Ren, X.-J. Ji, S.-L. Chen, D.-S. Guo, and H. Huang, "Adaptive evolution of *Schizochytrium* sp. by continuous high oxygen stimulations to enhance docosahexaenoic acid synthesis," *J Bioresource Technology,* vol. 211, pp. 374-381, 2016.
[201] Z. Yu, T. Zhang, and Y. Zhu, "Whole-genome re-sequencing and transcriptome reveal cadmium tolerance related genes and pathways in *Chlamydomonas reinhardtii*," *J Ecotoxicology Environmental Safety,* vol. 191, p. 110231, 2020.
[202] S. Yu, Q. Zhao, X. Miao, and J. Shi, "Enhancement of lipid production in low-starch mutants *Chlamydomonas reinhardtii* by adaptive laboratory evolution," *J Bioresource Technology,* vol. 147, pp. 499-507, 2013.
[203] A. J. LaPanse, T. A. Burch, J. M. Tamburro, J. C. Traller, A. Pinowska, and M. C. Posewitz, "Adaptive laboratory evolution for increased temperature tolerance of the diatom *Nitzschia inconspicua*," *J MicrobiologyOpen,* vol. 12, no. 1, p. e1343, 2023.
[204] R. Barten, T. Peeters, S. Navalho, L. Fontowicz, R. H. Wijffels, and M. Barbosa, "Expanding the upper‐temperature boundary for the microalga *Picochlorum* sp.(BPE23) by adaptive laboratory evolution," *J Biotechnology Journal,* vol. 17, no. 5, p. 2100659, 2022.
[205] X. Li, G. Pei, L. Liu, L. Chen, and W. Zhang, "Metabolomic analysis and lipid accumulation in a glucose tolerant *Crypthecodinium cohnii* strain obtained by adaptive laboratory evolution," *J Bioresource Technology,* vol. 235, pp. 87-95, 2017.

[206] Z.-H. Kim *et al.*, "Enhanced fatty acid productivity by *Parachlorella* sp., a freshwater microalga, via adaptive laboratory evolution under salt stress," *J Biotechnology Bioprocess Engineering,* vol. 26, no. 2, pp. 223-231, 2021.
[207] L. Hu *et al.*, "Divergent metabolic and transcriptomic responses of *Synechocystis* sp. PCC 6803 to salt stress after adaptive laboratory evolution," *J Algal Research,* vol. 47, 2020, doi: 10.1016/j.algal.2020.101856.
[208] C. Xu, T. Sun, S. Li, L. Chen, and W. Zhang, "Adaptive laboratory evolution of cadmium tolerance in *Synechocystis* sp. PCC 6803," *J Biotechnology for Biofuels and Bioproducts,* vol. 11, p. 205, 2018, doi: 10.1186/s13068-018-1205-x.
[209] Y. Wang *et al.*, "Metabolomic basis of laboratory evolution of butanol tolerance in photosynthetic Synechocystis sp. PCC 6803," *J Microbial Cell Factories,* vol. 13, pp. 1-12, 2014.
[210] K. Hosoda *et al.*, "Adaptation of a cyanobacterium to a biochemically rich environment in experimental evolution as an initial step toward a chloroplast-like state," *J PloS One,* vol. 9, no. 5, p. e98337, 2014.
[211] C. Bowler *et al.*, "The *Phaeodactylum* genome reveals the evolutionary history of diatom genomes," *J Nature,* vol. 456, no. 7219, pp. 239-244, 2008.
[212] K. E. Apt, A. Grossman, and P. Kroth-Pancic, "Stable nuclear transformation of the diatom *Phaeodactylum tricornutum*," *J Molecular General Genetics MGG,* vol. 252, pp. 572-579, 1996.
[213] S. Stork, D. Moog, J. M. Przyborski, I. Wilhelmi, S. Zauner, and U. G. Maier, "Distribution of the SELMA translocon in secondary plastids of red algal origin and predicted uncoupling of ubiquitin-dependent translocation from degradation," *J Eukaryotic cell,* vol. 11, no. 12, pp. 1472-1481, 2012.
[214] Y.-F. Niu *et al.*, "Transformation of diatom *Phaeodactylum tricornutum* by electroporation and establishment of inducible selection marker," *J Biotechniques,* vol. 52, no. 6, pp. 1-3, 2012.
[215] W.-H. Xie *et al.*, "Construction of novel chloroplast expression vector and development of an efficient transformation system for the diatom *Phaeodactylum tricornutum*," *J Marine Biotechnology,* vol. 16, pp. 538-546, 2014.
[216] M. L. Hamilton, R. P. Haslam, J. A. Napier, and O. Sayanova, "Metabolic engineering of *Phaeodactylum tricornutum* for the enhanced accumulation of omega-3 long chain polyunsaturated fatty acids," *J Metabolic Engineering,* vol. 22, pp. 3-9, 2014.
[217] S. Seo, H. Jeon, S. Hwang, E. Jin, and K. S. Chang, "Development of a new constitutive expression system for the transformation of the diatom *Phaeodactylum tricornutum*," *J Algal Research,* vol. 11, pp. 50-54, 2015.
[218] M. Moosburner, A. E. Allen, and F. Daboussi, "Genetic Engineering in Marine Diatoms: Current Practices and Emerging Technologies," *J The Molecular Life of Diatoms,* pp. 743-773, 2022.
[219] A. Oeltjen, J. Marquardt, and E. Rhiel, "Differential circadian expression of genes fcp2 and fcp6 in *Cyclotella cryptica*," *J International Microbiology,* vol. 7, no. 2, pp. 127-131, 2004.
[220] A. Falciatore, R. Casotti, C. Leblanc, C. Abrescia, and C. Bowler, "Transformation of nonselectable reporter genes in marine diatoms," *J Marine Biotechnology,* vol. 1, pp. 239-251, 1999.

[221] M. Siaut *et al.*, "Molecular toolbox for studying diatom biology in *Phaeodactylum tricornutum*," *J Gene,* vol. 406, no. 1-2, pp. 23-35, 2007.
[222] C. Leblanc, A. Falciatore, M. Watanabe, and C. Bowler, "Semi-quantitative RT-PCR analysis of photoregulated gene expression in marine diatoms," *J Plant Molecular Biology,* vol. 40, pp. 1031-1044, 1999.
[223] N. Poulsen and N. Kröger, "A new molecular tool for transgenic diatoms: control of mRNA and protein biosynthesis by an inducible promoter–terminator cassette," *J The FEBS journal,* vol. 272, no. 13, pp. 3413-3423, 2005.
[224] Y. Niu *et al.*, "A new inducible expression system in a transformed green alga, *Chlorella vulgaris*," *J Genet Mol Res,* vol. 10, no. 4, pp. 3427-34, 2011.
[225] N. Poulsen, P. M. Chesley, and N. Kröger, "Molecular genetic manipulation of the diatom *Thalassiosira pseudonana* (bacillariophyceae) 1," *J Journal of Phycology,* vol. 42, no. 5, pp. 1059-1065, 2006.
[226] L. Chu, D. Ewe, C. R. Bártulos, P. G. Kroth, and A. Gruber, "Rapid induction of GFP expression by the nitrate reductase promoter in the diatom *Phaeodactylum tricornutum*," *J PeerJ,* vol. 4, p. e2344, 2016.
[227] A. Falciatore, M. Jaubert, J.-P. Bouly, B. Bailleul, and T. Mock, "Diatom molecular research comes of age: model species for studying phytoplankton biology and diversity," *Plant Cell,* vol. 32, no. 3, pp. 547-572, 2020.
[228] K. Sakaue, H. Harada, and Y. Matsuda, "Development of gene expression system in a marine diatom using viral promoters of a wide variety of origin," *J Physiologia Plantarum,* vol. 133, no. 1, pp. 59-67, 2008.
[229] T. Kadono *et al.*, "Effect of an introduced phytoene synthase gene expression on carotenoid biosynthesis in the marine diatom *Phaeodactylum tricornutum*," *J Marine Drugs,* vol. 13, no. 8, pp. 5334-5357, 2015.
[230] H. Harada, D. Nakatsuma, M. Ishida, and Y. Matsuda, "Regulation of the expression of intracellular β-carbonic anhydrase in response to CO_2 and light in the marine diatom *Phaeodactylum tricornutum*," *J Plant Physiology,* vol. 139, no. 2, pp. 1041-1050, 2005.
[231] H.-Y. Lin *et al.*, "Alkaline phosphatase promoter as an efficient driving element for exogenic recombinant in the marine diatom *Phaeodactylum tricornutum*," *J Algal Research,* vol. 23, pp. 58-65, 2017.
[232] Y. Watanabe *et al.*, "Development of endogenous promoters that drive high-level expression of introduced genes in the model diatom *Phaeodactylum tricornutum*," *J Marine Genomics,* vol. 42, pp. 41-48, 2018.
[233] E. Erdene-Ochir, B.-K. Shin, B. Kwon, C. Jung, and C.-H. Pan, "Identification and characterisation of the novel endogenous promoter HASP1 and its signal peptide from *Phaeodactylum tricornutum*," *J Scientific Reports,* vol. 9, no. 1, p. 9941, 2019.
[234] E. Erdene‐Ochir *et al.*, "Characterization of endogenous promoters of GapC1 and GS for recombinant protein expression in *Phaeodactylum tricornutum*," *J MicrobiologyOpen,* vol. 10, no. 5, p. e1239, 2021.
[235] L. A. Zaslavskaia, J. C. Lippmeier, P. G. Kroth, A. R. Grossman, and K. E. Apt, "Transformation of the diatom *Phaeodactylum tricornutum* (Bacillariophyceae) with a variety of selectable marker and reporter genes," *J Journal of Phycology,* vol. 36, no. 2, pp. 379-386, 2000.
[236] M. Miyahara, M. Aoi, N. Inoue-Kashino, Y. Kashino, and K. Ifuku, "Highly efficient transformation of the diatom *Phaeodactylum tricornutum* by multi-

pulse electroporation," *J Bioscience, Biotechnology, Biochemistry,* vol. 77, no. 4, pp. 874-876, 2013.
[237] A. Miyagawa, T. Okami, N. Kira, H. Yamaguchi, K. Ohnishi, and M. Adachi, "Research note: high efficiency transformation of the diatom *Phaeodactylum tricornutum* with a promoter from the diatom *Cylindrotheca fusiformis*," *J Phycological Research,* vol. 57, no. 2, pp. 142-146, 2009.
[238] C. Zhang and H. Hu, "High-efficiency nuclear transformation of the diatom Phaeodactylum tricornutum by electroporation," *J Marine genomics,* vol. 16, pp. 63-66, 2014.
[239] B. J. Karas *et al.*, "Designer diatom episomes delivered by bacterial conjugation," *J Nature Communications,* vol. 6, no. 1, p. 6925, 2015.
[240] W. Huang and F. Daboussi, "Genetic and metabolic engineering in diatoms," *J Philosophical Transactions of the Royal Society B: Biological Sciences,* vol. 372, no. 1728, p. 20160411, 2017.
[241] V. De Riso, R. Raniello, F. Maumus, A. Rogato, C. Bowler, and A. Falciatore, "Gene silencing in the marine diatom *Phaeodactylum tricornutum*," *J Nucleic Acids Research,* vol. 37, no. 14, pp. e96-e96, 2009.
[242] T. J. Erb, P. R. Jones, and A. Bar-Even, "Synthetic metabolism: metabolic engineering meets enzyme design," *J Current Opinion in Chemical Biology,* vol. 37, pp. 56-62, 2017.
[243] B. Behera, Y. Unpaprom, R. Ramaraj, G. P. Maniam, N. Govindan, and B. Paramasivan, "Integrated biomolecular and bioprocess engineering strategies for enhancing the lipid yield from microalgae," *J Renewable Sustainable Energy Reviews,* vol. 148, p. 111270, 2021.
[244] A. Mühlroth *et al.*, "Pathways of lipid metabolism in marine algae, co-expression network, bottlenecks and candidate genes for enhanced production of EPA and DHA in species of Chromista," *J Marine Drugs,* vol. 11, no. 11, pp. 4662-4697, 2013.
[245] N. N. Zulu, K. Zienkiewicz, K. Vollheyde, and I. Feussner, "Current trends to comprehend lipid metabolism in diatoms," *J Progress in Lipid Research,* vol. 70, pp. 1-16, 2018.
[246] S. Seo, J. Kim, J.-W. Lee, O. Nam, K. S. Chang, and E. Jin, "Enhanced pyruvate metabolism in plastids by overexpression of putative plastidial pyruvate transporter in *Phaeodactylum tricornutum*," *J Biotechnology for Biofuels and Bioproducts,* vol. 13, no. 1, pp. 1-11, 2020.
[247] Y.-H. Ma *et al.*, "Antisense knockdown of pyruvate dehydrogenase kinase promotes the neutral lipid accumulation in the diatom *Phaeodactylum tricornutum*," *J Microbial Cell Factories,* vol. 13, pp. 1-9, 2014.
[248] D.-W. Li *et al.*, "Constitutive and chloroplast targeted expression of acetyl-CoA carboxylase in oleaginous microalgae elevates fatty acid biosynthesis," *J Marine Biotechnology,* vol. 20, pp. 566-572, 2018.
[249] J. Xue, Y.-F. Niu, T. Huang, W.-D. Yang, J.-S. Liu, and H.-Y. Li, "Genetic improvement of the microalga *Phaeodactylum tricornutum* for boosting neutral lipid accumulation," *J Metabolic Engineering,* vol. 27, pp. 1-9, 2015.
[250] B.-H. Zhu, R.-H. Zhang, N.-N. Lv, G.-P. Yang, Y.-S. Wang, and K.-H. Pan, "The role of malic enzyme on promoting total lipid and fatty acid production in *Phaeodactylum tricornutum*," *J Frontiers in Plant Science,* vol. 9, p. 826, 2018.
[251] R. Zhang, B. Zhu, C. Tu, Y. Li, Y. Zhao, and K. Pan, "The combined effect of nitrogen deprivation and overexpression of malic enzyme gene on growth

and lipid accumulation in *Phaeodactylum tricornutum*," *J Journal of Applied Phycology,* vol. 33, pp. 3637-3645, 2021.
[252] J. Xue *et al.*, "Glucose-6-phosphate dehydrogenase as a target for highly efficient fatty acid biosynthesis in microalgae by enhancing NADPH supply," *J Metabolic Engineering,* vol. 41, pp. 212-221, 2017.
[253] S. Wu *et al.*, "Elevated CO_2 improves both lipid accumulation and growth rate in the glucose-6-phosphate dehydrogenase engineered *Phaeodactylum tricornutum*," *J Microbial Cell Factories,* vol. 18, no. 1, pp. 1-16, 2019.
[254] Y. Yao *et al.*, "Glycerol and neutral lipid production in the oleaginous marine diatom *Phaeodactylum tricornutum* promoted by overexpression of glycerol-3-phosphate dehydrogenase," *J Biotechnology for Biofuels and Bioproducts,* vol. 7, no. 1, pp. 1-9, 2014.
[255] X. Wang *et al.*, "Dual expression of plastidial GPAT1 and LPAT1 regulates triacylglycerol production and the fatty acid profile in Phaeodactylum tricornutum," *J Biotechnology for Biofuels and Bioproducts,* vol. 11, pp. 1-14, 2018.
[256] X. Wang *et al.*, "TAG pathway engineering via GPAT2 concurrently potentiates abiotic stress tolerance and oleaginicity in Phaeodactylum tricornutum," *J Biotechnology for Biofuels and Bioproducts,* vol. 13, no. 1, pp. 1-14, 2020.
[257] Y. Zhang, Y. Pan, W. Ding, H. Hu, and J. Liu, "Lipid production is more than doubled by manipulating a diacylglycerol acyltransferase in algae," *J GCB Bioenergy,* vol. 13, no. 1, pp. 185-200, 2021.
[258] R. P. Haslam *et al.*, "Overexpression of an endogenous type 2 diacylglycerol acyltransferase in the marine diatom *Phaeodactylum tricornutum* enhances lipid production and omega-3 long-chain polyunsaturated fatty acid content," *J Biotechnology for Biofuels and Bioproducts,* vol. 13, pp. 1-17, 2020.
[259] J. Dinamarca, O. Levitan, G. K. Kumaraswamy, D. S. Lun, and P. G. Falkowski, "Overexpression of a diacylglycerol acyltransferase gene in *Phaeodactylum tricornutum* directs carbon towards lipid biosynthesis," *J Journal of Phycology,* vol. 53, no. 2, pp. 405-414, 2017.
[260] Y.-F. Niu *et al.*, "Improvement of neutral lipid and polyunsaturated fatty acid biosynthesis by overexpressing a type 2 diacylglycerol acyltransferase in marine diatom *Phaeodactylum tricornutum*," *J Marine Drugs,* vol. 11, no. 11, pp. 4558-4569, 2013.
[261] B.-H. Zhu, H.-P. Shi, G.-P. Yang, N.-N. Lv, M. Yang, and K.-H. Pan, "Silencing UDP-glucose pyrophosphorylase gene in *Phaeodactylum tricornutum* affects carbon allocation," *J New Biotechnology,* vol. 33, no. 1, pp. 237-244, 2016.
[262] X. Jiang *et al.*, "Silencing 1, 3-β-glucan synthase gene promotes total lipid production and changes fatty acids composition by affecting carbon flow distribution in *Phaeodactylum tricornutum*," *J Algal Research,* vol. 67, p. 102827, 2022.
[263] F. Barka, M. Angstenberger, T. Ahrendt, W. Lorenzen, H. B. Bode, and C. Büchel, "Identification of a triacylglycerol lipase in the diatom *Phaeodactylum tricornutum*," *J Biochimica et Biophysica Acta -Molecular Cell Research,* vol. 1861, no. 3, pp. 239-248, 2016.
[264] K.-T. Peng *et al.*, "Delta 5 fatty acid desaturase upregulates the synthesis of polyunsaturated fatty acids in the marine diatom *Phaeodactylum*

tricornutum," *J Journal of Agricultural Food Chemistry,* vol. 62, no. 35, pp. 8773-8776, 2014.
[265] B.-H. Zhu, C.-C. Tu, H.-P. Shi, G.-P. Yang, and K.-H. Pan, "Overexpression of endogenous delta-6 fatty acid desaturase gene enhances eicosapentaenoic acid accumulation in *Phaeodactylum tricornutum*," *J Process Biochemistry,* vol. 57, pp. 43-49, 2017.
[266] U. Eilers, A. Bikoulis, J. Breitenbach, C. Büchel, and G. Sandmann, "Limitations in the biosynthesis of fucoxanthin as targets for genetic engineering in *Phaeodactylum tricornutum*," *J Journal of Applied Phycology,* vol. 28, pp. 123-129, 2016.
[267] S.-Y. Cen *et al.*, "Crucial carotenogenic genes elevate hyperaccumulation of both fucoxanthin and β-carotene in *Phaeodactylum tricornutum*," *J Algal Research,* vol. 64, p. 102691, 2022.
[268] T.-B. Hao *et al.*, "Hyperaccumulation of fucoxanthin by enhancing methylerythritol phosphate pathway in *Phaeodactylum tricornutum*," *J Applied Microbiology Biotechnology,* vol. 105, no. 23, pp. 8783-8793, 2021.
[269] F. Manfellotto, G. R. Stella, A. Falciatore, C. Brunet, and M. I. Ferrante, "Engineering the unicellular alga *Phaeodactylum tricornutum* for enhancing carotenoid production," *J Antioxidants,* vol. 9, no. 8, p. 757, 2020.
[270] C. Castell, P. Bernal‐Bayard, J. M. Ortega, M. Roncel, M. Hervás, and J. A. Navarro, "The heterologous expression of a plastocyanin in the diatom *Phaeodactylum tricornutum* improves cell growth under iron‐deficient conditions," *J Physiologia Plantarum,* vol. 171, no. 2, pp. 277-290, 2021.
[271] S. Seo, H. Jeon, K. S. Chang, and E. Jin, "Enhanced biomass production by *Phaeodactylum tricornutum* overexpressing phosphoenolpyruvate carboxylase," *J Algal Research,* vol. 31, pp. 489-496, 2018.
[272] W. Fu *et al.*, "Intracellular spectral recompositioning of light enhances algal photosynthetic efficiency," *J Science Advances,* vol. 3, no. 9, p. e1603096, 2017.
[273] G.-B. Ye *et al.*, "3-Oxoacyl acyl carrier protein reductase overexpression reveals its unprecedented roles in biofuel production and high-temperature tolerance in diatom," *J Fuel,* vol. 325, p. 124844, 2022.
[274] Z. Shemesh, S. Leu, I. Khozin-Goldberg, S. Didi-Cohen, A. Zarka, and S. Boussiba, "Inducible expression of *Haematococcus* oil globule protein in the diatom *Phaeodactylum tricornutum*: association with lipid droplets and enhancement of TAG accumulation under nitrogen starvation," *J Algal Research,* vol. 18, pp. 321-331, 2016.
[275] J. Yang, Y. Pan, C. Bowler, L. Zhang, and H. Hu, "Knockdown of phosphoenolpyruvate carboxykinase increases carbon flux to lipid synthesis in *Phaeodactylum tricornutum*," *J Algal Research,* vol. 15, pp. 50-58, 2016.
[276] Y.-F. Yang, D.-W. Li, S. Balamurugan, X. Wang, W.-D. Yang, and H.-Y. Li, "Chrysolaminarin biosynthesis in the diatom is enhanced by overexpression of 1, 6-β-transglycosylase," *J Algal Research,* vol. 66, p. 102817, 2022.
[277] M. T. Russo *et al.*, "The first genetic engineered system for ovothiol biosynthesis in diatoms reveals a mitochondrial localization for the sulfoxide synthase OvoA," *J Open Biology,* vol. 13, no. 2, p. 220309, 2023.
[278] N. Baiden, C. Gandini, P. Goddard, and O. Sayanova, "Heterologous expression of antimicrobial peptides S-thanatin and bovine lactoferricin in the marine diatom *Phaeodactylum tricornutum* enhances native

antimicrobial activity against Gram-negative bacteria," *J Algal Research*, vol. 69, p. 102927, 2023.
[279] F. Hempel, J. Lau, A. Klingl, and U. G. Maier, "Algae as protein factories: expression of a human antibody and the respective antigen in the diatom *Phaeodactylum tricornutum*," *J PloS One*, vol. 6, no. 12, p. e28424, 2011.
[280] M. Windhagauer, R. M. Abbriano, D. A. Pittrich, and M. A. Doblin, "Phosphate-inducible poly-hydroxy butyrate production dynamics in CO_2 supplemented upscaled cultivation of engineered *Phaeodactylum tricornutum*," *J Journal of Applied Phycology*, vol. 34, no. 5, pp. 2259-2270, 2022.
[281] F. Hempel *et al.*, "Microalgae as bioreactors for bioplastic production," *J Microbial Cell Factories*, vol. 10, pp. 1-6, 2011.
[282] L. C. Krämer, D. Wasser, F. Haitz, B. Sabel, and C. Büchel, "Heterologous expression of HUP1 glucose transporter enables low-light mediated growth on glucose in *Phaeodactylum tricornutum*," *J Algal Research*, vol. 64, p. 102719, 2022.
[283] W. Zhang *et al.*, "Heterotrophic modification of *Phaeodactylum tricornutum* Bohlin," *J Algal Research*, vol. 72, p. 103137, 2023.
[284] L. Zaslavskaia, J. Lippmeier, C. Shih, D. Ehrhardt, A. Grossman, and K. Apt, "Trophic conversion of an obligate photoautotrophic organism through metabolic engineering," *J Science*, vol. 292, no. 5524, pp. 2073-2075, 2001.
[285] Á. Ragnarsson, B. Steingrímsson, and S. Thorhallsson, "Geothermal development in Iceland 2015-2019," in *Proceedings World Geothermal Congress*, 2020, vol. 1.
[286] I. Gunnarsson, E. S. Aradóttir, B. Sigfússon, E. Gunnlaugsson, and B. M. Júlíusson, "Geothermal gas emission from Hellisheiði and Nesjavellir power plants, Iceland," *Energy, Reykjavík J GRC Transactions*, vol. 37, p. 7859, 2013.
[287] B. Sigfússon, M. Þ. Arnarson, S. Ó. Snæbjörnsdóttir, M. R. Karlsdóttir, E. S. Aradóttir, and I. Gunnarsson, "Reducing emissions of carbon dioxide and hydrogen sulphide at Hellisheidi power plant in 2014-2017 and the role of CarbFix in achieving the 2040 Iceland climate goals," *J Energy Procedia*, vol. 146, pp. 135-145, 2018.
[288] S. R. Chia, K. W. Chew, H. Y. Leong, S.-H. Ho, H. S. H. Munawaroh, and P. L. Show, "CO_2 mitigation and phycoremediation of industrial flue gas and wastewater via microalgae-bacteria consortium: Possibilities and challenges," *J Chemical Engineering Journal*, vol. 425, p. 131436, 2021.
[289] W. A. Wan Mahari *et al.*, "Recent advances on microalgae cultivation for simultaneous biomass production and removal of wastewater pollutants to achieve circular economy," *J Bioresource Technology*, vol. 364, p. 128085, Oct 8 2022, doi: 10.1016/j.biortech.2022.128085.
[290] J. Cheng, Y. Zhu, Z. Zhang, and W. Yang, "Modification and improvement of microalgae strains for strengthening CO_2 fixation from coal-fired flue gas in power plants," *J Bioresource Technology*, vol. 291, p. 121850, 2019.
[291] M. Xie, Y. Qiu, C. Song, Y. Qi, Y. Li, and Y. Kitamura, "Optimization of *Chlorella sorokiniana* cultivation condition for simultaneous enhanced biomass and lipid production via CO_2 fixation," *J Bioresource Technology Reports*, vol. 2, pp. 15-20, 2018.

[292] E. C. Camargo and A. T. Lombardi, "Effect of cement industry flue gas simulation on the physiology and photosynthetic performance of *Chlorella sorokiniana*," *J Journal of Applied Phycology*, vol. 30, pp. 861-871, 2018.
[293] Y. J. Sung, J. S. Lee, H. K. Yoon, H. Ko, and S. J. Sim, "Outdoor cultivation of microalgae in a coal-fired power plant for conversion of flue gas CO_2 into microalgal direct combustion fuels," *Systems Microbiology*, vol. 1, pp. 90-99, 2021.
[294] X. Jin, S. Gong, Z. Chen, J. Xia, and W. Xiang, "Potential microalgal strains for converting flue gas CO_2 into biomass," *J Journal of Applied Phycology*, vol. 33, pp. 47-55, 2021.
[295] M. Sakarika and M. Kornaros, "Effect of pH on growth and lipid accumulation kinetics of the microalga *Chlorella vulgaris* grown heterotrophically under sulfur limitation," *J Bioresource Technology*, vol. 219, pp. 694-701, Nov 2016, doi: 10.1016/j.biortech.2016.08.033.
[296] A. Solovchenko and I. Khozin-Goldberg, "High-CO_2 tolerance in microalgae: possible mechanisms and implications for biotechnology and bioremediation," *Biotechnol Lett*, vol. 35, no. 11, pp. 1745-1752, 2013.
[297] H. I. Choi *et al.*, "Augmented CO_2 tolerance by expressing a single H^+-pump enables microalgal valorization of industrial flue gas," *J Nature Communications*, vol. 12, no. 1, pp. 1-15, 2021.
[298] Y. Guo *et al.*, "Metabolic acclimation mechanism in microalgae developed for CO_2 capture from industrial flue gas," *J Algal Research*, vol. 26, pp. 225-233, 2017.
[299] S. Nagappan, P.-C. Tsai, S. Devendran, V. Alagarsamy, and V. K. Ponnusamy, "Enhancement of biofuel production by microalgae using cement flue gas as substrate," *Environmental Science and Pollution Research*, vol. 27, pp. 17571-17586, 2020.
[300] B. Zhu *et al.*, "Large-scale cultivation of Spirulina for biological CO_2 mitigation in open raceway ponds using purified CO_2 from a coal chemical flue gas," *J Frontiers in Bioengineering*, vol. 7, p. 441, 2020.
[301] X. Wang *et al.*, "A waste upcycling loop: Two-factor adaptive evolution of microalgae to increase polyunsaturated fatty acid production using food waste," *J Journal of Cleaner Production*, vol. 331, p. 130018, 2022/01/10/ 2022, doi: https://doi.org/10.1016/j.jclepro.2021.130018.
[302] J. Uchiyama *et al.*, "Genomic analysis of parallel-evolved cyanobacterium *Synechocystis* sp. PCC 6803 under acid stress," *Photosynthesis research*, vol. 125, no. 1-2, pp. 243-254, 2015, doi: 10.1007/s11120-015-0111-3.
[303] Y. Jiang, X. Peng, W. Zhang, and T. Liu, "Enhancement of acid resistance of *Scenedesmus dimorphus* by acid adaptation," *J Journal of Applied Phycology*, vol. 24, pp. 1637–1641, 2012, doi: 10.1007/s10811-012-9827-z.
[304] E. Bautista-Chamizo, A. R. Borrero-Santiago, M. R. De Orte, A. DelValls, and I. Riba, "Effects of CO_2 enrichment on two microalgae species: A toxicity approach using consecutive generations," *J Chemosphere*, vol. 213, pp. 84-91, Dec 2018, doi: 10.1016/j.chemosphere.2018.09.001.
[305] R. R. L. Guillard, "Culture of Phytoplankton for Feeding Marine Invertebrates," in *Culture of Marine Invertebrate Animals: Proceedings — 1st Conference on Culture of Marine Invertebrate Animals Greenport*, W. L. Smith and M. H. Chanley Eds. Boston, MA: Springer US, 1975, pp. 29-60.
[306] C. Zhu and Y. Lee, "Determination of biomass dry weight of marine microalgae," *J Journal of Applied Phycology*, vol. 9, pp. 189-194, 1997.

[307] R. J. Ritchie, "Consistent sets of spectrophotometric chlorophyll equations for acetone, methanol and ethanol solvents," *Photosynthesis research,* vol. 89, no. 1, pp. 27-41, 2006.
[308] E. M. Zetsche and F. J. R. Meysman, "Dead or alive? Viability assessment of micro- and mesoplankton," *Journal of Plankton Research,* vol. 34, no. 6, pp. 493-509, 2012, doi: 10.1093/plankt/fbs018.
[309] E. Ryckebosch, K. Muylaert, and I. Foubert, "Optimization of an analytical procedure for extraction of lipids from microalgae," *Journal of the American Oil Chemists' Society,* vol. 89, no. 2, pp. 189-198, 2011, doi: 10.1007/s11746-011-1903-z.
[310] F. Mus *et al.*, "Physiological and molecular analysis of carbon source supplementation and pH stress-induced lipid accumulation in the marine diatom *Phaeodactylum tricornutum*," *J Applied Microbiology Biotechnology,* vol. 97, no. 8, pp. 3625-42, Apr 2013, doi: 10.1007/s00253-013-4747-7.
[311] J. F. Kennedy and M. Chaplin, *Carbohydrate analysis: a practical approach*. Oxford University Press, 1994.
[312] A. M. Bolger, M. Lohse, and B. Usadel, "Trimmomatic: a flexible trimmer for Illumina sequence data," *Bioinformatics,* vol. 30, no. 15, pp. 2114-20, Aug 1 2014, doi: 10.1093/bioinformatics/btu170.
[313] D. Kim, B. Langmead, and S. L. Salzberg, "HISAT: a fast spliced aligner with low memory requirements," *J Nature Methods,* vol. 12, no. 4, pp. 357-60, Apr 2015, doi: 10.1038/nmeth.3317.
[314] B. Langmead and S. L. Salzberg, "Fast gapped-read alignment with Bowtie 2," *Nat Methods,* vol. 9, no. 4, pp. 357-359, 2012.
[315] A. Roberts and L. Pachter, "Streaming fragment assignment for real-time analysis of sequencing experiments," *Nat Methods,* vol. 10, no. 1, pp. 71-73, 2013.
[316] S. Chen, Y. Zhou, Y. Chen, and J. Gu, "fastp: an ultra-fast all-in-one FASTQ preprocessor," *Bioinformatics,* vol. 34, no. 17, pp. i884-i890, Sep 1 2018, doi: 10.1093/bioinformatics/bty560.
[317] H. Li and R. Durbin, "Fast and accurate long-read alignment with Burrows-Wheeler transform," *Bioinformatics,* vol. 26, no. 5, pp. 589-95, Mar 1 2010, doi: 10.1093/bioinformatics/btp698.
[318] A. McKenna *et al.*, "The Genome Analysis Toolkit: a MapReduce framework for analyzing next-generation DNA sequencing data," (in eng), *Genome research,* vol. 20, no. 9, pp. 1297-303, Sep 2010, doi: 10.1101/gr.107524.110.
[319] Z. Wu *et al.*, "Evaluation of flocculation induced by pH increase for harvesting microalgae and reuse of flocculated medium," *J Bioresource Technology,* vol. 110, pp. 496–502, 2012, doi: 10.1016/j.biortech.2012.01.101.
[320] B. Pérez, I. C. Pina, and L. P. Rodríguez, "Kinetic model for growth of *Phaeodactylum tricornutum* in intensive culture photobioreactor," *J Biochemical Engineering Journal,* vol. 40, pp. 520–525, 2008, doi: 10.1016/j.bej.2008.02.007.
[321] J. Hayward, "Studies on the growth of *Phaeodactylum tricornutum* IV. Comparison of different isolates," *J. mar. biol. Ass. U.K.*, vol. 48, pp. 657-666, 1968.

[322] G. F. Humphrey, "The photosynthesis: respiration ratio of some unicellular marine algae," *J. mar. biol. Ass. U.K.*, vol. 18, pp. 111-119, 1975.
[323] K. R. Hinga, "Effects of pH on coastal marine phytoplankton," *Marine Ecology Progress Series*, vol. 238, pp. 281–300, 2002.
[324] D. C. O. Thornton, "Effect of low pH on carbohydrate production by a marine planktonic diatom (*Chaetoceros muelleri*)," *Research Letters in Ecology*, vol. 2009, pp. 1-4, 2009, doi: 10.1155/2009/105901.
[325] P. S. Schulze, L. A. Barreira, H. G. Pereira, J. A. Perales, and J. C. Varela, "Light emitting diodes (LEDs) applied to microalgal production," *J Trends in Biotechnology*, vol. 32, no. 8, pp. 422-430, 2014.
[326] N. Sharma *et al.*, "Red Light Variation an Effective Alternative to Regulate Biomass and Lipid Profiles in *Phaeodactylum tricornutum*," *Applied Sciences*, vol. 10, no. 7, p. 2531, 2020. [Online]. Available: https://www.mdpi.com/2076-3417/10/7/2531.
[327] R. Yang and D. Wei, "Improving fucoxanthin production in mixotrophic culture of marine diatom *Phaeodactylum tricornutum* by LED light shift and nitrogen supplementation," *J Frontiers in Bioengineering*, vol. 8, p. 820, 2020.
[328] A. D. Martino, A. Meichenin, J. Shi, K. Pan, and C. Bowler, "Genetic and phenotypic characterization of *Phaeodactylum tricornutum* (Bacillariophyceae) accessions," *J Journal of Phycology*, vol. 43, no. 5, pp. 992-1009, 2007.
[329] A. Bartual, J. A. Ga´lvez, and F. Ojeda, "Phenotypic response of the diatom *Phaeodactylum tricornutum* Bohlin to experimental changes in the inorganic carbon system," *J Botanica Marina*, vol. 51, pp. 350–359, 2008, doi: 10.1515/BOT.2008.047.
[330] R. Nagao, M. Yokono, Y. Ueno, J. R. Shen, and S. Akimoto, "pH-Sensing Machinery of Excitation Energy Transfer in Diatom PSI-FCPI Complexes," *J Phys Chem Lett*, vol. 10, no. 13, pp. 3531-3535, Jul 5 2019, doi: 10.1021/acs.jpclett.9b01314.
[331] L. Qu, J. Beardall, X. Jiang, and K. Gao, "Elevated pCO_2 enhances under light but reduces in darkness the growth rate of a diatom, with implications for the fate of phytoplankton below the photic zone," *J Limnology Oceanography*, vol. 66, no. 10, pp. 3630-3642, 2021, doi: 10.1002/lno.11903.
[332] V. López-Rodas, E. Maneiro, and E.Costas, "Adaptation of cyanobacteria and microalgae to extreme environmental changes derived from anthropogenic pollution," *Limnetica*, vol. 25(1-2), pp. 403-410, 2006.
[333] B. Scholz, "Effects of varying pH on the growth and physiology of five marine microphytobenthic diatoms isolated from the Solthörn tidal flat (southern North Sea, Germany)," *J Physiologia Plantarum*, vol. 53, no. 3, pp. 252-264, 2019, doi: 10.2216/13-240.1.
[334] C. Büchel, "Evolution and function of light harvesting proteins," *Journal of Plant Physiology*, vol. 172, pp. 62-75, 2015.
[335] A. Falciatore *et al.*, "Light-driven processes: key players of the functional biodiversity in microalgae," *Comptes Rendus. Biologies*, vol. 345, no. 2, pp. 1-24, 2022.
[336] A. R. Taylor, C. Brownlee, and G. L. Wheeler, "Proton channels in algae: reasons to be excited," *Trends in Plant Science*, vol. 17, no. 11, pp. 675-684, 2012.

[337] V. Hervé, J. Derr, S. Douady, M. Quinet, L. Moisan, and P. J. Lopez, "Multiparametric analyses reveal the pH-dependence of silicon biomineralization in diatoms," *J PloS One,* vol. 7, no. 10, p. e46722, 2012.
[338] R. Höhner, A. Aboukila, H.-H. Kunz, and K. Venema, "Proton gradients and proton-dependent transport processes in the chloroplast," *J Frontiers in Plant Science,* vol. 7, p. 218, 2016.
[339] R. Huang *et al.*, "A Potential Role for Epigenetic Processes in the Acclimation Response to Elevated pCO_2 in the Model Diatom *Phaeodactylum tricornutum*," *J Frontiers in Microbiology,* vol. 9, p. 3342, 2018, doi: 10.3389/fmicb.2018.03342.
[340] J. Levering, C. L. Dupont, A. E. Allen, B. O. Palsson, and K. Zengler, "Integrated regulatory and metabolic networks of the marine diatom *Phaeodactylum tricornutum* predict the response to rising CO_2 levels," *Msystems,* vol. 2, no. 1, pp. e00142-16, 2017.
[341] M. Gachelin *et al.*, "Enhancing PUFA-rich polar lipids in *Tisochrysis lutea* using adaptive laboratory evolution (ALE) with oscillating thermal stress," (in eng), *J Applied Microbiology Biotechnology,* vol. 105, no. 1, pp. 301-312, Jan 2021, doi: 10.1007/s00253-020-11000-4.
[342] F. Taddei, M. Radman, J. Maynard-Smith, B. Toupance, P. H. Gouyon, and B. Godelle, "Role of mutator alleles in adaptive evolution," *J Nature,* vol. 387, no. 6634, pp. 700-2, Jun 12 1997, doi: 10.1038/42696.
[343] A. Olabi *et al.*, "Role of microalgae in achieving sustainable development goals and circular economy," *J Science of The Total Environment,* vol. 854, p. 158689, 2023.
[344] A. Pawlowski, J. Mendoza, J. Guzmán, M. Berenguel, F. Acién, and S. Dormido, "Effective utilization of flue gases in raceway reactor with event-based pH control for microalgae culture," *J Bioresource Technology,* vol. 170, pp. 1-9, 2014.
[345] S.-C. Ong, C.-Y. Kao, S.-Y. Chiu, M.-T. Tsai, and C.-S. Lin, "Characterization of the thermal-tolerant mutants of *Chlorella* sp. with high growth rate and application in outdoor photobioreactor cultivation," *J Bioresource Technology,* vol. 101, no. 8, pp. 2880-2883, 2010.
[346] C.-M. Kuo *et al.*, "Ability of an alkali-tolerant mutant strain of the microalga *Chlorella* sp. AT1 to capture carbon dioxide for increasing carbon dioxide utilization efficiency," *J Bioresource Technology,* vol. 244, pp. 243-251, 2017.
[347] Y. Su, M. Xu, S. Brynjólfsson, and W. Fu, "Physiological and molecular insights into adaptive evolution of the marine model diatom *Phaeodactylum tricornutum* under low-pH stress," *J Journal of Cleaner Production,* vol. 412, p. 137297, 2023.
[348] S. Siripornadulsil, S. Traina, D. P. S. Verma, and R. T. Sayre, "Molecular mechanisms of proline-mediated tolerance to toxic heavy metals in transgenic microalgae," *J The Plant Cell,* vol. 14, no. 11, pp. 2837-2847, 2002.
[349] C. Celi, D. Fino, and F. Savorani, "*Phaeodactylum tricornutum* as a source of value-added products: A review on recent developments in cultivation and extraction technologies," *J Bioresource Technology Reports,* p. 101122, 2022.

[350] T. Butler, R. V. Kapoore, and S. Vaidyanathan, "*Phaeodactylum tricornutum*: a diatom cell factory," *J Trends in Biotechnology,* vol. 38, no. 6, pp. 606-622, 2020.
[351] K. Nakajima, A. Tanaka, and Y. Matsuda, "SLC4 family transporters in a marine diatom directly pump bicarbonate from seawater," *J Proceedings of the National Academy of Sciences,* vol. 110, no. 5, pp. 1767-1772, 2013.
[352] G. Hanke and P. Mulo, "Plant type ferredoxins and ferredoxin‐dependent metabolism," *J Plant, Cell Environment,* vol. 36, no. 6, pp. 1071-1084, 2013.
[353] L.-F. Huang, J.-Y. Lin, K.-Y. Pan, C.-K. Huang, and Y.-K. Chu, "Overexpressing ferredoxins in Chlamydomonas reinhardtii increase starch and oil yields and enhance electric power production in a photo microbial fuel cell," *J International Journal of Molecular Sciences,* vol. 16, no. 8, pp. 19308-19325, 2015.
[354] Y.-H. Lin *et al.*, "Overexpression of ferredoxin, PETF, enhances tolerance to heat stress in Chlamydomonas reinhardtii," *J International Journal of Molecular Sciences,* vol. 14, no. 10, pp. 20913-20929, 2013.
[355] M. Tsujii, E. Tanudjaja, and N. Uozumi, "Diverse physiological functions of cation proton antiporters across bacteria and plant cells," *J International Journal of Molecular Sciences,* vol. 21, no. 12, p. 4566, 2020.
[356] V. Correa Galvis *et al.*, "H^+ transport by K^+ EXCHANGE ANTIPORTER3 promotes photosynthesis and growth in chloroplast ATP synthase mutants," *J Plant Physiology,* vol. 182, no. 4, pp. 2126-2142, 2020.
[357] H. Nawaly *et al.*, "Multiple plasma membrane SLC4s contribute to external HCO_3^-acquisition during CO_2 starvation in the marine diatom *Phaeodactylum tricornutum*," *J Journal of Experimental Botany,* vol. 74, no. 1, pp. 296-307, 2023.
[358] J. A. Berges, D. J. Franklin, and P. J. Harrison, "Evolution of an artificial seawater medium: improvements in enriched seawater, artificial water over the last two decades," *J Journal of Phycology,* vol. 37, no. 6, pp. 1138-1145, 2001.
[359] M. Pertea, G. M. Pertea, C. M. Antonescu, T. C. Chang, J. T. Mendell, and S. L. Salzberg, "StringTie enables improved reconstruction of a transcriptome from RNA-seq reads," *J Nature Biotechnology,* vol. 33, no. 3, pp. 290-5, Mar 2015, doi: 10.1038/nbt.3122.
[360] S. Anders, P. T. Pyl, and W. Huber, "HTSeq-a Python framework to work with high-throughput sequencing data," *Bioinformatics,* vol. 31, no. 2, pp. 166-169, Jan 2015, doi: 10.1093/bioinformatics/btu638.
[361] U. Raudvere *et al.*, "g: Profiler: a web server for functional enrichment analysis and conversions of gene lists (2019 update)," *J Nucleic Acids Research,* vol. 47, no. W1, pp. W191-W198, 2019.
[362] N. R. Cohen *et al.*, "Iron storage capacities and associated ferritin gene expression among marine diatoms," *J Limnology Oceanography,* vol. 63, no. 4, pp. 1677-1691, 2018.
[363] N. R. Baker, "Chlorophyll fluorescence: a probe of photosynthesis in vivo," *J Annu. Rev. Plant Biol.,* vol. 59, pp. 89-113, 2008.
[364] M. Schieber and N. S. Chandel, "ROS function in redox signaling and oxidative stress," *J Current Biology,* vol. 24, no. 10, pp. R453-R462, 2014.
[365] T. M. Roberts *et al.*, "Identification and Characterisation of a pH-stable GFP," *J Scientific Reports,* vol. 6, no. 1, p. 28166, 2016.

[366] Y. Liu, J. Yang, and L. Chen, "Structure and function of SLC4 family HCO_3^- transporters," *J Frontiers in Physiology,* vol. 6, p. 355, 2015.
[367] K. Shi *et al.*, "Reactive oxygen species-mediated cellular stress response and lipid accumulation in oleaginous microorganisms: the state of the art and future perspectives," *J Frontiers in Microbiology,* vol. 8, p. 793, 2017.
[368] Q. Yang *et al.*, "Development and characterization of acidic-pH-tolerant mutants of *Zymomonas mobilis* through adaptation and next-generation sequencing-based genome resequencing and RNA-Seq," *J Biotechnology for Biofuels and Bioproducts,* vol. 13, no. 1, pp. 1-17, 2020.
[369] M. M. Kuypers, H. K. Marchant, and B. Kartal, "The microbial nitrogen-cycling network," *J Nature Reviews Microbiology,* vol. 16, no. 5, pp. 263-276, 2018.
[370] X. Z. Fang, W. H. Tian, X. X. Liu, X. Y. Lin, C. W. Jin, and S. J. Zheng, "Alleviation of proton toxicity by nitrate uptake specifically depends on nitrate transporter 1.1 in Arabidopsis," *J New Phytologist,* vol. 211, no. 1, pp. 149-158, 2016.
[371] A. Filonova, P. Haemsch, C. Gebauer, W. Weisheit, and V. Wagner, "Protein disulfide isomerase 2 of *Chlamydomonas reinhardtii* is involved in circadian rhythm regulation," *Molecular plant,* vol. 6, no. 5, pp. 1503-1517, 2013.
[372] K. Greenham and C. R. McClung, "Integrating circadian dynamics with physiological processes in plants," *J Nature Reviews Genetics,* vol. 16, no. 10, pp. 598-610, 2015.
[373] E. M. Farré, "The brown clock: circadian rhythms in stramenopiles," *J Physiologia Plantarum,* vol. 169, no. 3, pp. 430-441, 2020.
[374] K. Tanaka, M. Ishikawa, M. Kaneko, K. Kamiya, S. Kato, and S. Nakanishi, "The endogenous redox rhythm is controlled by a central circadian oscillator in cyanobacterium *Synechococcus elongatus* PCC7942," *Photosynthesis research,* vol. 142, no. 2, pp. 203-210, 2019.
[375] M. S. Chauton, P. Winge, T. Brembu, O. Vadstein, and A. M. Bones, "Gene regulation of carbon fixation, storage, and utilization in the diatom *Phaeodactylum tricornutum* acclimated to light/dark cycles," *J Plant Physiology,* vol. 161, no. 2, pp. 1034-48, Feb 2013, doi: 10.1104/pp.112.206177.
[376] A. N. Dodd, J. Kusakina, A. Hall, P. D. Gould, and M. Hanaoka, "The circadian regulation of photosynthesis," *Photosynthesis research,* vol. 119, no. 1, pp. 181-190, 2014.
[377] K. P. Wright Jr, A. W. McHill, B. R. Birks, B. R. Griffin, T. Rusterholz, and E. D. Chinoy, "Entrainment of the human circadian clock to the natural light-dark cycle," *J Current Biology,* vol. 23, no. 16, pp. 1554-1558, 2013.
[378] K. R. Arrigo and G. L. van Dijken, "Secular trends in Arctic Ocean net primary production," *Journal of Geophysical Research: Oceans,* vol. 116, no. C9, 2011.
[379] K. Lewis, G. Van Dijken, and K. R. Arrigo, "Changes in phytoplankton concentration now drive increased Arctic Ocean primary production," *J Science,* vol. 369, no. 6500, pp. 198-202, 2020.
[380] J. Terhaar, R. Lauerwald, P. Regnier, N. Gruber, and L. Bopp, "Around one third of current Arctic Ocean primary production sustained by rivers and coastal erosion," *J Nature Communications,* vol. 12, no. 1, pp. 1-10, 2021.

[381] C. Beer *et al.*, "Terrestrial gross carbon dioxide uptake: global distribution and covariation with climate," *J Science,* vol. 329, no. 5993, pp. 834-838, 2010.
[382] L. R. Welp *et al.*, "Interannual variability in the oxygen isotopes of atmospheric CO_2 driven by El Niño," *J Nature,* vol. 477, no. 7366, pp. 579-582, 2011.
[383] M. Ragni, *Circadian patterns in key physiological processes of the marine diatom Phaeodactylum tricornutum*. Open University (United Kingdom), 2005.
[384] L. de Winter, I. T. D. Cabanelas, D. E. Martens, R. H. Wijffels, and M. J. Barbosa, "The influence of day/night cycles on biomass yield and composition of *Neochloris oleoabundans*," *J Biotechnology for Biofuels and Bioproducts,* vol. 10, no. 1, pp. 1-10, 2017.
[385] S. Pabi, G. L. van Dijken, and K. R. Arrigo, "Primary production in the Arctic Ocean, 1998–2006," *Journal of Geophysical Research: Oceans,* vol. 113, no. C8, 2008.
[386] K. R. Arrigo, G. L. van Dijken, and S. Bushinsky, "Primary production in the Southern Ocean, 1997–2006," *Journal of Geophysical Research: Oceans,* vol. 113, no. C8, 2008.
[387] K. R. Arrigo, D. Worthen, A. Schnell, and M. P. Lizotte, "Primary production in Southern Ocean waters," *Journal of Geophysical Research: Oceans,* vol. 103, no. C8, pp. 15587-15600, 1998.
[388] L. de Winter, A. J. Klok, M. C. Franco, M. J. Barbosa, and R. H. Wijffels, "The synchronized cell cycle of *Neochloris oleoabundans* and its influence on biomass composition under constant light conditions," *J Algal Research,* vol. 2, no. 4, pp. 313-320, 2013.
[389] E. Poliner *et al.*, "Transcriptional coordination of physiological responses in *Nannochloropsis oceanica* CCMP1779 under light/dark cycles," *Plant J,* vol. 83, no. 6, pp. 1097-113, Sep 2015, doi: 10.1111/tpj.12944.
[390] G. Bilcke *et al.*, "Diurnal transcript profiling of the diatom *Seminavis robusta* reveals adaptations to a benthic lifestyle," *Plant J,* vol. 107, no. 1, pp. 315-336, Jul 2021, doi: 10.1111/tpj.15291.
[391] C. Ferrari *et al.*, "Kingdom-wide comparison reveals the evolution of diurnal gene expression in Archaeplastida," *J Nature Communications,* vol. 10, no. 1, p. 737, Feb 13 2019, doi: 10.1038/s41467-019-08703-2.
[392] S. R. Smith *et al.*, "Transcriptional Orchestration of the Global Cellular Response of a Model Pennate Diatom to Diel Light Cycling under Iron Limitation," *J PLoS Genetics,* vol. 12, no. 12, p. e1006490, Dec 2016, doi: 10.1371/journal.pgen.1006490.
[393] J. M. Zones, I. K. Blaby, S. S. Merchant, and J. G. Umen, "High-Resolution Profiling of a Synchronized Diurnal Transcriptome from *Chlamydomonas reinhardtii* Reveals Continuous Cell and Metabolic Differentiation," *Plant Cell,* vol. 27, no. 10, pp. 2743-69, Oct 2015, doi: 10.1105/tpc.15.00498.
[394] R. Annunziata *et al.*, "bHLH-PAS protein RITMO1 regulates diel biological rhythms in the marine diatom *Phaeodactylum tricornutum*," *Proc Natl Acad Sci USA,* vol. 116, no. 26, pp. 13137-13142, Jun 25 2019, doi: 10.1073/pnas.1819660116.
[395] K.-i. Kucho, K. Okamoto, S. Tabata, H. Fukuzawa, and M. Ishiura, "Identification of novel clock-controlled genes by cDNA macroarray

analysis in *Chlamydomonas reinhardtii*," *J Plant Molecular Biology,* vol. 57, no. 6, pp. 889-906, 2005.
[396] M. Moulager *et al.*, "Light-dependent regulation of cell division in Ostreococcus: evidence for a major transcriptional input," *J Plant Physiology,* vol. 144, no. 3, pp. 1360-1369, 2007.
[397] E. Ryckebosch, K. Muylaert, M. Eeckhout, T. Ruyssen, and I. Foubert, "Influence of drying and storage on lipid and carotenoid stability of the microalga *Phaeodactylum tricornutum*," *J. Agric. Food Chem.,* vol. 59, no. 20, pp. 11063-11069, 2011.
[398] A. Roberts, H. Pimentel, C. Trapnell, and L. Pachter, "Identification of novel transcripts in annotated genomes using RNA-Seq," *Bioinformatics,* vol. 27, no. 17, pp. 2325-2329, Sep 2011, doi: 10.1093/bioinformatics/btr355.
[399] B. Langmead, "Aligning short sequencing reads with Bowtie," *Current Protocols in Bioinformatics,* vol. 32, no. 1, pp. 11.7. 1-11.7. 14, 2010.
[400] S. F. Altschul, W. Gish, W. Miller, E. W. Myers, and D. J. Lipman, "Basic local alignment search tool," *Journal of molecular biology,* vol. 215, no. 3, pp. 403-410, 1990.
[401] S. Griffiths-Jones, A. Bateman, M. Marshall, A. Khanna, and S. R. Eddy, "Rfam: an RNA family database," *J Nucleic Acids Research,* vol. 31, no. 1, pp. 439-441, 2003.
[402] S. Griffiths-Jones, H. K. Saini, S. Van Dongen, and A. J. Enright, "miRBase: tools for microRNA genomics," *Nucleic acids research,* vol. 36, no. suppl_1, pp. D154-D158, 2007.
[403] M. R. Friedländer, S. D. Mackowiak, N. Li, W. Chen, and N. Rajewsky, "miRDeep2 accurately identifies known and hundreds of novel microRNA genes in seven animal clades," *J Nucleic Acids Research,* vol. 40, no. 1, pp. 37-52, 2012.
[404] M. I. Love, W. Huber, and S. Anders, "Moderated estimation of fold change and dispersion for RNA-seq data with DESeq2," *Genome Biology,* vol. 15, no. 12, pp. 1-21, 2014.
[405] A. Enright, B. John, U. Gaul, T. Tuschl, C. Sander, and D. Marks, "MicroRNA targets in *Drosophila*," *Genome Biology,* vol. 4, no. 11, pp. 1-27, 2003.
[406] A. Huang, L. He, and G. Wang, "Identification and characterization of microRNAs from *Phaeodactylum tricornutum* by high-throughput sequencing and bioinformatics analysis," *J BMC Genomics,* vol. 12, no. 1, pp. 1-11, 2011.
[407] N. Tuteja, N. Q. Tran, H. Q. Dang, and R. Tuteja, "Plant MCM proteins: role in DNA replication and beyond," *J Plant Molecular Biology,* vol. 77, no. 6, pp. 537-545, 2011.
[408] P. Bulankova, G. Bilcke, W. Vyverman, and L. De Veylder, "Cellular Hallmarks and Regulation of the Diatom Cell Cycle," in *The Molecular Life of Diatoms,* A. Falciatore and T. Mock Eds. Cham: Springer International Publishing, 2022, pp. 229-263.
[409] M. Ragni and M. R. d'Alcalà, "Circadian variability in the photobiology of *Phaeodactylum tricornutum*: pigment content," *Journal of Plankton Research,* vol. 29, no. 2, pp. 141-156, 2007, doi: 10.1093/plankt/fbm002 %J Journal of Plankton Research.
[410] Y. Xu, I. M. Ibrahim, and P. J. Harvey, "The influence of photoperiod and light intensity on the growth and photosynthesis of *Dunaliella salina*

(chlorophyta) CCAP 19/30," *Plant Physiology and Biochemistry*, vol. 106, pp. 305-315, 2016.
[411] A. Monnier *et al.*, "Orchestrated transcription of biological processes in the marine picoeukaryote *Ostreococcus* exposed to light/dark cycles," *J BMC Genomics*, vol. 11, p. 192, Mar 22 2010, doi: 10.1186/1471-2164-11-192.
[412] T. Yamashino *et al.*, "A link between circadian-controlled bHLH factors and the APRR1/TOC1 quintet in *Arabidopsis thaliana*," *Plant and Cell Physiology*, vol. 44, no. 6, pp. 619-629, 2003.
[413] C. Lim *et al.*, "Clockwork orange encodes a transcriptional repressor important for circadian-clock amplitude in *Drosophila*," *J Current Biology*, vol. 17, no. 12, pp. 1082-1089, 2007.
[414] N. H. Nguyen and H. Lee, "MYB-related transcription factors function as regulators of the circadian clock and anthocyanin biosynthesis in Arabidopsis," *Plant signaling & behavior*, vol. 11, no. 3, p. e1139278, 2016.
[415] R. Saini, M. Jaskolski, and S. J. Davis, "Circadian oscillator proteins across the kingdoms of life: structural aspects," *J BMC Biology*, vol. 17, no. 1, pp. 1-39, 2019.
[416] R. Y. Poon, "Cell cycle control: a system of interlinking oscillators," *J Cell Cycle Oscillators: Methods Protocols*, pp. 3-19, 2016.
[417] M. Björklund, "Cell size homeostasis: Metabolic control of growth and cell division," *J Biochimica et Biophysica Acta -Molecular Cell Research*, vol. 1866, no. 3, pp. 409-417, 2019.
[418] L. Robert, M. Hoffmann, N. Krell, S. Aymerich, J. Robert, and M. Doumic, "Division in *Escherichia coli* is triggered by a size-sensing rather than a timing mechanism," *J BMC Biology*, vol. 12, pp. 1-10, 2014.
[419] A. R. Jones *et al.*, "Cell-size dependent progression of the cell cycle creates homeostasis and flexibility of plant cell size," *J Nature Communications*, vol. 8, no. 1, p. 15060, 2017.
[420] M. B. Ginzberg, N. Chang, H. D'Souza, N. Patel, R. Kafri, and M. W. Kirschner, "Cell size sensing in animal cells coordinates anabolic growth rates and cell cycle progression to maintain cell size uniformity," *J Elife*, vol. 7, p. e26957, 2018.
[421] K. Kobayashi *et al.*, "Transcriptional repression by MYB 3R proteins regulates plant organ growth," *The EMBO Journal*, vol. 34, no. 15, pp. 1992-2007, 2015.
[422] J. K. Waititu, C. Zhang, J. Liu, and H. Wang, "Plant Non-Coding RNAs: origin, biogenesis, mode of action and their roles in abiotic stress," *International Journal of Molecular Sciences*, vol. 21, no. 21, p. 8401, 2020.
[423] E. Bautista-Chamizo, M. Sendra, M. De Orte, and I. Riba, "Comparative effects of seawater acidification on microalgae: Single and multispecies toxicity tests," *J Science of The Total Environment*, vol. 649, pp. 224-232, 2019.
[424] X. Liu *et al.*, "Formation of resting cells is accompanied with enrichment of ferritin in marine diatom Phaeodactylum tricornutum," *J Algal Research*, vol. 61, p. 102567, 2022.
[425] A. Eisentraeger, W. Dott, J. Klein, and S. Hahn, "Comparative studies on algal toxicity testing using fluorometric microplate and Erlenmeyer flask growth-inhibition assays," *J Ecotoxicology Environmental Safety*, vol. 54, no. 3, pp. 346-354, 2003.

[426] H. S. Kim *et al.*, "High-throughput droplet microfluidics screening platform for selecting fast-growing and high lipid-producing microalgae from a mutant library," *J Plant Direct,* vol. 1, no. 3, p. e00011, 2017.
[427] M. Serif, B. Lepetit, K. Weißert, P. G. Kroth, and C. R. Bartulos, "A fast and reliable strategy to generate TALEN-mediated gene knockouts in the diatom *Phaeodactylum tricornutum*," *J Algal Research,* vol. 23, pp. 186-195, 2017.
[428] O. Levitan, J. Dinamarca, E. Zelzion, M. Y. Gorbunov, and P. G. Falkowski, "An RNA interference knock-down of nitrate reductase enhances lipid biosynthesis in the diatom *Phaeodactylum tricornutum*," *J The Plant Journal,* vol. 84, no. 5, pp. 963-973, 2015.
[429] D. R. Ort *et al.*, "Redesigning photosynthesis to sustainably meet global food and bioenergy demand," *J Proceedings of the National Academy of Sciences,* vol. 112, no. 28, pp. 8529-8536, 2015.
[430] J. Beckmann *et al.*, "Improvement of light to biomass conversion by de-regulation of light-harvesting protein translation in *Chlamydomonas reinhardtii*," *J Journal of Biotechnology,* vol. 142, no. 1, pp. 70-77, 2009.
[431] J. H. Mussgnug *et al.*, "Engineering photosynthetic light capture: impacts on improved solar energy to biomass conversion," *J Plant Biotechnology Journal,* vol. 5, no. 6, pp. 802-814, 2007.
[432] M. Oey *et al.*, "RNAi knock-down of LHCBM1, 2 and 3 increases photosynthetic H_2 production efficiency of the green alga *Chlamydomonas reinhardtii*," *J PloS One,* vol. 8, no. 4, p. e61375, 2013.
[433] P.-H. Chen *et al.*, "Enhancing CO 2 bio-mitigation by genetic engineering of cyanobacteria," *Energy & Environmental Science,* vol. 5, no. 8, pp. 8318-8327, 2012.
[434] S. Seo, H. Jeon, K. S. Chang, and E. Jin, "Enhanced biomass production by Phaeodactylum tricornutum overexpressing phosphoenolpyruvate carboxylase," *Algal Research,* 2017.

Appendix A

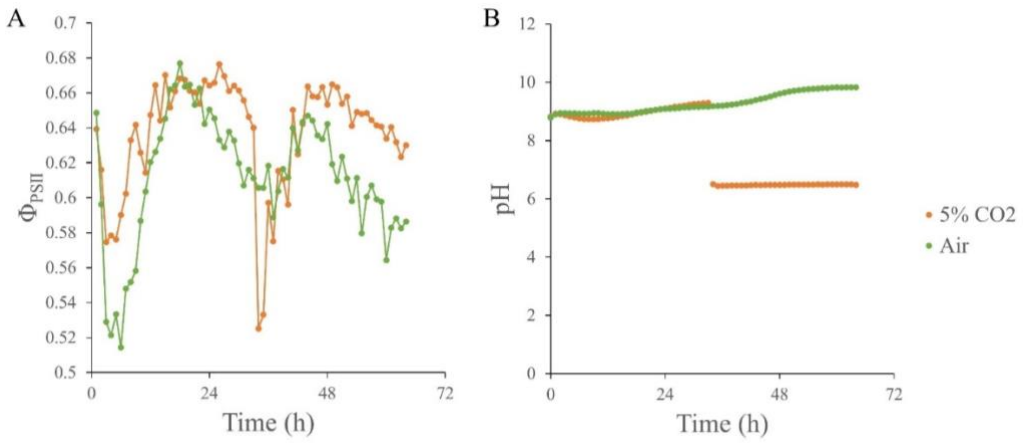

Figure A2. Monitoring of growth parameters under continuous illumination. (A) Effective quantum yield. (B) pH. Batch cultures were conducted in FMT150 photobioreactors with constant light and temperature; 5% CO_2 was pumped into one reactor after 33 h.

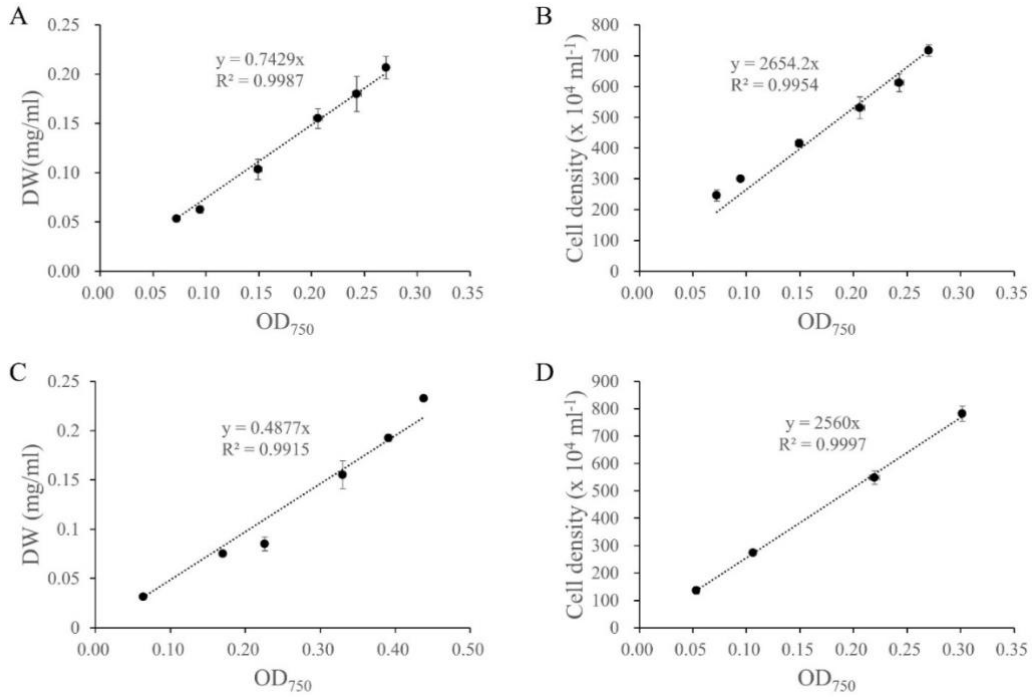

Figure A3. Optical density (OD) calibration to dry weight (DW) and cell concentration with different spectrophotometers. (A) OD-DW calibration with DR1900. (B) OD-cell concentration calibration with DR1900. (C) OD-DW calibration with DR3900. (D) OD-cell concentration calibration with DR3900.

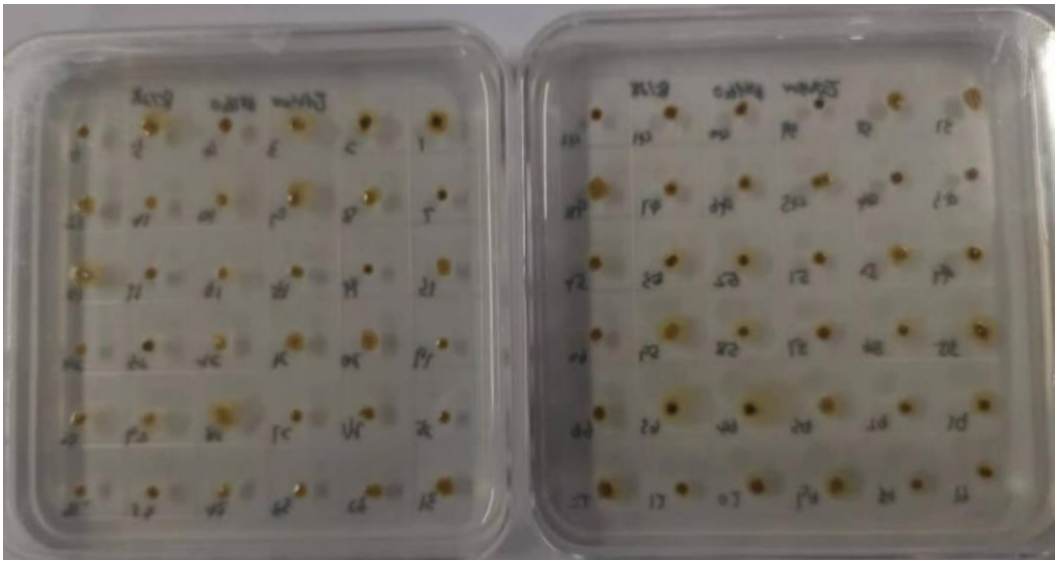

Figure A3. Isolated colonies from ALE strains grown on acidic agar plates (pH 6.0).